Design and Synthesis of Artificial Photosynthetic Molecules to Mimic Aspects of Natural Photosynthetic Mechanisms

by

Smitha Pillai

A Dissertation Presented in Partial Fulfillment
of the Requirements for the Degree
Doctor of Philosophy

Approved July 2011 by the
Graduate Supervisory Committee:

Ana Moore, Chair
Ian Gould
Thomas Moore

ARIZONA STATE UNIVERSITY

August 2011

ABSTRACT

Natural photosynthesis features a complex biophysical/chemical process that requires sunlight to produce energy rich products. It is one of the most important processes responsible for the appearance and sustainability of life on earth.

The first part of the thesis focuses on understanding the mechanisms involved in regulation of light harvesting, which is necessary to balance the absorption and utilization of light energy and in that way reduce the effect caused by photooxidative damage. In photosynthesis, carotenoids are responsible not only for collection of light, but also play a major role in protecting the photosynthetic system. To investigate the role of carotenoids in the quenching of the excited state of cyclic tetrapyrroles, two sets of dyads were studied. Both sets of dyads contain zinc phthalocyanine (Pc) covalently attached to carotenoids of varying conjugation lengths. In the first set of dyads, carotenoids were attached to the phthalocyanine via amide linkage. This set of dyads serves as a good model for understanding the molecular "gear-shift" mechanism, where the addition of one double bond can turn the carotenoid from a nonquencher to a very strong quencher of the excited state of a tetrapyrrole. In the second set of dyads, carotenoids were attached to phthalocyanine via a phenyl amino group. Two independent studies were performed on these dyads: femtosecond transient absorption and steady state fluorescence induced by two-photon excitation. In the transient absorption study it was observed that there is an instantaneous population of the carotenoid S_1 state after Pc excitation, while two-photon

excitation of the optically forbidden carotenoid S_1 state shows ^{1}Pc population. Both observations provide a strong indication of the existence of a shared excitonic state between carotenoid and Pc. Similar results were observed in LHC II complexes in plants, supporting the role of such interactions in photosynthetic down regulation.

In the second chapter we describe the synthesis of porphyrin dyes functionalized with carboxylate and phosphonate anchoring groups to be used in the construction of photoelectrochemical cells containing a porphyrin-$IrO_2 \cdot nH_2O$ complex immobilized on a TiO_2 electrode. The research presented here is a step in the development of high potential porphyrin-metal oxide complexes to be used in the photooxidation of water.

The last chapter focuses on developing synthetic strategies for the construction of an artificial antenna system consisting of porphyrin-silver nanoparticle conjugates, linked by DNA of varied length to study the distance dependence of the interaction between nanoparticles and the porphyrin chromophore. Preliminary studies indicate that at the distance of about 7–10 nm between porphyrin and silver nanoparticle is where the porphyrin absorption leading to fluorescence shows maximum enhancement. These new hybrid constructs will be helpful for designing efficient light harvesting systems.

This dissertation is dedicated to my loving husband Sandip for his support and motivation during this graduate program.

ACKNOWLEDGMENTS

First and foremost, I would like to express my most sincere gratitude to my advisor, Dr. Ana Moore for providing me with the opportunity to work with her. Her continuous guidance and support have helped me in getting my thesis in the present form. She has shown enormous patience during the course of my Ph.D studies and constantly gives me encouragement to think positively. I would like to thank Dr. Thomas Moore and Dr. Devens Gust for their support and guidance. Special thanks to my committee members Dr. Seth Rose and Dr. Ian Gould for their guidance and support as a part of my examination committee. I am very grateful to our collaborators Dr. John Kennis, Dr. Peter Walla, Dr. Thomas Mallouk and their students. I would like to thank Dr. Paul Liddell and Dr. Yuichi Terazono for sharing their knowledge of synthetic chemistry. A special thanks to Dan Brune, John Lopez and Zachery Laughery at the protein lab facility for all their help in teaching me HPLC and MALDI. I would like to thank Dr. Brain Cherry who had patience to help me do all 2D NMR spectroscopy. I would also like to thank Dr. Hao Yan's group for teaching me DNA chemistry especially Dr. Reji Varghese and Suchetan Pal. It is a pleasure to thank the entire Gust Moore Moore group for being helpful and creating a friendly environment. I would like to thank Dr. Michael Hambourger, Dr. Miguel Gervaldo and Benjamin Sherman for teaching me electrochemistry. Special thanks to Dr. Gerdenis Kodis and Dr. Amy Keirstead for teaching me spectroscopy. I would like to thank Benjamin Sherman and Larry Orr for proofreading this document. I am indebted to my lab

partners Elina. S and Jesse Bergkamp. Thanks to Katherine Wong for her cheerful presence in the office. Special acknowledgements are also given to Department of Energy and National Institutes of Health for their financial support.

I would like to thank those in my personnel life that supported me through the graduate years, especially my mother and sister for all their support throughout my life. I am very grateful to all my teachers and my students for their contribution throughout my carrier. Finally I like to dedicate my thesis to my husband Sandip for his continuous motivation and support.

TABLE OF CONTENTS

Page

LIST OF TABLES

CHAPTER 2

CHAPTER 3

LIST OF FIGURES

CHAPTER 1

Figure Page

CHAPTER 2

CHAPTER 3

Figure Page

LIST OF ABBREVIATIONS

BINAP……2,2’-bis(diphenylphosphino)-1,1’-binapthyl

Calcd……...Calculated

CDI……1,1'-Carbonyldiimidazole

DBU……1,8-Diazabicyclo[5.4.0]undec-7-ene

DCC…….Dicyclohexylcarbodimide

DDQ……....2,3-Dichloro-5,6-dicyano-1,4-benzoquinone

DIBAL…….Diisobutylaluminium hydride

DMF……Dimethyl formamide

DMAE……..Dimethylethanolamine

DMAP……..Dimethylaminopyridine

DMSO……..Dimethyl sulfoxide

DNA……Deoxyribonucleic Acid

EADS……...Evolution Associated Difference Spectra

$E_{1/2}$……Midpoint Potential

E_p……..Peak Potential

E^0……..Standard Potential

EDCI……1-Ethyl-3-(3-dimethylaminopropyl)carbodiimide

FTO…….....Fluorine Doped Tin Oxide

HOBt……. Hydroxybenzotriazole

HPLC…… High Performance Liquid Chromatography

ICT…… Intramolecular Charge Transfer Spectra

ITO…… Indium Doped Tin Oxide

LHC……... Light Harvesting Complex

MALDI……..Matrix Assisted Laser Desorption Ionization

Me……..Methyl

MOPS……3-(N-morpholino)propanesulfonic acid

MS…….Mass Spectrometry

NPQ…… Non-Photochemical Quenching

NMR……..Nuclear Magnetic Resonance

NP…… Nanoparticle

Obsd…… Observed

OEC…… Oxygen Evolving Complex

OPE…… One Photon Excitation

P680…… The Primary Electron Donor of Photosystem II

PSII…….Photosystem II

SCE…… Standard Calomel Electrode

TBE……Tris-Borate-EDTA

TOF…… Time of Flight

THF……Tetrahyrofuran

TPE……Two Photon Excitation

TLC……Thin Layer Chromatography

UV…… Ultraviolet

Vis…… Visible

Chapter 1

CAROTENOIDS PHOTOPROTECTION IN ARTIFICIAL LIGHT HARVESTING DYADS

I. Introduction

Photosynthesis is one of the most important processes on earth, one in which photosynthetic organisms harvest light energy from the sun and then convert this energy to chemically useful forms.[1] The photosynthetic process involves a complex mechanism, which includes organic pigments and other cofactors that are situated in the protein matrix.[2] The photosynthetic assembly mainly consists of two components: light harvesting complexes (LHC) and reaction centers (RC). The first step of photosynthesis is absorption of photons, which is performed by the LHC.[3] This energy is then funneled into a reaction center where charge separation takes place. The two essential classes of pigments in photosynthetic complexes involved in light harvesting function are chlorophylls and carotenoids. Light received from the sun is crucial for the existence of plants, algae, and other photosynthetic organisms, however too much light can lead to undesirable reactions byproducts causing photooxidative damage to the organisms. To survive these conditions plants have developed numerous biochemical processes to optimize photosynthesis and their growth. The organisms can adapt themselves to the environment in such a way that, in addition to adjusting light absorption, they have developed ways of getting rid of excess light energy that has already been absorbed.[3,4] The research presented in this

chapter is to understand the role of chlorophyll and carotenoids pigments in performing these functions in artificial systems.

Light harvesting complexes

In photosynthetic organisms, the light-harvesting complexes absorb solar radiant energy and transfer it to the reaction centers where electronic excitation energy is converted to electrochemical energy. The first step of this conversion starts with the absorption of sunlight by the light-harvesting pigments such as chlorophyll and carotenoids. In general, biological pigments are non-covalently attached to proteins, forming pigment protein complexes.[5] The proteins function as a framework to support these pigments and align them in a way to enable efficient absorption of light and transfer of energy in these complexes. In purple bacteria the photosynthetic antenna system consists of two types of pigment-proteins known as light-harvesting 1 and 2 complexes, LH1 and LH2.[6] LH1 is found close to the reaction center, while LH2 is a peripheral light-harvesting complex known as accessory antenna that is found only in some organisms.[7] The structure of LH2 has been determined by X-ray diffraction for *Rhodopseudomonas (Rsp.) acidophila* (Figure 1). It consists of a circular aggregate of α and β polypeptides (grey), along with bacteriochlorophyll (green) and carotenoid (red) molecules. In green plants and algae the major light-harvesting complex (LHC) is located in photosystem II (PSII). The structure of pea LHCII has been determined by X-ray crystallography as shown in Figures 2 and 3.[8] It consists of chlorophyll *a*, chlorophyll *b* and carotenoids, which help to hold the complex together. In the LHC of dinoflagellate algae there is a unique

antenna complex known as the peridinin-chlorophyll protein (PCP) complex, which contains chlorophyll *a* and the carotenoid peridinin.[9,10]

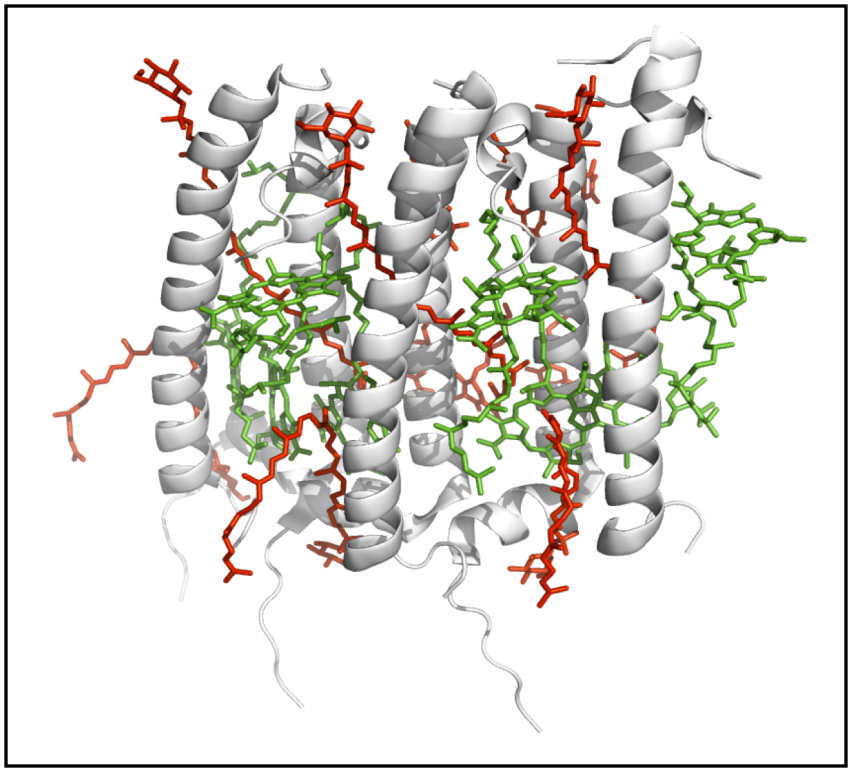

Figure 1: The structure of the LH2 complex of R*ps*. *Acidophila*. The bacteriochlorophylls are shown in green, carotenoid are shown in red and protein in light grey.[5]

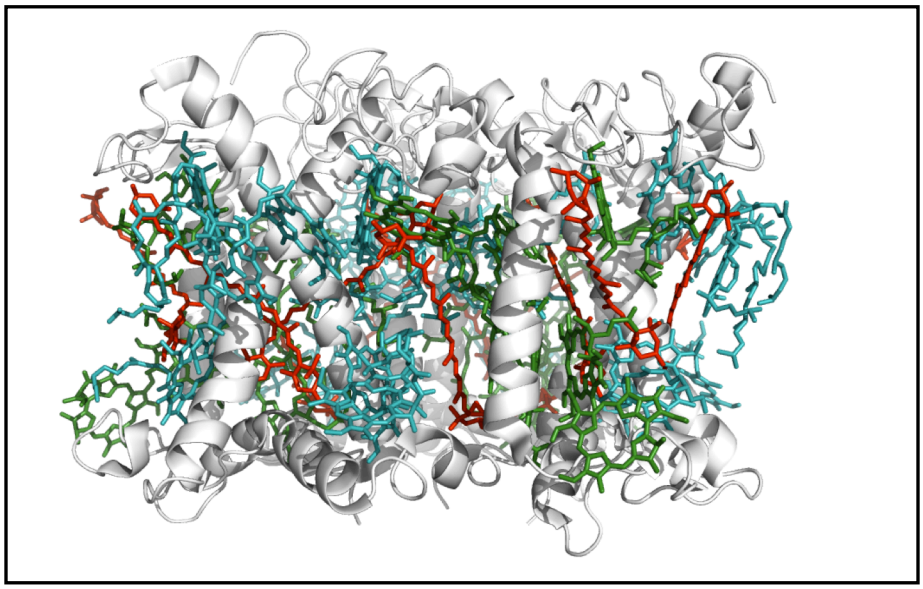

Figure 2: LHCII trimer: side view from the stromal side. Chl *a* is shown in blue, Chl *b* is shown in green, carotenoids are shown in red and protein in light grey.[8]

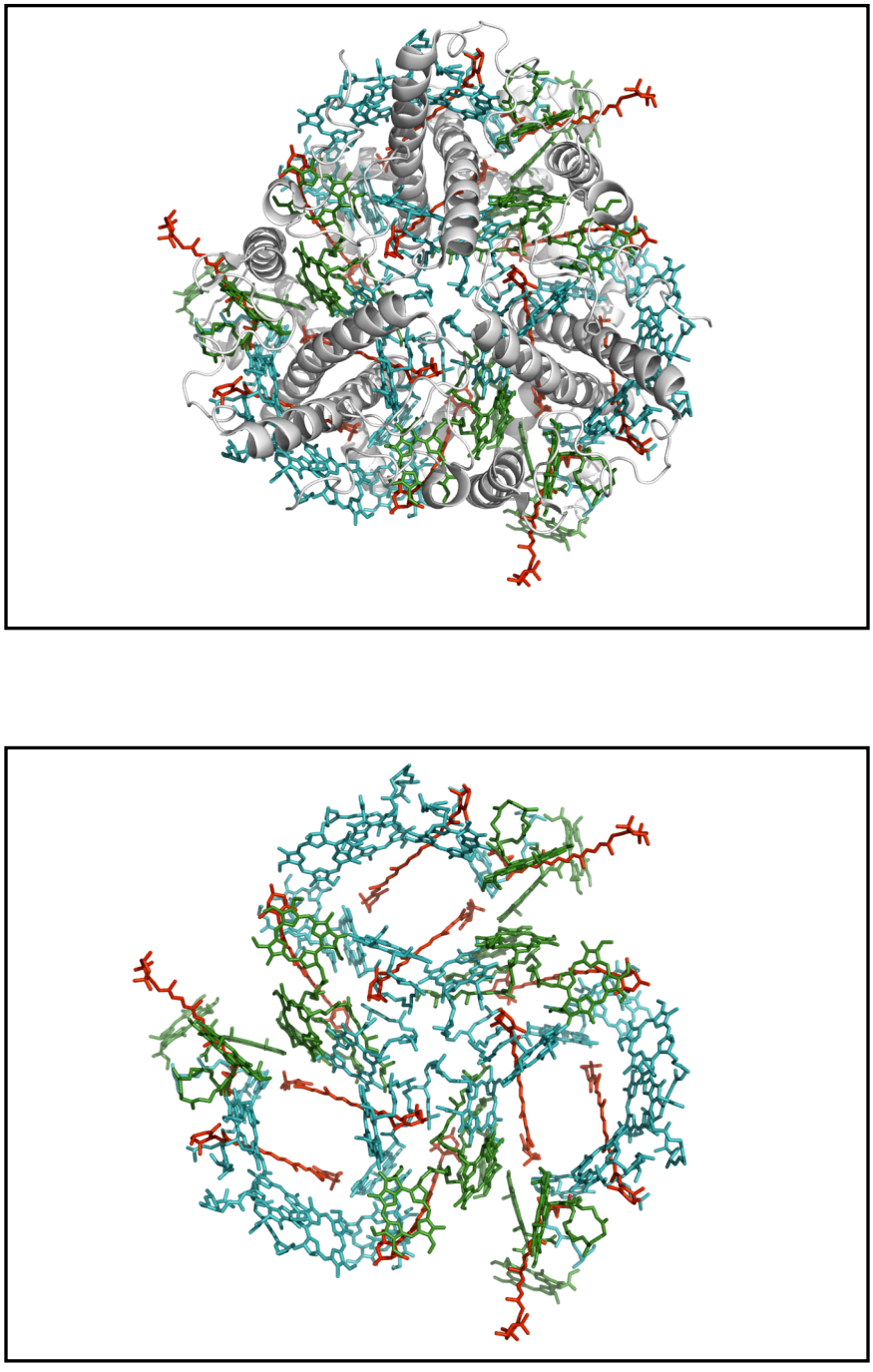

Figure 3: LHCII trimer: top view from the stromal side. Chl *a* is shown in blue, Chl *b* is shown in green, carotenoids are shown in red and protein in light grey.[8]

Carotenoids in nature

Carotenoids and chlorophyll are the most abundant pigments found in nature. The light-harvesting complexes of green plants and many other photosynthetic organisms consist of arrays of chlorophyll (Chl) and carotenoid molecules, which are the primary chromophores of the photosynthetic apparatus.[1]

A. Role of Carotenoids in Photosynthesis

In photosynthetic organisms carotenoids can serve different functions:

Antenna function

Carotenoids can absorb light in the blue/green region of the visible spectrum where the chlorophyll has less absorption, and transfer this energy to the neighboring chlorophylls.[11] Therefore, carotenoids enhance the efficiency of light harvesting in the photosynthetic apparatus.[1]

Photoprotection

In photosynthesis, some dangerous byproducts such as chlorophyll triplets and singlet oxygen are generated. Carotenoids can protect the system from the effect of these species very efficiently due to their low-lying excited triplet states; energy transfer from chlorophyll triplet or singlet oxygen, in the case that it is formed, results in the formation of carotenoid triplet, which decays harmlessly to the ground state by internal conversion. Another photoprotective mechanism in which the carotenoids are involved is known as non-photochemical quenching (NPQ).[12] It is a regulatory mechanism that results in the quenching of the excited state of the chlorophylls in the antennas under conditions of high light illumination.

Structural stability

Carotenoids are essential for the structural stability of light-harvesting proteins, without them the protein would disassemble.[13]

B. Symmetry and electronic states

Carotenoids are divided into two categories: the non-polar carotenoids and the oxygen-containing xanthophylls. The ability of carotenoids to act as light harvesters is linked to their spectroscopic properties. The complicated excited states of carotenoids limit the knowledge of their photophysics and our understanding of their role in nature. Carotenoids have a highly conjugated π-electron system and are all *trans*, with C_{2h} symmetry in most antennas complexes. The commonly used symmetry labels for the singlet states of the carotenoids, which belong to the C_{2h} group symmetry, are A_g^- and B_u^+.[4]

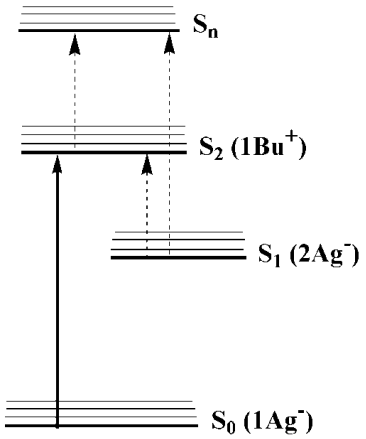

Figure 4: General energy level scheme of carotenoids.[14]

The S_2 state

The carotenoids ground state (S_0) and first excited state (S_1) both possess A_g^- symmetry; the second excited state (S_2) possesses B_u^+ symmetry. According to selection rules of optical transition, only S_0 to S_2 transition is optically dipole-allowed and is responsible for the absorption spectra of the carotenoid around 400–550 nm. The absorption spectra of carotenoid in solution have a characteristic three-peak structure with each peak corresponding to the transition from the ground state to different vibration sub-level of S_2.[4]

The S_1 state

Carotenoids after excitation to S_2 undergo rapid internal conversion (IC) to the S_1 state within few hundred femtoseconds.[15] The lifetime of S_1 depends on N (number of conjugated double bonds) and is between 1 and 200 ps for most natural carotenoids.[16] The S_1 state has the same A_g symmetry as the ground state and hence S_0 to S_1 transition is forbidden and cannot be observed by conventional absorption or fluorescence spectroscopy.[17] A convenient way to overcome this limitation is by two-photon excitation (TPE) because $A_g \rightarrow A_g$ transitions are generally two-photon allowed. Two-photon excitation of LHCII and other photosynthetic proteins has been studied as since this allows selective direct excitation of the optically forbidden carotenoid S_1 state.[18] Electronic interactions between carotenoid S_1 and chlorophylls can be studied by measuring the chlorophyll fluorescence upon TPE excitation; these studies provide an evidence of the energy transfer from the carotenoid S_1 to chlorophyll Q_y state (Car $S_1 \rightarrow$Chl).[19,20] Carotenoid S_1-clorophyll interactions have been measured

quantitatively by comparing the chlorophyll fluorescence intensity detected upon selective two-photon excitation of the carotenoid dark states (Fl^{TPE}), and direct one-photon excitation of the chlorophyll (Fl^{OPE}).[21]

$$\phi_{Coupling}^{CarS_1-Chl/Pc} \propto \frac{Fl^{TPE}}{Fl^{OPE}}$$

It has been shown recently that the fluorescence quenching and photosynthetic down-regulation in LHCII and entire plants are closely related to the electronic interactions between the carotenoids and the chlorophylls.[22,23] It has also been demonstrated that there is an instantaneous energy flow in the opposite direction from the chlorophylls to the carotenoids (Chl→ Car S_1) in these systems.[15]

Other states

Theoretical calculations performed by Tavan and Schulten on polyenes with more than 8-conjugated π-electrons such as carotenoids, determined that there could be additional states besides the S_1 and S_2 states.[24-26] Extrapolating the state energies to longer polyenes it became clear that there are two other excited states, $1Bu^-$ and $3A_g^-$. The $1Bu^-$ is expected to appear between the $1B_u^+$ and the $2A_g^-$ states of polyenes having N≈9 (N is equal to the number of double bonds), and $3A_g^-$ state was predicted to be in the vicinity of the S_2 state for N≈13 and thus above the S_2 state for most of carotenoids. The transition from the ground state to both $1Bu^-$ and $3A_g^-$ are forbidden (for $1Bu^-$ it is both one- and two-photon forbidden), and is challenging to experimentally resolve these states as these states if populated, will relax quickly to the S_1 state, reducing their lifetime to the femtosecond timescale.[4]

Intramolecular charge transfer state (ICT)

Carotenoids with a carbonyl group conjugated with the π–electron system of double bonds show the presence of intramolecular charge transfer states. Transient signals from both S_1 and ICT states exhibited identical dynamics over a broad spectral range and this has led to the S_1/ICT representation for the combined system of states.[27] The major influence of the ICT state is that it modulates the lifetime of the S_1 state with which it might be electronically coupled. It is observed that when a carbonyl group is present the S_1 lifetime becomes shorter and the S_2–S_1 energy gap decreases as compared to the carotenoids of similar length lacking the carbonyl groups.[28-31] This makes the coupled S_1/ICT state sufficiently higher so that there is a favorable spectral overlap with the Q_y band of Chl *a*.[29-31]

Non-photochemical quenching

When photosynthetic organisms experience higher levels of light than they are capable of utilizing, thermal dissipation of the excess absorbed photons occurs. This protects the photosynthetic membrane against damage by the generation of harmful species.[3] This process is referred to as non-photochemical quenching (NPQ) of chlorophyll fluorescence. NPQ arises from a number of factors in the thylakoid membrane, but the major factor depends on the activity of xanthophyll cycle and change in pH across the membrane.[32] The interconversion of violaxanthin (nine double bonds) to zeaxanthin (eleven double bonds) via antheraxanthin (ten double bonds) is referred to as the xanthophyll cycle as shown in Figure 5. In some groups of micro algae, a different type of xanthophyll cycle

called the diadinoxanthin cycle is observed which involves diadinoxanthin and diaatoxanthin.[33] In the past few years it has been generally accepted that NPQ correlates linearly with the acidification of the lumen and the combined concentrations of the monoepoxide antheraxanthin and epoxide-free zeaxanthin.

Xanthophyll cycle in photosynthesis

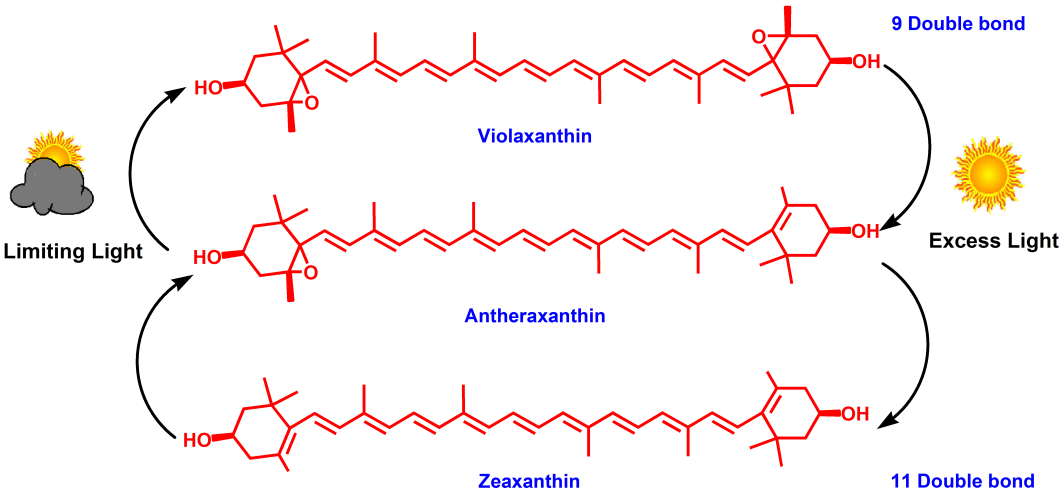

Figure 5: The xanthophyll cycle.[33]

In plants de-epoxidation reaction is carried out by violaxanthin de-epoxidase enzyme (VDE), which is localized in the thylakoid lumen. VDE utilizes ascorbic acid (vitamin C) to reduce the epoxide ring. The xanthophyll cycle is then completed with the zeaxanthin epoxidase (ZE), which catalyzes the epoxidation reaction. As ZE activity is optimum at pH 8, it is believed to be located on the stromal side of the thylakoid membrane. The major component of NPQ is energy-dependent quenching (qE), which is rapidly reversible, and normally functions to protect PSII. There is no single mechanism of NPQ for

natural photosynthetic systems; different organisms have developed different ways to protect themselves. There is evidence of both energy transfer and electron-transfer quenching of the chlorophylls excited state in the NPQ of higher plants, but it is unclear whether these processes are induced by conformational changes within the pigment-protein complexes or in its position in antenna systems.[34,35] Alternatively excitonic carotenoid S_1-chlorophyll interactions have been proposed as one of photosynthetic down-regulation mechanisms. Excitonic interactions between carotenoids and chlorophylls take place when two chromophores with similar excited-state energies come close together to form two new excited states; one having a lower energy level than the original chromophore energies and the other having a higher energy level. The excess energy of the entire pigment can be trapped in the lower energy level of the excitonic state.[36,37] Figure 6 represents the proposed regulation (quenching) mechanisms for light-harvesting in photosynthesis.[21] Simple artificial light-harvesting systems such as ones discussed below containing carotenoid-tetrapyrrole systems have served as good mimics to understand these mechanisms.

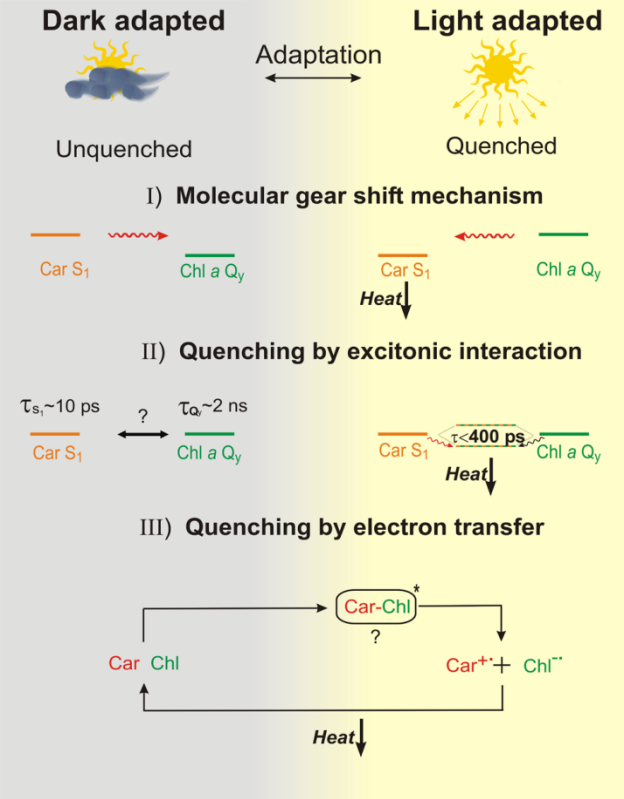

Figure 6: The electronic carotenoid-chlorophyll (Car–Chl) interactions that have been proposed as regulation mechanisms for light harvesting in photosynthesis.[34]

Artificial light-harvesting antennae

Our group has extensively studied the role of photosynthetic pigments in artificial synthetic compounds where they show behavior similar to that observed in natural systems. To explore the functions of carotenoids in natural photosynthesis many artificial light-harvesting antennae have been used. The following brief outline will focus on the attempt to understand the structural and environmental effects on the interaction between the carotenoids and tetrapyrroles, thereby defining their roles in natural photosynthesis.

A. Carotenoids containing terminal carbonyl group covalently attached to a tetrapyrrole system

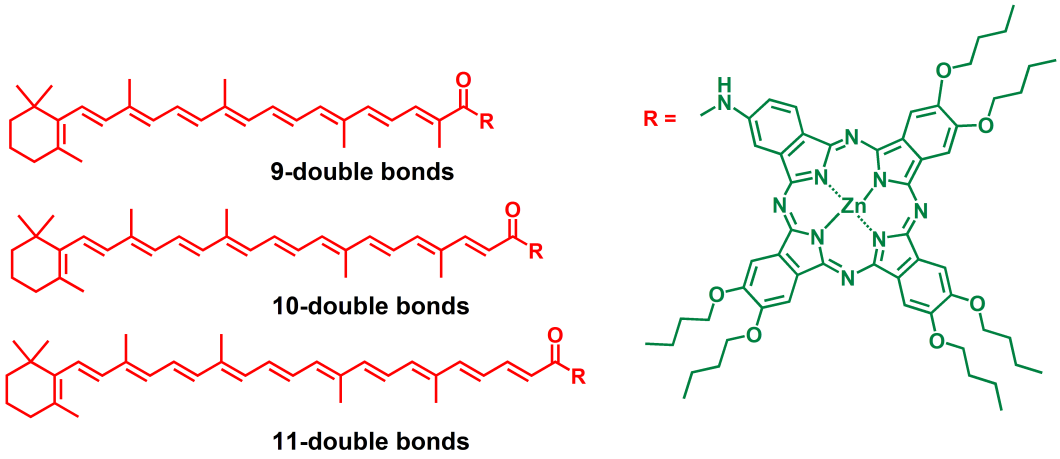

Figure 7: Molecular structures of dyads with 9-, 10- and 11-double-bond carotenoids covalently attached to phthalocyanine.

A set of dyads was synthesized to study the excess energy dissipation in oxygenic photosynthesis. These dyads consist of zinc phthalocyanine (Pc), which mimics Chl *a*, covalently linked to a series of carotenoids having 9-, 10-, and 11-double bonds. Changing the conjugation length from 9- to 10-double bonds brings the energy level of the carotenoid S_1 state below that of the Q_y state of chlorophyll, which can allow the carotenoids to quench the Chl (Pc) excited state by energy transfer.[38,39] However, quenching the Chl (Pc) excited state could be caused by electron transfer, as an increase in conjugation lowers the first oxidation potential of the carotenoid.[12,40]

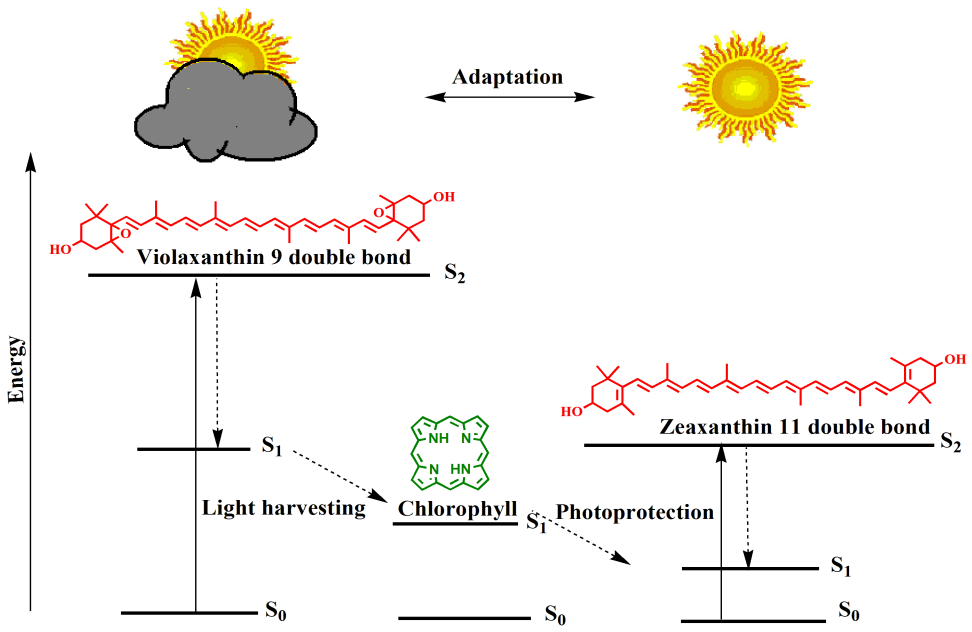

Figure 8: Molecular gear-shift mechanism.[33]

Transient absorption spectroscopic studies were performed on these dyads. Experiments show that carotenoid can act as an acceptor of Pc excitation energy, thereby reducing Pc singlet excited state lifetime. The conjugation length of the carotenoid plays a major role in the quenching mechanism; the addition of only one double bond can convert the carotenoid from a nonquencher to a very strong quencher (see Figure 8). The quenching is dependent on the polarity of the solvent used. These results were thought to arise from the participation of the carotenoid ICT (internal charge transfer state) that in the case of carbonyl containing carotenoids are known to be strongly coupled to their S_1 state and thereby mediating energy transfer.[39] The transient spectra of the S_1 state of the model carbonyl containing carotenoids were comparable with those of fucoxanthin and

peridinin the naturally occurring carotenoids containing carbonyl groups conjugated to the polyene. Fucoxanthin and peridinin show considerable charge-transfer character in their S_1 states, which is essential for their efficient light harvesting function.[16]

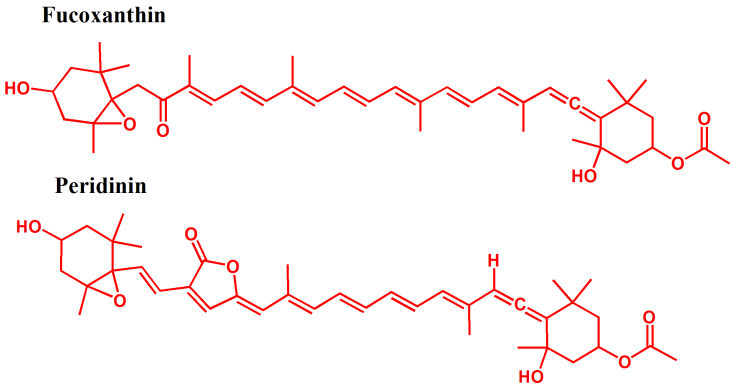

Figure 9: Molecular structure of fucoxanthin and peridinin.[27]

B. Carotenoids lacking terminal carbonyl group covalently attached to a tetrapyrrole system

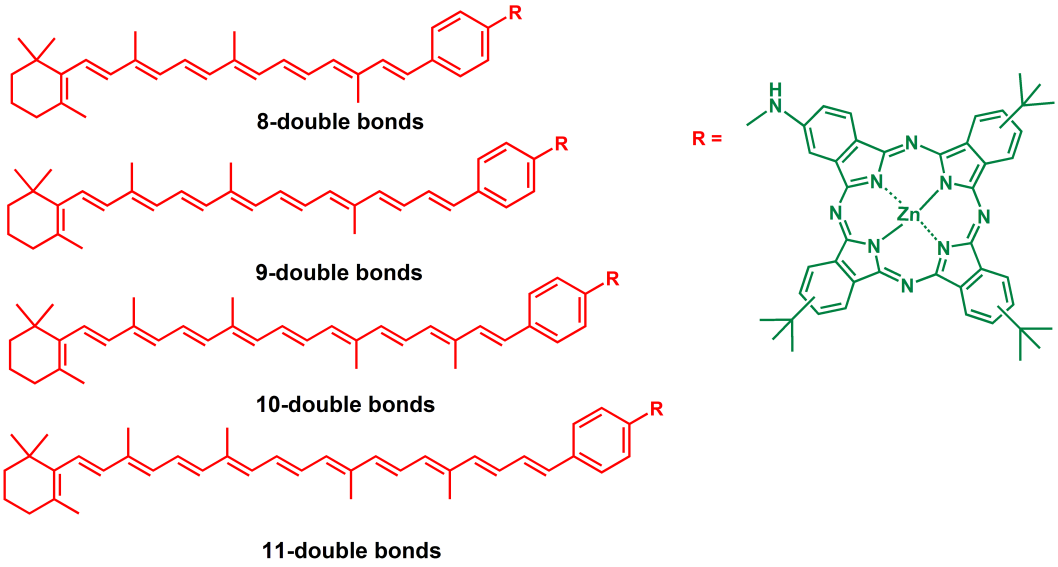

Figure 10: Molecular structures of dyads with 8-, 9-, 10- and 11-double bond carotenoids covalently attached to phthalocyanine.

The second part of this project was to address the question of whether or not carotenoids lacking the carbonyl group, but otherwise structurally similar to the dyads mentioned above, can act as quenchers of the excited states of the pyrrole. As shown above in Figure 5, the xanthophylls involved in NPQ of higher plants do not include carbonyl groups. For this reason, a new series of dyads with carotenoids lacking the carbonyl group was synthesized. These dyads contain a secondary amine group as a linker between the carotenoids and Pc. The carotenoid moieties of the dyads contain 8-, 9-, 10-, and 11-conjugated double bonds, respectively, in addition to the phenyl group.[41]

II. Carotenoids containing terminal carbonyl group covalently attached to a phthalocyanine

General carotenoid synthesis

A. 12'-Apo-*β*-caroten-12'-al

Alkoxylation of furan was performed by reacting methyl alcohol and bromine to give 1,1,4,4-tetramethoxy-2-butene in 78% yield. This compound was then treated with vinylmethyl ether in presence of zinc chloride and $BF_3.O(C_2H_5)_2$ to give compound **2** in 71% yield. The desired 2,4,6-octatrien-1,8-dial was obtained by heating the alkoxyacetal with dilute phosphoric acid followed by simultaneous distillation of the methanol to give the desired product **3** in 54% yield.[42]

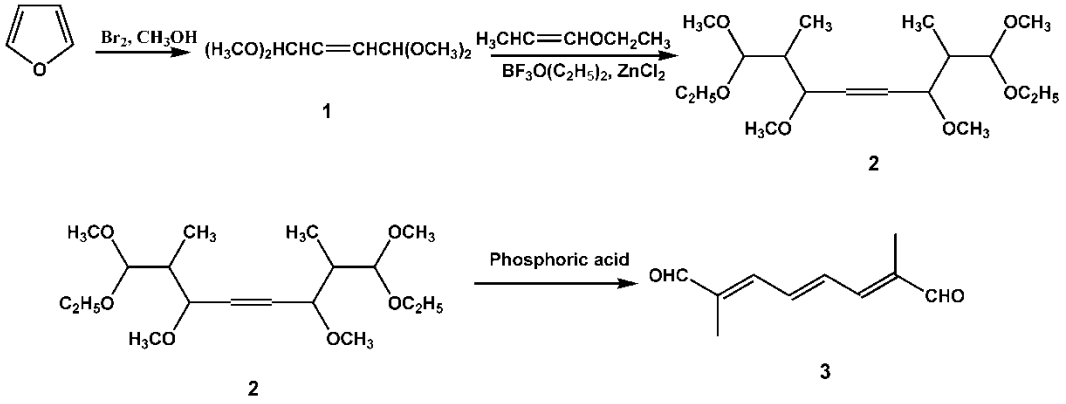

Scheme 1: Synthesis of compound **3**

Synthesis of phosphonium salt **5** was achieved by the Grignard reaction of *β*–ionone with vinylmagnesium bromide to give vinyl-*β*-ionol **4**. Treatment of this allylic alcohol with triphenylphosphinehydrogenbromide gave the desired product as salt **5** in 82% yield.[42]

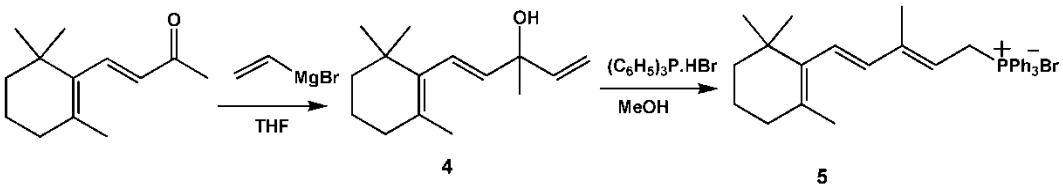

Scheme 2: Synthesis of compound **5.**

Wittig olefination of **3** with salt **5** was initiated with sodium methoxide in methanol to give the desired carotenoid **6** with 65% yield. The reaction also produced double olefination of **3** to give *β*-carotene, which was easily removed by column chromatography due to its non-polar nature.[43]

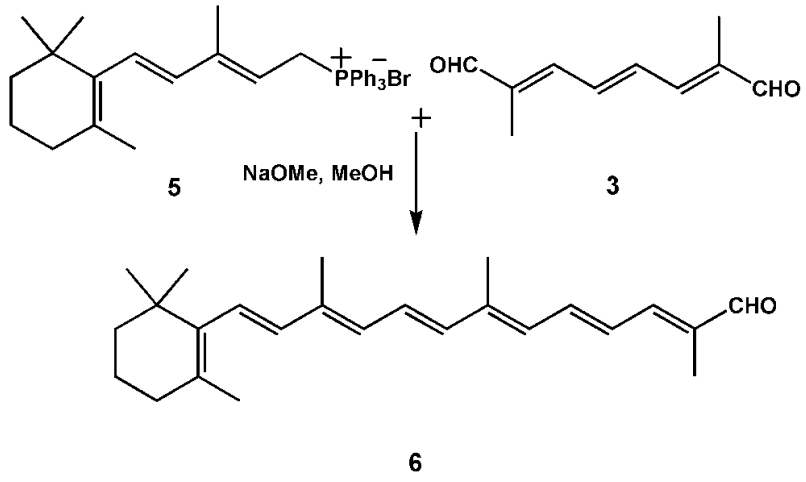

Scheme 3: Synthesis of compound **6**.

B. 10'-Apo-*β*-caroten-10'-al

Extension of the conjugated chain of the carotene was achieved by a Wittig reaction to a give a polyene-ester. Two alternate ylides $(Ph)_3PCHCO_2Me$ and $(Ph)_3PC(CH_3)CO_2Et$ were used in the Wittig reaction with the carotenoid aldehydes to introduce methyl groups as observed in natural carotenoids.[44]

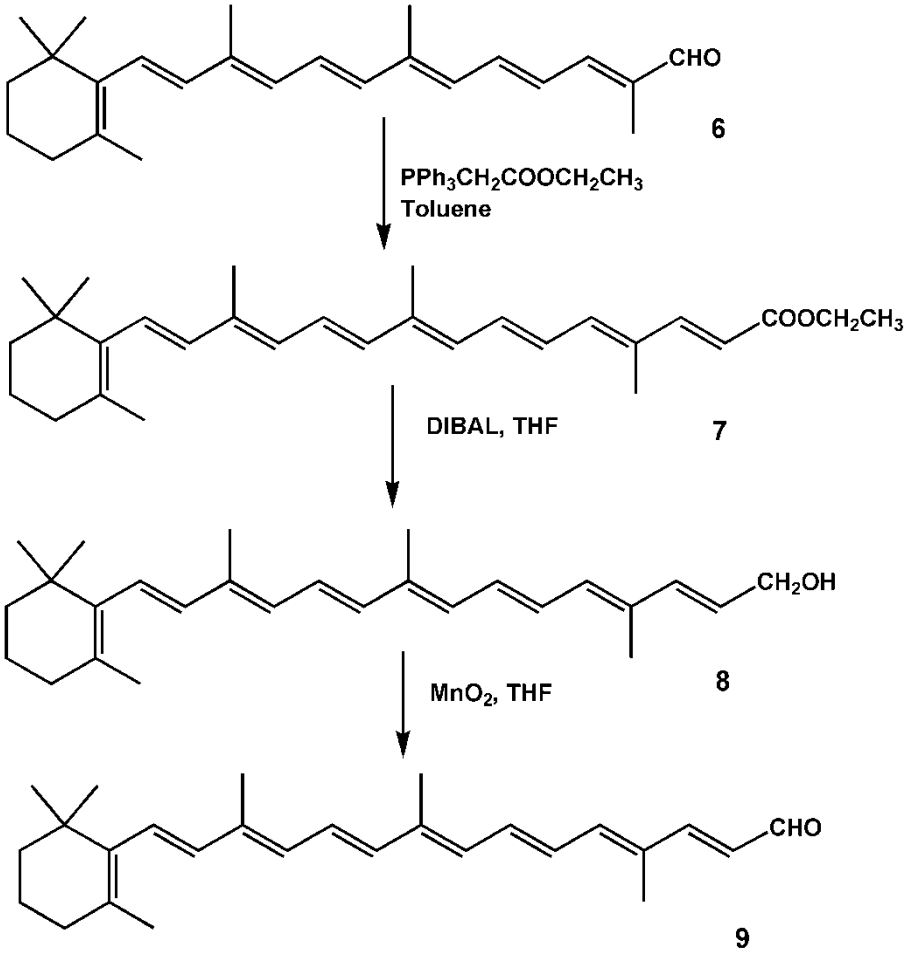

Scheme 4: Synthesis of compound **9**.

The conversion of the ester obtained after the Wittig reaction to an aldehyde was necessary in the next step to perform another Wittig reaction. This

was achieved by reducing the ester to the alcohol using DIBAL in THF, followed by oxidation of the alcohol with MnO_2 to give the corresponding aldehyde.

Synthesis of amide linked caroteno phthalocyanine dyads

Dyads **20**, **21** and **22** consist of two components, a carotenoid and a phthalocyanine, which were synthesized individually and coupled via an amide bond. The amide bond offers an excellent linkage between the phthalocyanine and the carotenoid moieties. Unsymmetrical zinc phthalocyanine with an amino group was coupled with carotenoids **10**, **11** and **12**, that contained acid functional groups.[39]

A. Synthesis of carotenoic acids

Basic hydrolysis of the carotenoid ester generated the corresponding carboxylic acids 9'-apo-*β*-caroten-9'-oic acid (**10**), 7'-apo-*β*-caroten-7'-oic acid (**11**) and 5'-apo-*β*-caroten-5'-oic acid (**12**).

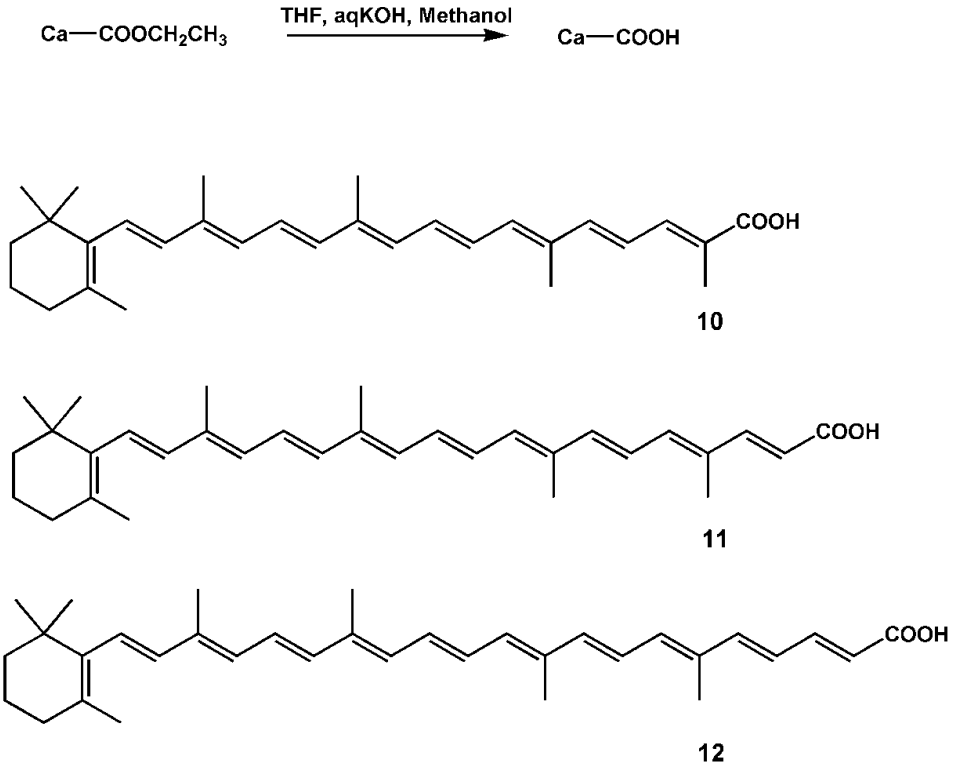

Scheme 5: Synthesis of compounds **10, 11** and **12.**

B. Synthesis of phthalonitriles

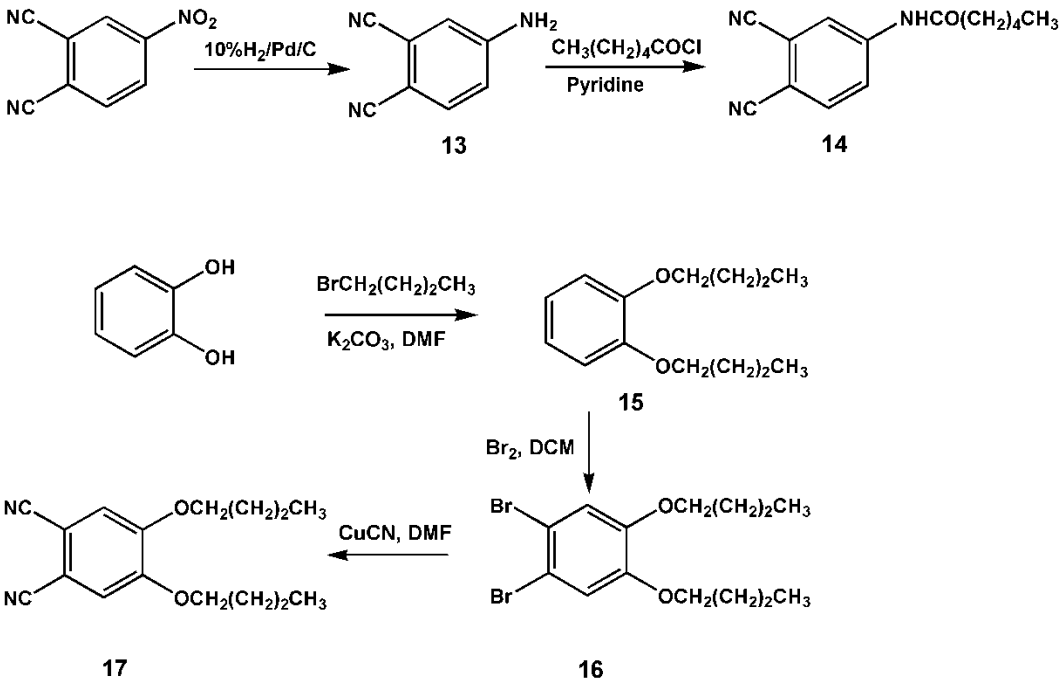

Scheme 6: Synthesis of phthalonitriles **14** and **17**.

4-Hexanamidophthalonitrile was synthesized in two steps: 4-nitrophthalonitrile was first catalytically reduced to 4-aminophthalonitrile, which was later on condensed with hexanoyl chloride in presence of pyridine to produce compound **14** in 33% yield. 1,2-Dibutoxybenzene was synthesized via Williamson ether synthesis by treating 1,2-dihydroxybenzene with potassium carbonate and 1-bromobutane. Compound **15** was brominated to give a mixture of brominated products from which the product was isolated by column chromatography to yield 81% of 1,2-dibromo-4,5-dibutoxybenzene (**16**). This

compound was then treated with copper cyanide to give the desired 4,5-dibutoxyphthalonitrile (**17**).

C. Synthesis of phthalocyanines

Condensation of two phthalonitriles, 4,5-dibutoxyphthalonitrile (**17**) and 4- hexanamidophthalonitrile (**14**) in 3:1 proportion resulted in five phthalocyanines including the desired phthalocyanine **18 (model Pc)** in 8% yield. Deprotection of the amide group was achieved by the hydrolysis of **18** with methanolic potassium hydroxide in THF, which yielded the desired zinc phthalocyanine **19** in 86% yield.

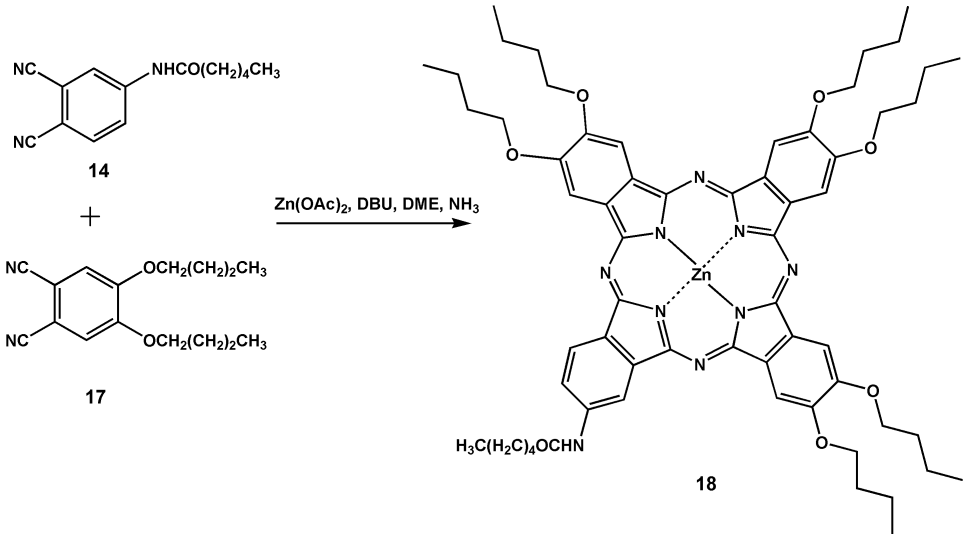

Scheme 7: Synthesis of compound **18.**

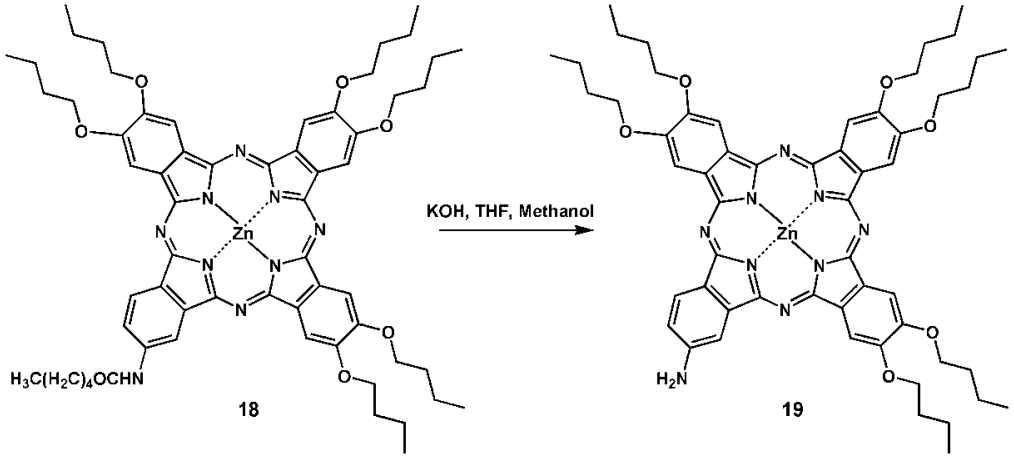

Scheme 8: Synthesis of compound **19.**

D. Synthesis of dyads

In order to prepare the dyads, phthalocyanine **19** was linked with the corresponding carotenoid acids using EDCI as coupling reagent (see Scheme 9). The coupling reaction between phthalocyanine and carotenoic acid was also accomplished via an acid chloride coupling method.[39]

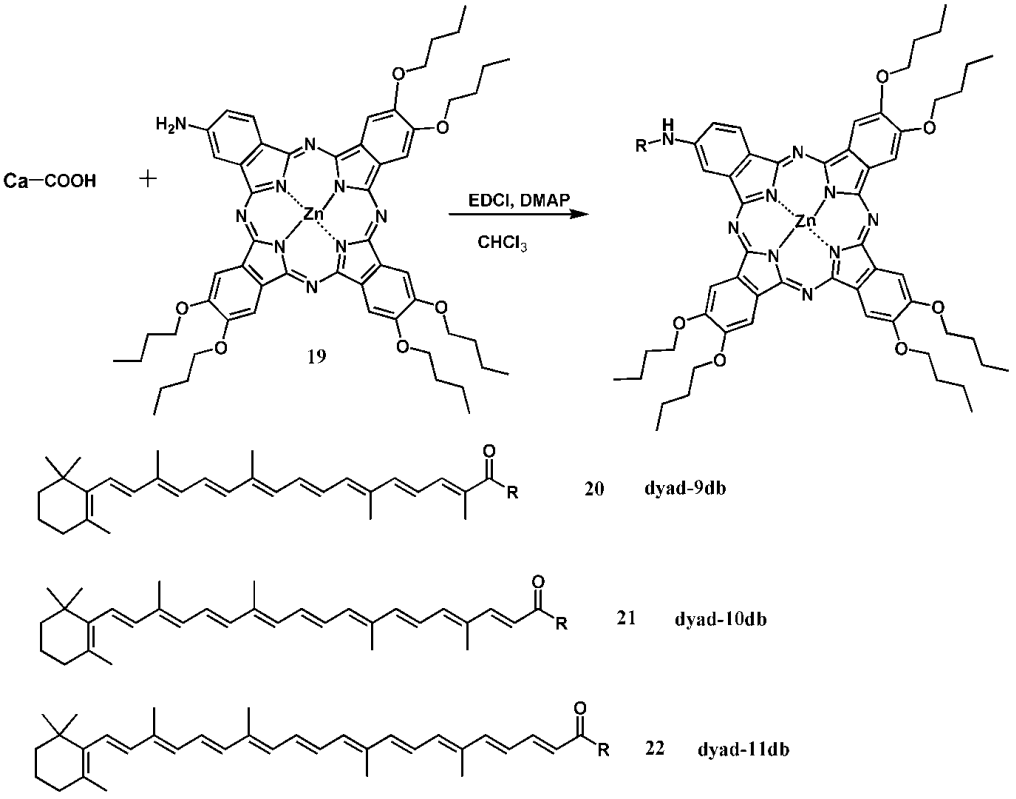

Scheme 9: Synthesis of dyads **20, 21 and 22.**

Spectroscopic studies

Dyads made up of zinc phthalocyanine (Pc) attached covalently to carotenoids with 9-, 10- and 11-double bonds via amide linkages were used as models for artificial light harvesting systems. Zinc phthalocyanine was chosen as a model of chlorophyll because of its spectroscopic similarities. The next step after the preparation of the dyads was to perform spectroscopic studies to explore the photophysics of each dyad. A summary of the photophysical data is presented here but a complete photophysical characterization of these artificial photosynthetic antenna models can be found in recently published work by our group.[34,35,38,39]

A. Steady state absorption and fluorescence spectra

The absorption spectra are linear combinations of the model tetrapyrrole macro cycles and the carotenoids, except for a shift of the Q-band to longer wavelengths, indicative of some electronic interaction between the carotenoids and the phthalocyanine.

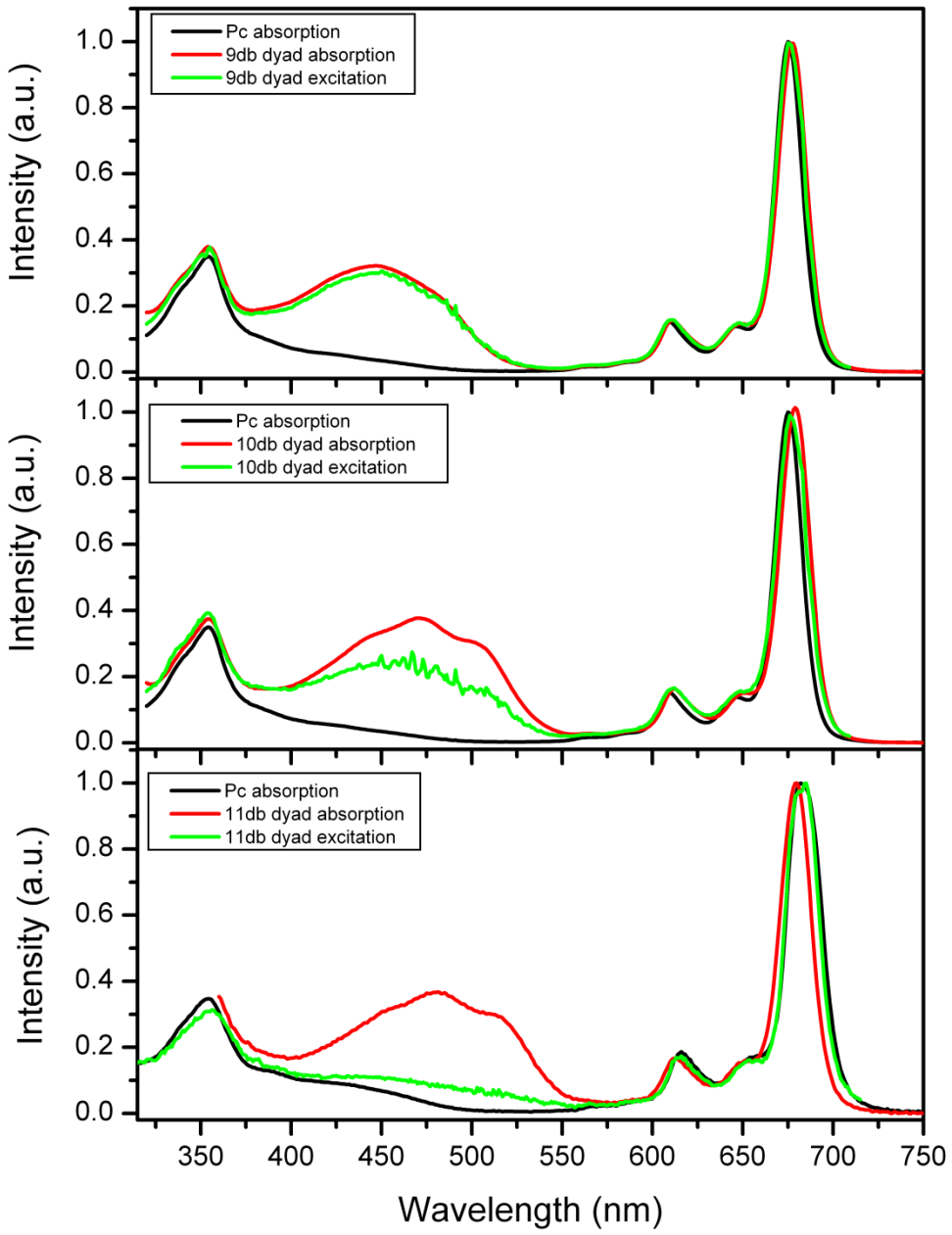

Figure 11: Absorption spectra in THF of 9-, 10- and 11-db dyads (red lines), corrected fluorescence excitation spectra of 9-, 10- and 11-db dyads (green line), and absorption spectrum of model Pc (black line).

From the ratio of the absorption and the corrected fluorescence excitation spectra the yield of energy transfer from the carotenoid to the phthalocyanine was evaluated. The quantum yield of such energy transfer is 100% for the 9-db dyad, 60% for the 10-db dyad and 20% for the 11-db dyad.

The absorption and fluorescence emission spectra of 9-db and 11-db dyads and model Pc excited at the Q_y peak of Pc in THF is shown in Figure 12. The concentrations of all samples were adjusted to give equal absorbance in the region of Pc Q_y peak. The reduction in fluorescence emission in the case of dyad 11-db is an indication that the excited state of the Pc is quenched by some photochemical process(es).

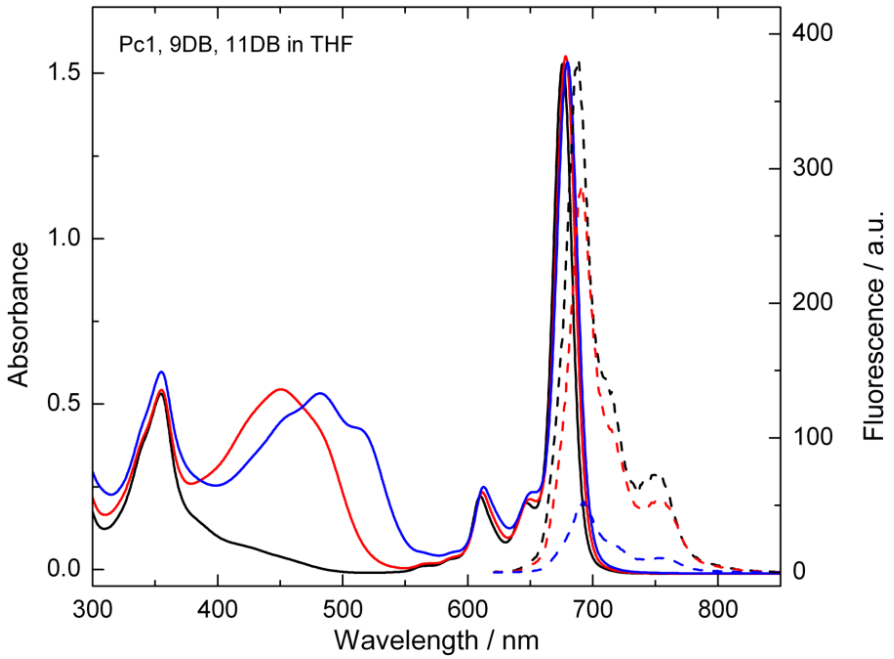

Figure 12: Absorption and fluorescence spectra of the model Pc (black), dyad 9-db (red), dyad 11-db (blue) in THF. Dashed lines show the corresponding fluorescence spectra.

B. Transient absorption spectroscopy (performed by John Kennis et al. at the Vrije Universiteit, Amsterdam)

Details of the energy transfer from the carotenoid to the phthalocyanine were obtained by applying ultrafast time-resolved spectroscopy, with the excitation wavelength tuned to 475 nm to selectively excite the S_2 state of the carotenoid moiety and the laser pulse width set to 100 fs. Dyad 9-db exhibited perfect antenna function through energy transfer from the S_2 state and the optically forbidden S_1 state to phthalocyanine. In dyad 10-db, efficient energy transfer from S_2 was evident, but energy transfer from S_1 was not observed, most likely as a result of unfavorable energetics. In dyad 11-db, energy transfer efficiency from the carotenoid to the phthalocyanine is relatively low. The carotenoid S_1 state does not transfer energy, for similar reasons to that of dyad 10-db and the energy transfer quantum yield from S_2 is only ~24%. These results are in agreement with the steady state measurements (see Figure 11).[38,39]

When the excitation was tuned to 680 nm to selectively excite the Q_y state of Pc, the explanation for the quenching of the fluorescence of Pc by the attached carotenoid, most evident in the case of dyad 11-db (see Figure 12) was investigated. From the transient absorption study, we can conclude that carotenoids with appropriate number of double bonds can efficiently shorten the Pc excited state lifetime and in THF solution an increase in conjugation length from 9-db to 10-db can convert the carotenoid from a nonquencher into a very strong quencher.

Transient absorption spectroscopy was performed on these dyads in solvents of varying polarity. The dyads show stronger quenching in more polar

solvents than THF, such as dimethyl sulfoxide and acetone; in these cases even the 9-db dyad show strong quenching of the fluorescence of Pc. This dependence on solvent polarity can be explained in terms of the existence of an intramolecular charge transfer state (ICT) in the excited state of the carotenoid moiety. The ICT state is believed to arise from the photoexcitation of the extended π-electron system containing a carbonyl group.[39] It was conclusively shown that the quenching in dyad-10 and dyad-11-db in THF and all of the dyads in more polar solvents, proceeds by energy transfer from the Q_y state of Pc to the carotenoid S_1 state. However, the dependence in solvent polarity indicates that the ICT modulates the process as shown in the Figure 13.

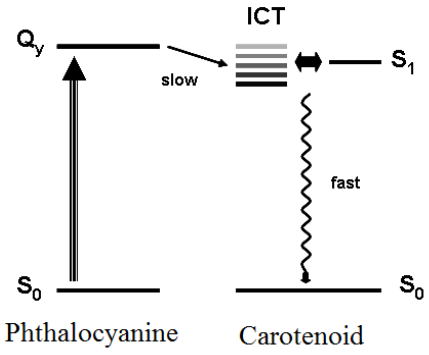

Figure 13: Schematic illustration of the proposed quenching process of the Q_y state of Pc by transferring the energy to the S_1/ICT state.[39]

The Q_y state of Pc transfers energy to the S_1/ICT state. Both states S_1 and ICT could be in equilibrium or are strongly coupled and are better represented by a mixed state.[39] The S_1/ICT state of the carotenoid relaxes quickly to the ground state (S_0) on the time scale of several picoseconds by internal conversion. Energy

transfer from the excited Pc to the S_1/ICT state depends on the polarity of the solvent. As the polarity of the solvent is increased the quenching is increased as the ICT state moves downwards making it more accessible from the Q_y state of Pc.

B. Two-Photon Spectroscopy (performed by Peter Walla et al. at Technische Universität Braunschweig, Braunschweig, and The Max Planck Institute for Biophysical Chemistry, Göttingen, Germany)

Two-photon excitation spectroscopy studies were performed on dyad 9-db, dyad 11-db, and model Pc in THF. The purpose of these experiments was to access directly the S_1 state of the carotenoid, which is forbidden by one-photon excitation. Phthalocyanine fluorescence intensity was measured after two-photon excitation of the S_1 state of carotenoid.

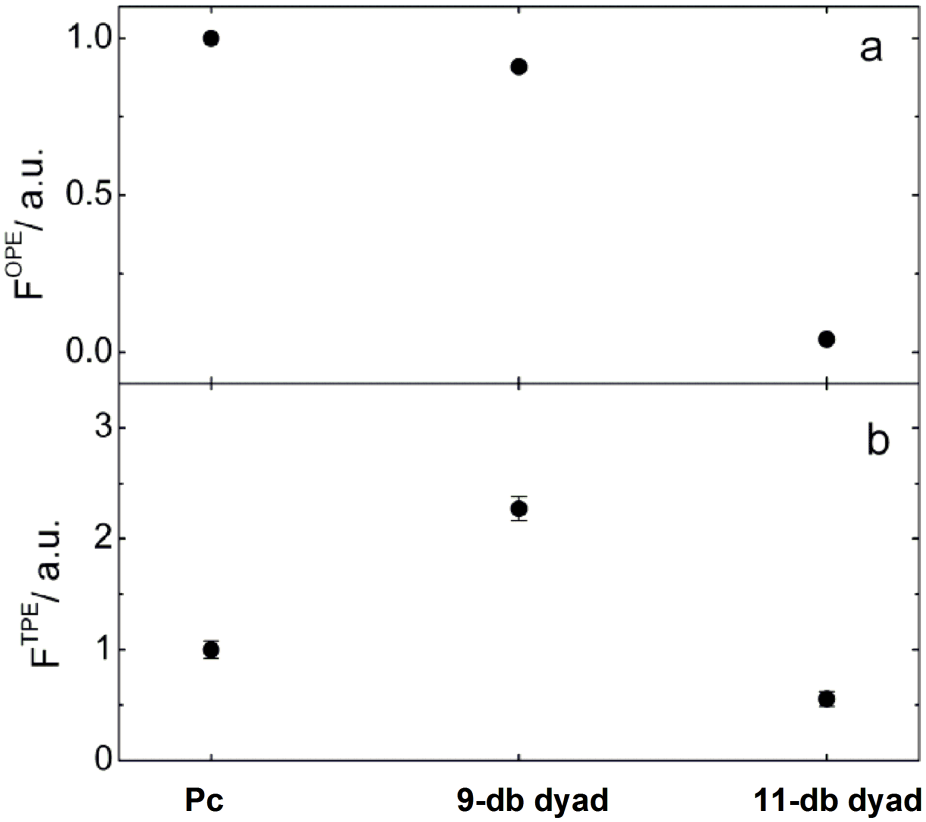

Figure 14: (a) Pc fluorescence after OPE (one-photon excitation) and (b) after TPE (two- photon excitation) of the Pc model compound and amide-linked dyad 9-db and dyad 11-db. These measurements were obtained in THF solutions of samples of identical concentration. The excitation was for the one-photon excitation at 594 nm and for the two-photon excitation at 1188 nm.

Figure 14a shows that the fluorescence quantum yield of the 11-db dyad is more than 17 times smaller than that of the model Pc whereas the 9-db dyad fluorescence yield is about 90% of that of Pc. This is an expected result as these compounds have been shown to demonstrate the molecular gear shift mechanism.[39] In the 9-db dyad the carotenoid acts as an energy donor to Pc, while

the 11-db dyad fluorescence is significantly quenched due to the opposite Pc→Car S_1 energy transfer.

Figure 14b shows the Pc fluorescence intensities observed after the Car S_1 two-photon excitation (Fl^{TPE}). The 9-db dyad shows significantly more fluorescence intensity than both the model Pc and the 11-db dyad. In the 9-db dyad, effective two-photon excitation of Car S_1 with subsequent energy transfer to Pc, Car S_1→Pc, occurs, giving rise to the high values for Fl^{TPE}. In contrast, Fl^{TPE} for the 11-db dyad is much smaller because almost no Car S_1→Pc energy transfer occurs there. Instead, Pc→Car S_1 energy transfer occurs. The two-photon sensitized Pc fluorescence observed with the pure Pc is significantly smaller than the Fl^{TPE} observed with the 9-db dyad, because the excitation Car S_0→Car S_1 is by far more two-photon allowed than a direct two-photon excitation of tetrapyrroles. These results provide clear evidence that the observation of Pc fluorescence sensitized by selective two-photon excitation of Car S_1 sensitively monitors the extent of Car S_1→Pc energy flow and that direct Pc two-photon excitation occurs only to a minor extend.

III Carotenoids lacking terminal carbonyl group covalently attached to a phthalocyanine

Synthesis.

The main objective for the second set of dyads was to link the carotenoid lacking the terminal carbonyl group of different conjugation lengths to a phthalocyanine. The new set of dyads was synthesized via an amine-linkage utilizing the conditions developed by Buchwald-Hartwig.[45] A variety of amination reactions utilizing different palladium catalyst and ligands are reported in the literature. This coupling chemistry is frequently performed by reacting aryl halides with a variety of amino derivatives under relatively milder conditions. The dyads were synthesized by coupling phthalocyanine bearing an aryl iodide with various amino carotenoids using a palladium catalyst and BINAP as a ligand.[45-47]

A. Synthesis of amino carotenoids

An amino group can be attached to a carotenoid by a Wittig type reaction of a carotenoid bearing an aldehyde functional group with 4-(N-acetylamino)benzylphosphoniumbromide followed by base hydrolysis.[35]

The first step was the acetylation of 4-aminobenzylalcohol in presence of acetic anhydride to give 4-acetamidobenzylalcohol.[48] The second step was the bromination of the alcohol with PBr_3 to give N-(4-[bromethyl]phenyl)acetamide in 86% yield. This compound reacted with triphenyphosphine in toluene to give the Wittig salt in 89% yield.

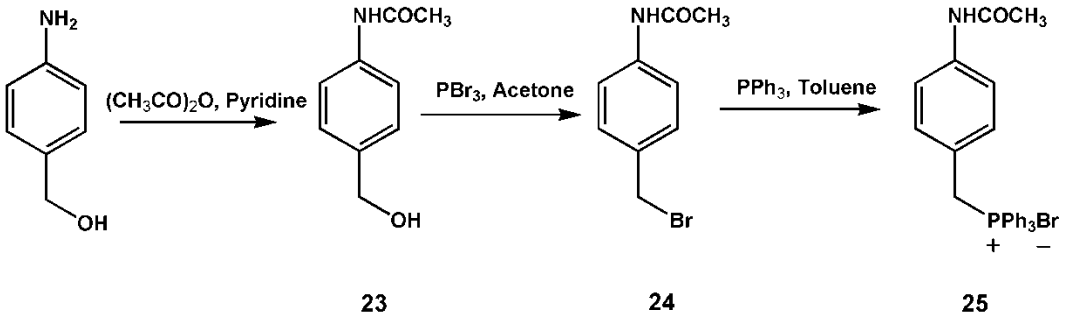

Scheme 10: Synthesis of compound **25**

The Wittig salt was then reacted with the required carotenal in presence of sodium methoxide to give the carotenoid with an amide group. Deprotection to the amino carotenoid, under basic conditions occurred over 24 hours.[49]

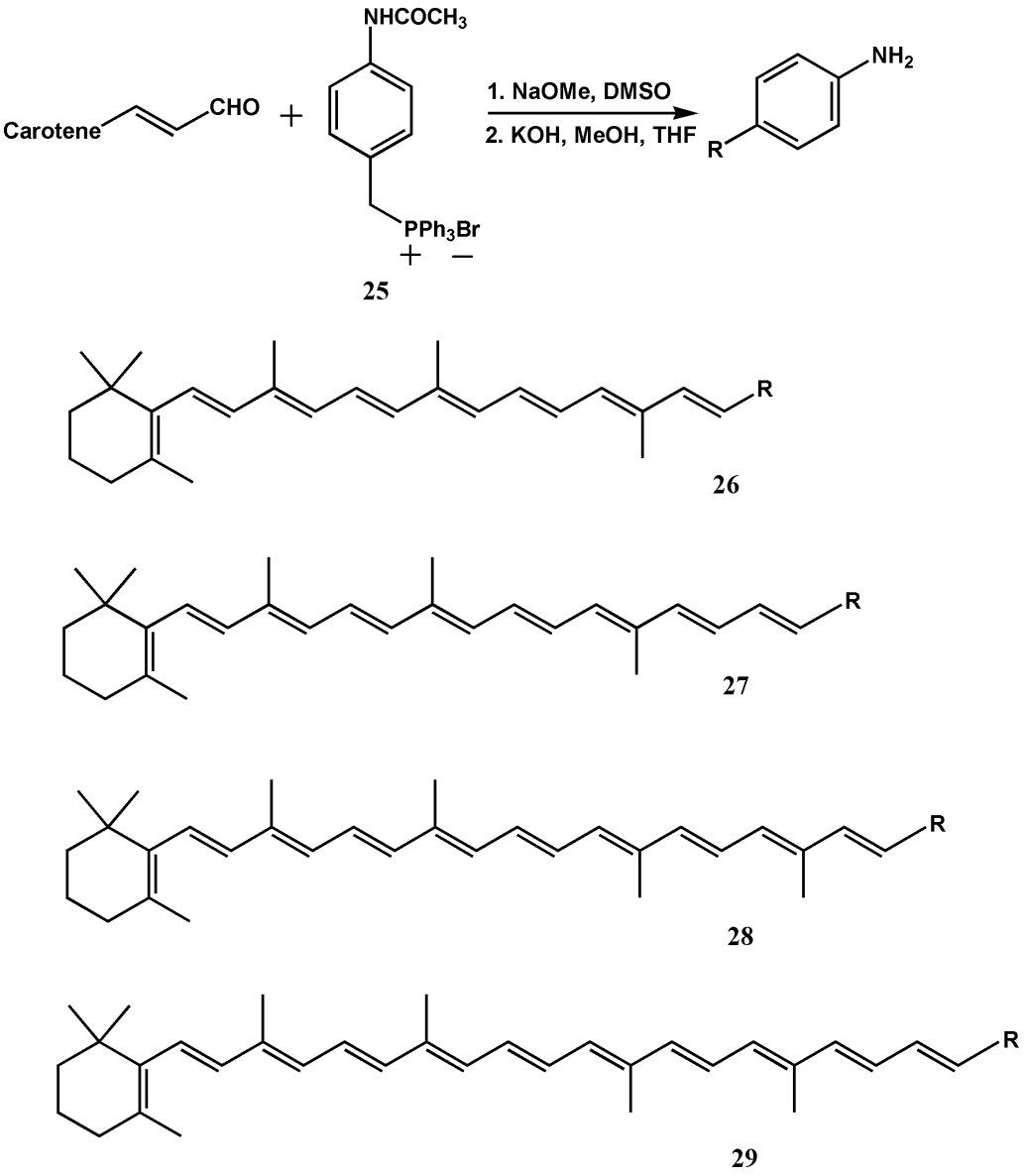

Scheme 11: Synthesis of compounds **26, 27, 28** and **29.**

B. Synthesis of phthalocyanine

Mixed condensation of 4-iodophthalonitrile (1 equiv) and 4-(*tert*-butyl)phthalonitile (3 equiv) in presence of zinc chloride and N,N-dimethylaminoethanol (DMAE) afforded tri-*tert*-butyliodophthalocyanine **30** in 15% yield after isolation from the statistical mixture of phthalocyanines by column chromatography on silica gel.[50]

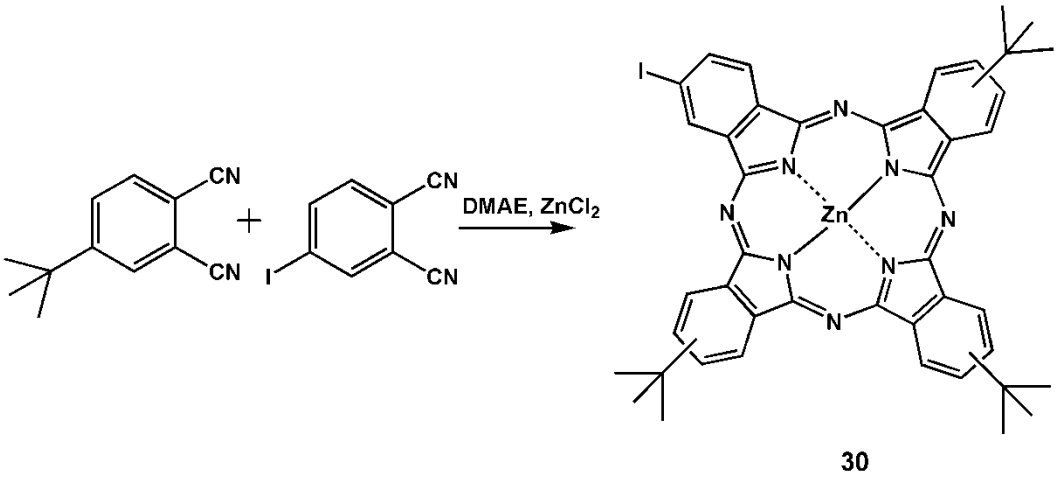

30

Scheme 12: Synthesis of compound **30.**

C. Synthesis of the amine-linked dyads

Mild one pot amination reaction of the phthalocyanine bearing an aryl iodide was performed with various aminocarotenoids under conditions developed by Buchwald and coworkers.[45] The coupling was carried out in presence of tris(dibenzylideneacetone)dipalladium, sodium *tert*-butoxide and BINAP in toluene under argon atmosphere.

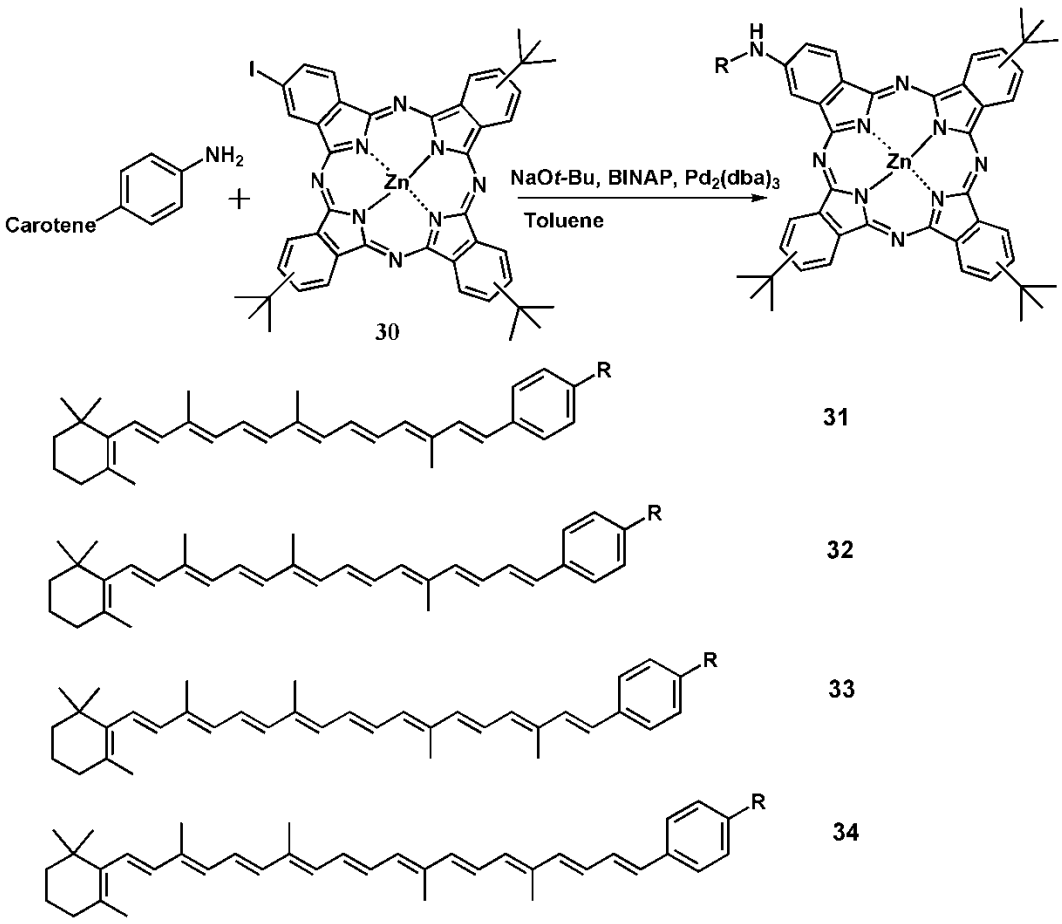

Scheme 13: Synthesis of compounds **31, 32, 33 and 34** (**amine-dyad-8db**, **amine-dyad-9db**, **amine-dyad-10** and **amine-dyad-11-db**).

D. Synthesis model compounds

In addition to the dyads, model compounds were necessary to completely analyze the spectroscopic data collected from the dyads. Along with the dyads model Pc and model carotenoids were also synthesized via the amination reaction.

Synthesis of model phthalocyanine

Model Pc was synthesized by using the same methodology as described for the dyads; 4-amino-1-methylbenzene was used to couple with the phthalocyanine **30**.

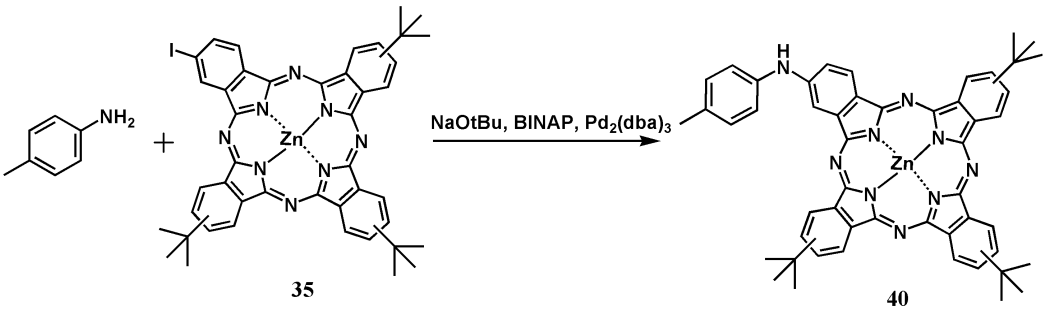

35 40

Scheme 14: Synthesis of compound **44** (model-Pc).

Synthesis of model carotenoids

The amination reaction using aminocarotenoid and 4-iodotoluene was performed, but the reaction did not go to completion and the product could not be separated from the starting aminocarotenoids, so the functional groups were switched by making the iodocarotenoid and treating it with 4-amino-1-methylbenzene. Unreacted iodocarotenoids could be easily separated from the product due to their non-polar nature. Reacting 4-iodobenzylbromide with triphenyphosphine in toluene for 24 hours gave the required Wittig salt **35** in 82% yield.

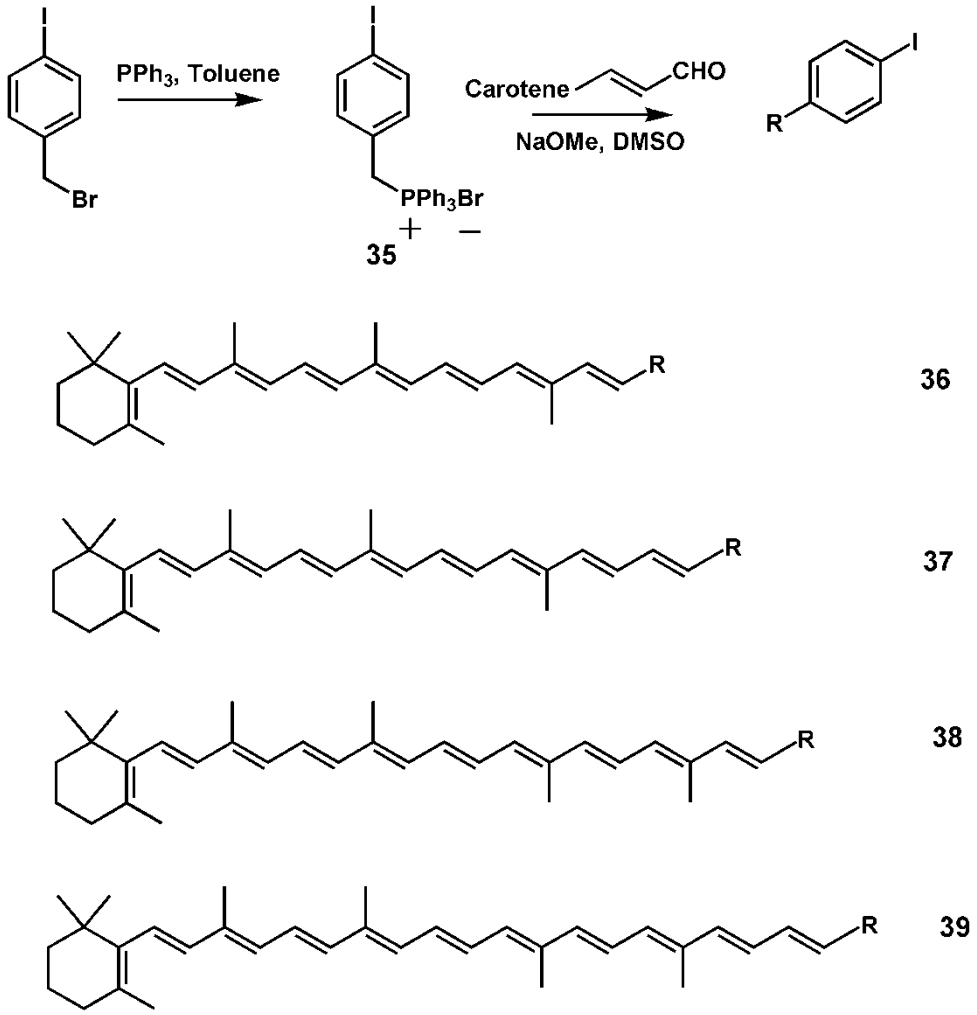

Scheme 15: Synthesis of compounds **36, 37, 38** and **39** (iodocarotenoids with 8-, 9-, 10-, and 11-double bond)

The carotenoids with the iodo group were then coupled to 4-amino-1-methylbenzene using the same methodology as described for the dyads.

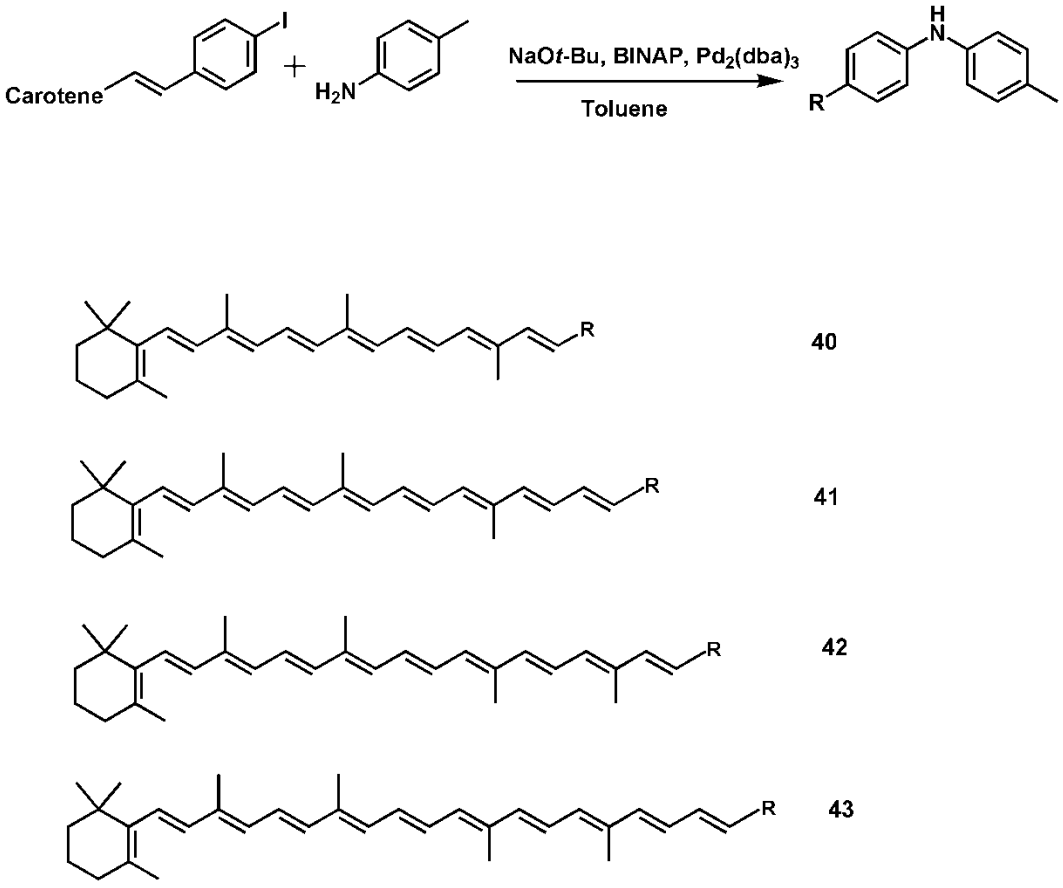

Scheme 16: Synthesis of compounds **40, 41, 42** and **43** (model carotenoid with 8, 9, 10, and 11-double bond).

Spectroscopic studies

The carotenoids involved in NPQ of higher plants do not contain carbonyl groups. Thus, to understand the role of these carotenoids and to compare them with carotenoids containing carbonyl groups a new series of dyads was synthesized. These dyads contain a secondary amine group as a linker between the carotenoid and the Pc. The dyads contain carotenoid moieties of 8-, 9-, 10-, and 11-double bond in addition to a phenyl group. Spectroscopic studies were performed on the dyads in two different solvents with varying polarities: toluene, a less polar solvent, and THF being a more polar solvent.

A. Absorption and fluorescence of dyads in toluene

Absorption spectra of the dyads and model Pc measured in toluene are shown in Figure 15. The absorption spectra show the expected red shift of the carotenoid band as a function of the number of conjugated double bonds. The fluorescence excitation spectra clearly indicate that efficiency of energy transfer from the carotenoid to Pc (antenna function) is a function of the number of conjugated double bonds (see Figure 16).

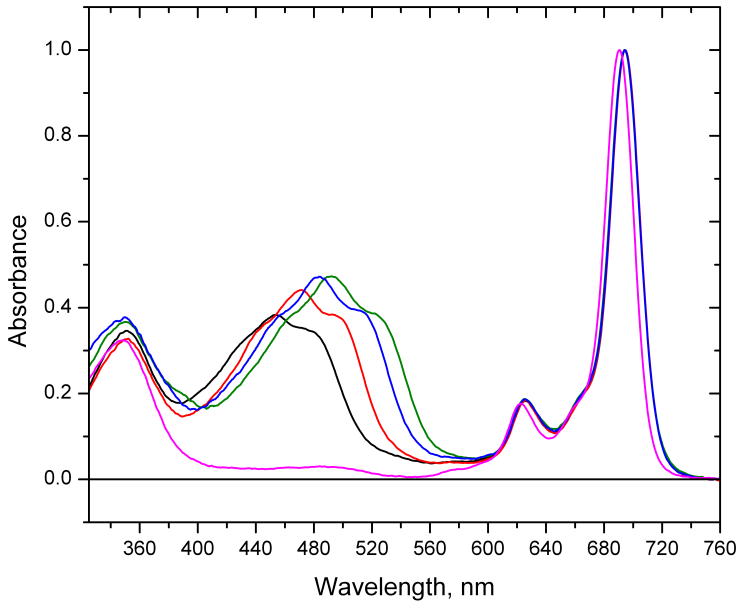

Figure 15: Absorption spectra of **amine-dyad-8-db** (black), **amine-dyad-9-db** (red), **amine-dyad-10-db** (blue), **amine-dyad-11-db** (green) and **Pc** model (magenta) in toluene.

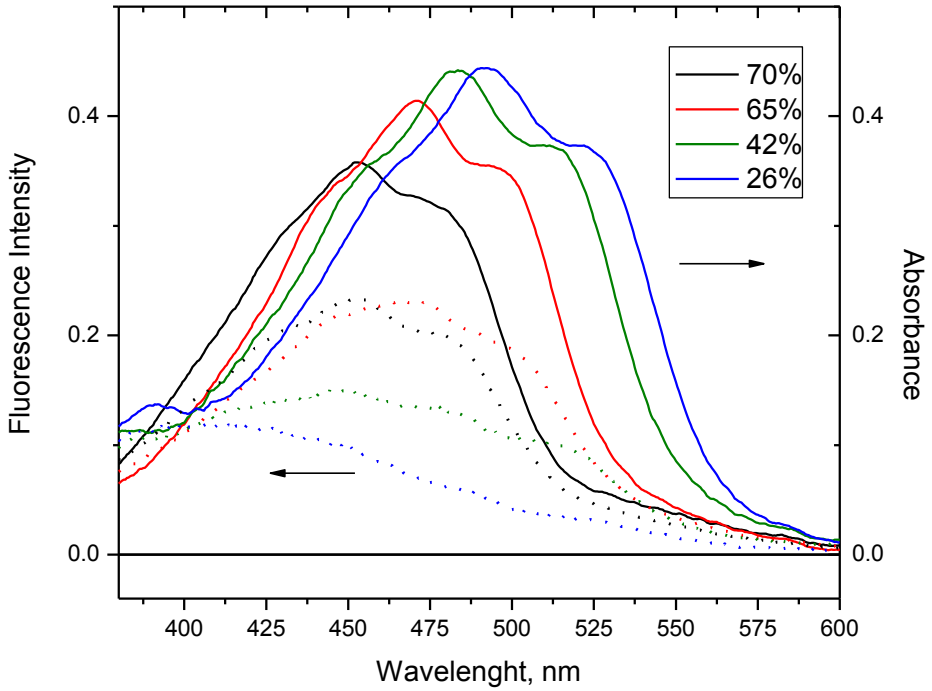

Figure 16: Absorption (solid line) and corrected fluorescence excitation (dotted-line) spectra of **amine-dyad-8-db** (black), **amine-dyad-9-db** (red), **amine-dyad-10-db** (green), **amine-dyad-11-db** (blue) in toluene.

Transient absorption spectroscopy (performed by John Kennis et al. at the Vrije Universiteit, Amsterdam)

The evolution associated decay spectra (EADS) of amine-dyads with 8-, 9-, 10- and 11-double bond dissolved in toluene with excitation at 670 nm is discussed below. The time-resolved spectroscopic study of Pc model compounds showed no significant impact of the solvent polarity on the singlet excited state lifetimes, which in both cases were around 2.7 ns. This number represents the

decay of Pc by internal conversion, fluorescence, and intersystem crossing. The dashed black line in the EADS spectra (Figure 17) represents the relaxed excited state of Pc model. In the dyads, quenching of the Pc excited states was found to depend upon the number of conjugated double bonds present on the carotenoid. The transient spectra data required three time constants and a nondecaying component to obtain a satisfactory fit of the data to a sequential kinetic model (EADS).

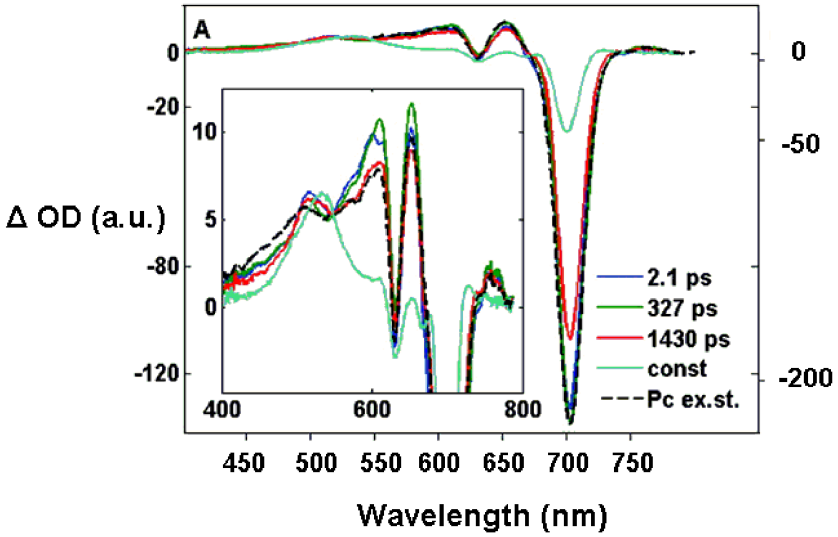

Figure 17: Evolution associated decay spectra (EADS) extracted from time-resolved spectra recorded for toluene solutions of **amine-dyad-8-db** after 670 nm excitation. The black dashed lines denote the EADS of the Pc model compound, shifted by 5 nm so as to overlap with the signal of the dyad-bound Pc moieties.

In **amine-dyad 8-db**, lifetimes of 2.1, 327, and 1430 ps were obtained; the first EDAS (blue line) shows a negative band near 700 nm, which results from Pc ground state bleach and stimulated emission. Broad positive signal of excited state

absorption at wavelengths shorter than 670 nm was observed. The first EADS evolves in 2.1 ps to the second EADS, which has a lifetime of 327 ps (green line). A small increase in Pc ground state bleaching at 700 nm and small rise in excited state absorption between 550 and 650 nm was observed. The first and the second EADS resemble the excited state of Pc. The second EADS evolves with a lifetime of 327 ps into third EADS, which has a lifetime of 1430 ps. The third EADS shows an 80% drop in Pc excited state transient absorption signatures. The nondecaying EADS is identified as a mixture of Pc and carotenoid triplet states as it shows a characteristic broad peak at 520 nm and a small amount of Pc ground state bleach. In this dyad the excited state of Pc decays with a minor decay component of 327 ps and a major component of 1430 ps. These experiments show that Pc excited state is weakly to moderately quenched (1.4 ns) by the carotenoid.

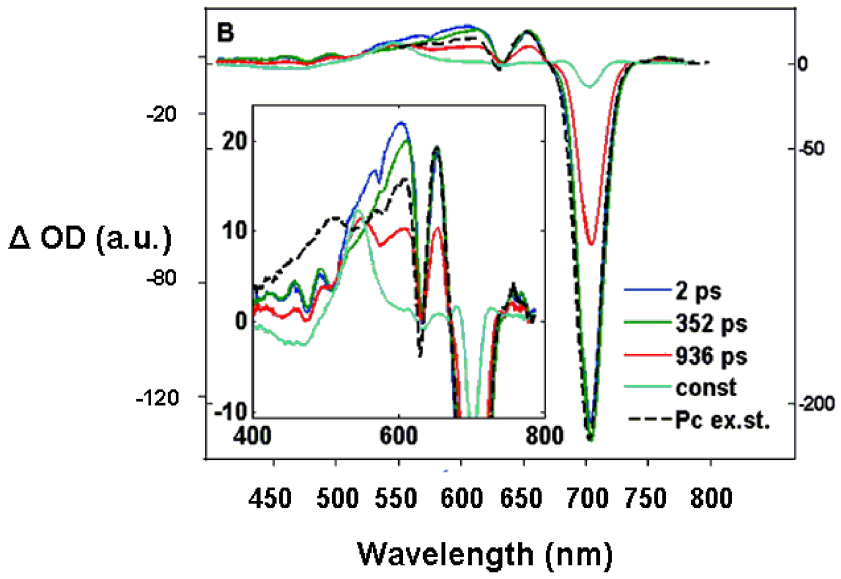

Figure 18: Evolution associated decay spectra (EADS) extracted from time-resolved spectra recorded for toluene solutions of **amine-dyad-9-db** after 670 nm excitation. The black dashed lines denote the EADS of the Pc model compound, shifted by 5 nm so as to overlap with the signal of the dyad-bound Pc moieties.

Amine-dyad-9-db shows similar evolution to that of the above example with lifetimes of 2, 352, 936 ps and a nondecaying component. The 352 ps component has larger amplitude as compared to the corresponding 327 ps component in the previous example. In general these results show that ^{1}Pc in this dyad is somehow more quenched than that of the **amine-dyad-8-db**.

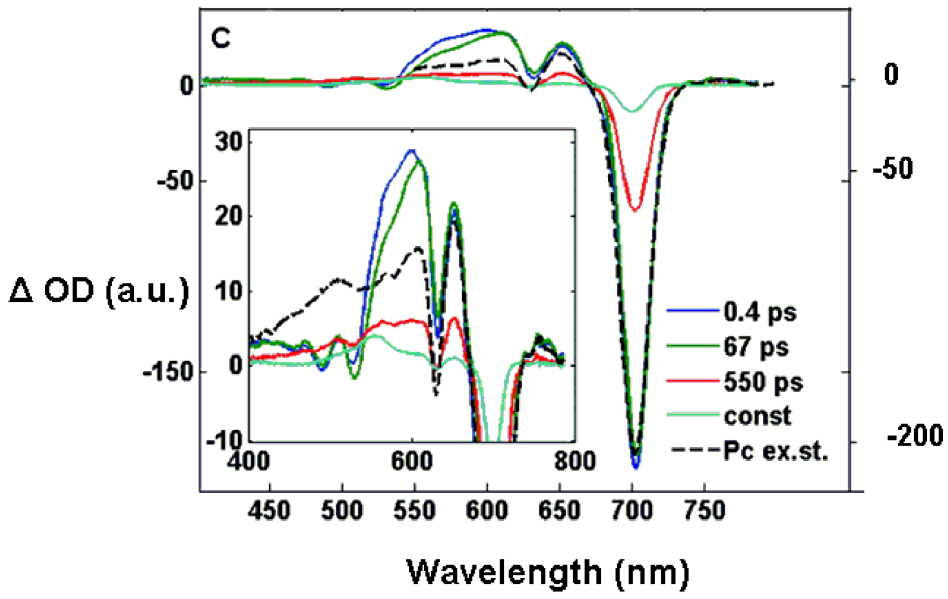

Figure 19: Evolution associated decay spectra (EADS) extracted from time-resolved spectra recorded for toluene solutions of **amine-dyad-10-db** after 670 nm excitation. The black dashed lines denote the EADS of the Pc model compound, shifted by 5 nm so as to overlap with the signal of the dyad-bound Pc moieties.

In **amine-dyad-10-db** there is an appearance of a distinct carotenoid bleaching between 400 and 500 nm and small additional excited state absorption between 500 and 610 nm in the 400 fs and 67 ps EADS. The spectral region for Pc model compound is flat and featureless in this spectral region. This observation suggested that a carotenoid excited state is populated along with ^{1}Pc. The spectral feature and induced absorption of the 67 ps component is consistent with the presence of carotenoid S_1 state. There is no transient carotenoid cation

band in the near-IR region, which excludes the possibility of the $Car^{\bullet+}$-$Pc^{\bullet-}$ radical pair.

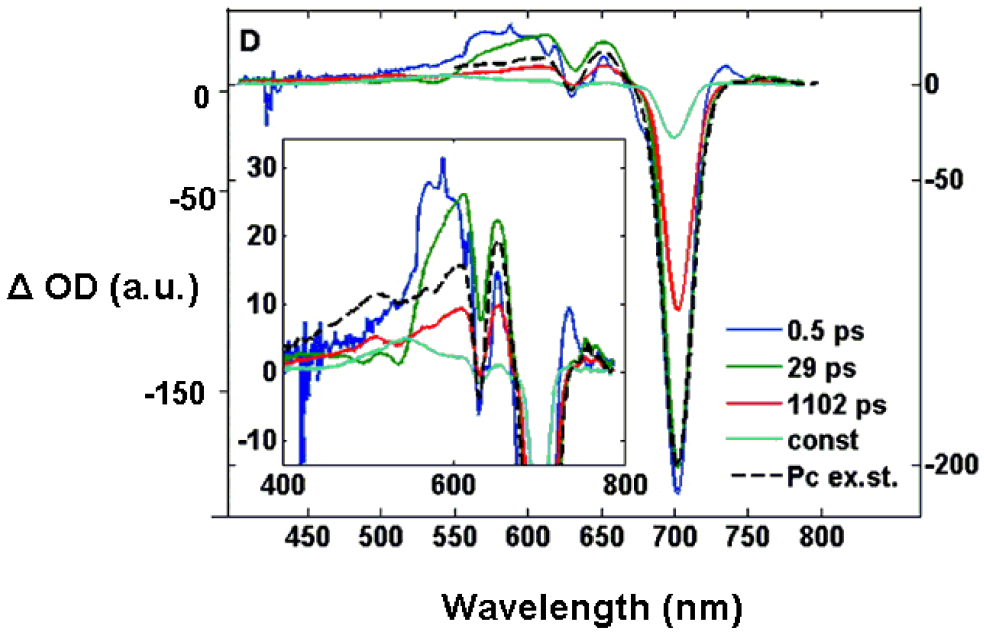

Figure 20: Evolution associated decay spectra (EADS) extracted from time-resolved spectra recorded for toluene solutions of **amine-dyad 11-db** after 670 nm excitation. The black dashed lines denote the EADS of the Pc model compound, shifted by 5 nm so as to overlap with the signal of the dyad-bound Pc moieties.

Amine-dyad-11-db shows similarities to that of **amine-dyad-10-db**. The EADS data reveal that a larger fraction of dyad 11-double bond is only weekly to moderately quenched. Excitation of Pc resulted in Car S_1 signature immediately within the time resolution of 100 fs. Remarkably, the third EADS (1102 ps) does not follow the trend, it is longer than in the examples.

The difference between the amide-linked dyads and the amine-linked dyads is that in amine-linked dyads there is no rise component of the carotenoid S_1 state; this is more clearly seen in the **amine-dyad-10-db and 11-db**. Instead the carotenoid S_1 was observed in the transient spectra immediately after Pc excitation. These observations imply that the quenching mechanism in the amine-linked dyads could not be simply assigned to a sequential $^1Pc \rightarrow$ carotenoid S_1 energy transfer. These results suggest that the quenching might be mediated through excitonic coupling between the ^1Pc and the optically forbidden carotenoid S_1 state. Upon excitation, the excited states are instantaneously shared between the Pc and the carotenoid moieties in the case of an excitonic state.[35]

Two-photon spectroscopy (performed by Peter Walla et al. at Technische Universität Braunschweig, Braunschweig, and The Max Planck Institute for Biophysical Chemistry, Göttingen, Germany)

To further exploring the mechanism for the quenching of the excited state of Pc in amine-linked dyads, two-photon excitation spectroscopy studies were performed on **amine-dyad-8-db** and **amine-dyad-10-db** in toluene and the results compared to Chl *a* in acetone and LHC II in water.[34]

All samples had the same concentration, essentially equal absorbance in the Q_y peak region, allowing a direct comparison of their relative fluorescence intensities. The fluorescence intensity of Pc-model is similar to that of Chl *a* in acetone at the same absorbance. The Chl fluorescence intensity of unquenched LHC II is smaller than that of pure Chl *a*. It has been previously reported in the

literature that there is aggregation-induced quenching which leads to reduction in the fluorescence in these systems.[34]

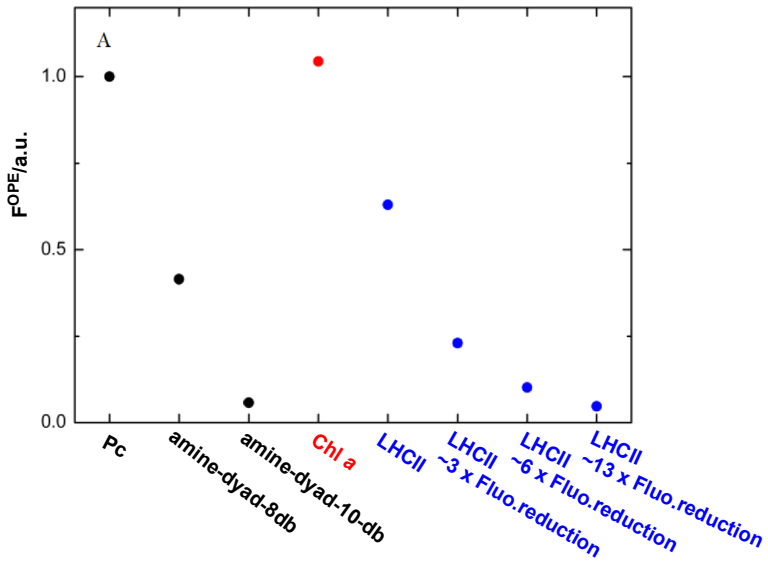

Figure 21: **Pc/chlorophyll** fluorescence intensity observed after one photon excitation (Fl^{OPE}): **Pc** (black), **amine-dyad-8-db** (black), **amine-dyad-10-db** (black), **Chl *a*** (red), and **LHC II** (blue) in various quenched states. The three right-most LHC II samples have been treated by aggregation quenching so that their fluorescence was 3, 6 and 13 times reduced in comparison to un-aggregated LHC II, respectively. The excitation was at 594 nm.[34]

Figure 21 shows that in **amine-dyad-8-db,** the carotenoid has much more quenching effect on the Pc fluorescence than in the **amide-linked-9-db** dyad described earlier and that the 10-double bond carotenoid has an extremely high quenching effect on Pc fluorescence.

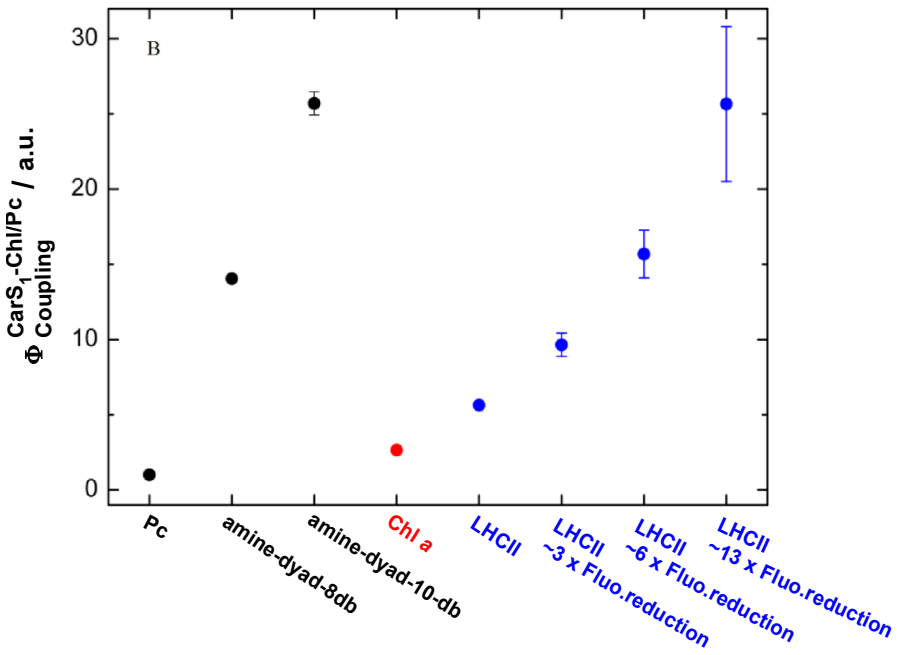

Figure 22: $\phi_{Coupling}^{CarS_1-Chl\,/\,Pc}$ of **Pc** (model), **amine-dyad-8-db**, **amine-dyad-10-db**, Chl *a* (red) and LHC II in various quenched states (blue). The three right-most LHC II samples have been treated by aggregation quenching so that their fluorescence was 3, 6 and 13 times reduced in comparison to un-aggregated LHC II, respectively.[34]

Figure 22 shows calculated using equation (1) which was obtained from the fluorescence intensities of Chl/Pc after one-photon excitation (Fl^{OPE}), and after selective carotene two-photon excitation (Fl^{TPE}). It is related to carotenoid S_1-Pc Q_y electronic interactions.[34] **Amine-dyad-10-db** showed a very large $\phi_{Coupling}^{CarS_1-Chl\,/\,Pc}$, the largest ever observed.

$$\phi_{Coupling}^{CarS_1-Chl\,/\,Pc} \propto \frac{Fl^{TPE}}{Fl^{OPE}} \qquad (1)$$

From the transient absorption measurements discussed above it was shown that there is energy flow in the direction Pc→ S_1 and, from the two-photon excitation spectroscopy measurements it was shown that energy transfer in the opposite direction, carotenoid S_1→ Pc, also takes place. If the energy transfer process was unidirectional between the two pigments, this would correspond to a simple energy transfer process from one pigment to another and would be similar to that observed with the amide-linked Pc-carotenoid dyads (they show the molecular gearshift mechanism). In the case of the amine-liked dyads, it is observed that there is energy transfer in both directions simultaneously. An explanation for such behavior would be the existence of an excitonic state where both moieties, carotenoid and Pc, share the excitation energy.

B. Amine-dyads in THF

An alternative mechanism that has been reported to play a role in the regulation of light harvesting in photosynthesis involves electron transfer from carotenoids to chlorophyll molecules.[51-53]

Transient absorption spectroscopy

In contrast to the case of toluene, in a more polar solvent such as THF, all amine-dyads behave similarly; excitation of Pc shows an immediate carotenoid S_1 population, suggesting excitonic interactions between carotenoid S_1 – Pc Q_y and considerable quenching of the excited state of ^{1}Pc. The EADS for **amine-dyad-10-db** is shown in Figure 23. After excitation, a charge separation takes place in ~1 ps as evidenced by the rise of both a carotenoid radical cation and $Pc^{\bullet-}$ band in

the near IR region (980 nm, a small signal is possibly indicative of inverted kinetics).

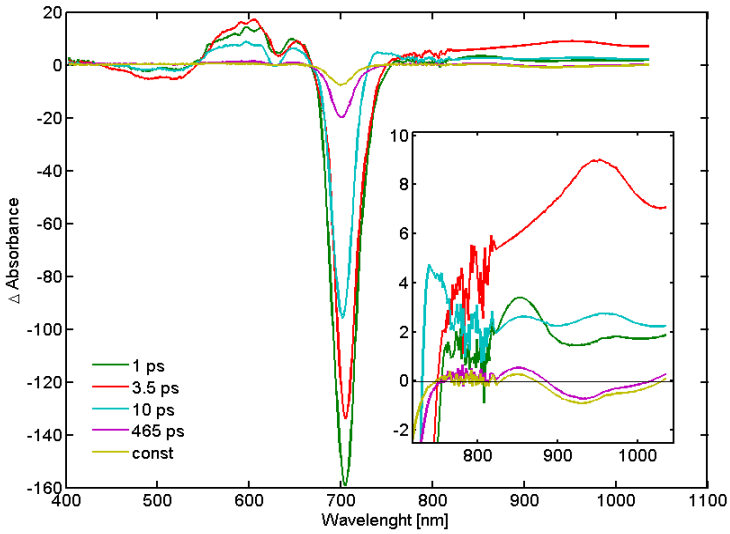

Figure 23: Evolution-associated decay spectra of **amine-dyad-10-db** in the visible and near-IR regions. The excitation wavelength was 680 nm.

IV. Conclusion

The two carotene-phthalocyanine sets of dyads presented here serve as good models for studying the regulation mechanisms for light harvesting in photosynthetic organisms. Factors that determine the quenching of the excited state of the Pc model of the chlorophyll were the conjugation length of the carotenoid moiety, the solvent polarity, and the linker between the phthalocyanine and the carotene.

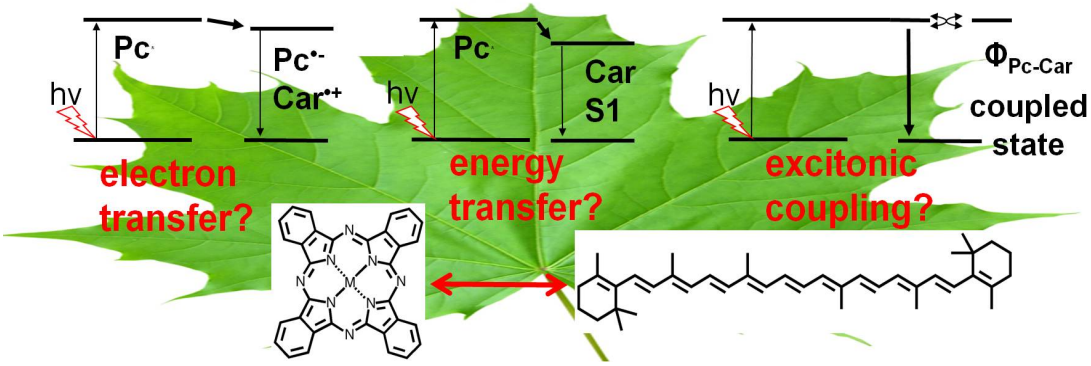

Figure 24: Mechanisms for the quenching of the excited state of tetrapyrroles described in this chapter: (1) quenching via formation of a short-lived charge separated state; (2) quenching via energy transfer to the carotenoid dark S_1 state; (3) quenching via the population of a Pc-carotenoid excitonic state.

In summary, in dyads with the amide linkage a change in the conjugation length from 9-double bonds to 10-double bonds changes the properties of the carotenoid from a nonquencher to a very strong quencher of Pc excited state lifetime. When solvent polarity is increased, even the dyad with 9-double bond shows some degree of quenching. Dependence on solvent polarity and the results obtained from transient spectroscopy reveal that the quenching proceeds through

energy transfer from the excited state of Pc to the optically forbidden S_1 state of the carotenoid coupled to an ICT state. These dyads displayed an excellent example of molecular gear shift mechanism where an addition of one double bond can activate the quenching.[39] This mechanism has been suggested to operate in the xanthophyll cycle: the 9-double bond carotenoid, violaxanthin, transfers its excitation energy to the chlorophyll, while in the 11-double bond carotenoid, zeaxanthin, the excess excitation energy gathered by the chlorophyll is effectively transferred to the carotenoids. Carotenoids then dissipate this excess energy as heat by internal conversion from S_1 to the S_0 state.

In the second set of dyads, where the amide linkage is replaced with a phenyamino group (lacking carbonyl group), there is a large electronic interaction between the carotenoid S_1-Pc Q_y. There is an instantaneous population of carotenoid S_1 (faster than 100 fs) when Pc is excited. This instantaneous population of carotenoid S_1 is highest in the dyads with 10- and 11-double bond carotenoids. Dyads with 8-double bond and 10-double bond carotenoids were further studied by two-photon excitation spectroscopy, where Pc fluorescence was observed after two-photon excitation of the optically forbidden carotenoid S_1 state. It was observed that the coupling value, $\phi_{Coupling}^{CarS_1-Chl/Pc}$, which is an indication of the level of electronic interaction between the carotenoid and the Pc system, is higher for the dyad with 10-double bonds compared to the dyad with 8-double bond carotenoids. The combined results obtained led to the conclusion that the quenching proceeds through excitonic coupling between the Pc singlet excited state, Q_y, and the carotenoid excited state, S_1. A dyad with 10-double bonds acts

as a good model to understand the situation of the light adapted plants where the excess energy is successfully trapped by the lower carotenoid S_1–Chl Q_y excitonic state, and is then dissipated in a short period of time. Even in a polar solvent like THF, the phenlyamino dyads show excitonic interactions and some part of the quenching was mediated through charge separation and recombination.

Thus, from the extensive spectroscopic study on these model dyads containing the tetrapyrroles and carotenoids, it is evident that the carotenoid can quench effectively the tetrapyrrole-excited states in at least three different ways: energy transfer, electron transfer and excitonic coupling.[7,52,54,55]

V. Experimental

General Methods

The NMR spectra were recorded on Varian spectrometers at 300, 400 or 500 MHz. Most of the samples were dissolved in deuteriochloroform with tetramethysilane as an internal reference unless specified otherwise. Mass spectra were obtained with matrix-assisted laser desorption/ionization time-of-flight spectrometer (MALDI-TOF) in positive mode using terthiophene matrix. Steady-state ultraviolet-visible absorption spectra were measured on a Shimadzu UV-2100U UV-vis spectrometer. Steady-state fluorescence spectra were measured using a Photon Technology International MP-1 spectrometer and corrected for detection response.

Solvents and reagents

Chemicals used were purchased from Aldrich, Acros or Alfa Aesar. Solvents were bought from EM Science. The reagent 8'-apo-β-carotene-8'-al (Hoffmann-La Roche) was purified by flash column chromatography, 100% dichloromethane, before use. Tetrahyrdofuran was distilled from sodium metal and benzophenone in an argon atmosphere immediately prior to use. Toluene was distilled from CaH_2, and dichloromethane was distilled from potassium carbonate. All solvents were stored over the appropriate molecular sieves prior to use. Thin layer chromatography was done using silica coated glass plates from Analtech. Column chromatography was carried out using Silicycle silica gel 60 with 230-400 mesh. Unless otherwise specified all reactions were carried out under a

nitrogen atmosphere except for Pd-catalyzed reactions that were carried out under an argon atmosphere.

Synthesis

Carotenoids containing terminal carbonyl group covalently attached to tetrapyrrole system

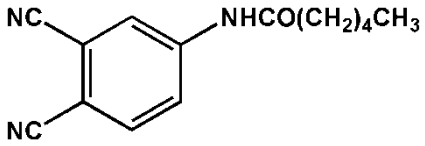

14

4-Hexanamidophthalonitrile[39]

A solution of 4-nitrophthalonitrile (4 g, 23 mmol) in methanol (97 mL) was flushed with N_2, and a portion of 10% Pd/C (0.4 g) was added. This mixture was then stirred under H_2 (50 psi) for 1 h. The reaction mixture was then passed through celite to remove the catalyst, and the solvent was distilled under vacuum to obtain the desired amine (3.16 g, 95% yield). A portion of the amine obtained (2.5 g, 17.7 mmol) was dissolved in pyridine (62.5 mL), and then hexanoyl chloride (6 ml, 43 mmol) was added. The mixture was stirred under N_2 for 2 h. The solvent was distilled under vacuum, and the mixture was redissolved in dichloromethane, washed with 0.1 M HCl several times, and then with 5% $NaHCO_3$ to neutral pH. The solution was dried over Na_2SO_4 and filtered and the solvent distilled under vacuum. The crude product was chromatographed on silica gel 5% methanol in dichloromethane and 1.41 g (33% yield) of the desired nitrile was obtained. ^{1}H-NMR (300 MHz, $CDCl_3$): δ 0.92 (3H, t), 1.36 (4H, m), 1.72

(2H, q), 2.43 (2H, t), 7.63 (1H, bs), 7.73 (1H, d, J = 9 Hz, Ar-H), 7.87 (1H, dd, J = 9 Hz, J = 2 Hz, Ar-H), 8.18 (1H, d, J = 2 Hz, Ar-H).

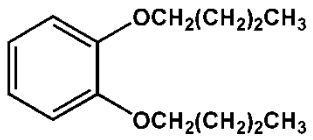

15

1,2-Dibutoxybenzene[39]

1,2-Dihyroxybenzene (1.7 g, 15.5 mmol) was dissolved in 15.5 mL of dimethylformamide. Potassium carbonate (5.35 g, 39 mmol) and 1-bromobutane (6.38 g, 46.56 mmol) were added, and the reaction mixture was stirred at 95°C under N_2 for 24 h. Additional portions of potassium carbonate (3.87 g, 28 mmol) and 1-bromobutane (3.82 g, 27.87 mmol) were added and the stirring continued for 3 h. Again, potassium carbonate (3.87 g, 28 mmol) was added and the reaction was continued overnight. The mixture was allowed to cool down to room temperature and ether (1 liter) was added. The organic layer was washed with water several times. The organic layer was dried over Na_2SO_4, the solvent was distilled under vacuum, and the liquid obtained was purified by column chromatography with 20% dichloromethane in hexanes. (2.646 g, 77.2% yield). ^{1}H-NMR (300 MHz, $CDCl_3$): δ 0.9 (6H, t), 1.38-1.45 (4H, m), 1.65-1.8 (4H, m), 3.93 (4H, t), 6.81(4H, s, Ar-H).

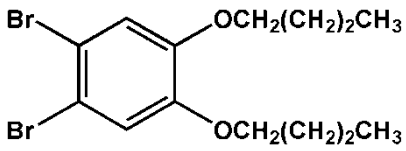

16

1,2-Dibromo-4,5-dibutoxybenzene[39]

A portion of 1, 2-dibutoxybenzene (1.8 g, 8.2 mmol) was dissolved in dichloromethane (20 ml) and cooled to 0°C under N_2. Bromine (0.836 mL, 16.3 mmol) was added slowly, half at 0°C and the other half at room temperature in the course of 40 min. The reaction mixture was monitored by thin layer chromatography. The solution was washed with a 10% $NaHSO_3$ solution and then with 10% $NaHCO_3$ solution. The organic layer was dried over Na_2SO_4, and the solvent was distilled under vacuum to yield 2.52 g (81.8%) of the desired compound. ^{1}H-NMR (300 MHz, $CDCl_3$): δ 0.98 (6H, t), 1.4-1.6 (4H, m), 1.85-1.95 (4H, m), 3.95 (4H, t), 7.08 (2H, s, Ar-H).

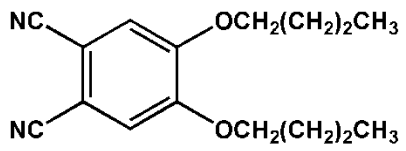

17

4,5-Dibutoxyphthalonitrile[39]

A portion of 1,2-dibromo-4,5-dibutoxybenzene (1.5 g, 3.95 mmol) was dissolved in dichloromethane (18 mL), CuCN (1.06 g, 11.84 mmol) was added and the reaction mixture was heated to reflux under N_2 for 8 h. The mixture was cooled to

room temperature and the solvent was evaporated under vacuum. To the residue dichloromethane (18 mL) and 30% aqueous ammonia were added and the reaction mixture was stirred for 24 h. The organic extracts were combined and dried over Na_2SO_4 and evaporated under vacuum. The compound was recrystallized from ethanol. The desired compound was obtained, 0.46 g (43.4%). ^{1}HNMR (300 MHz, $CDCl_3$): δ 0.99 (6H, t), 1.48-1.53 (4H, m), 1.81-1.87 (4H, m), 4.06 (4H, t), 7.11(2H, s, Ar-H).

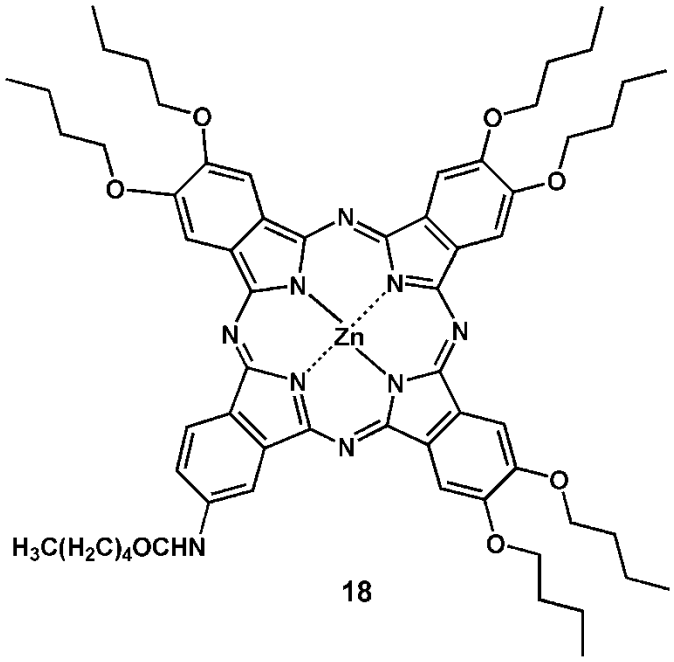

18

Zinc 9,10,16,17,23,24-hexabutoxy-2-hexanamidophthalocyanine[39]

A portion of 4-hexanamidophthalonitrile (0.8 g, 3.3 mmol) and 4,5-dibutoxyphthalonitrile (2.7 g, 9.95 mmol) were dissolved in 42.6 mL of dimethoxyethane (DME) and stirred under an ammonia flow at 100°C for 2 h. A portion of 1,8-diazabicyclo[5.4.0]undec-7-ene (DBU, 0.7 mL) was added and the stirring was continued for 15 min. Zinc acetate (0.61 g) was added and the mixture was stirred at 100°C overnight. The green mixture was cooled to room

temperature and 30 mL of a water/methanol mixture (1:1) was added. The precipitate that formed was collected, washed with water, and dried. The product was purified by column chromatography using 1% methanol in chloroform. Zinc-9,10,16,17,23,24-hexabutoxy-2-hexanamidophthalocyanine was obtained in 8.1% yield (330 mg). ^{1}H-NMR (500 MHz, DMSO-$CDCl_3$): δ 1.02 (3H, t), 1.12 - 1.20 (18H, m), 1.47 - 1.53 (4H, m), 1.70 - 1.80 (12H, m), 1.87(2H, q), 2.00 - 2.10 (12H, m), 2.63 (2H, t), 4.47 - 4.55 (12H, m), 8.40 (1H, d, J = 8 Hz, Pc-H), 8.45 - 8.60 (6H, m, Pc-H), 9.10 (1H, d, J = 8 Hz, Pc-H), 9.60 (1H, d, J = 8 Hz, Pc-H), 10.6 (1H, s, Pc-H); MALDI-TOF-MS *m/z:* calcd. for $C_{62}H_{75}N_9O_7Zn$ 1123.47, obsd. 1123.50; UV/vis (95% chloroform/5% methanol) 355, 612, and 679 nm.

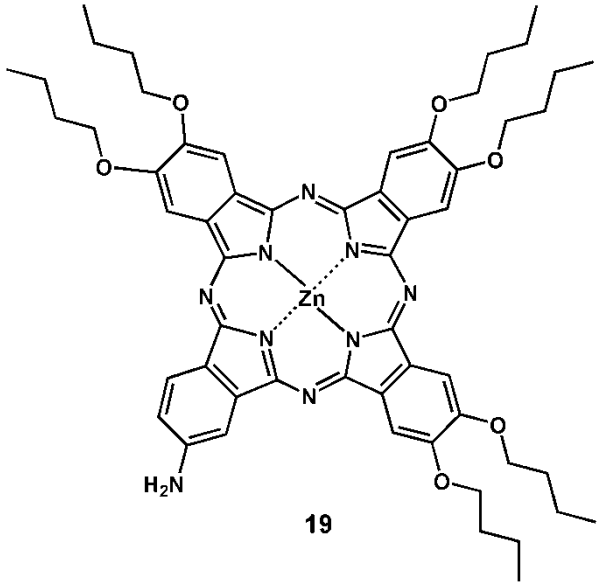

19

Zinc 2-amino-9,10,16,17,23,24-hexabutoxyphthalocyanine[39]

A portion of the hexanamidophthalocyanine obtained in the above reaction (0.3 g, 0.3 mmol) was dissolved in 40 mL of tetrahydrofuran and 40 mL of a saturated methanolic solution of potassium hydroxide. The solution was heated to 75°C and stirred overnight under N_2 after the addition of another 20 mL of tetrahydrofuran.

The reaction mixture was diluted with chloroform and washed with water several times. The organic layer was dried over Na_2SO_4 and filtered, and the solvent was distilled at reduced pressure to give 236 mg (86.4%) of the desired zinc 2-amino-9,10,16,17,23,24-hexabutoxyphthalocyanine. MALDI-TOF-MS *m/z:* calcd, for $C_{56}H_{65}N_9O_6Zn$ 1025.48, obsd. 1025.43.

General procedure for amide formation reaction: Carotenoid-acid (23.2 mg, 0.05 mmole) and aminophthalocyanine (50 mg, 0.05 mmol) were dissolved in 25 mL of chloroform. To this reaction mixture EDCI (14.03 mg, 0.073 mmol), DMAP (11.9 mg, 0.10 mmol) were added and stirred at room temperature for 24 h under N_2 atmosphere. The reaction mixture was diluted with chloroform, washed with water, and dried under vacuum. The product was purified by flash chromatography on silica gel using 7% acetone in dichloromethane.

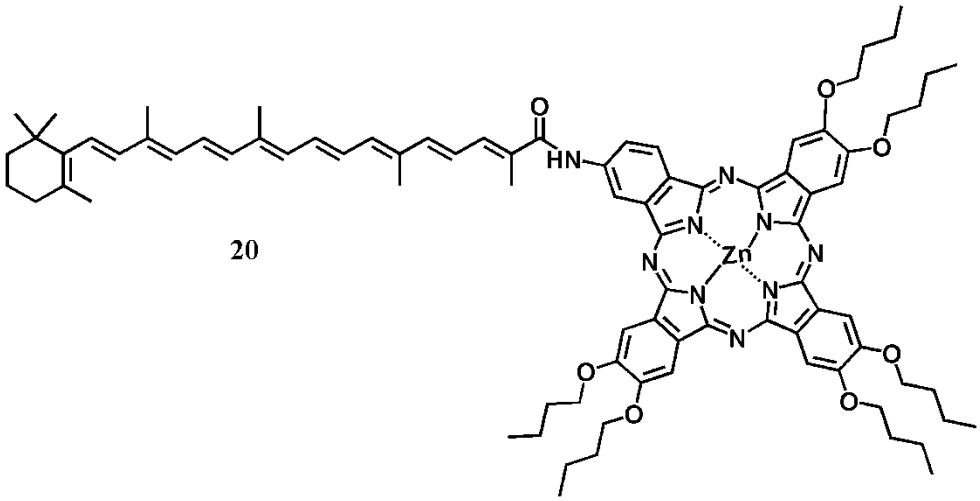

20

Dyad 9-db

The general procedure using 8'-apo-β-caroten-8'-oic acid gave 19 mg (27% yield) of pure title compound **20**. ^{1}H-NMR (500 MHz, DMSO/$CDCl_3$): δ 1.03 (6H, m,

Car 16- CH_3, Car 17-CH_3), 1.16-1.21 (18H, m, -$OCH_2CH_2CH_2CH_3$), 1.46 (2H, s, Car-2), 1.59 (2H, s, Car-3), 1.71 (3H, s, Car18), 1.75-1.83 (12H, m, -$OCH_2CH_2CH_2CH_3$), 1.96 (3H, s, Car-19), 1.98-2 (5H, m, Car- 20, Car-4), 2.08 (15H, m, Car-20', -$OCH_2CH_2CH_2CH_3$), 2.32 (3H, s, Car 19'), 4.50-4.57 (12H, m, -$OCH_2CH_2CH_2CH_3$), 6.16-6.81 (11H, m, vinyl H), 7.44 (1H, s, J = 10), 8.45-8.6 (7H, m, Pc-H), 9.1 (1H, d, Pc-H), 9.63 (1H, s, Pc-H), 10.4 (1H, s, -NH-CO-); MALDI-TOF-MS *m/z:* calcd. for $C_{86}H_{103}N_9O_7Zn$ 1440.75, obsd. 1440.71; UV/vis (95% chloroform/5% methanol) 352, 454, 616, and 683 nm.

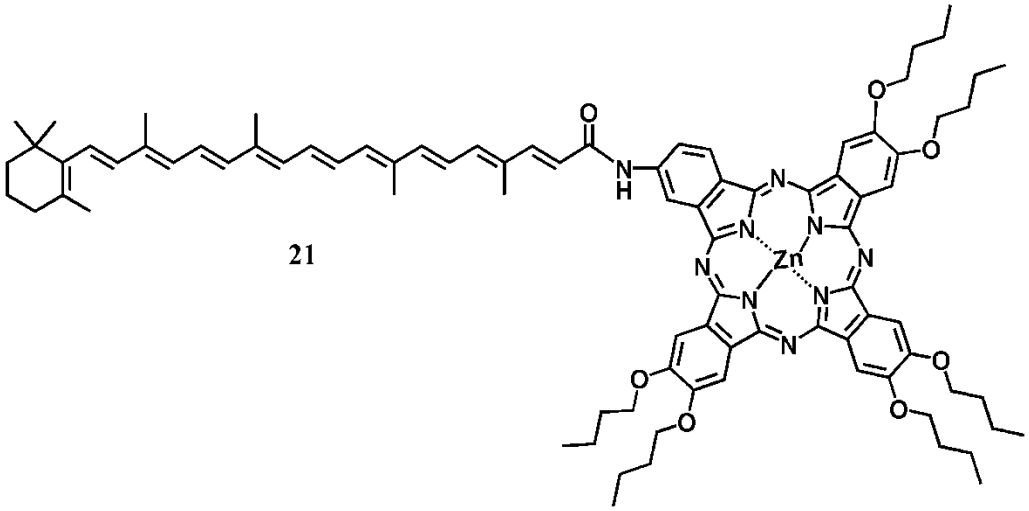

21

Dyad 10-db

The general procedure using 6'-apo-β-caroten-6'-oic acid gave 16 mg (27% yield) of pure title compound **21**. ^{1}H-NMR (500 MHz, DMSO/$CDCl_3$): δ 1.01 - 1.04 (6H, m, Car 16-CH_3, Car 17-CH_3), 1.16 - 1.21 (18H, m, -$OCH_2CH_2CH_2CH_3$), 1.46 (2H, m, Car 2-CH_2), 1.59 (2H, m, Car 3-CH_2), 1.71 (3H, s, Car 18-CH_3), 1.75 - 1.83 (12H, m, -$OCH_2CH_2CH_2CH_3$), 1.96 (3H, s, Car 19-CH_3), 2.00 (5H, m, Car 20-CH_3, Car-4), 2.08 (15H, m, -$OCH_2CH_2CH_2CH_3$, Car 20'-CH_3), 2.32 (3H,

s, Car 19'-CH_3), 4.50 - 4.57 (12H, m, -O-$CH_2CH_2CH_2CH_3$), 6.16 - 6.81 (13H, m, vinyl H), 7.44 (1H, d, J = 10 Hz), 8.45 - 8.60 (7H, m, Pc-H), 9.10 (1H, d, J = 8 Hz, Pc-H), 9.63 (1H, s, Pc-H), 10.40 (1H, s, -NHCO-); MALDI-TOF-MS *m/z:* calcd. for $C_{88}H_{105}N_9O_7Zn$ 1466.76, obsd. 1440.73; UV/vis (97% chloroform/3% methanol) 356, 476, 616, and 684 nm; UV/vis (tetrahydrofuran) 354, 468, 612, and 679 nm.

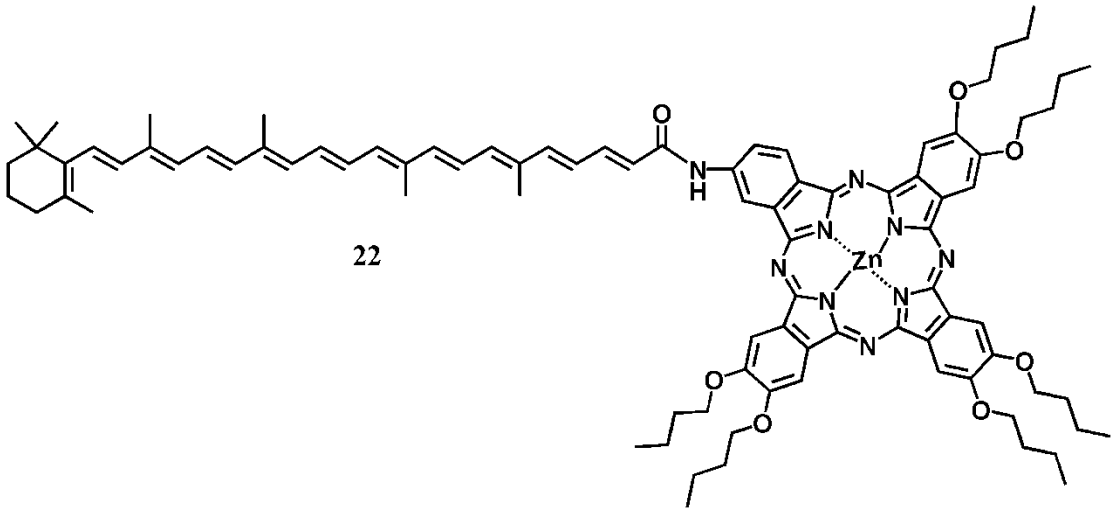

22

Dyad 11-db

The general procedure using 4'-apo-β-caroten-4'-oic acid gave 15 mg (31% yield) of pure title compound **22**. ^{1}H-NMR (500 MHz, DMSO/$CDCl_3$): δ 0.96 - 0.98 (6H, m, Car 16-CH_3, Car 17-CH_3), 1.12 - 1.21 (18H, m, -$OCH_2CH_2CH_2CH_3$), 1.41 (2H, m, Car 2-CH_2), 1.56 (2H, m, Car 3-CH_2), 1.65 (3H, s, Car 18-CH_3), 1.75 (12H, s, -$OCH_2CH_2CH_2CH_3$), 1.91 (3H, s, Car 19-CH_3), 1.92 (3H, s, Car 20-CH_3), 1.95 - 2.00 (5H, m, Car-4, Car 20'-CH_3), 2.08 (15H, m, -$OCH_2CH_2CH_2CH_3$, Car 19'-CH_3), 4.53 - 4.57 (12H, m, -O-$CH_2CH_2CH_2CH_3$), 6.05 - 7.32 (16H, m, vinyl-H), 8.29 (1H, bs, Pc-H), 8.65 - 8.73 (6H, m, Pc-H),

9.19 (1H, bs, Pc-H), 9.75 (1H, s, Pc-H), 10.37 (1H, s, -NHCO-); MALDI-TOF-MS *m/z:* calcd. for $C_{90}H_{107}N_9O_7Zn$ 1492.67, obsd. 1492.73; UV/vis (97% chloroform/3% methanol) 356, 476, 616, and 684 nm; UV/vis (tetrahydrofuran) 354, 468, 612, and 679 nm.

Carotenoids lacking terminal carbonyl group covalently attached to phthalocyanines

General procedure for the synthesis of amino carotenoids: Carotene-aldehyde (0.7 mmol), 4-(N-acetylamino)benzyltriphenylphosphonium bromide (1.4 mmol) and sodium methoxide (1.8 mmol) in 40 mL of dimethyl sulfoxide were heated under argon atmosphere at 65ºC for 8 h. Adding the dark orange solution to 250 mL of water quenched the reaction mixture. The compound was then extracted with diethyl ether. The organic layer was dried over anhydrous sodium sulfate filtered, and the solvent evaporated under reduced pressure. The resulting crude carotenoid amide was dissolved in 15 mL of tetrahydrofuran to which 35 mL of saturated methanolic potassium hydroxide solution was added. This solution was heated to 63ºC, stirred under an argon atmosphere for 6 h, and then poured into 250 mL of ether and washed several times with 100 mL portions of water. The organic layer was dried over anhydrous sodium sulfate, filtered, and the solvent evaporated. The residue was chromatographed on silica gel column using 15% ethyl acetate in hexane.

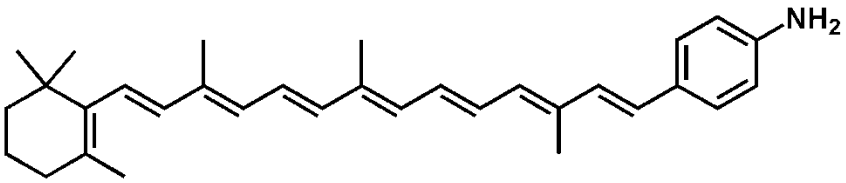

26

11'-Apo-11'-(4-aminophenyl)-*β*-carotene

The general procedure using 12'-apo-*β*-caroten-12'-al gave 195 mg (63%) of compound **26**. ^{1}HNMR (400MHz, $CDCl_3$): δ 1.02 (6H, s, CH_3-16C and CH_3-17C), 1.43-1.49 (2H, m, CH_2-2C), 1.57-1.65 (2H, m, CH_2-3C), 1.7 (3H, s, CH_3-19C), 1.9-2 (11H, m, CH_3-18C, CH_3-20C, CH_3-20'C, CH_2-4C), 3.7 (2H, s, -NH_2), 6.1-6.7 (13H, m, vinyl H, ArH), 7.22 (2H, d, J=8.2Hz, ArH); MALDI-TOF-MS *m/z:* calcd. for $C_{32}H_{41}N$ 439.32, obsd. 439.31; UV-vis (dichloromethane): 353, 442 and 470 nm.

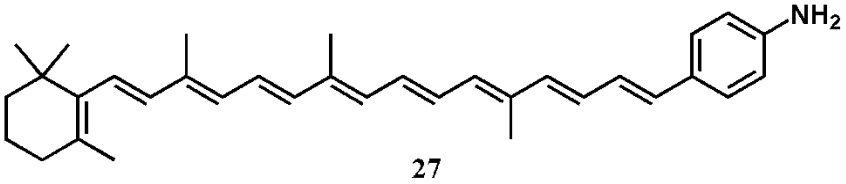

27

9'-Apo-9'-(4-aminophenyl)-*β*-carotene

The general procedure using 10'-apo-*β*-caroten-10'-al gave 186 mg (57%) of compound **27**. ^{1}HNMR (400MHz, $CDCl_3$): δ 1.03 (6H, s, CH_3-16C and CH_3-17C), 1.44-1.5 (2H, m, CH_2-2C), 1.57-1.66 (2H, m, CH_2-3C), 1.72 (3H, s, CH_3-19C), 1.89-2 (11H, m, CH_3-18C, CH_3-20C, CH_3-20'C, CH_2-4C), 3.72 (2H, s, -NH_2), 6-6.8 (15H, m vinyl H, ArH), 7.23 (2H, d, J=8.4Hz, ArH); MALDI-TOF-MS *m/z:* calcd. for $C_{34}H_{43}N$ 465.71, obsd. 465.72; UV-vis (dichloromethane): 372, 461, and 489 nm.

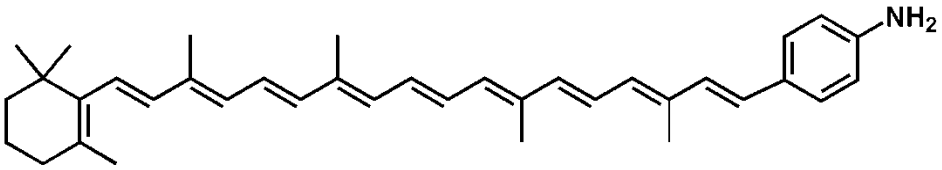

28

7'-Apo-7'-(4-aminophenyl)-*β*-carotene

The general procedure using 8'-apo-*β*-caroten-8'-al gave 216 mg (61%) of compound **28**. ^{1}HNMR (400MHz, $CDCl_3$): δ 1.01 (6H, s, CH_3-16C and CH_3-17C), 1.44-1.48 (2H, m, CH_2-2C), 1.57-1.64 (2H, m, CH_2-3C), 1.7 (3H, s, CH_3-19C), 1.94-2.04 (14H, m, CH_3-18C, CH_3-20C, CH_3-19'C, CH_3-20'C, and CH_2-4C), 3.8 (2H, s, -NH_2), 6.06-6.98 (16H, m, vinyl H, ArH), 7.24 (2H,d, J=8.1Hz ArH); MALDI-TOF-MS *m/z:* calcd. for $C_{37}H_{47}N$ 505.37, obsd. 505.37; UV-vis (dichloromethane): 376, 479, and 509 nm.

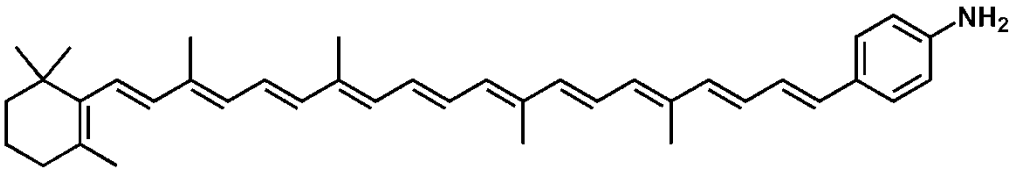

29

5'-Apo-5'-(4-aminophenyl)-*β*-carotene

The general procedure using 6'-apo-*β*-caroten-6'-al gave 218 mg (58 %) of compound **29**. ^{1}HNMR (400MHz, $CDCl_3$): δ 1.03 (6H, s, CH_3-16C and CH_3-17C), 1.45-1.5 (2H, m, CH_2-2C), 1.57-1.65 (2H, m, CH_2-3C), 1.72 (3H, s, CH_3-19C), 1.95-2 (14H, m, CH_3-18C, CH_3-20C, CH_3-19'C, CH_3-20'C, and CH_2-4C), 3.73 (2H, s, NH_2), 6-6.9 (18H, m, vinyl H, ArH), 7.22 (2H, d, J=8.2Hz ArH);

MALDI-TOF-MS *m/z*: calcd. for $C_{39}H_{49}N$ 531.39, obsd. 531.40; UV-vis (dichloromethane): 395, 488, and 519 nm.

General procedure for amination reaction to prepare the amino-dyads: Zinc tri-*tert*-butyliodophthalocyanine (0.1 mmol), amine (0.12 mmol), sodium *tert*-butoxide (0.14 mmol), tris(dibenzylideneacetone)dipalladium (0.001 mmol), and BINAP (0.005 mmol), were stirred in toluene (5 mL) at 80ºC under argon atmosphere until the starting material had been consumed (6-7 h). The solution was then allowed to cool to room temperature and filtered through a short silica gel column to remove compounds having low solubility. The solvent was evaporated and the residue was chromatographed on silica gel using 20% THF in hexanes.

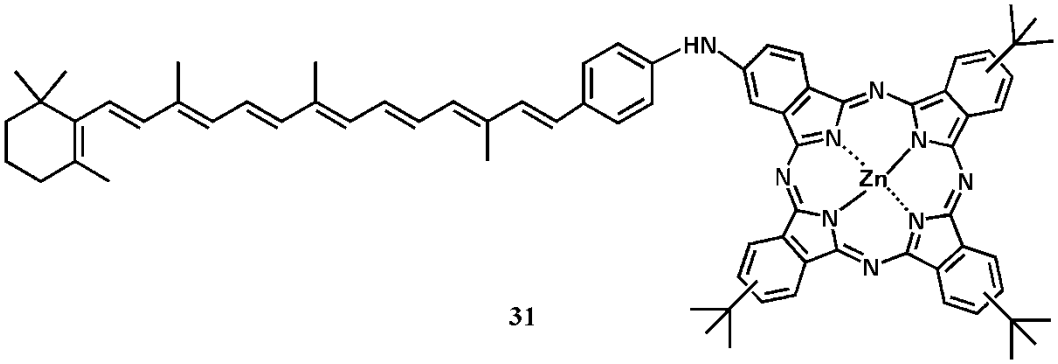

31

Amine-dyad-8-db

The general procedure using 11'-apo-11'-(4-aminophenyl)-*β*-carotene gave 78 mg (66%) of the title compound **31**. ^{1}HNMR (500MHz, THF-d_8): δ 1.07 (6H, s, CH_3-16C and CH_3-17C), 1.48-1.54 (2H, m, CH_2-2C), 1.62-1.69 (2H, m, CH_2-3C), 1.74 (3H, s, CH_3,-19C), 1.84 (27H, s, CH_3-*t*Bu), 1.97-2.15 (8H, m, CH_3-18C, CH_3-20C, and CH_2-4C), 2.32 (3H, s, CH_3-20'C), 5.52 (1H, s, NH), 6.07-7.24 (11H, m

vinyl H), 7.53-7.73 (4H, m, Car-1', 2', 4', 5'), 8.22-8.33 (3H, m, Pc-H), 8.42-8.45 (1H, m, Pc-H), 8.83-9.57 (8H, m, Pc-H); MALDI-TOF-MS *m/z*: calcd. for $C_{76}H_{79}N_9Zn$ 1181.57, obsd. 1181.58; UV-vis (toluene) 350, 453, 625, and 696 nm.

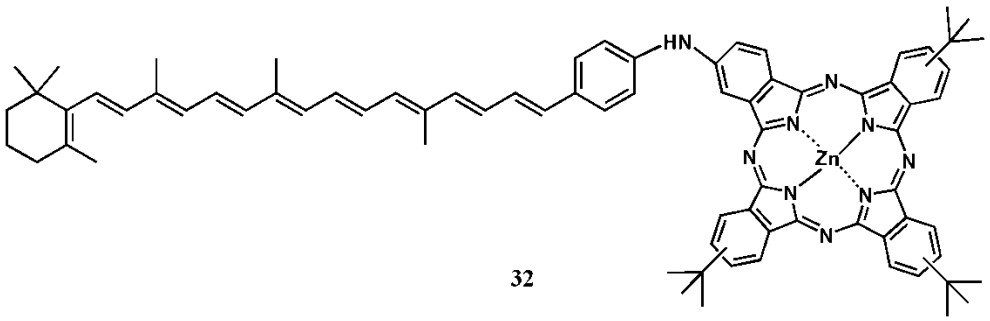

32

Amine-dyad-9-db

The general procedure using 9'-apo-9'-(4-aminophenyl)-*β*-carotene gave 75 mg (62%) of the title compound **32**. ^{1}HNMR (500MHz, THF-d_8): δ 1.05 (6H, s, CH_3-16C and CH_3-17C), 1.46-1.53 (2H, m, CH_2-2C), 1.6-1.67 (2H, m, CH_2-3C), 1.73 (3H, s, CH_3,-19C), 1.81 (27H, s, CH_3-*t*Bu), 1.94-2.07 (8H, m, CH_3-18C, CH_3-20C, and CH_2-4C), 2.3 (3H, s, CH_3-20'C), 5.52 (1H, s, NH), 6.06-7.23 (13H, m vinyl H), 7.5-7.65 (4H, m, Car-1', 2', 4', 5'), 8.23-8.32 (3H, m, Pc-H), 8.45-8.54 (1H, m, Pc-H), 8.89-9.55 (8H, m, Pc-H); MALDI-TOF-MS *m/z*: calcd. for $C_{78}H_{81}N_9Zn$ 1209.59 obsd. 1209.60; UV-vis (toluene) 351, 471, 626, and 696 nm.

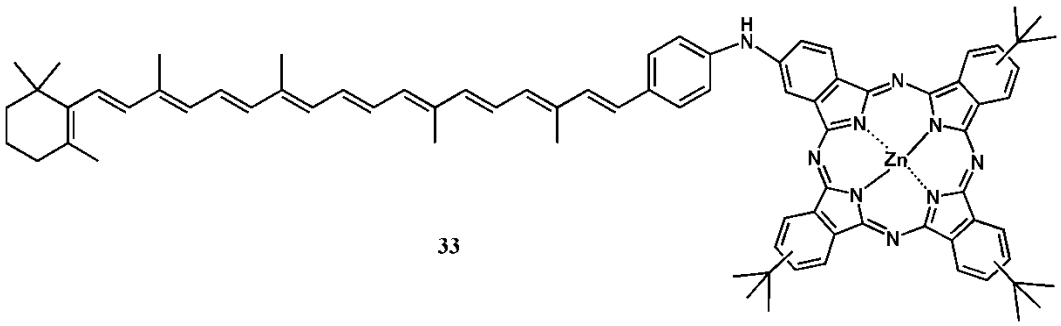

33

Amine-dyad-10-db

The general procedure using 7'-apo-7'-(4-aminophenyl)-*β*-carotene gave 80 mg (64%) of the title compound **33**.[1]HNMR (500MHz, THF-d_8): δ 1.07 (6H, s, CH_3-16C and CH_3-17C), 1.48-1.54 (2H, m, CH_2-2C), 1.62-1.69 (2H, m, CH_2-3C), 1.78 (3H, s, CH_3,-19C), 1.84 (27H, s, CH_3-*t*Bu), 1.96-2.16 (11H, m, CH_3-18C, CH_3-20C, CH_3-19'C, CH_2-4C,), 2.32 (3H, s, CH_3-20'C), 5.52 (1H, s, NH), 6.09-7.24 (14H, m vinyl H), 7.53-7.7 (4H, m, Car-1', 2', 4', 5'), 8.22-8.32 (3H, m, Pc-H), 8.42-8.5 (1H, m, Pc-H), 9.03-9.57 (8H, m, Pc-H); MALDI-TOF-MS *m/z*: calcd for $C_{81}H_{85}N_9Zn$ 1247.62, obsd 1247.65; UV-vis (toluene) 349, 483, 625, and 696 nm.

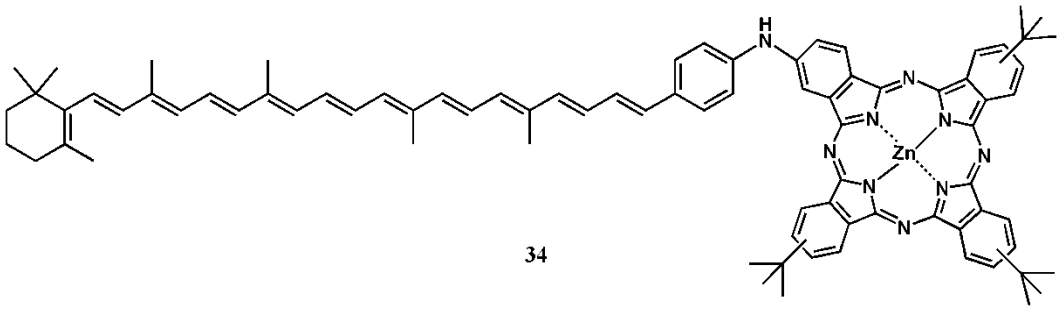

34

Amine-dyad-11-db

The general procedure using 5'-apo-5'-(4-aminophenyl)-*β*-carotene gave 73mg (57%) of the title compound **34**.[1]HNMR (500MHz, THF-d_8): δ 1.2 (6H, s, CH_3-16C and CH_3-17C), 1.47-1.5 (2H, m, CH_2-2C), 1.6-1.67 (2H, m, CH_2-3C), 1.79

(3H, s, CH_3,-19C), 1.8 (27H, s, CH_3-*t*Bu), 1.94-2 (14H, m, CH_3-18C, CH_3-20C, CH_3-19'C, CH_3-20'C, and CH_2-4C), 5.85 (1H, s, NH), 6.13-7.22 (16H, m vinyl H), 7.4-7.6 (4H, m, Car-1', 2', 4', 5'), 8.2-8.33 (3H, m, Pc-H), 8.45-8.55 (1H, m, Pc-H), 9-9.58 (8H, m, Pc-H); MALDI-TOF-MS *m/z*: calcd. for $C_{83}H_{87}N_9Zn$ 1273.64, obsd. 1273.67; UV-vis (toluene) 350, 492, 625, and 694 nm.

Synthesis of model phthalocyanine

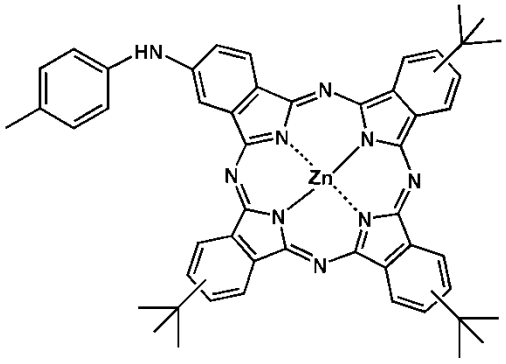

44

Pc-Model

The general procedure using 2-amino-1-methylbenzene gave 63 mg (74%) of the title compound **44**.^{1}HNMR (500MHz, THF-d_8): δ 1.79 (27H, s, CH_3-*t*Bu), 2.46 (3H, s, CH_3), 5.5 (1H, s, NH), 7.26-7.3 (2H, m, 1', 5'), 7.4-7.48 (2H, m, 2', 4'), 7.7-7.9 (2H, m, Pc-H), 8.2-8.32 (3H, m, Pc-H), 9-9.5 (7H, m, Pc-H); MALDI-TOF-MS *m/z.* calcd. for $C_{51}H_{47}N_9Zn$ 849.34, obsd. 849.34; UV-vis (toluene) 348, 622, and 690 nm.

Synthesis of model carotenoids.

General procedure for the synthesis of iodocarotenoids: Carotenoid-aldehyde (0.5 mmol), 4-iodobenzyltriphenylphosphonium bromide (1 mmol), and sodium

methoxide (1.25mmol) were added to 30 mL of dimethylsulfoxide and stirred at 65ºC for 24 h. The reaction mixture was quenched by adding the dark orange solution to 250 mL water and extracting the compound with diethyl ether. The organic layer was dried over anhydrous magnesium sulfate, filtered, and the solvent evaporated under reduced pressure. The crude reaction mixture was then purified by column chromatography on silica using 20% dichloromethane in hexanes as the eluent. The product was recrystallized from dichloromethane/methanol.

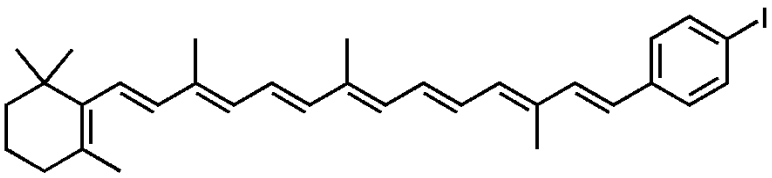

36

11'-Apo-11'-(4-iodophenyl)-*β*-carotene

The general procedure using 12'-apo-*β*-caroten-12'-al gave 187 mg (68%): ^{1}HNMR (400MHz, $CDCl_3$): δ 1.03 (6H, s, CH_3-16C and CH_3-17C), 1.45-1.49 (2H, m, CH_2-2C), 1.58-1.65 (2H, m, CH_2-3C), 1.72(3H, s, CH_3-19C), 1.96-2.05 (11H, m, CH_3-18C, CH_3-20C, CH_3-20'C, CH_2-4C), 6.04-6.86 (11H, m vinyl H), 7.15 (2H, d, J=8Hz, ArH), 7.6 (2H, d, J=8Hz, ArH). MALDI-TOF-MS *m/z.* calcd. for $C_{32}H_{39}I$ 550.56, obsd.550.51; UV-vis (dichloromethane) 422, 440, 462 nm.

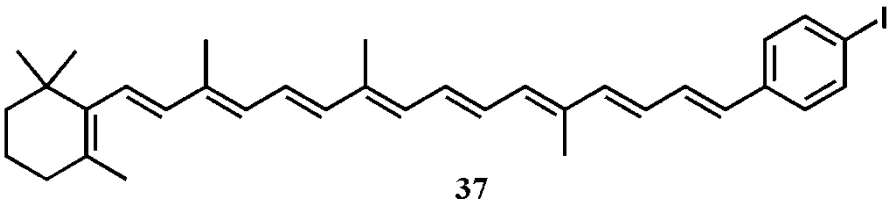

37

9'-Apo-9'-(4-iodophenyl)-*β*-carotene

The general procedure using 10'-apo-*β*-caroten-10'-al gave 198 mg (68%): ^{1}HNMR (400MHz, $CDCl_3$): δ 1.02 (6H, s, CH_3-16C and CH_3-17C), 1.43-1.48 (2H, m, CH_2-2C), 1.57-1.64 (2H, m, CH_2-3C), 1.7 (3H, s, CH_3,-19C), 1.9-2 (11H, m, CH_3,-18C, CH_3-20C, CH_3-20'C, CH_2-4C), 6.07-6.9 (13H, m vinyl H, ArH), 7.11 (2H, d, J=8.2Hz, ArH), 7.6 (2H, d, J=8.2Hz, ArH). MALDI-TOF-MS *m/z.*: calcd. for $C_{34}H_{41}I$ 576.81, obsd. 576.85; UV-vis (dichloromethane) 434, 455, 483 nm.

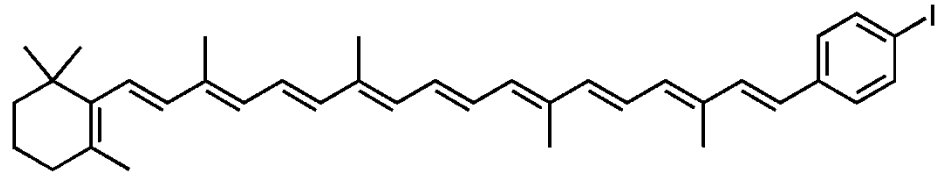

38

7'-Apo-7'-(4-iodophenyl)-*β*-carotene

The general procedure using 8'-apo-*β*-caroten-8'-al gave 206 mg (66.8%): ^{1}HNMR (400MHz, $CDCl_3$): δ 1.03 (6H, s, CH_3-16C and CH_3-17C), 1.45-1.48 (2H, m, CH_2-2C), 1.58-1.63 (2H, m, CH_2-3C), 1.7(3H, s, CH_3-19C), 1.96-2.4 (14H, m, CH_3-18C, CH_3-20C, CH_3-20'C, CH_2-4C, and CH_3-19'C), 6.11-6.87(14H, m vinyl H), 7.15 (2H, d, J=8.4Hz, ArH), 7.62(2H, d, J=8.4Hz, ArH).

MALDI-TOF-MS *m/z.* calcd. for $C_{37}H_{45}I$ 616.20, obsd. 616.23; UV-vis (dichloromethane) 362, 449, 475, and 507 nm.

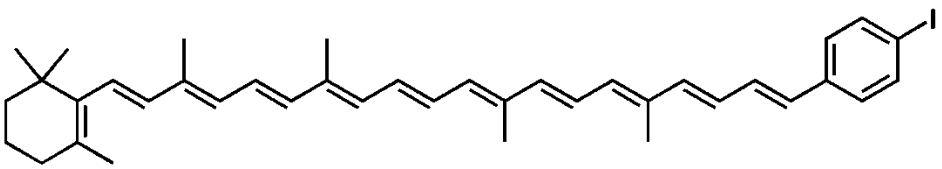

39

5'-Apo-5'-(4-iodophenyl)-*β*-carotene

The general procedure using 6'-apo-*β*-caroten-6'-al gave 195 mg (60%) of compound: ^{1}HNMR (400MHz, $CDCl_3$): δ 1.03 (6H, s, CH_3-16C and CH_3-17C), 1.44-1.45 (2H, m, CH_2-2C), 1.58-1.66 (2H, m, CH_2-3C), 1.7(3H, s, CH_3-19C), 1.93-2 (14H, m, CH_3-18C, CH_3-20C, CH_3-20'C, CH_2-4C, and CH_3-19'C), 6.1-6.9 (16H, m vinyl H), 7.13 (2H, d, J=7.8Hz, ArH), 7.27 (2H, d, J=7.8Hz, ArH). MALDI-TOF-MS *m/z.* calcd. for $C_{39}H_{47}I$ 642.69, obsd. 642.72.

General procedure for the amination reaction to prepare model aminocarotenoids: Iodocarotene (0.1 mmol), 4-amino-1-methylbenzene (0.12 mmol), sodium *tert*-butoxide (0.14 mmol), tris(dibenzylideneacetone)dipalladium (0.003 mmol), and BINAP (0.008 mmol), were stirred in toluene (5 mL) at 80ºC under argon atmosphere until the starting material had been consumed (8h). The solution was then allowed to cool to room temperature and filtered through a short silica gel column to remove compounds having low solubility. The solvent was evaporated and the residue was chromatographed on silica gel using 30% dichloromethane in hexanes.

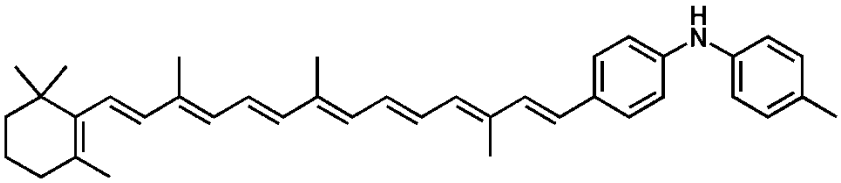

40

11'-Apo-11'-(4-amino-N-[4-methylphenyl]phenyl)-*β*-carotene

The general procedure using 11'-Apo-11'-(4-iodophenyl)-*β*-carotene gave 42 mg (66%): ^{1}HNMR (500MHz, $CDCl_3$): δ 1.02 (6H, s, CH_3-16C and CH_3-17C), 1.43-1.48 (2H, m, CH_2-2C), 1.58-1.65 (2H, m, CH_2-3C), 1.7 (3H, s, CH_3-19C), 1.93-2.05 (11H, m, CH_3,-18C, CH_3-20C, CH_3-20'C, CH_2-4C), 2.29 (3H, s, Ar-CH_3), 5.68 (1H, s, NH), 6.02-6.8 (11H, m vinyl H), 6.9 (2H, d, J=8Hz, ArH), 7 (2H, d, J=8Hz, ArH), 7.08 (2H, d, J=8Hz, ArH), 7.3 (2H, d, J=8Hz, ArH). MALDI-TOF-MS *m/z* calcd. for $C_{39}H_{47}N$ 529.31, obsd. 529.29; UV-vis (dichloromethane) 356, 430,452, and 475 nm.

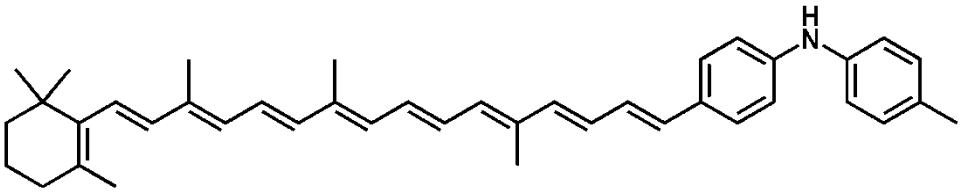

41

9'-Apo-9'-(4-amino-N-[4-methylphenyl]phenyl)-*β*-carotene

The general procedure using 9'-apo-9'-(4-iodophenyl)-*β*-carotene gave 35 mg (63%): ^{1}HNMR (400MHz, $CDCl_3$): δ 1.06 (6H, s, CH_3-16C and CH_3-17C), 1.48-1.52 (2H, m, CH_2-2C), 1.62-1.68 (2H, m, CH_2-3C), 1.75 (3H, s, CH_3-19C), 1.96-2 (11H, m, CH_3,-18C, CH_3-20C, CH_3-20'C, CH_2-4C), 2.34 (3H, s, Ar-CH_3), 5.73

(1H, s, NH), 6.07-6.9 (13H, m vinyl H, ArH), 6.97 (2H, d, J=8Hz, ArH), 7.04 (2H, d, J=8Hz, ArH), 7.12 (2H, d, J=8Hz, ArH), 7.32 (2H, d, J=8Hz, ArH). MALDI-TOF-MS *m/z.*: calcd. for $C_{41}H_{49}N$ 555.40, obsd. 555.46; UV-vis (dichloromethane) 371, 441, 466, 493 nm.

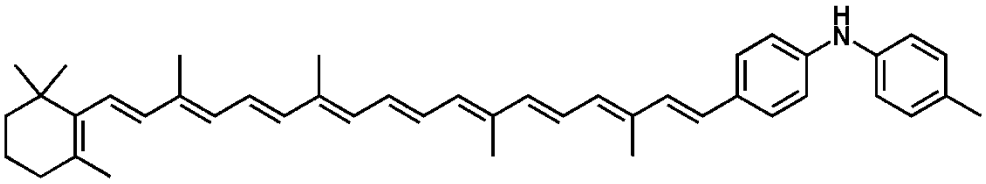

42

7'-Apo-7'-(4-amino-N-[4-methylphenyl]phenyl)-*β*-carotene

The general procedure using 7'-apo-7'-(4-iodophenyl)-*β*-carotene gave 46 mg (77%): ^{1}HNMR (500MHz, $CDCl_3$): δ 1.03 (6H, s, CH_3-16C and CH_3-17C), 1.45-1.49 (2H, m, CH_2-2C), 1.6-1.64 (2H, m, CH_2-3C), 1.72(3H, s, CH_3-19C), 1.97-2.03 (14H, m, CH_3-18C, CH_3-20C, CH_3-20'C, CH_2-4C, and CH_3-19'C), 2.31 (3H, s, Ar-CH_3**),** 6.09-6.77 (15H, m vinyl H, NH), 6.96 (2H, d, J=8.5Hz, ArH), 7.01 (2H, d, J=8Hz, ArH), 7.1 (2H, d, J=8Hz, ArH), 7.3 (2H, d, J=8.5Hz, ArH). MALDI-TOF-MS *m/z*: calcd. for $C_{44}H_{53}N$ 595.21, obsd. 595.27; UV-vis (dichloromethane) 382, 455, 480, and 510 nm.

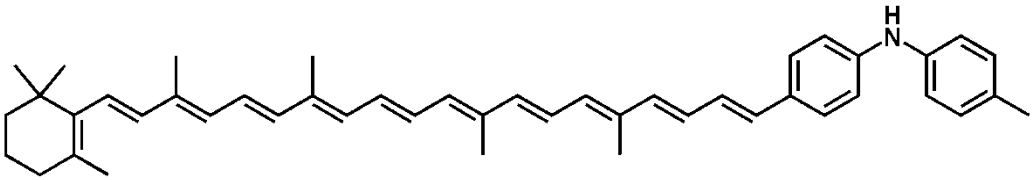

43

5'-Apo-5'-(4-amino-N-[4-methylphenyl]phenyl)-*β*-carotene

The general procedure using 5'-apo-5'-(4-iodophenyl)-*β*-carotene gave 38 mg (61%). ^{1}HNMR (400MHz, $CDCl_3$): δ 1.01 (6H, s, CH_3-16C and CH_3-17C), 1.45-1.46 (2H, m, CH_2-2C), 1.58-1.64 (2H, m, CH_2-3C), 1.7(3H, s, CH_3-19C), 1.96-2.1 (14H, m, CH_3-18C, CH_3-20C, CH_3-20'C, CH_2-4C, and CH_3-19'C), 2.2 (3H, s, Ar-CH_3), 6.06-6.9 (17H, m vinyl H, NH), 6.95 (2H, d, J=8Hz, ArH), 7.01 (2H, d, J=8Hz, ArH), 7.08 (2H, d, J=8Hz, ArH), 7.27 (2H, d, J=8Hz, ArH). MALDI-TOF-MS *m/z*: calcd. for $C_{46}H_{55}N$ 621.94, obsd.621.93; UV-vis (dichloromethane) 395, 461, 491, and 521 nm.

VI. References

(1) Gust, D.; Moore, T. A. *Science* **1989**, *244*, 35.

(2) Gust, D.; Moore, T. A.; Moore, A. L. *Accounts of Chemical Research* **1993**, *26*, 198.

(3) Muller, P.; Li, X. P.; Niyogi, K. K. *Plant Physiology* **2001**, *125*, 1558.

(4) Polivka, T.; Sundstrom, V. *Chemical Reviews* **2004**, *104*, 2021.

(5) Vaswani, H. M.; Holt, N. E.; Fleming, G. R. *Pure and Applied Chemistry* **2005**, *77*, 925.

(6) Ahn, T. K.; Avenson, T. J.; Ballottari, M.; Cheng, Y. C.; Niyogi, K. K.; Bassi, R.; Fleming, G. R. *Science* **2008**, *320*, 794.

(7) Ruban, A. V.; Berera, R.; Ilioaia, C.; van Stokkum, I. H. M.; Kennis, J. T. M.; Pascal, A. A.; van Amerongen, H.; Robert, B.; Horton, P.; van Grondelle, R. *Nature* **2007**, *450*, 575.

(8) Standfuss, R.; van Scheltinga, A. C. T.; Lamborghini, M.; Kuhlbrandt, W. *Embo Journal* **2005**, *24*, 919.

(9) Ishizaki, A.; Calhoun, T. R.; Schlau-Cohen, G. S.; Fleming, G. R. *Physical Chemistry Chemical Physics* **2010**, *12*, 7319.

(10) Papagiannakis, E.; Larsen, D. S.; van Stokkum, I. H. M.; Vengris, M.; Hiller, R. G.; van Grondelle, R. *Biochemistry* **2004**, *43*, 15303.

(11) Dreuw, A.; Fleming, G. R.; Head-Gordon, M. *Physical Chemistry Chemical Physics* **2003**, *5*, 3247.

(12) Fungo, F.; Otero, L.; Durantini, E.; Thompson, W. J.; Silber, J. J.; Moore, T. A.; Moore, A. L.; Gust, D.; Sereno, L. *Physical Chemistry Chemical Physics* **2003**, *5*, 469.

(13) Frank, H. A.; Cogdell, R. J. *Photochemistry and Photobiology* **1996**, *63*, 257.

(14) Polivka, T.; Kaligotla, S.; Chabera, P.; Frank, H. A. *Physical Chemistry Chemical Physics* **2011**, *13*, 10787.

(15) Wehling, A.; Walla, P. J. *Journal of Physical Chemistry B* **2005**, *109*, 24510.

(16) Polivka, T.; Sundstrom, V. *Chemical Physics Letters* **2009**, *477*, 1.

(17) Polivka, T.; Frank, H. A. *Accounts of Chemical Research* **2010**, *43*, 1125.

(18) Liao, P. N.; Bode, S.; Wilk, L.; Hafi, N.; Walla, P. J. *Chemical Physics* **2010**, *373*, 50.

(19) Frank, H. A.; Farhoosh, R.; Gebhard, R.; Lugtenburg, J.; Gosztola, D.; Wasielewski, M. R. *Chemical Physics Letters* **1993**, *207*, 88.

(20) Wehling, A.; Walla, P. J. *Photosynthesis Research* **2006**, *90*, 101.

(21) Bode, S.; Quentmeier, C. C.; Liao, P. N.; Hafi, N.; Barros, T.; Wilk, L.; Bittner, F.; Walla, P. J. *Proceedings of the National Academy of Sciences of the United States of America* **2009**, *106*, 12311.

(22) Liao, P. N.; Holleboom, C. P.; Wilk, L.; Kuhlbrandt, W.; Walla, P. J. *Journal of Physical Chemistry B* **2010**, *114*, 15650.

(23) Walla, P. J.; Yom, J.; Krueger, B. P.; Fleming, G. R. *Journal of Physical Chemistry B* **2000**, *104*, 4799.

(24) Schulten, K.; Ohmine, I.; Karplus, M. *Journal of Chemical Physics* **1976**, *64*, 4422.

(25) Tavan, P.; Schulten, K. *Journal of Chemical Physics* **1979**, *70*, 5407.

(26) Tavan, P.; Schulten, K. *Physical Review B* **1987**, *36*, 4337.

(27) Zigmantas, D.; Hiller, R. G.; Sharples, F. P.; Frank, H. A.; Sundstrom, V.; Polivka, T. *Physical Chemistry Chemical Physics* **2004**, *6*, 3009.

(28) Frank, H. A.; Bautista, J. A.; Josue, J.; Pendon, Z.; Hiller, R. G.; Sharples, F. P.; Gosztola, D.; Wasielewski, M. R. *Journal of Physical Chemistry B* **2000**, *104*, 4569.

(29) Polivka, T.; Pellnor, M.; Melo, E.; Pascher, T.; Sundstrom, V.; Osuka, A.; Naqvi, K. R. *Journal of Physical Chemistry C* **2007**, *111*, 467.

(30) Enriquez, M. M.; Fuciman, M.; LaFountain, A. M.; Wagner, N. L.; Birge, R. R.; Frank, H. A. *Journal of Physical Chemistry B* **2010**, *114*, 12416.

(31) Kosumi, D.; Kusumoto, T.; Fujii, R.; Sugisaki, M.; Iinuma, Y.; Oka, N.; Takaesu, Y.; Taira, T.; Iha, M.; Frank, H. A.; Hashimoto, H. *Physical Chemistry Chemical Physics* **2011**, *13*, 10762.

(32) Pascal, A. A.; Liu, Z. F.; Broess, K.; van Oort, B.; van Amerongen, H.; Wang, C.; Horton, P.; Robert, B.; Chang, W. R.; Ruban, A. *Nature* **2005**, *436*, 134.

(33) Young, A. J.; Phillip, D.; Ruban, A. V.; Horton, P.; Frank, H. A. *Pure and Applied Chemistry* **1997**, *69*, 2125.

(34) Liao, P. N.; Pillai, S.; Gust, D.; Moore, T. A.; Moore, A. L.; Walla, P. J. *Journal of Physical Chemistry A* **2011**, *115*, 4082.

(35) Kloz, M.; Pillai, S.; Kodis, G.; Gust, D.; Moore, T. A.; Moore, A. L.; van Grondelle, R.; Kennis, J. T. M. *Journal of the American Chemical Society* **2011**, *133*, 7007.

(36) van Amerongen, H.; van Grondelle, R. *Journal of Physical Chemistry B* **2001**, *105*, 604.

(37) Delasrivas, J.; Telfer, A.; Barber, J. *Biochimica Et Biophysica Acta* **1993**, *1142*, 155.

(38) Berera, R.; van Stokkum, I. H. M.; Kodis, G.; Keirstead, A. E.; Pillai, S.; Herrero, C.; Palacios, R. E.; Vengris, M.; van Grondelle, R.; Gust, D.; Moore, T. A.; Moore, A. L.; Kennis, J. T. M. *Journal of Physical Chemistry B* **2007**, *111*, 6868.

(39) Berera, R.; Herrero, C.; van Stokkum, I. H. M.; Vengris, M.; Kodis, G.; Palacios, R. E.; van Amerongen, H.; van Grondelle, R.; Gust, D.; Moore, T. A.; Moore, A. L.; Kennis, J. T. M. *Proceedings of the National Academy of Sciences of the United States of America* **2006**, *103*, 5343.

(40) Fungo, F.; Otero, L.; Durantini, E. N.; Silber, J. J.; Sereno, L.; Marino-Ochoa, E.; Moore, T. A.; Moore, A. L.; Gust, D. *Journal of Physical Chemistry B* **2001**, *105*, 4783.

(41) Pillai, S. T.; Berera, R.; Kennis, J.; Gust, D.; Moore, T. A.; Moore, A. L. *Abstracts of Papers of the American Chemical Society* **2009**, *238*, 507.

(42) S.M, M.; Telegina, N. I.

(43) Reddy, P. V.; Rabago-Smith, M.; Borhan, B. *Journal of Labelled Compounds & Radiopharmaceuticals* **2002**, *45*, 79.

(44) Cardoso, S. L.; Nicodem, D. E.; Moore, T. A.; Moore, A. L.; Gust, D. *Journal of the Brazilian Chemical Society* **1996**, *7*, 19.

(45) Wolfe, J. P.; Buchwald, S. L. *Journal of Organic Chemistry* **2000**, *65*, 1144.

(46) Sadighi, J. P.; Singer, R. A.; Buchwald, S. L. *Journal of the American Chemical Society* **1998**, *120*, 4960.

(47) Wolfe, J. P.; Wagaw, S.; Marcoux, J. F.; Buchwald, S. L. *Accounts of Chemical Research* **1998**, *31*, 805.

(48) Byramova, N. E.; Mochalova, L. V.; Belyanchikov, I. M.; Matrosovich, M. N.; Bovin, N. V. *Journal of Carbohydrate Chemistry* **1991**, *10*, 691.

(49) Gust, D.; Moore, T. A.; Moore, A. L.; Devadoss, C.; Liddell, P. A.; Hermant, R.; Nieman, R. A.; Demanche, L. J.; Degraziano, J. M.; Gouni, I. *Journal of the American Chemical Society* **1992**, *114*, 3590.

(50) Maya, E. M.; Vazquez, P.; Torres, T. *Chemistry-a European Journal* **1999**, *5*, 2004.

(51) Avenson, T. J.; Ahn, T. K.; Niyogi, K. K.; Ballottari, M.; Bassi, R.; Fleming, G. R. *Journal of Biological Chemistry* **2009**, *284*, 2830.

(52) Bassi, R.; Avenson, T.; Ahn, T. K.; Zigmantas, D.; Zirong, L.; Matteo, B.; Li, Z.; Fleming, G. *Photosynthesis Research* **2007**, *91*, PS362.

(53) Holt, N. E.; Zigmantas, D.; Valkunas, L.; Li, X. P.; Niyogi, K. K.; Fleming, G. R. *Science* **2005**, *307*, 433.

(54) Berera, R.; van Stokkum, I. H. M.; d'Haene, S.; Kennis, J. T. M.; van Grondelle, R.; Dekker, J. P. *Biophysical Journal* **2009**, *96*, 2261.

(55) Li, Z. R.; Ahn, T. K.; Avenson, T. J.; Ballottari, M.; Cruz, J. A.; Kramer, D. M.; Bassi, R.; Fleming, G. R.; Keasling, J. D.; Niyogi, K. K. *Plant Cell* **2009**, *21*, 1798.

Chapter 2

PORPHYRIN STABILIZED IRIDIUM OXIDE WATER OXIDATION CATALYST

I. Introduction

Photosynthesis is a complex process that has sustained life on our planet for over three billion years. During oxygenic photosynthesis, fuel production results from the absorption of sunlight through the antenna/reaction center and then the conversion of this excitation energy to electrochemical energy.[1,2] The electrochemical potential formed after photoexcitation of photosystem II (PSII) is transferred to the oxygen evolving complex (OEC) and drives the catalytic oxidation of water to hydrogen ions and molecular oxygen, with the electrons freed during this process stored as reducing equivalents. Photosystem I (PSI) then uses the generated reducing equivalents and further light absorption to make a fuel (NADPH).[3] Photosynthesis ultimately has provided most of the energy needs required by human society as the fossil fuels we depend on for our energy, such as oil, gas, and coal, come from plants that lived millions of years ago.[4] With the growing demand for energy, humans are on their way to consuming all the available fossil fuels and soon will have to find other sources of energy. Additionally, while consuming these available energy sources, we are continuously generating higher levels of carbon dioxide and other greenhouse gases that contribute to global climate change. Alternatively, artificial photosynthesis is a promising approach of utilizing energy providing possibility that utilizes sunlight to produce a fuel.[5] Solar fuel production by artificial photosynthesis can be achieved either by reduction of carbon dioxide to methanol or hydrocarbons or by water

splitting into hydrogen and oxygen.[6,7] Different approaches have been pursued to mimic the fundamental steps of natural photosynthesis which has led to the development of artificial photosynthesis. Inspired by nature, artificial constructs have been developed to mimic the process of photosynthesis including the use of semiconductor particles as photocatalyst and photoelectrodes, molecular donor-acceptor systems linked to catalysts for hydrogen and oxygen evolution, and photovoltaic cells coupled directly or indirectly to electrocatalysts.[8]

Due to tremendous research in this area, researchers have been successful in developing artificial photosynthetic systems that use sunlight to produce fuel in the laboratory. Unfortunately, practical solar-driven catalysts for water oxidation and fuel production composed of earth-abundant elements have not yet been discovered.[9] Our current research aims to use water as an electron source for fuel production without generating any harmful byproducts. In this chapter, research related towards developing a porphyrin-based photoanode for use in a photoelectrochemical water splitting cell is presented.

Natural photosynthesis and water splitting

Natural photosynthesis features a complex photophysical and biochemical process, using sunlight to produce energy rich products that are then utilized for the growth of the organism.[2] Plants algae and cyanobacteria can efficiently absorb light energy at all wavelengths of the visible spectrum, but the energy used for splitting water and reducing carbon dioxide comes from the red region of the spectrum.[10] The energy of two red photons is required for every electron extracted from water, which is then used to reduce CO_2. This complex mechanism is achieved by connecting

together two different photosystems, photosystem I (PSI) and photosystem II (PSII). PSII uses light to power the extraction of electrons/protons from water, and PSI uses light to provide additional energy to the PSII-energized electrons so as to drive the CO_2 fixation process.[1,11]

The main steps that account for the operation of photosynthesis are as follows:

Light Harvesting

Solar energy is absorbed by chlorophylls, carotenoids, and other antenna pigments at wavelengths available in their environment. The resulting excitation energy of these pigments is transferred to PSII, the reaction center where charge separation takes place. This initial conversion of light energy to electrochemical potential occurs with high quantum yield.[2,10,11]

Charge separation

In the reaction center complex, upon excitation of the primary donar (P680, which is chlorophyll *a* dimer) and electron is transferred from the donor to the acceptor, creating a charge-separated state. This charge separation produces $P680^{\cdot +}$ (P680 is a chlorophyll *a* dimer) and $Pheo^{\cdot -}$ (Pheo is a chlorophyll molecule lacking an Mg ion in the tetrapyrrole ring). After the initial charge separation, it takes about 200 ps for the electron to move 26 Å away from the highly oxidizing $P680^{\cdot +}$.[10,11]

Charge transport

After charge separation, the reducing equivalent is passed from $Pheo^{\cdot -}$ along an electron transport chain to PSI, where the absorption of a second photon at P700 (a chlorophyll molecule) is used to generate a more powerful reductant. The energy accumulated in this process is used for carbon dioxide fixation, the production of NADPH (nicotinamide adenine dinucleotide phosphate), the generation of a proton gradient then used for the synthesis of the energy rich molecule ATP (adenosine triphosphate).[9]

Water Oxidation

The catalytic site for water oxidation involves a four manganese (Mn) cluster and calcium ion (Ca^{2+}) in the protein subunit of PSII known as the oxygen evolving complex (OEC). The OEC is repeatedly oxidized by $P680^{\cdot +}$ until it acquires four oxidizing equivalents; it then converts water to dioxygen and resets itself to a reduced state. Thus, the overall process includes storing solar energy as fuel by producing hydrogen (i.e., NADPH) and releasing oxygen as a byproduct to the atmosphere.[9,11,12]

Artificial photosynthesis

Researchers over the past several years have been trying to utilize the sun's energy for fuel production. For an artificial photosynthetic fuel-producing system to work, it should have components similar to those observed in nature. The main components required are: (a) an antenna/reaction center complex, which can harvest the sun's energy to generate electrochemical potential, (b) molecular

structures capable of forming and stabilizing light induced charge-separated states, and (c) catalysts capable of using the light generated charges to oxidize water and produce hydrogen or other reduced carbon based fuel.[5,9,13] This brief introduction will focuses on earlier work in artificial photosynthesis that was performed in an attempts to mimic natural photosynthesis using synthetic compounds similar to those found in nature.

Many artificial photosynthetic systems aim to use the energy of sunlight to drive the production of hydrogen. Hydrogen is considered an ideal fuel for the future as it can be produced from water; consuming hydrogen simply regenerates water and does not create harmful gases such as carbon dioxide.[5,9] Renewable hydrogen production by photovoltaic driven water electrolysis is still limited because of its high cost, though it is becoming more cost effective with developing technology.[14]

An alternative to generating electricity with light and then using that electricity to split water is the photocatalytic water-splitting using a photoelectrochemical cell. Such a device uses solar energy directly to convert water to hydrogen and oxygen. One of the first designs was that of Fujishima and Honda reported in the early 1970s. Their design carried out light driven water splitting using a TiO_2 electrode as a photoanode in combination with a Pt cathode.[15] In this system TiO_2 is used as the light absorber; as TiO_2 is a semiconductor, the absorption of photons with energy equal to or greater than its band gap energy leads to the generation of electrons in the conduction band and generates holes in the valence band.[12] The photogenerated holes in the valence

band lead to the oxidation of water to form oxygen on the TiO_2 surface and light generated electrons in the conduction band then drive the reduction of protons to hydrogen at the platinum counter electrode. Unfortunately, the band gap of TiO_2 is about 3.2 eV, which only allows this system to utilize ultraviolet light. This limits the usefulness of this design as ultraviolet light accounts for only about 4% of the solar spectrum while visible light makes up about 50%.[7,12] The main goal of artificial photosynthesis is to accomplish efficient hydrogen production using solar light and, therefore, significant research in this field has sought to develop a visible light driven photocatalyst.

In 1991 Grätzel developed a dye-sensitized photovoltaic cell, which utilizes visible light for the generation of electricity.[16] Under illumination by visible light, the excited state of the dye can inject electrons into the conduction band of certain semiconductors, such as TiO_2. These electrons are then transferred from the conduction band to the noble metal particles loaded on the surface of the cathode to drive the reduction of the redox mediator in solution (I_3^-/I^-). The ground state dye is then regenerated by electron transfer from the reduced form of the redox mediator in the solution.[16]

TiO_2 is most commonly used in dye-sensitized solar cells (DSSC) as it can form high surface area mesoporous surfaces to increase light absorption by the dye layer, has a high chemical stability, and provides a long lifetime of electron/hole pairs.[14,17] Furthermore, with a conduction band energy near –0.5 V

vs. NHE, electrons generated in the TiO_2 layer have sufficient energy to reduce I_3^- to I^- in a typical Grätzel style DSSC.[4,18]

Researchers have developed several catalysts for water oxidation. Nocera and coworkers developed a system using a film containing a cobalt oxide material on an ITO electrode formed from a solution of Co^{2+} and phosphate for electrochemical water oxidation.[4,19] Meyer and coworkers have reported a Ru-based molecular catalyst called the "blue" Ru dimer, *cis,cis*-$[(bpy)_2(H_2O)RuIIIORuIII(OH_2)(bpy)_2]^{4+}$ (bpy is 2,2′-bipyridine), which is capable of water oxidation.[13,20–22] Over twenty years ago Harriman and coworkers revealed transition metal oxides as some of the best candidates for catalyzing water oxidation; among these were metal oxides like Co_3O_4, RuO_2, $NiCo_2O_4$, Rh_2O_3, IrO_2, and Mn_2O_3. A RuO_2-based catalyst was found to be effective and was studied extensively in homogenous, heterogeneous, and colloidal forms.[23,24] Even though RuO_2 colloids are effective catalysts, they undergo anodic corrosion under strong oxidizing conditions, making them less stable.[25] Catalytic activity of IrO_2 was comparable to RuO_2 and was found to be much more stable under oxidizing conditions than RuO_2. Several groups have reported water oxidation by $IrO_2 \cdot nH_2O$ nanoparticles in both electrochemical and photochemical systems.[5,26]

Photochemical generation of O_2 from water was performed by utilizing dyes such as $Ru(II)(bpy)_3$ complexes or porphyrins.[23,27–29] These studies, however, required the presence of a strong oxidant ($S_2O_8^{2-}$) to generate the photo-oxidized dye $[Ru(bpy)_3]^{3+}$ or porphyrin radical cation which then oxidizes the catalyst

($IrO_2 \cdot nH_2O$). Typically in these studies the $IrO_2 \cdot nH_2O$ colloidal suspension was prepared by using citrate molecules as stabilizers.[27]

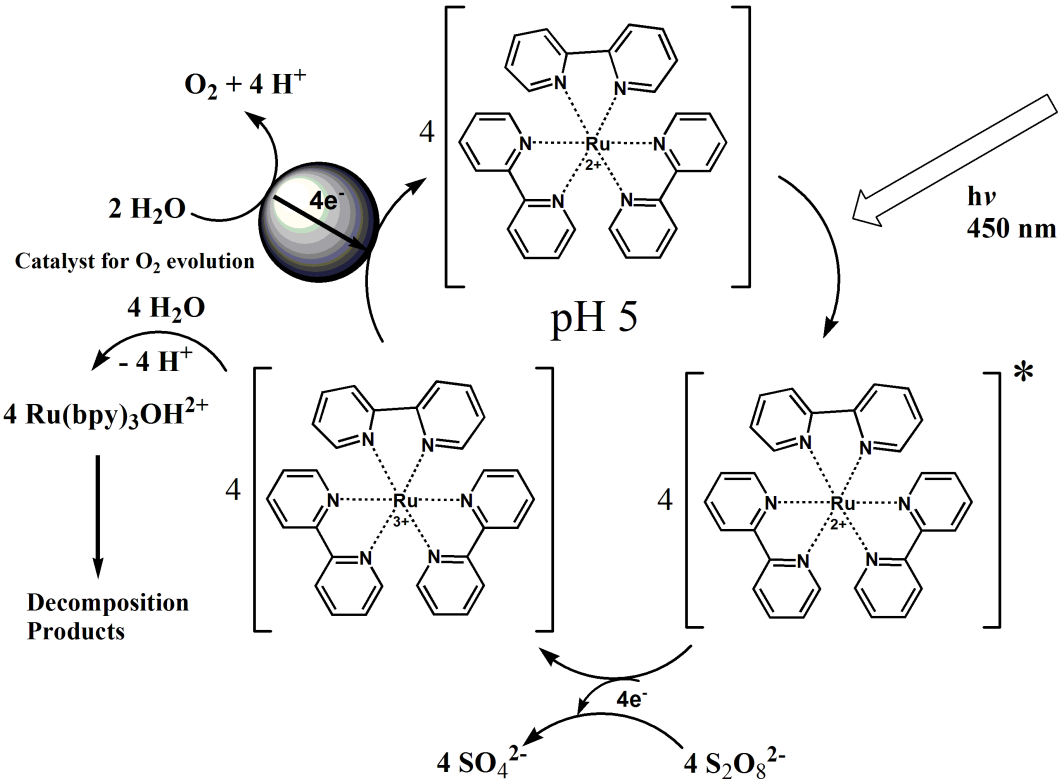

Figure 1: Photocatalytic oxidation of water by the $[Ru(bpy)_3]^{2+}$-catalyst system.[26]

As shown in the Figure 1, visible light is absorbed by $[Ru(bpy)_3]^{2+}$, and a metal-to-ligand charge transfer state is formed in the excited state of the dye, $[Ru(bpy)_3]^{2+}*$. This is then oxidized to $[Ru(bpy)_3]^{3+}$ by the sacrificial acceptor $S_2O_8^{2-}$. In presence of a catalyst such as RuO_2 or IrO_2, the photosensitizer can be recycled to the ground state and O_2 is produced as the reaction product. The

reaction proceeds at pH 5, but a change in pH reduces the rate of oxygen production.[26]

Comparative studies performed on Nafion-stabilized and citrate-stabilized $IrO_2 \cdot nH_2O$ colloids for O_2 evolution showed that there was higher quantum efficiency for Nafion-stabilized colloids than with those formed with citrate.[30] The high activity of these polyanion-stabilized colloids suggested the use of other polyanionic/polycationic stabilizers could increase the catalytic rate.[26] Further studies were focused on controlling the size of the IrO_2 colloids by using bidentate dicarboxylic (malonate and succinate) capping groups. Techniques such as transmission electron microscopy revealed that monodentate (acetate), tridentate (citrate), phosphonate, and diphosphonate ligands are less effective as stabilizers and lead to various degrees of colloidal aggregation. Formation of IrO_2 colloids stabilized by succinate groups form 2 nm IrO_2 colloidal particles that can catalyze the oxidation of water in persulfate-sensitizer solutions similarly to that of citrate stabilized colloidal suspensions.[31] The smaller size of the $IrO_2 \cdot nH_2O$ colloidal particles formed with succinate (2 nm vs. >100 nm) implies a more efficient use of iridium, i.e., a greater surface area to mass ratio. In the (succinate-$IrO_2 \cdot nH_2O$)-$Ru(bpy)_3$ system, the excited state of the sensitizer is quenched in 30 ns, indicating a good electronic coupling between the sensitizer and IrO_2. Other bidendate ligands such as phosphonate were tried as capping agents, but bidentate carboxylate groups showed better activity than phosphonate groups for binding to the surface of $IrO_2 \cdot nH_2O$ colloids.[31] These findings led to the design of bifunctional sensitizer molecules that had a dicarboxylic acid group for

attachment to the IrO_2 and a phosphonate groups for attachment to semiconductor surfaces like TiO_2; this would ultimately lead to the introduction of sensitizer-IrO_2 dyads into to the photochemical water splitting system.[31,32]

Yagi and coworkers showed that 50–100 nm diameter citrate stabilized IrO_2 colloids could be self-assembled on the surface of the indium tin oxide (ITO) electrodes when the electrode is dipped in a colloidal solution (pH 5.3). This self-assembly could be due to the chemical interaction between the carboxylic acid groups of the citrate molecules bound to the IrO_2 surface and hydroxyl groups of the ITO surface.[6,33] In the resulting films, about 16% of the Ir sites were active in catalyzing water oxidation, and, when poised at a potential of +1.3 V vs. Ag/AgCl, an average turnover (TO) frequency (mol of O_2/mol of Ir of ~6.6 s^{-1} (23 600 h^{-1}) was observed.[6]

Murray and coworkers studied 2 nm diameter IrO_2 nanoparticles formed without the use of stabilizing groups on glassy carbon electrodes at pH 13, formed without the use of stabilizing groups, both on the electrode surface and in solution. Their work has shown the need for only 0.15 V of overpotential for the onset of water oxidation and 100% current efficiency for the generation of O_2 from water at an overpotential of 0.29 V.[34,35]

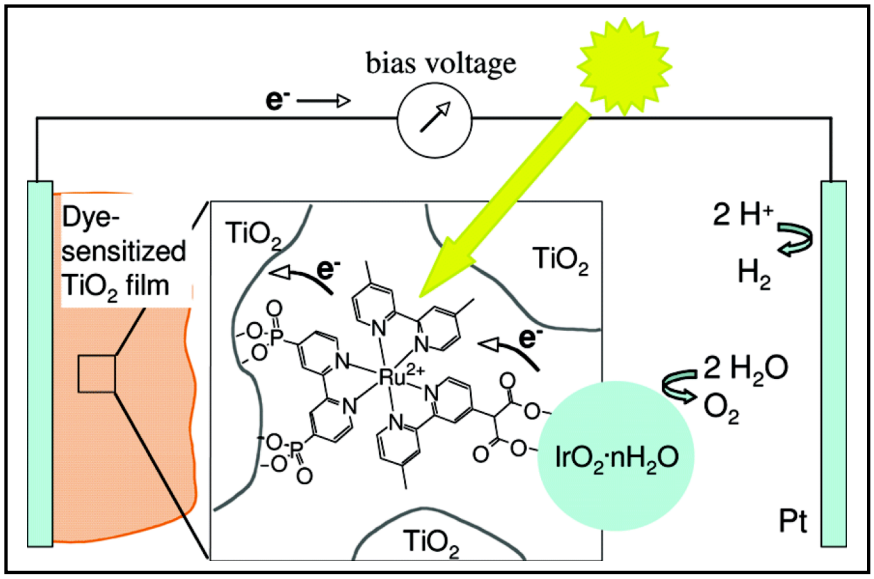

Figure 2: Schematic of a water splitting dye sensitized photoelectrochemical cell using a $[Ru(bpy)_3]$-$IrO_2{\cdot}nH_2O$ complex.[32]

Recently, our group in collaboration with T. E. Mallouk's group reported a photoelectrochemical cell that carries out visible light driven water splitting. In this system, the photoanode consists of the heteroleptic dye–$IrO_2{\cdot}nH_2O$ complex adsorbed to a TiO_2 layer on top of an FTO (fluorine-doped tin oxide) electrode.[32] When this photoanode is combined with a platinum cathode in a photoelectrochemical cell, it produces a photocurrent of 12.7 μA cm^{-2} upon illumination with 450 nm light at intensity of 7.8 mW cm^{-2} giving an internal quantum yield of 0.9%. The system has some limiting factors, such as slow electron transfer from the $IrO_2{\cdot}nH_2O$ catalyst to the oxidized dye. Transient

spectroscopic studies revealed electron transfer from the $IrO_2 \cdot nH_2O$ to the photo-oxidized dye (2.8 ms) to be about an order of magnitude slower than the back electron transfer from TiO_2 to the oxidized dye (0.37 ms). Additionally, there is bleaching of the $Ru(bpy)_3$ dye after ~2 h of illumination which could be due to the nucleophilic attack on the oxidized dye, limiting the durability of the system. The system also requires an applied bias to achieve overall water splitting.[32,36] Finally, the $Ru(II)(bpy)_3$ complexes used in this system absorb strongly in the blue region and cannot efficiently utilize light from the red region of the spectrum.[32]

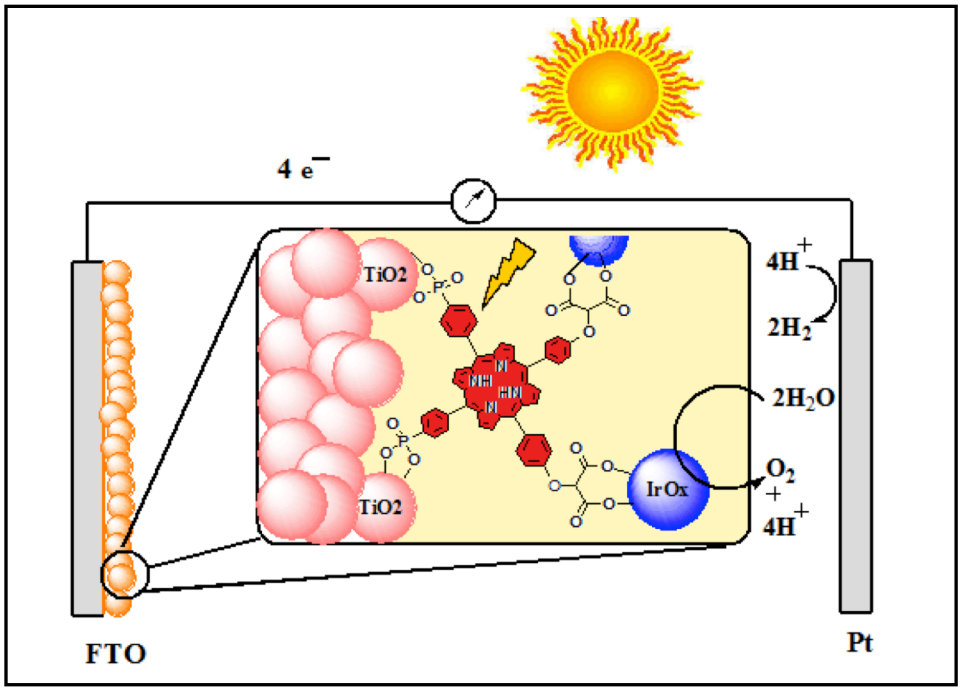

Figure 3: Schematic of the water splitting dye-sensitized solar cell using a porphyrin-$IrO_2 \cdot nH_2O$ complex.

The work outlined in this chapter marks a step forward to improving the stability, electron transfer rate, and spectral properties of the dye-$IrO_2 \cdot nH_2O$ complex by incorporating a porphyrin rather than a ruthenium-based dye. Porphyrins would better mimic natural photosynthesis as phorphyrin-based chromophores are used by plants and bacteria for capturing solar energy and converting it to chemical energy.[7] Porphyrins are used in dye-sensitized solar cells because it is easy to introduce different functional groups onto them synthetically, allowing for modulation of their photophysical properties.[29] Porphyrins have been shown to mimic photosynthesis by converting solar energy into chemical potential in the form of a long-lived charge separated state.[9] Porphyrins strongly absorb in the 400–450 nm region (Soret band) as well as in the 500–700 nm region (Q-bands), allowing them to utilize light from blue to the red region of the solar spectrum.[28]

The first step to developing the porphyrin-$IrO_2 \cdot nH_2O$ complex was the synthesis of a model compound having malonate and phosphonate groups to utilize in developing the synthetic methodology for the system. Developing the synthetic route for making the model compound would then be used for the synthesis of a porphyrin bearing phosphonate and malonate functional groups. Initially, a small molecule was be used to refine the synthetic method for forming the dye-$IrO_2 \cdot nH_2O$ complex. After successful synthesis of such model and demonstrating its ability to form $IrO_2 \cdot nH_2O$ colloids, the next step was the synthesis of a water-soluble porphyrin with four malonate groups. This molecule was used to form the porphyrin-$IrO_2 \cdot nH_2O$ complex that showed an

electrochemical catalytic response similar to other $IrO_2 \cdot nH_2O$ complexes reported in literature.[31] Fluorescence lifetime measurements were also performed indicating that the porphyrin fluorescence is quenched in the porphyrin-$IrO_2 \cdot nH_2O$ complex.[36]

The next step in constructing the target photoanode was to attach this porphyrin-$IrO_2 \cdot nH_2O$ complex to TiO_2. For this purpose, a new porphyrin was designed having malonate and phosphonate groups such that the malonate groups could attach to the $IrO_2 \cdot nH_2O$ to make stable colloids while the phosphonate group could attach to the TiO_2 surface. This porphyrin served both as a sensitizer, as well as a bridge to connect the $IrO_2 \cdot nH_2O$ catalyst to the metal oxide semiconductor.[32]

II. Model Compound

The work presented herein establishes a method to use porphyrins as stabilizers for the formation of $IrO_2 \cdot nH_2O$ colloidal solutions and demonstrate the use of this complex in a visible light driven photoelectrochemical water-splitting cell. We first describe the synthesis of the model compound-$IrO_2 \cdot nH_2O$ colloidal particles and then extend our work with porphyrins bearing malonate and phosphonate functional groups. It is expected that the colloidal particles formed by these stabilizers will be similar in structure to the iridium oxide complexes formed with ruthenium tris(2,2'-bipyridyl) sensitizers as demonstrated by Hoertz *et al.* [31]

1. Synthesis

The first approach was to synthesize a simple model compound bearing a malonate group and a phosphonate group on a benzene ring. This model compound was chosen to develop a synthetic methodology for attaching the malonate groups and the phosphonate groups and deprotecting their esters in presence of each other. The initial scheme for the synthesis involved the direct attachment of the malonate and the phosphonate groups on 1-bromo-4-iodobenzene via a coupling reaction using a palladium catalyst. The coupling reaction for attaching the phosphonate group gave very poor yields, while the coupling reaction to attach malonate group failed. Thus, the reaction scheme was modified by using 1,4-bis(bromomethyl)benzene as the starting material for the reaction.

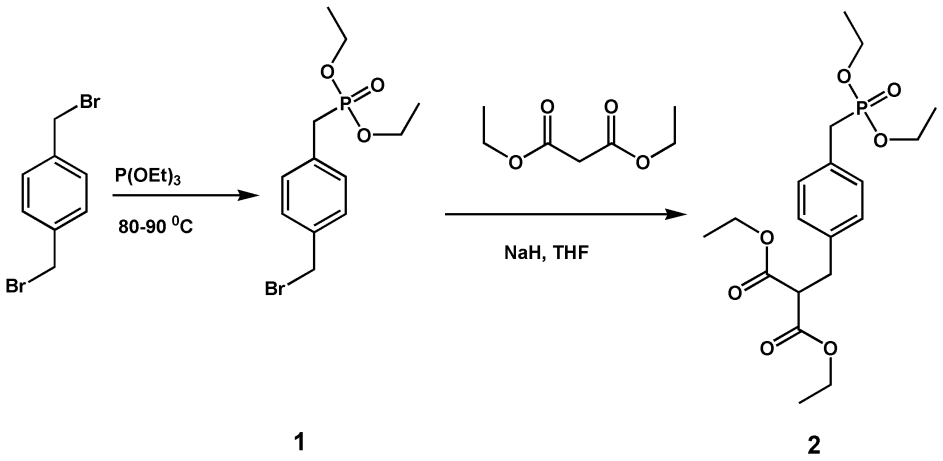

Scheme 1: Synthesis of model compound **2.**

The first step in the sequence was to attach the phosphonate group, which was achieved by heating 1,4-bis(bromomethyl)benzene with triethylphosphite to 80-90 ºC. The reaction was monitored by thin layer chromatography (TLC). After 3 h, a sufficient amount of mono-phosphonate was observed with some unreacted starting material.[37] The product was purified by column chromatography to give compound **1** in 62% yield. In the second step, a malonate group was attached by first treating the diethylmalonate with sodium hydride in THF to form a carbanion by abstraction of the acidic methylene hydrogen.[38] After stirring this reaction mixture for 30 min, compound **1** was slowly added and the mixture further stirred for 30 min. Analysis by TLC indicated that the reactant was consumed and there was formation of a more polar compound. The reaction mixture was quenched with ammonium chloride, and the desired product was extracted with ethyl acetate and further purified by using column chromatography to yield 84% of compound **2**.

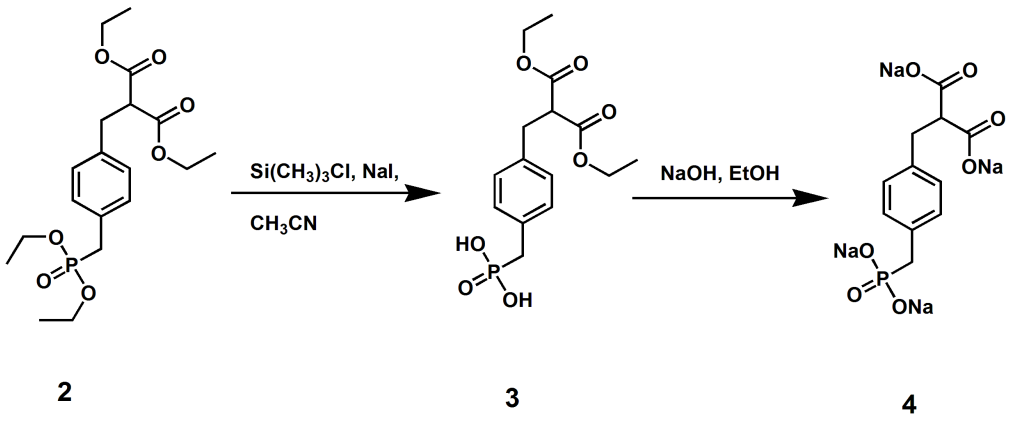

Scheme 2: Synthesis of model compound **4.**

The next step was the deprotection of both the malonate and phosphonate protecting groups. Phosphonic acids can be generated from their dialkyl esters by reaction with concentrated HCl or HBr, however these conditions were too harsh for many functional groups including the malonate groups. To find milder conditions for cleavage of the dialkyl groups, the Rabinowitz method, using chloromethylsilane (TMSCl) followed by hydrolysis, was followed with minor modifications.[39] Bromotrimethylsilane (TMSBr) can also be used to cleave the dialkyl groups, and it is reported in the literature that the yield can be further improved by adding sodium or lithium iodide. Compound **2** was deprotected by iodotrimethysilane, which was generated *in situ* by treating chlorotrimethylsilane with sodium iodide.[40] Hydrolysis of the reaction mixture was done with water, and the product was extracted with DCM to give 83% of compound **3**. Deprotection of the malonate ester group was tried using different conditions. In the first attempt, deprotection was carried out using KOH in THF at RT for 18 h, but the reaction did not go to completion. In the second successful attempt, the

compound was treated with sodium hydroxide in presence of ethanol and the reaction mixture was refluxed for 12 h.[41] The product was obtained as the sodium salt, which was filtered and washed with cold ethanol and dried under vacuum to yield 84% of compound **4**.

2. Results and discussion

Synthesis of the model compound **4**-$IrO_2 \cdot nH_2O$ complex resulted from heating a solution containing K_2IrCl_6 and model compound **4** in deionized water. After preparing a solution containing 6 mM of compound **4** and 1 mM K_2IrCl_6, the pH of the solution was adjusted to near pH 8 by the addition of NaOH. The resulting reddish brown solution was then heated on a hot plate with continuous stirring at 80–85ºC for approximately 40 mins. During the synthesis, the color of the solution gradually turns to orange, then light yellow, and then develops to light purple-blue color. The purple-blue solution is indicative of the formation of $IrO_2 \cdot nH_2O$ colloid.[31] This solution was allowed to cool to room temperature and basic conditions were maintained throughout the preparation. Figure 4 shows the absorption spectrum of the model compound **4**-$IrO_2 \cdot nH_2O$ colloid solution; the spectrum shows with an intense UV absorbance below 400 nm and a low, broad absorbance band centered at 580 nm that extends into the near-IR. According to the literature, the wavelength of maximum absorbance for the visible band is usually dependent on the identity of surface stabilizer, for succinate ~572 nm and malonate ~586 nm (reaction time >15 min).[32] Additionally, it is reported that the formation of small 2 nm $IrO_2 \cdot nH_2O$ particles, such as those formed using malonate, give purple colloidal solutions while larger (≥10 nm) colloidal particles, such as those formed using citrate, usually give blue colloidal solutions.[31]

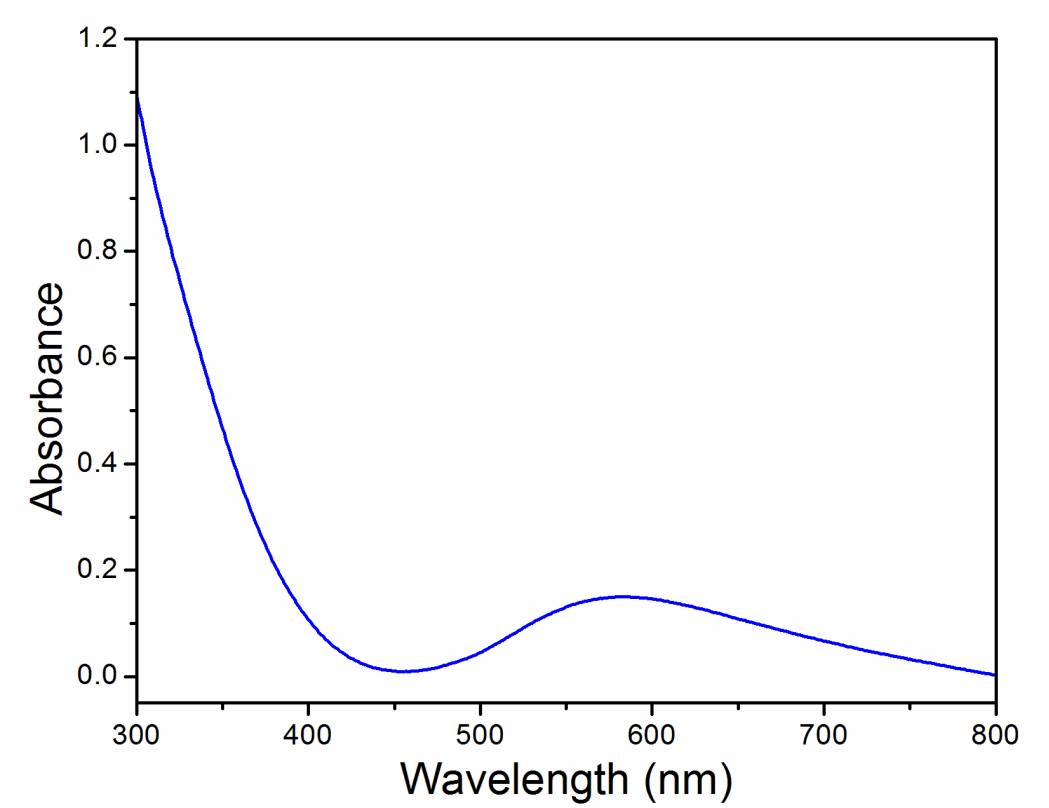

Figure 4: Absorption spectrum of model compound **4**-$IrO_2 \cdot nH_2O$ colloidal solution.

Cyclic voltammetry was performed on the compound **4**-$IrO_2 \cdot nH_2O$ colloid to study its electrochemical characteristics. Voltammograms taken of this preparation reveal the onset of strong anodic current near 1.1 V vs. Ag/AgCl, indicative of water oxidation. When poised at sufficiently positive potential, bubbles begin to form on the face of a glassy carbon electrode when immersed in a solution-containing compound **4**-$IrO_2 \cdot nH_2O$, again consistent with catalytic water oxidation. Comparison with a scan using a polished electrode in the absence

of any $IrO_2 \cdot nH_2O$ particles shows that the signal originates from the presence of the catalyst.

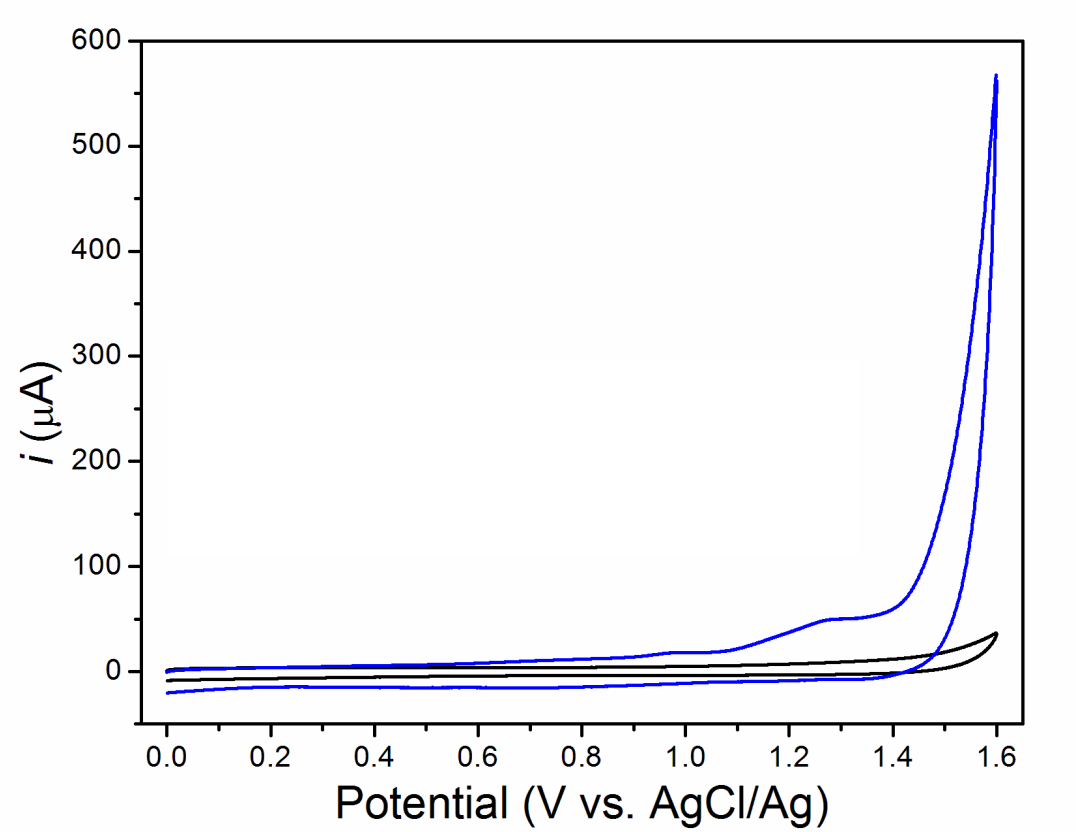

Figure 5: Comparison of cyclic voltammograms taken in solutions containing (blue) model compound **4**-$IrO_2 \cdot nH_2O$ and with only supporting electrolyte (black). All scans taken with a glassy carbon working electrode, at a scan rate of 100 mV/s, in solutions containing 0.1 M KNO_3 supporting electrolyte, and with voltages referenced to a Ag/AgCl electrode.

III. Porphyrin functionalized with malonate groups

1. Synthesis

The success in developing the model compound-$IrO_2.nH_2O$ colloidal solution led us to the next step of switching the model compound **4** for a porphyrin containing malonate groups at the para position of the four *meso* phenyl groups. The malonic acid functional group allowed the porphyrin to be completely soluble in water, an essential property for incorporating a porphyrin dye into this system. Compound **5** the precursor for porphyrin **6**, was synthesized by a modified version of Bookser and Bruice's method. For easier work up, chlorobenzene was used in place of toluene.[42]

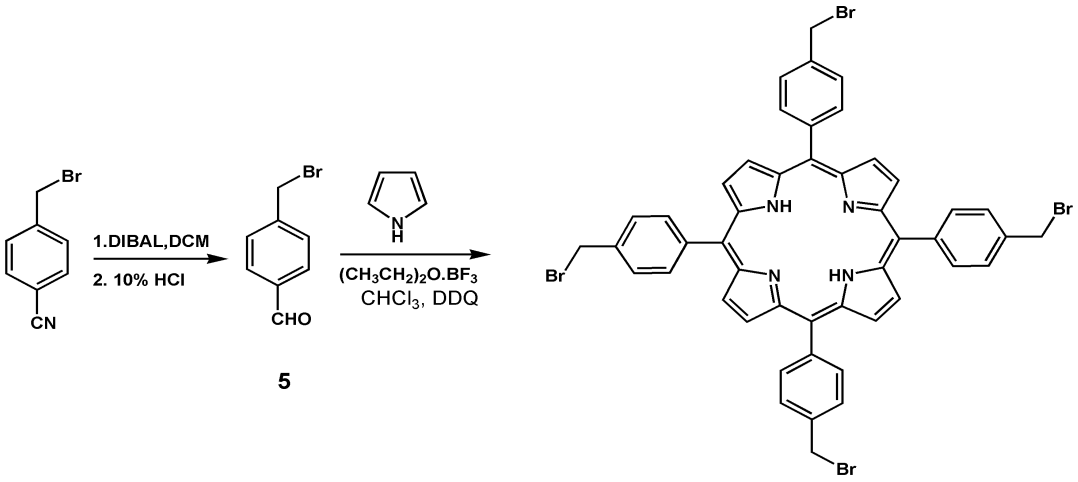

Scheme 3: Synthesis of porphyrin **6.**

Porphyrin **6** was synthesized by condensation of compound **5** with pyrrole in presence of $BF_3.(OEt)_2$ as catalyst. The condensation, followed by oxidation

with DDQ, gave a 28% yield of porphyrin 5,10,15,20-tetra(4-bromomethylphenyl)porphyrin.[42]

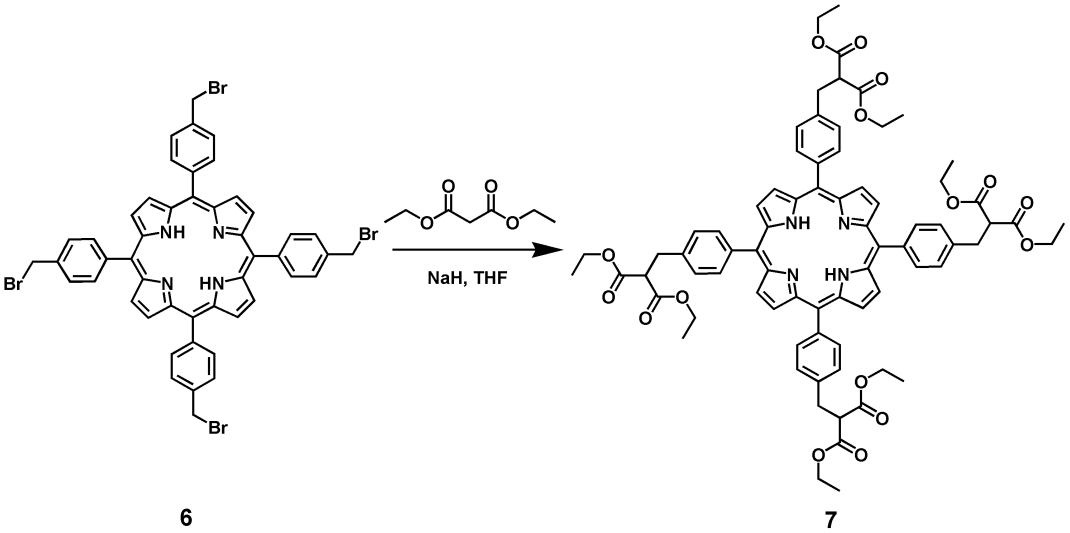

6 7

Scheme 4: Synthesis of porphyrin **7.**

The malonate groups were incorporated using the methodology established for the model compound to give a 45% yield of porphyrin **7**.[41] The hydrolysis of the malonate ester groups was achieved by refluxing porphyrin **7** with sodium hydroxide in ethanol. After 15 h of reflux, the sodium salt form of the porphyrin was obtained with an 89% yield. The octasodium salt of porphyrin **9** obtained was completely water-soluble and was characterized by H^1NMR and MALDI-TOF-MS.

Palladium was inserted into the porphyrin after the incorporation of the malonate groups as the palladium chloride was found to react with the benzyl bromide precursor to give undesired compounds that could not be characterized. Palladium insertion was achieved by treating the porphyrin **7** with palladium (II)

chloride in DMF for 1 h at 55ºC, the reaction was monitored by UV-Vis spectroscopy.[43] The malonate ester deprotection was performed in a similar manner as described for compound **7**.

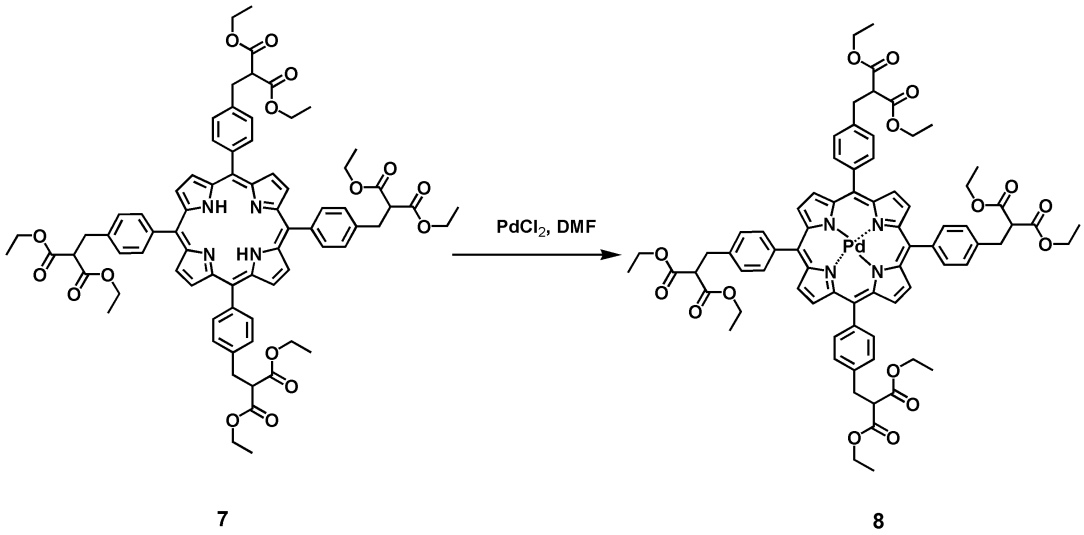

Scheme 5: Synthesis of porphyrin **8.**

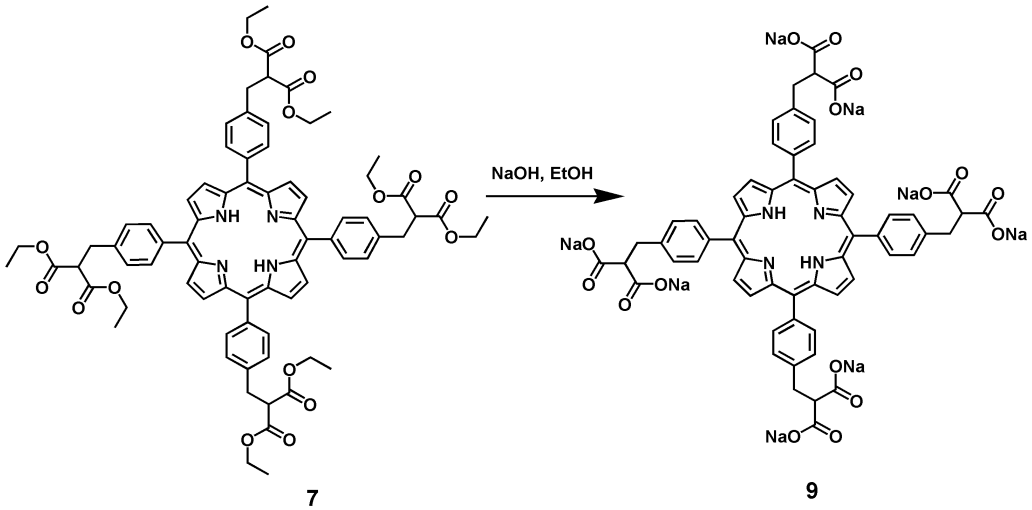

Scheme 6: Synthesis of porphyrin **9.**

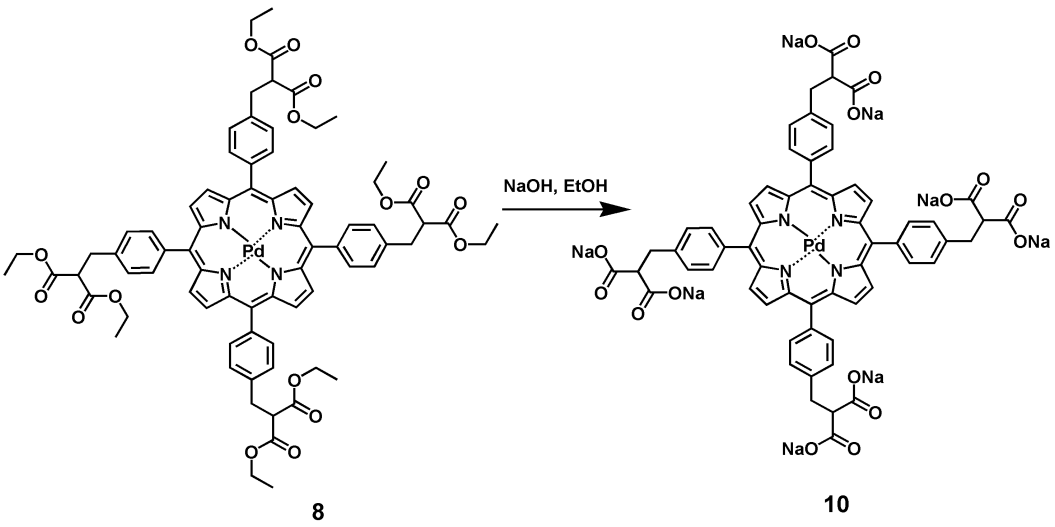

Scheme 7: Synthesis of porphyrin **10.**

2. Results and discussion

The porphyrin-$IrO_2{\cdot}nH_2O$ colloidal solution was prepared with slight modifications from the model compound. To form the colloid complex, an aqueous solution containing K_2IrCl_6 and porphyrin was heated at 35ºC for 2–3 days under basic conditions. Size exclusion column chromatography was preformed on some of the preparations to remove salts and unused starting material. The final color of the porphyrin-$IrO_2{\cdot}nH_2O$ colloid was pale yellow. The colloidal solutions were stored under mildly basic conditions and were stable for several months at room temperature.

A typical voltammogram performed on solutions containing the porphyrin-$IrO_2{\cdot}nH_2O$ complex revealed the onset of strong anodic current near 1.1 V vs. Ag/AgCl, indicative of water oxidation. Poising the working electrode at sufficiently positive potentials causes the generation of bubbles at the electrode

surface in solutions containing the porphyrin-$IrO_2 \cdot nH_2O$. Figure 6 shows an overlay of several voltammograms performed in the presence of $IrO_2 \cdot nH_2O$ catalysts. The various $IrO_2 \cdot nH_2O$ complexes give comparable voltammograms, with strong anodic signals indicative of water oxidation. Comparison with the scan in the absence of any $IrO_2 \cdot nH_2O$ clearly shows the signal originates from the catalyst. It should be noted that Figure 6 is not intended as a quantitative comparison between the various $IrO_2 \cdot nH_2O$ complexes as the concentration and likely the size of the colloid was different in each case, but rather as a means of demonstrating that the behavior of the porphyrin-$IrO_2 \cdot nH_2O$ complexes is similar to that of the carboxylic acid (malonate or citrate) stabilized $IrO_2 \cdot nH_2O$ complexes described in the literature.

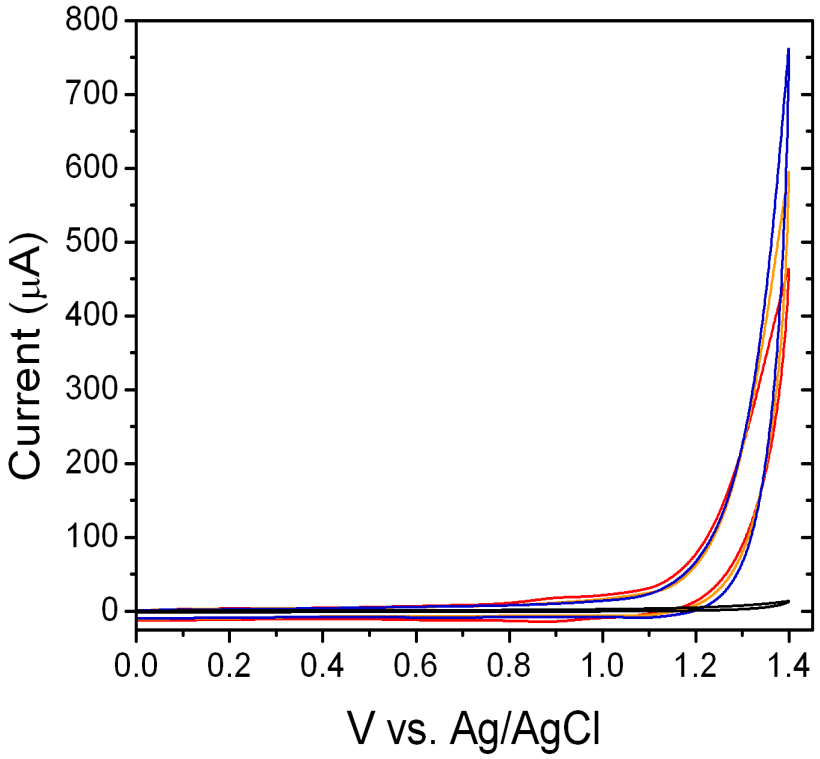

Figure 6. Comparison of cyclic voltammograms taken in solutions containing (red) porphyrin **9**-$IrO_2 \cdot nH_2O$, (orange) porphyrin **10**-$IrO_2 \cdot nH_2O$, (blue) malonate-$IrO_2 \cdot nH_2O$ and only supporting electrolyte (black). All scans taken with a glassy carbon working electrode, at a scan rate of 100 mV/s, with voltages referenced to a Ag/AgCl electrode. The solutions contained $IrO_2 \cdot nH_2O$ colloidal catalyst at different concentrations and the currents observed should not be taken as a quantitative comparison of catalytic activity.

In order to demonstrate that the observed catalytic signal corresponds to the oxidation of water to O_2, a Clark electrode was employed to monitor the O_2

concentration in the solution during the electrochemical measurements. After purging the cell of O_2 by bubbling with argon, the cell was sealed and the O_2 concentration was monitored while poising the glassy carbon working electrode at various potentials vs. Ag/AgCl (Figure 7). With porphyrin **10**–$IrO_2 \cdot nH_2O$ in solution, the O_2 concentration does not increase with time at 0.6 V vs. Ag/AgCl, but does increase at 1.4 V. When the same working electrode is used in a solution containing only supporting electrolyte and no catalyst no increase in O_2 occurs at either 0.6 or 1.4 V vs. Ag/AgCl. Thus, oxygen is produced only in the presence of the catalyst at a suitable potential.

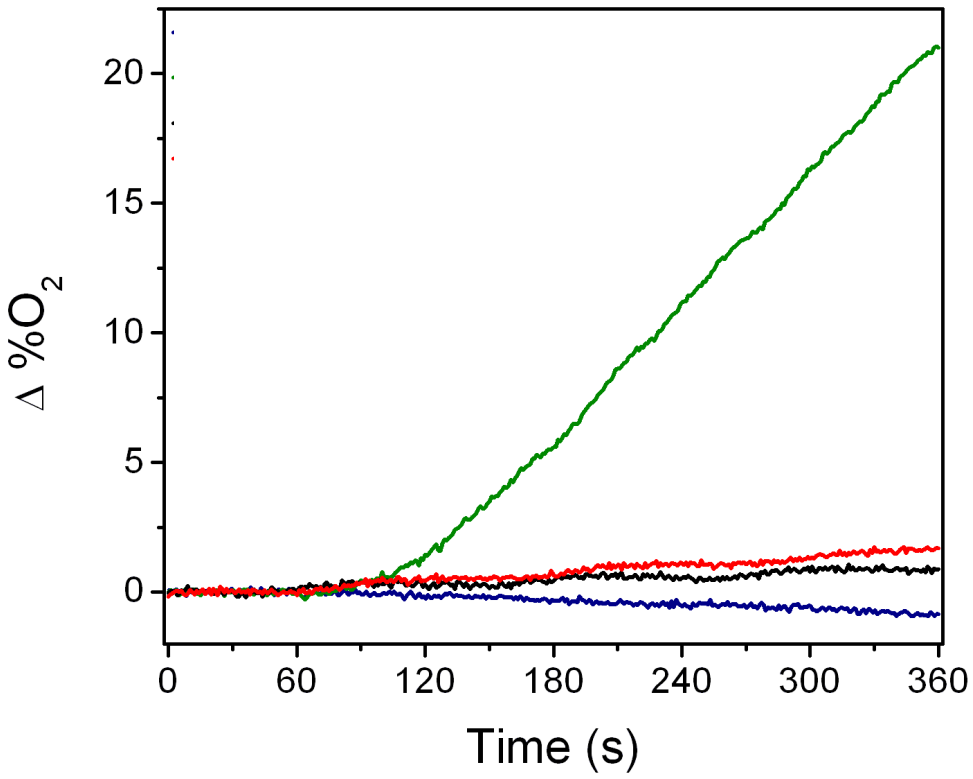

Figure 7: Oxygen concentration relative to air-saturated water measured with a Clark electrode. Porphyrin **10**-$IrO_2 \cdot nH_2O$ (green), glassy carbon working electrode poised at 1.4 V vs. Ag/AgCl, porphyrin **10**-$IrO_2 \cdot nH_2O$ (blue), glassy carbon working electrode poised at 0.6 V vs. Ag/AgCl and buffer only (black), glassy carbon working electrode poised at 0.6 V vs. Ag/AgCl, buffer only (red), and glassy carbon working electrode poised at 1.4 V vs. Ag/AgCl. All measurements were taken in H_2O at pH 6.95 with 0.1 M KNO_3 and 0.1 M phosphate buffer. Potential applied starting at t = 60 sec.

To probe the interaction between the porphyrin dye and the $IrO_2 \cdot nH_2O$, the porphyrin fluorescence lifetime in the porphyrin-$IrO_2 \cdot nH_2O$ complex was measured and compared with that of the porphyrin dissolved in a solution containing malonate-$IrO_2 \cdot nH_2O$. As shown in Figure **8**, the fluorescence lifetime of the free base porphyrin **9** in the presence of malonate-$IrO_2 \cdot nH_2O$ was 8.79 ns, which is typical for a freebase porphyrin of this general type. The fluorescence lifetime of the same porphyrin in complex with $IrO_2 \cdot nH_2O$ was quenched, with the major lifetime component of 46.7 ps (70.4%) and minor components with lifetimes of 316.9 ps (18.6 %), 1.81 ns (9.1%), and 7.09 ns (1.9%). These findings indicate that different populations of porphyrin molecules in the material experience different interactions with the $IrO_2 \cdot nH_2O$. The dominant short fluorescence lifetime component implies a significant interaction between the porphyrin and the $IrO_2 \cdot nH_2O$ particle. Quenching of the porphyrin fluorescence could occur by energy transfer, electron transfer, enhanced intersystem crossing, or some combination of these; the exact mechanism has not been assigned.

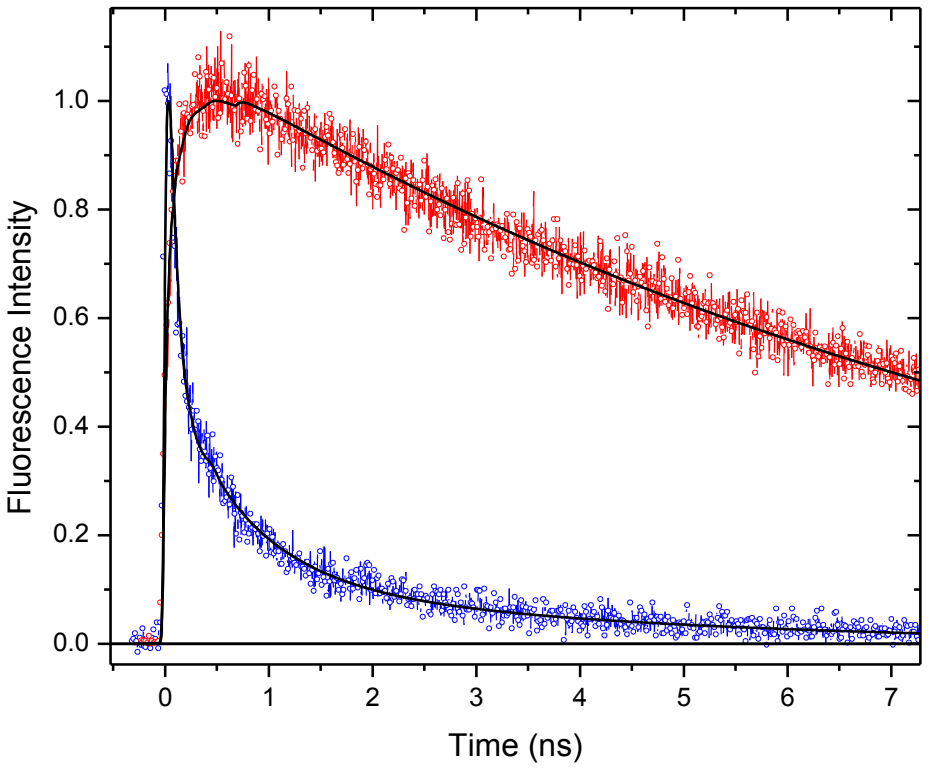

Figure 8. Porphyrin fluorescence lifetime measurements. Porphyrin **9** (red) in solution with malonate-stabilized $IrO_2 \cdot nH_2O$, lifetime 8.79 ns. Porphyrin **9**–$IrO_2 \cdot nH_2O$ (blue) colloidal particles, major component lifetime 46.7 ps.

In these photoanodes, the driving force for electron transfer from the $IrO_2 \cdot nH_2O$ catalyst to the sensitizer is provided by the electrochemical potential for the reduction of the porphyrin radical cation. Figure 9 shows cyclic voltammograms of free base porphyrin **7** and its Pd analog, porphyrin **8**. As seen in Table 1, the addition of Pd increases the potential for the first oxidation by ~160 mV.[36]

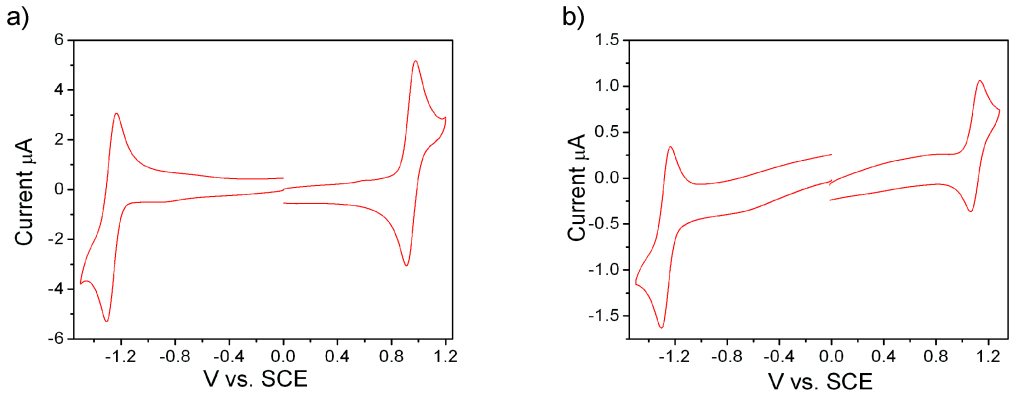

Figure 9. Cyclic voltammograms of (a) porphyrin **7** and (b) porphyrin **8**. Voltammograms were taken with a platinum working electrode, in benzonitrile with 0.1 M tetrabutylammonium hexafluorophosphate and at a scan rate of 100 mV/s.

Table 1. Electrochemical potentials for **7** and **8**

Porphyrin	1^{st} ox V vs. SCE	ΔE_p 1^{st} ox mV	1^{st} red V vs. SCE	ΔE_p 1^{st} red mV
(**7**)	0.94	67	–1.28	75
(**8**)	1.10	72	–1.28	71

ΔE_p: difference between anodic and cathodic peak potentials of the CV. Scan rate: 100 mV/s.

IV. Porphyrin functionalized with malonate and phosphonate groups

Having demonstrated the ability to form the porphyrin-$IrO_2 \cdot nH_2O$ complex, this project moved to incorporating porphyrins bearing malonate and phosphonate groups for the immobilization of the complex on TiO_2 semiconducting films. Along these lines, the first goal was to synthesize a porphyrin bearing phosphonate groups and a malonate groups. As mentioned earlier, phosphonates are chemically selective for attaching to TiO_2 while malonate groups show greater selectivity for $IrO_2.nH_2O$ surface.

1. Synthesis

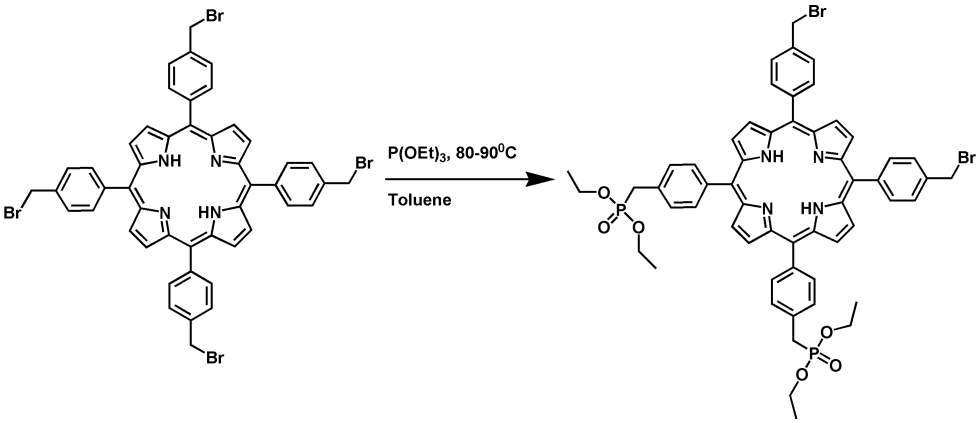

Scheme 8: Synthesis of porphyrin **11.**

Porphyrin **6** was available from the synthesis of porphyrin **7** mentioned above, so the reaction scheme was designed accordingly. The phosphonate groups were incorporated as described for the model compound **4**, except that in this case

there were four active benzyl bromide groups present. A mixture of porphyrins was obtained from this reaction, from which the desired porphyrin **11** was separated by column chromatography in 6.2% yield. Malonate groups were then attached to give porphyrin **12** with a 28% yield. Palladium was inserted in porphyrin **12** as described for porphyrin **8** to give porphyrin **13** with a 76% yield.

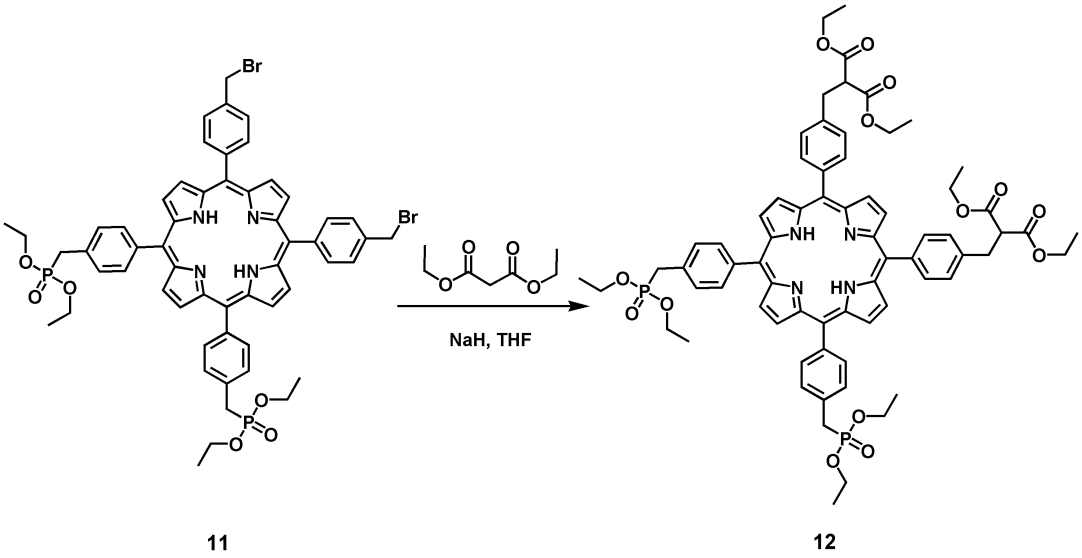

11 12

Scheme 9: Synthesis of porphyrin **12**.

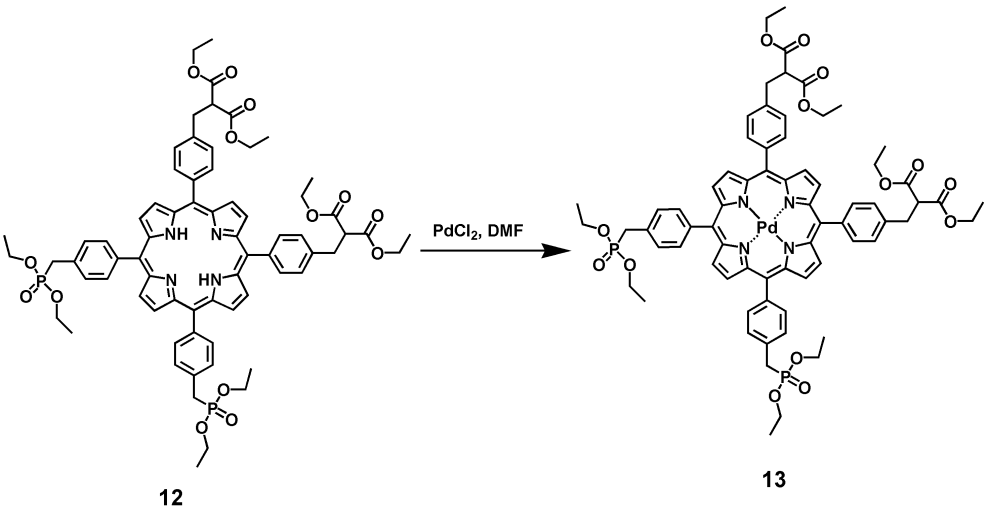

12 13

Scheme 10: Synthesis of porphyrin **13**.

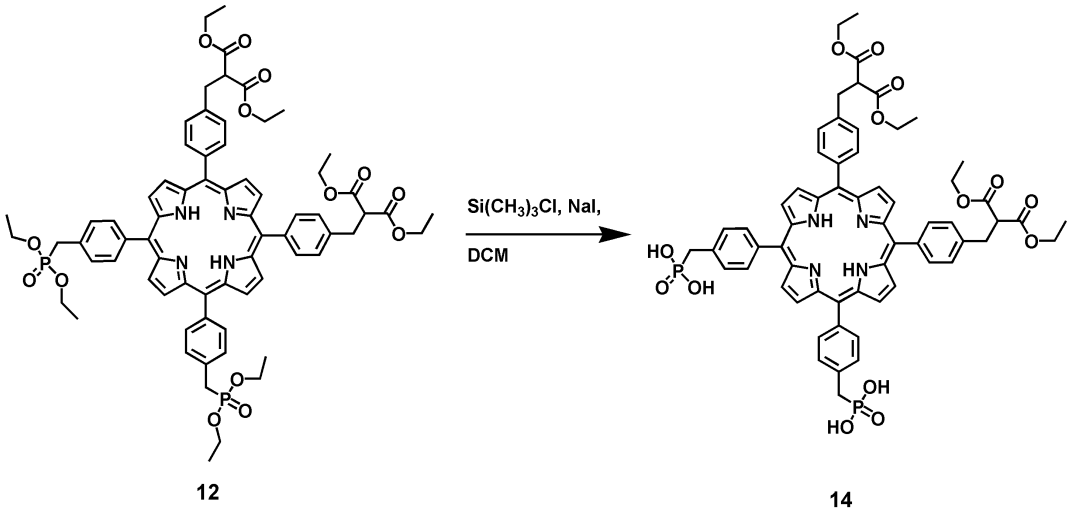

Scheme 11: Synthesis of porphyrin **14**.

The next step was the deprotection of the phosphonate group by chorotrimethylsilane in presence of sodium iodide to give porphyrin **14** as described for the model compound **4**. The last step was the deprotection of the malonate ester, which gave 77% of the desired product as the sodium salt form as porphyrin **15**. The product was completely soluble in water and was characterized by H^1NMR and MALDI-TOF-MS.

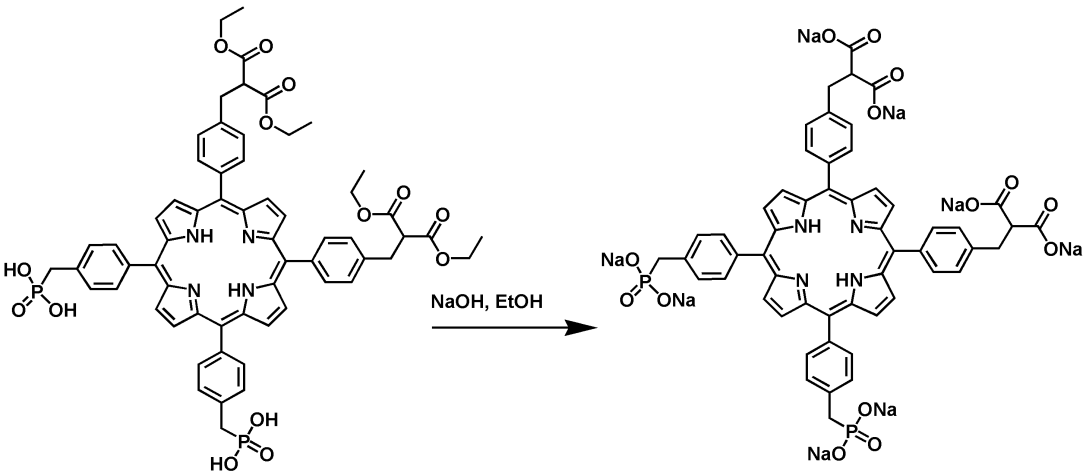

14 15

Scheme 12: Synthesis of porphyrin **15**.

With the aim of increasing the driving force for the electron transfer between $IrO_2 \cdot nH_2O$ and the porphyrin radical cation, the next goal was to synthesize a water soluble high potential porphyrin containing malonate and phosphonate groups. For this purpose a porphyrin was designed with phosphonate and malonate groups at the 5 and 15 positions of the porphyrin ring and pyridyl functional groups at the 10 and 20 positions.[44]

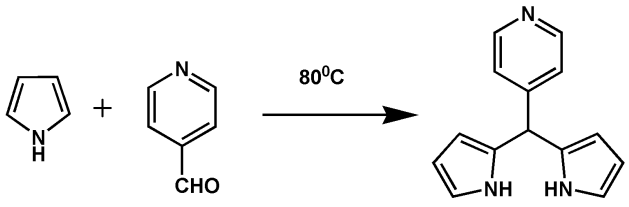

16

Scheme 13: Synthesis of compound **16**.

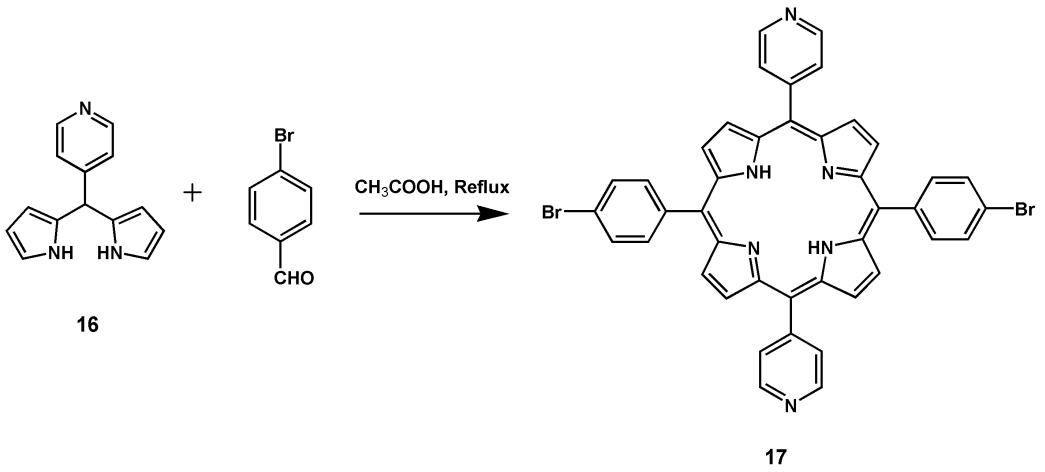

Scheme 14: Synthesis of compound **17**.

For the synthesis of this porphyrin the first requirement was the preparation of compound **16** is used as the starting material. Compound **16** was synthesized by stirring 4-pyridinecarboxaldehyde and pyrrole for 15 h at 85°C. Evaporation of the excess pyrrole, followed by chromatography, afforded a 48% yield of dipyrromethane **16**. The next step was the synthesis of the porphyrin by the Adler Longo method. This was done by refluxing compound **16** with 4-bromobenzaldehyde in propionic acid for 1 h. The desired product, porphyrin **17**, was obtained in a 3.8% yield after column chromatography.[44]

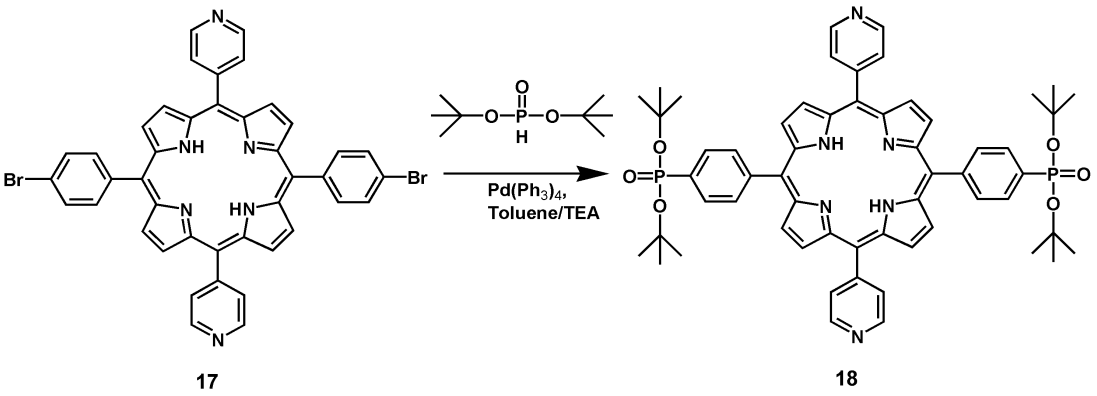

Scheme 15: Synthesis of porphyrin **18.**

The attachment of the phosphonate group was carried out by a palladium mediated coupling reaction, with the intention of obtaining the mono phosphonate porphyrin. Unfortunately, the reaction gave only di-substituted product.[39] Therefore, the reaction scheme was modified by incorporating the phosphonate group before the porphyrin synthesis. This was done by synthesizing the 4-(di-tert-butyloxyphosphoryl)benzaldehyde by a Pd-mediated coupling reaction of 4-bromobenzaldehydedimethylacetal. The *tert*-butyl protecting groups were not stable under the conditions used for the porphyrin synthesis (refluxing in propionic acid); therefore, this reaction was retried using ethyl groups as a protecting group for the phosphonates.[39]

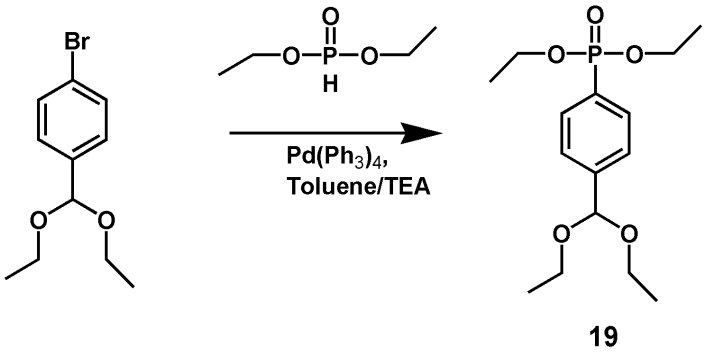

Scheme 16: Synthesis of compound **19.**

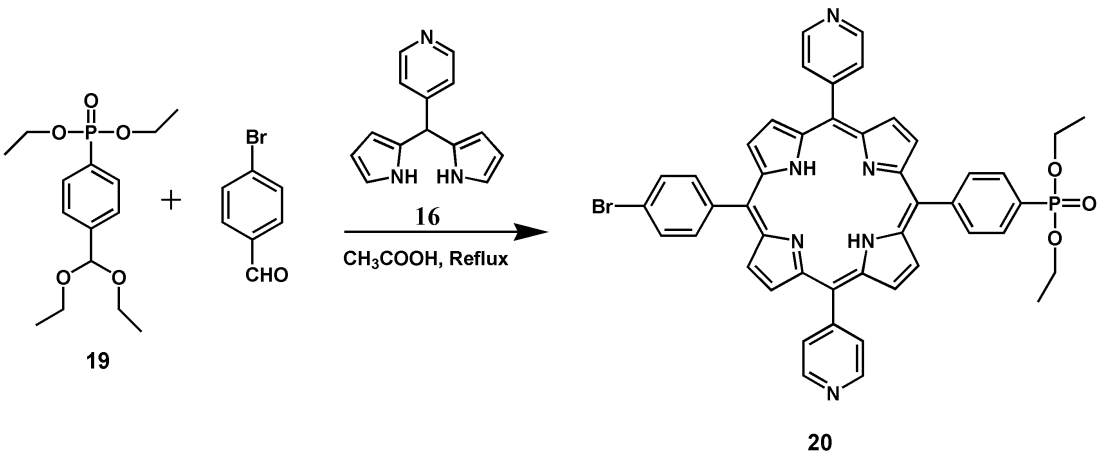

Scheme 17: Synthesis of porphyrin **20.**

The next step was to attach a malonate group and this was attempted by a Pd-mediated coupling reaction without any success. From the previous synthesis, it was clear that the attachment of the phosphonate group was comparatively easier than the attachment of the malonate group. Therefore, the challenge was to attach a malonate group to the pyridyl porphyrin. From the literature it was evident that the malonate group could be attached to a pyrridyl porphyrin via an ether linkage. A problem in designing the scheme was the necessity to perform

the deprotection of the phosphonate ester with chlorotrimethylsilane and sodium iodide, and there were concerns that this reagent might cleave the ether bond linking the porphyrin and the malonate.

The first step was the etherification of 4-hydroxybenzaldehyde, which was achieved by reacting 4-hydroxybenzaldehyde with diethyl bromomalonate in presence of sodium hydroxide, to yield 65% of diethyl-2-(4-formylphenoxy)malonate compound **21.**[45]

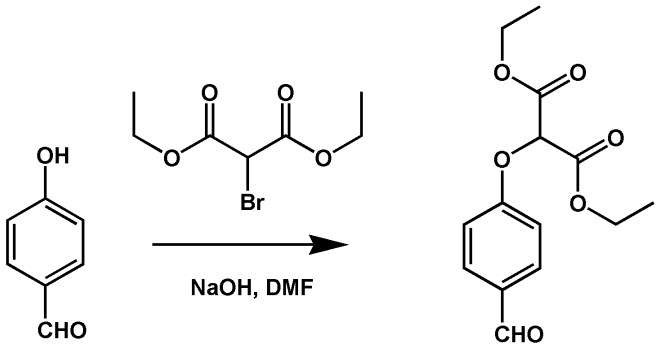

21

Scheme 18: Synthesis of compound **21.**

The second step was the synthesis of the porphyrin which was performed by Lindsey method.[46] During the synthesis, triethylorthoacetate was added in the reaction mixture as it has been reported in the literature to act as a moderately effective water scavenger and thereby increasing the extent of benzaldehyde-pyrrole bond formation. When triethylorthoacetate was added after 1 h, the

reaction yield increased.[46] The oxidation was completed by the addition of DDQ to yield 2% of the desired porphyrin **22**.

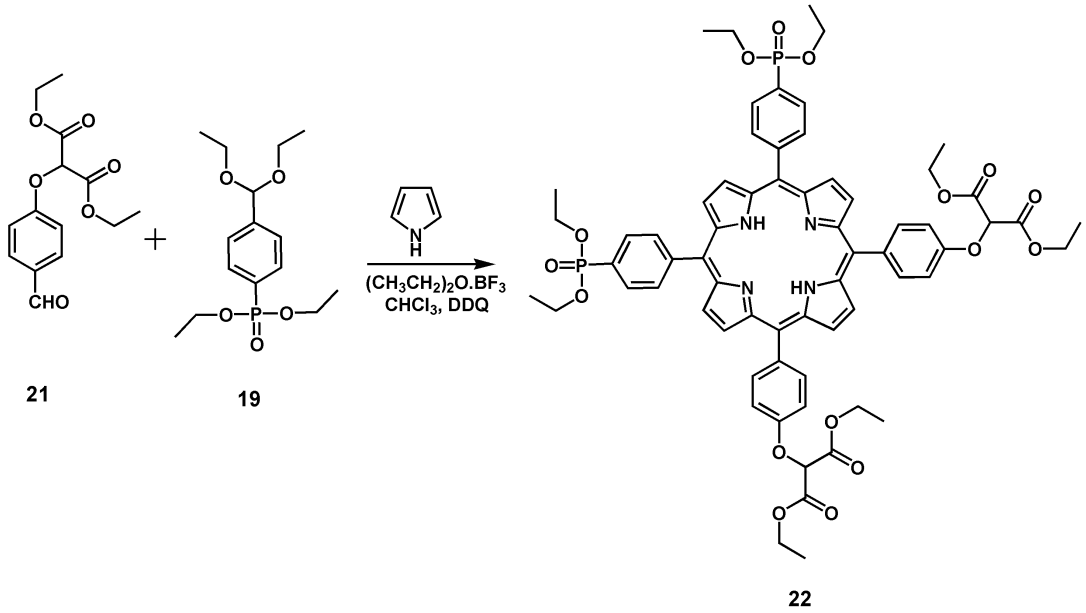

Scheme 19: Synthesis of porphyrin **22**.

The deprotection of the phosphonate group was carried out with chlorotrimethylsilane and sodium iodide and the reaction was monitored by MALDI-TOF-MS. It was observed that if the reaction was allowed to proceed for long periods of time, the malonate groups were cleaved from the porphyrin.

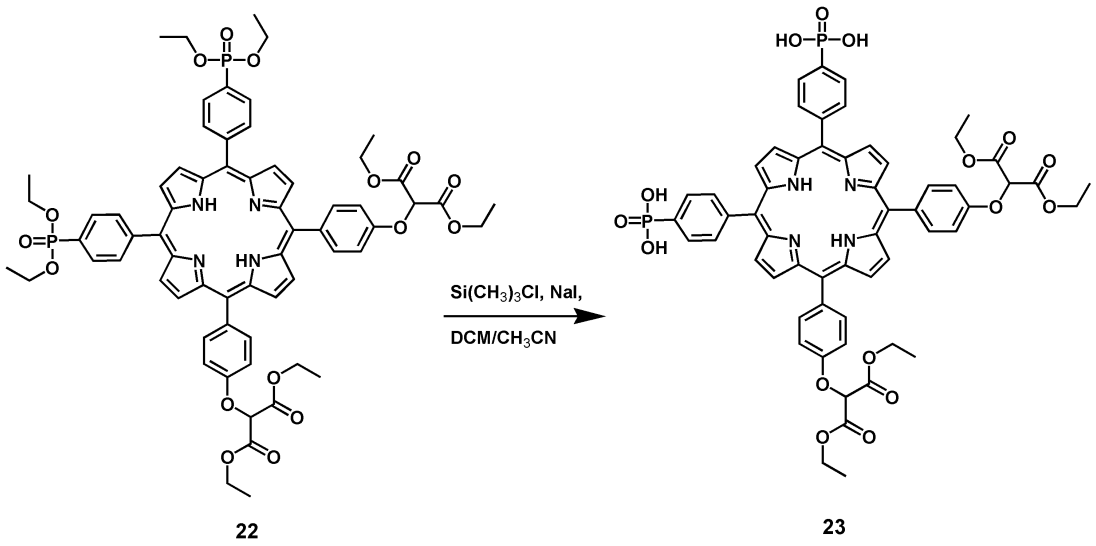

22 23

Scheme 20: Synthesis of porphyrin **23.**

The malonate ester was deprotected according to literature procedure.[45] The desired compound was completely water-soluble and was obtained in 82% yield as the potassium salt, porphyrin **24**.[45] The compounds were characterized by H^1NMR and MALDI-TOF-MS.

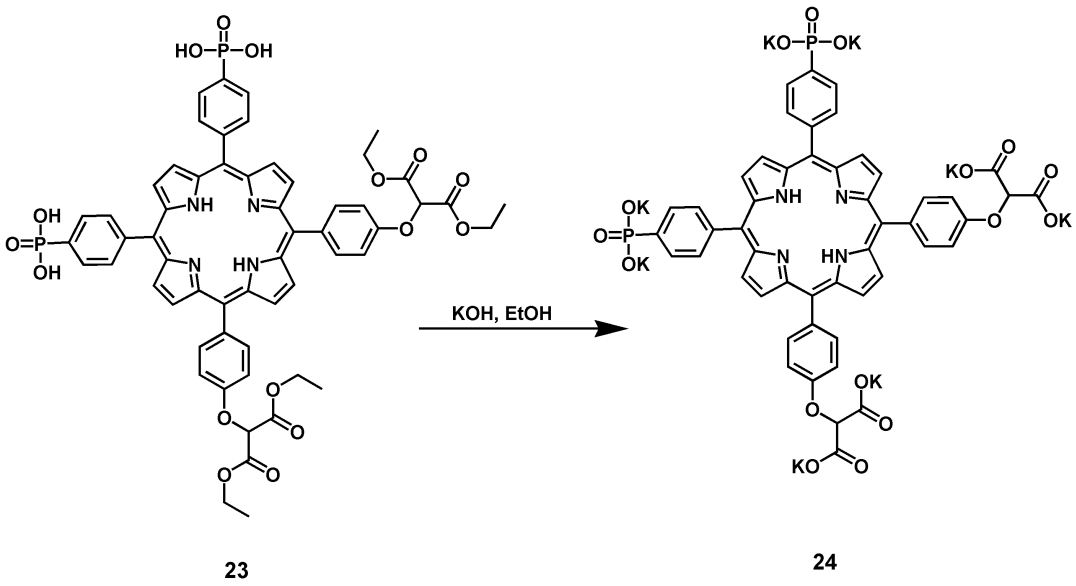

23 24

Scheme 21: Synthesis of porphyrin **24.**

2. Results and discussion

Various methods for forming the porphyrin-$IrO_2 \cdot nH_2O$ complex and then adsorbing this complex onto TiO_2 are being pursued. The most direct method for forming the $IrO_2 \cdot nH_2O$ colloid with porphyrin **24** and then adsorbing the complex to a TiO_2 electrode, has not yielded films containing sufficient amounts of the dye-$IrO_2 \cdot nH_2O$ complex to give appreciable photocurrent. One likely reason for this is that, though porphyrin **24** does stabilize the formation of the $IrO_2 \cdot nH_2O$, the resulting colloids are quite dilute and do not produce sufficiently dense films on TiO_2. A much more desirable method for forming the porphyrin-$IrO_2 \cdot nH_2O$ complex would be to form $IrO_2 \cdot nH_2O$ colloids without strong surface stabilizing groups and then introduce the porphyrin on the $IrO_2 \cdot nH_2O$ surface via a

stabilizing group. Our collaborators at Tom Mallouk's lab at Pennsylvania State University have developed such a method. Briefly, $IrO_2 \cdot nH_2O$ colloids are formed at pH 13 and then the pH is decreased by the rapid introduction of nitric acid. This results in a stable colloidal suspension of $IrO_2 \cdot nH_2O$ at neutral pH that showed a propensity to adsorb porphyrin **24** on the $IrO_2 \cdot nH_2O$ surface.

Using a porphyrin **24**-$IrO_2 \cdot nH_2O$ suspension provided to our lab by our collaborators, we have demonstrated the immobilization of the complex on a TiO_2 electrode and shown photocurrent indicative of light driven water oxidation. To form the electrode, an annealed film of anatase TiO_2 on FTO glass is soaked overnight in a solution containing the porphyrin **24**–$IrO_2 \cdot nH_2O$ complex. Figure 10 shows the absorption spectra of a TiO_2 after soaking in the solution of porphyrin **24**-$IrO_2 \cdot nH_2O$. The feature near 425 nm correlates to the Soret band of the porphyrin, demonstrating the attachment of porphyrin-$IrO_2 \cdot nH_2O$ complex on the surface of the electrode.

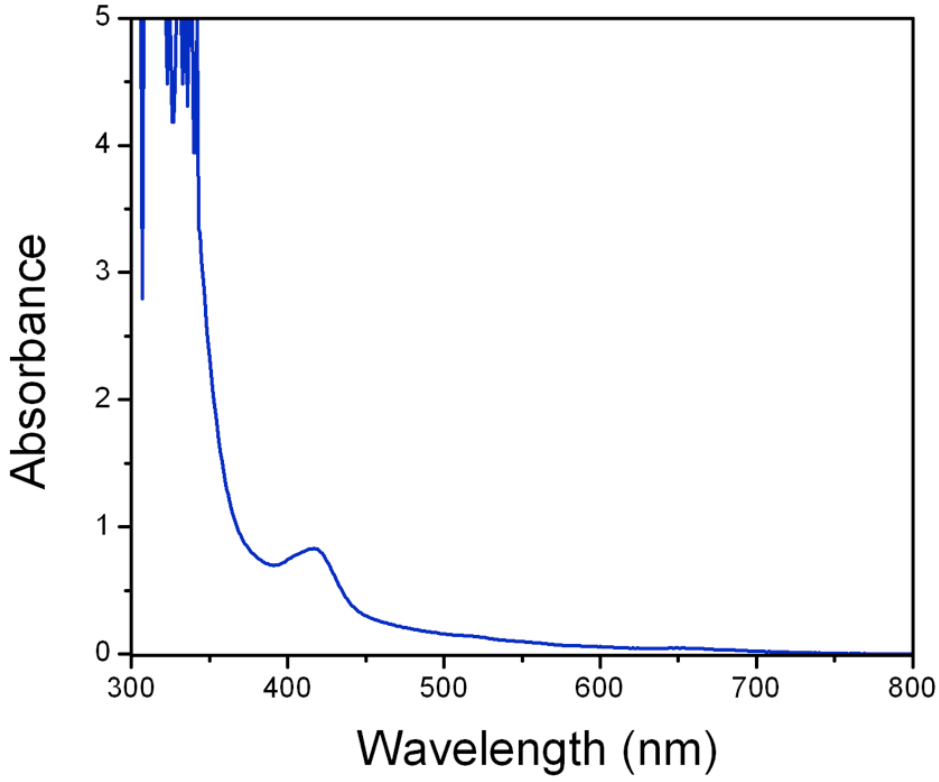

Figure 10: Absorption spectra of an FTO–TiO_2-porphyrin **24**-$IrO_2 \cdot nH_2O$ electrode.

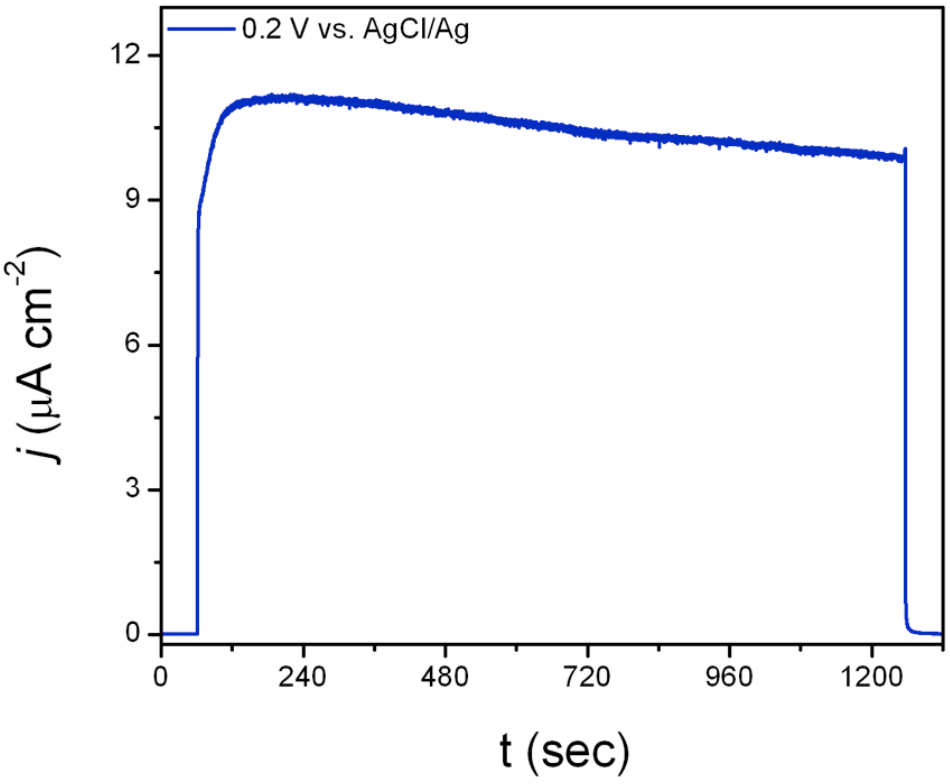

Figure 11: Photocurrent trace with the working electrode poised at 0.2 V vs. AgCl/Ag.

To test the ability of the FTO–TiO_2–porphyrin **24**–$IrO_2 \cdot nH_2O$ construct to carry out light driven water oxidation, this electrode was used with a Pt counter electrode to form a photoelectrochemical cell such as that shown in Figure 3 of this chapter. Figure 11 shows a typical photocurrent trace taken with such a cell. For this measurement, illumination was provided by a Xe arc lamp along with an AM 1.5 filter; and the cell was positioned to receive a light intensity of 100 mW cm^{-2} to best mimic solar light. The first 60 seconds of the trace were taken in the

dark to establish the level of the dark current, and cell was illuminated from 60 to 1260 sec of the trace. The large increase in the current during illumination arises from the oxidation of water by the $IrO_2 \cdot nH_2O$ catalyst as it is driven by photo-induced formation of the porphyrin radical cation. Similar to the system using a $Ru(bpy)_3$ dye, this cell needs ~200 mV of applied potential to achieve maximum photocurrent densities.

V. Conclusion

We have investigated the use of porphyrins containing carboxylate and phosphonate anchoring groups to construct a photoelectrochemical cell containing a porphyrin-$IrO_2 \cdot nH_2O$ complex immobilized on a TiO_2 electrode. The porphyrin was designed to incorporate bidentate carboxylic acid functional groups, which are known to interact with the $IrO_2 \cdot nH_2O$ surface. In this study we used a porphyrin-based stabilizer in the formation of $IrO_2 \cdot nH_2O$ colloidal particles and have demonstrated catalytic electrochemical water oxidation by this complex using visible light. The research presented here is a step towards the synthesis of a porphyrin-$IrO_2 \cdot nH_2O$ complex incorporating a high potential porphyrin that can be obtained by modifying the functional groups attached to the porphyrin. Future work would include the synthesis of pyridyl-functionalized porphyrin with malonate and phosphonate groups attached as described in this chapter.

VI. Experimental

General methods

The NMR spectra were recorded on Varian spectrometers at 400 MHz. Most of samples were dissolved in deuteriochloroform with tetramethysilane as an internal reference unless specified otherwise. Mass spectra were obtained with matrix-assisted laser desorption/ionization time-of-flight spectrometer (MALDI-TOF) in positive mode using terthiophene matrix. Steady state Ultraviolet-visible absorption spectra were measured on a Shimadzu UV-2100U UV-Vis spectrometer.

Solvents and reagents

Chemicals used were purchased from Aldrich, or Alfa Aesar. Solvents were bought from EM Science. Tetrahyrdofuran was distilled from sodium metal and benzophenone in an argon atmosphere immediately prior to use. Toluene was distilled from CaH_2, and dichloromethane was distilled from potassium carbonate. All solvents were stored over the appropriate molecular sieves prior to use. Thin layer chromatography was done using silica coated glass plates from Analtech. Column chromatography was carried out using Silicycle silica gel 60 with a 230–400 mesh. All reactions were carried out under a nitrogen atmosphere, except the Pd-catalyzed reactions that were carried out with an argon atmosphere.

Electrochemical measurements

All electrochemical measurements were done using a CH Instruments 760D potentiostat along with the software provided by the manufacturer. A glassy carbon or platinum working electrode was used as indicated along with a Ag^+/Ag

quasi reference or Ag/AgCl (in saturated KCl) reference as indicated and a Pt wire/mesh counter electrode. When using a Ag^+/Ag quasi reference, ferrocene was used to calibrate the potential of the reference with Cp_2Fe^+/Cp_2Fc taken as 0.45 V vs. SCE. Cyclic voltammetric (CV) measurements of were done in benzonitrile with 0.1 M tetrabutylammonium hexafluorophosphate or in aqueous solution with 0.1 M KNO_3 as indicated.

Clark electrode measurements

A Yellow Springs Instrument Co. 5300 Biological Oxygen Monitor was used to measure the $\%O_2$ in solution with air saturated solution set as 100% O_2. Solutions were purged of O_2 by bubbling Ar until reaching a level of 30–50% O_2. Argon was then flowed into the headspace of the cell to keep atmospheric O_2 from entering. After reading a stable $\%O_2$ level for 2–5 min, the amperometry experiment was initiated. A line was fitted to the stable $\%O_2$ reading for 60 s before applying potential in the experiment and was subtracted from the trace to give $\Delta\%O_2$ (change in $\%O_2$ during the experiment).

Time-resolved fluorescence measurements

Fluorescence decay measurements were performed by the time-correlated single-photon-counting method. The excitation source for the system was a mode-locked Ti:Sapphire laser (Spectra Physics, Millennia-pumped Tsunami) with a 130 fs pulse duration operating at 80 MHz. The laser output was sent through a frequency doubler and pulse selector (Spectra Physics Model 3980) to obtain 370–450 nm pulses at 4 MHz. Fluorescence emission was detected at the magic angle using a double grating monochromator (Jobin Yvon Gemini-180) and a

microchannel plate photomultiplier tube (Hamamatsu R3809U-50). The instrument response function was 35–55 ps. The spectrometer was controlled by software based on the LabView programming language and data acquisition was done using a single photon counting card (Becker-Hickl, SPC-830).

Data analysis was carried out using locally written software (ASUFIT) developed in a MATLAB environment (Mathworks Inc.). Random errors associated with the reported lifetimes obtained from fluorescence were typically ≤ 5%.

Synthesis

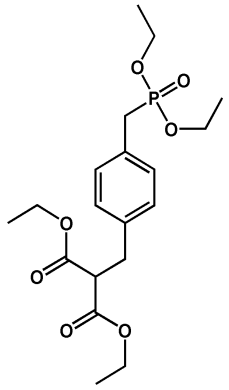

2

Diethyl 2-[4-(diethoxyphosphorylmethyl)benzyl]malonate (2)

In a 100 mL round bottom flask sodium hydride (360 mg, 15 mmol) was suspended in 10 mL of dry THF under nitrogen atmosphere. Diethyl malonate (1.98g, 15 mmol) in 20 mL THF was added drop-wise under ice cooling. After being stirred for 1 h at room temperature, a solution of diethyl (4-bromomethyl)benzylphosphonate (3.21g, 10 mmol) in 20 mL of dry THF was added drop-wise to the mixture and stirred for 1 h. The reaction mixture was then poured into an ice-cold saturated solution of NH_4Cl. The aqueous layer was extracted with ethyl acetate. The organic solution was washed thoroughly with water and dried over Na_2SO_4. The crude material was purified by column chromatography on silica gel using 20-50% ethyl acetate in hexanes. Yield 2.5g (62.5%). ^{1}H NMR: (400 MHz, $CDCl_3$, RT): δ 1.06-1.13 (m, 12H, -CH_3), 2.99 (d, 2H, J = 21.76 Hz, -CH_2), 3.06 (d, 2H, J = 7.68 Hz, -CH_2), 3.49(t, 1H, J = 7.08 Hz, ethyl -CH), 3.80-3.92(m, 4H, -CH_2), 3.97–4.08(m, 4H, -CH_2), 7.03 (d, 2H, J = 8 Hz, ArH), 7.09 (d, 2H, J = 2.24, 8 Hz, ArH).

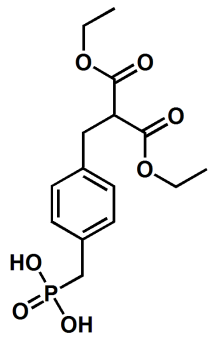

3

2-(4-Phosphonomethylbenzyl)malonic acid diethyl ester (3)

Chlorotrimethylsilane (280 mg, 2.58 mmol) was added drop-wise to a mixture of compound **2 (**0.43 mg, 1.08 mmol) and sodium iodide (0.387 mg, 2.58 mmol) in 3 mL of acetonitrile. The mixture was stirred for 2 h. The NaCl formed in the reaction mixture was removed by filtration. The precipitate was washed with dichloromethane and then evaporated under vacuum. The crude mixture was then purified by column chromatography on silica gel using 5% methanol in dichloromethane. Yield 310 mg (83.8%). ^{1}H NMR: (400 MHz, DMSO, RT): δ 1.08 (t, 6H, J = 7 Hz -CH_3), 2.83 (d, 2H, J = 20.44 Hz, -CH_2), 2.98 (d, 2H, J = 7.84 Hz, -CH_2), 3.70(t, 1H, J = 7.76 Hz, ethyl -CH), 3.97–4.09(m, 4H, -CH_2), 7.04 (d, 2H, J = 7.3 Hz, ArH), 7.12 (d, 2H, J = 2.24, 7.3 Hz, ArH).

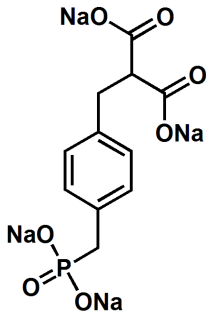

4

Tetrasodium 2-[4-(phosphonatemethyl)benzyl]malonate (4)

Compound **3** (300 mg, 0.87 mmol) and finely grounded sodium hydroxide (400 mg, 10 mmol) were suspended in 40 mL of ethanol. The mixture was refluxed for 15 h and a precipitate was formed. The mixture was cooled to room temperature and filtered. The residue was washed with ice-cold ethanol and dried in high vacuum. Yield: 274 mg (83.8%). ^{1}H NMR: (400 MHz, D_2O, RT): δ 2.52–2.59 (m, 2H, -CH_2), 2.84(t, 1H, J = 7.2 Hz, ethyl -CH), 3.07(d, 2H, J = 20.04 Hz, -CH_2), 7.09–7.2 (m, 4H, ArH).

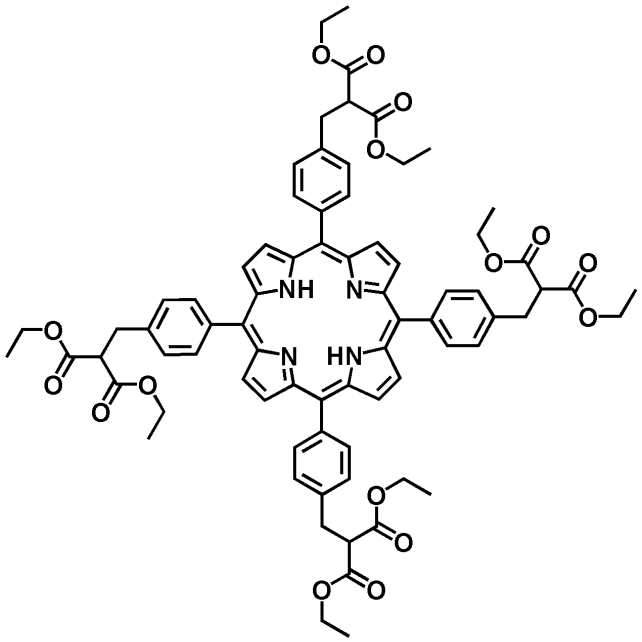

7

5,10,15,20-Tetra(4-diethyl methylphenylmalonate)porphyrin (7)

Sodium hydride (387 mg, 16 mmol) was suspended in 10 mL of dry THF under nitrogen atmosphere. Diethyl malonate (0.61 ml, 4 mmol) in 20 mL THF was added drop-wise under ice cooling. After being stirred for 1 h at room temperature, a solution of 5,10,15, 20-tetra(4-bromomethyl)phenylporphyrin (200 mg, 0.20 mmol) in 20 mL of dry THF was added drop-wise to the mixture and stirred for 1 h. The reaction mixture was then poured into an ice-cold saturated solution of NH_4Cl. The aqueous layer was extracted with dichloromethane. The organic solution was washed thoroughly with water and dried over Na_2SO_4. The crude material was purified by column chromatography on silica gel using 5% ethyl acetate in dichloromethane. Yield 120 mg (45%). ^1H NMR: (400 MHz, $CDCl_3$, RT): δ –2.82 (s, 2H, NH), 1.34 (t, 24H, J = 7.2 Hz, ethyl CH_3), 3.56 (d,

8H, J = 7.7 Hz, CH_2), 3.96 (t, 4H, J = 7.7 Hz, CH), 4.3(m, 16H, J = 7.2 Hz, ethyl CH_2), 7.58 (d, 8H, J = 8 Hz, phenyl–CH_2), 8.10 (d, 8H, J = 8 Hz, phenyl–CH_2), 8.77 (s, 8H pyrrolic H). MALDI-TOF-MS m/z: calcd. for $C_{76}H_{78}N_4O_{16}$ 1302.77, obsd. 1302.73. UV-vis (CH_2Cl_2): λ_{max} 419, 516, 551, 591, and 647 nm.

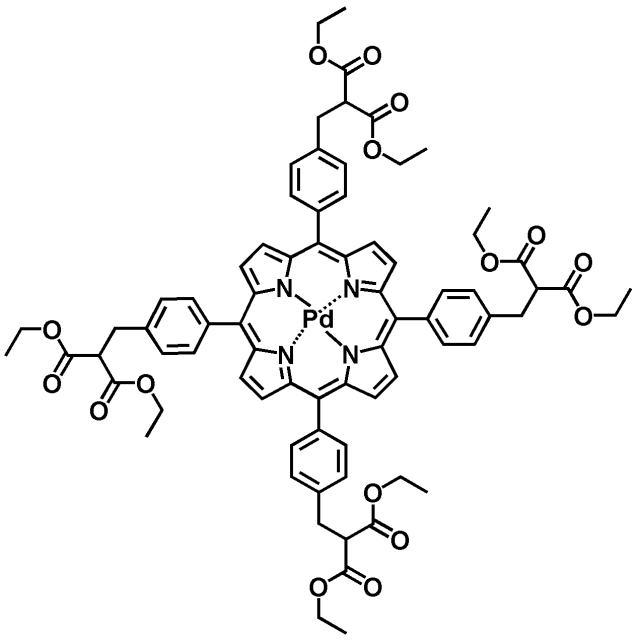

8

Palladium(II)5,10,15,20-tetra(4-diethylmethylphenylmalonate)porphyrin (8)

Palladium(II) chloride (33 mg 0.18 mmol) was added to a solution of porphyrin **7** (24 mg, 0.02 mmol) in 10 mL DMF. The mixture was stirred for 1 h at 55°C under nitrogen. The solvent was removed under reduced pressure and the compound was purified by column chromatography on silica gel using 5% ethyl acetate in dichloromethane. Yield: 21 mg (81%). ^{1}H NMR: (400 MHz, $CDCl_3$, RT): δ 1.35 (t, 24H, J = 7.2 Hz, ethyl CH_3), 3.56 (d, 8H, J = 7.7 Hz, CH_2), 3.96 (t, 4H, J = 7.7 Hz, CH), 4.3(m, 16H, J = 7.2 Hz, ethyl CH_2), 7.58 (d, 8H, J = 8 Hz, phenyl CH_2), 8.06 (d, 8H, J = 8 Hz, phenyl CH_2), 8.75 (s, 8H pyrrolic H)

MALDI-TOF-MS m/z: calcd. for $C_{76}H_{76}N_4O_{16}Pd$ 1407.85, obsd. 1408.84 UV-vis (dichloromethane): λ_{max} 416, and 523 nm.

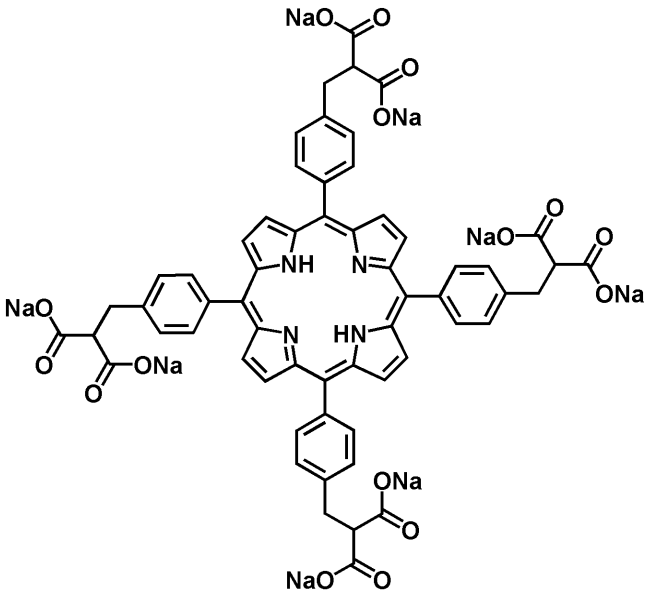

9

Octasodium 5,10,15,20-tetra(4-methylphenylmalonate)porphyrin (9)

Porphyrin **7** (50 mg, 0.04 mmol) and finely grounded sodium hydroxide (292 mg, 7.5 mmol) were suspended in 40 mL of ethanol. The mixture was refluxed for 15 h and a precipitate was formed. The mixture was cooled to room temperature and filtered. The residue was washed with ice-cold ethanol and dried in high vacuum. Yield 43 mg (89.5%). ^{1}H NMR: (400 MHz, D_2O, RT): δ 3.3 (d, 8H, *J* = 7.9 Hz, CH_2), 3.59 (t, 4H, *J* = 7.9 Hz, CH), 7.58 (d, 8H, *J* = 7.8 Hz, phenyl–CH_2), 7.9 (d, 8H, *J* = 7.8 Hz, phenyl–CH_2), 8.47 (s, 4H, pyrrolic H), 8.98 (s, 4H, pyrrolic H).

MALDI-TOF-MS m/z, after acidifying, calcd. for $C_{60}H_{46}N_4O_{16}$ 1079.39, obsd. 1079.41. UV-vis (water): λ_{max} 415, 519, 557, 582, and 635 nm.

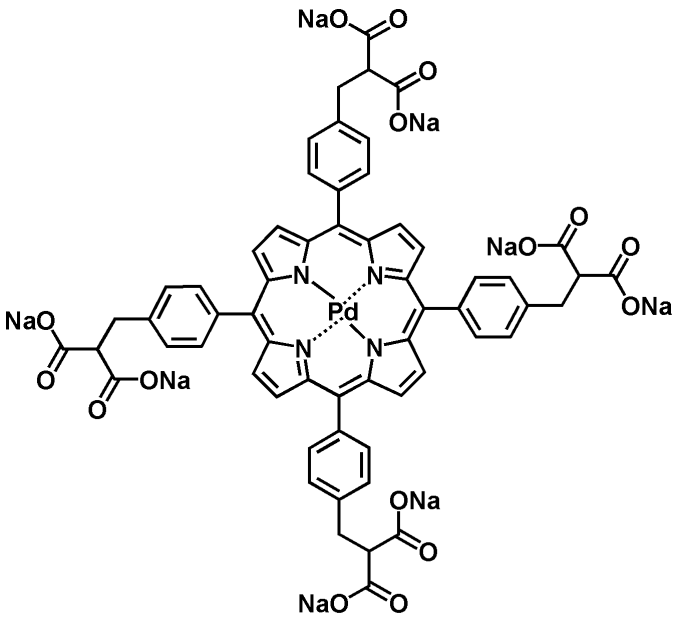

10

Palladium(II)octasodium5,10,15,20-tetra(4-methylphenylmalonate)porphyrin (10)

Palladium porphyrin **8** (20 mg, 0.02 mmol) and finely grounded sodium hydroxide (107 mg, 2.7 mmol) were suspended in 20 mL of ethanol. The mixture was refluxed for 15 h and a precipitate was formed. The mixture was cooled to room temperature and filtered. The residue was washed with ice-cold ethanol and dried in high vacuum. Yield 17 mg (88%). ^{1}H NMR: (400 MHz, D_2O, RT): δ 3.28 (d, 8H, J = 7.9 Hz, CH_2), 3.59 (t, 4H, J = 7.9 Hz, CH), 7.58 (d, 8H, J=7.8 Hz, phenyl CH_2), 7.96 (s, 8H phenyl CH_2), 8.47 (s, 8H, pyrrolic H). MALDI-TOF-MS m/z: calcd. for $C_{60}H_{44}N_4O_{16}Pd$ 1359.82, obsd. 1359.84, UV-vis (water): λ_{max} 413, and 522 nm.

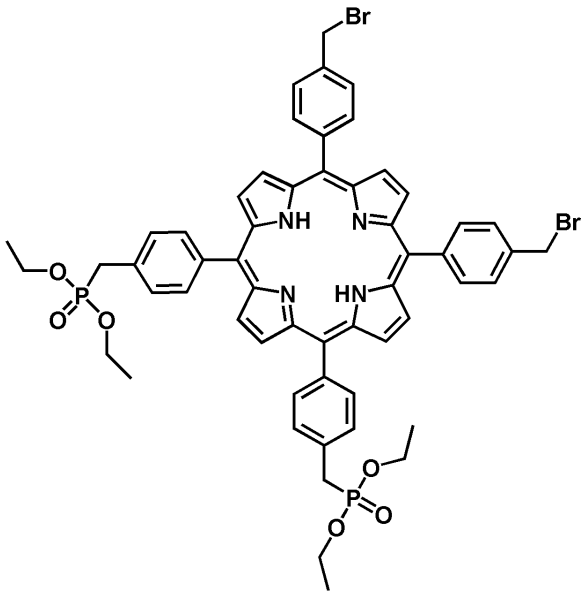

11

5,10-Bis[(4-bromomethyl)phenyl]-15,20-bis[4-(diethoxyphosphorylmethyl)phenyl]porphyrin (11)

Porphyrin **6** (500 mg, 0.51 mmol) and triethylphosphite (0.17 mL, 1.0 mmol) was heated in 10 mL of toluene at 85^0C for 2.5 h and then refluxed for 20 h. After the solvent was removed under reduced pressure, the crude product was purified by column chromatography on silica gel using 5% methanol in dichloromethane. Yield: 36mg (6.2%). ^{1}H NMR: (400 MHz, $CDCl_3$, RT): δ –2.81 (s, 2H, NH), 1.4 (t, 12H, J = 7.28 Hz, ethyl-CH_3), 3.49 (d, 4H, J = 21.88 Hz, CH_2), 4.18–4.26 (m, 8H, ethyl-CH_2), 4.84(s, 4H, J = 7.586Hz, CH_2), 7.69(dd, 4H, J = 4 Hz, J = 8 Hz), 7.77(d, 4H, J = 8 Hz), 8.16(t, 8H, J = 8.3Hz), 8.8(s, 8H pyrrolic H). MALDI-TOF-MS m/z: calcd. for $C_{56}H_{54}Br_2N_4O_6P_2$ 1100.80, obsd. 1100.86, UV-vis (dichloromethane): λ_{max} 415, 516, 556, 590, and 646 nm.

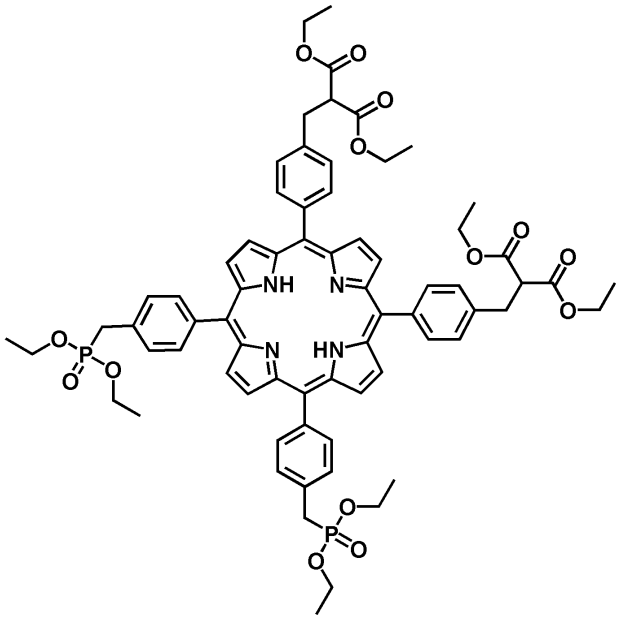

12

5,10-Bis[4-diethylmethylphenylmalonate)-15,20-bis(4-diethoxyphosphorylmethylphenyl]porphyrin (12)

Sodium hydride (122 mg, 5 mmol) was suspended in 10 mL of dry THF under a nitrogen atmosphere. Diethyl malonate (0.2 mL, 1.3 mmol) in 5 mL THF was added drop wise under ice cooling. After being stirred for 1 h at room temperature, a solution of porphyrin **11** (140 mg, 1.27 mmol) in 10 mL of dry THF was added drop-wise to the mixture and stirred for 1 h. The reaction mixture was then poured into an ice-cold saturated NH_4Cl solution. The aqueous layer was extracted with dichloromethane. The organic solution was washed thoroughly with water and dried over Na_2SO_4. The crude material was purified by column chromatography on silica gel using 2% methanol in dichloromethane. Yield: 40 mg (28.3%). ^{1}H NMR: (400 MHz, $CDCl_3$, RT): δ –2.82 (s, 2H, NH), 1.35 (t, 12H, J = 7.24 Hz, ethyl-CH_3), 1.4(t, 12H, J = 7.2 Hz, ethyl-CH_3), 3.49 (d, 4H, J =

21.76 Hz, CH_2), 3.56(d, 4H, *J* = 7.76 Hz, CH_2), 3.96(t, 2H, *J* = 8.28Hz, -CH), 4.18–4.26 (m, 8H, ethyl-CH_2), 4.23–4.34(m, 8H, 7.58, CH_2), 7.58(d, 4H, *J* = 8 Hz), 7.69(d, 4H, *J* = 8 Hz), 8.1–8.16(m, 8H) 8.76–8.83(m, 8H pyrrolic H). MALDI-TOF-MS m/z: calcd. for $C_{70}H_{76}N_4O_{14}P_2$ 1259.31, obsd. 1259.46 UV-vis (dichloromethane): λ_{max} 418, 515, 551, 590, and 646 nm.

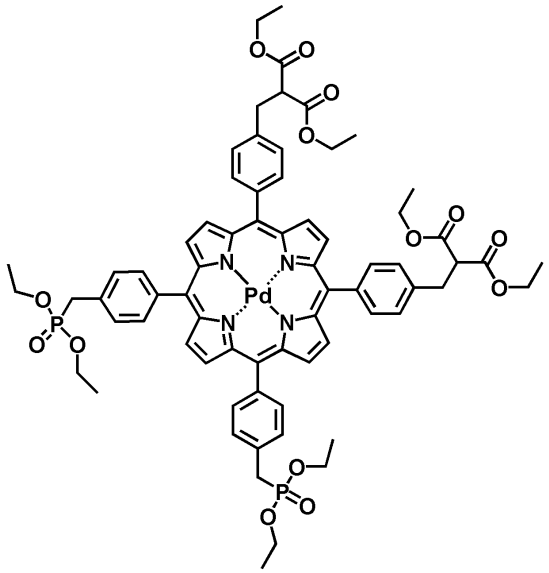

13

Palladium(II)5,10-bis[4-diethylmethylphenylmalonate)-15,20-bis(4-diethoxyphosphorylmethylphenyl]porphyrin (13)

To a solution of porphyrin **12** (18 mg, 0.02 mmol) in 5mL DMF was added palladium (II) chloride (25 mg 0.14 mmol). The mixture was stirred for 1 hr at 55°C under nitrogen. The reaction progress was monitored by UV-Vis spectroscopy. The solvent was removed under reduced pressure and the compound was passed over silica gel using 2% methanol in dichloromethane. Yield: 15 mg (76%). ^{1}H NMR: (400 MHz, $CDCl_3$, RT): δ 1.35 (t, 12H, *J* = 7.2 Hz, ethyl-CH_3), 1.41(t, 12H, *J* = 7.2 Hz, ethyl-CH_3), 3.48 (d, 4H, *J* = 21.92 Hz,

CH_2), 3.56(d, 4H, J = 7.44 Hz, CH_2), 3.96(t, 2H, J = 8.28Hz, -CH), 4.19–4.26 (m, 8H, ethyl-CH_2), 4.29–4.34(m, 8H, ethyl-CH_2), 7.57(d, 4H, J = 8 Hz), 7.68(d, 4H, J = 8 Hz), 8.06–8.12(m, 8H), 8.75–8.78(m, 8H pyrrolic H). MALDI-TOF-MS m/z: calcd. for $C_{70}H_{74}N_4O_{14}P_2Pd$ 1363.72, obsd. 1363.70 UV-vis (dichloromethane): λ_{max} 416, and 524nm.

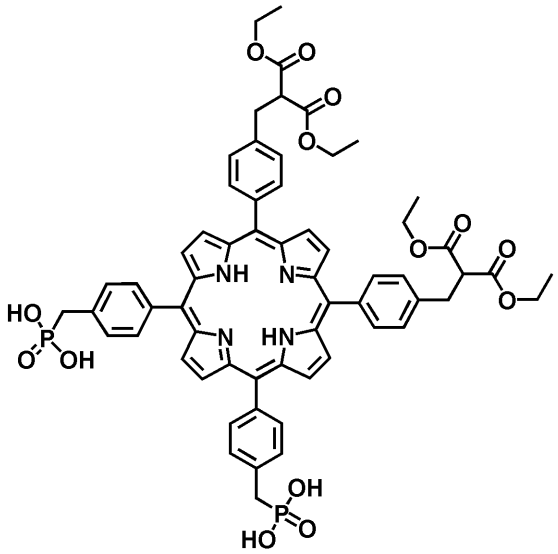

14

5,10-Bis(4-dihydroxyphosphorylmethylphenyl)-15,20-bis(4-diethylmethylphenylmalonate)porphyrin (14)

Chlorotrimethylsilane (23 mg, 0.21 mmol) was added to a mixture of porphyrin **13 (**110 mg, 0.09 mmol) and sodium iodide (32 mg, 0.21mmol) in 15 mL of dichloromethane. The mixture was stirred for 2 h. The reaction mixture was washed with water, followed by brine, and then dried over sodium sulfate and evaporated under vacuum. Yield: 78 mg (78%). MALDI-TOF-MS m/z: calcd. for $C_{62}H_{60}N_4O_{14}P_2$ 1147.11, obsd. 1147.18.

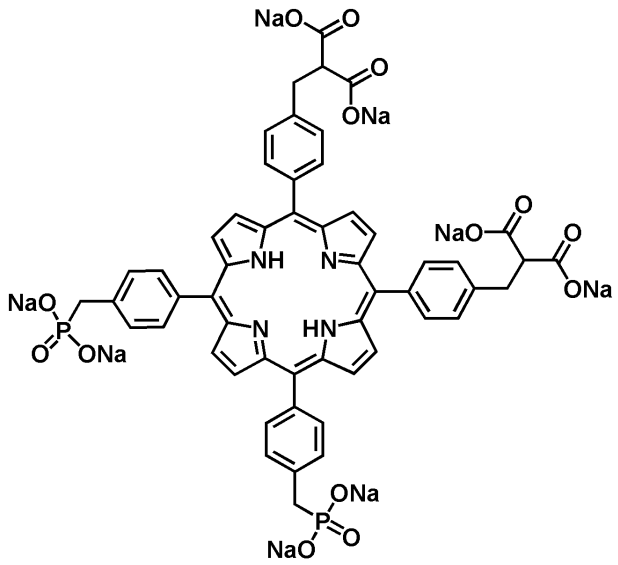

15

Octasodium5,10-bis(4-methylphenylphosphonate)-15,20-bis(4-methylphenylmalonate)porphyrin (15)

Porphyrin **14** (50 mg, 0.05 mmol) and finely grounded sodium hydroxide (292 mg, 7.5 mmol) were suspended in 40 mL of ethanol. The mixture was refluxed for 15 h and a precipitate formed. The mixture was cooled to room temperature and filtered. The residue was washed with ice-cold ethanol and dried in high vacuum. Yield: 41 mg (77.7%). ^{1}H NMR: (400 MHz, D_2O, RT): δ 1.32 (t, 12H, J = 7.2 Hz, ethyl-CH_3), 1.39(t, 12H, J = 7.2 Hz, ethyl-CH_3), 3.47 (d, 4H, J = 21.7 Hz, CH_2), 3.54(d, 4H, J = 7.72 Hz, CH_2), 3.96(t, 2H, J = 8.2Hz, -CH), 4.16-4.24 (m, 8H, ethyl-CH_2), 4.21-4.31(m, 8H, 7.58, CH_2), 7.58(d, 4H, J = 8 Hz), 7.69(d, 8H, J = 8 Hz), 8.1–8.16(m, 8H) 8.76–8.83(m, 8H pyrrolic H). MALDI-TOF-MS m/z: calcd. for $C_{54}H_{44}N_4O_{14}P_2$ 1034.89, obsd. 1057.07 (compound + Na) 1036.46 (compound +2H) UV-vis (CH_2Cl_2): λ_{max} 416, 520, 558, 579, and 637 nm.

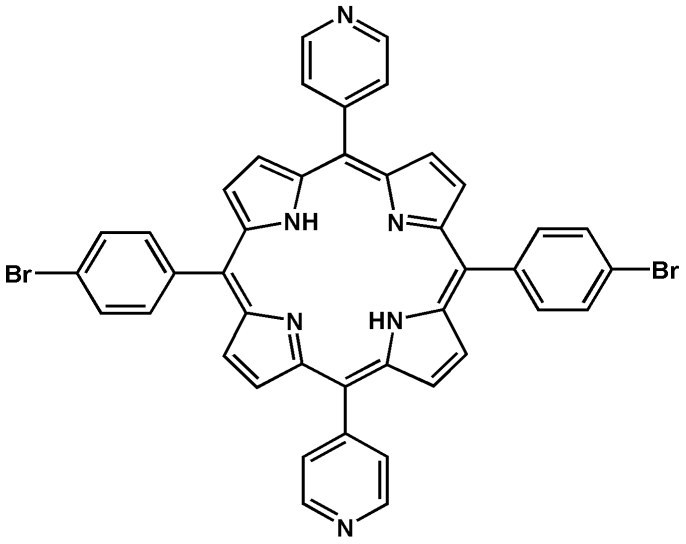

17

5,15-Bis(4-bromophenyl)-10,20-bis(4-pyridyl)porphyrin (17)

A mixture of compound **16** (3.5 g, 15.7 mmol) and 4-bromobenzaldehyde (2.9 g, 15.7 mmol) in 25 mL of propionic acid was refluxed for 1 h. The reaction mixture was cooled and the excess propionic acid was removed under vacuum. The residue was dissolved in dichloromethane and filtered through silica to remove the tar. The filtrate was concentrated and purified by column chromatography on silica gel using 2% methanol in dichloromethane as solvent. The obtained product was crystallized using methanol/dichloromethane. Yield 458 mg (3.8%). ^{1}H NMR: (400 MHz, $CDCl_3$, RT): δ –2.88 (s, 2H, NH), 7.90(4H, d, J = 8Hz), 8.06(4H, d, J = 8Hz), 8.15(4H, d, J = 5.6Hz), 8.83(4H, d, J = 5Hz), 8.89(4H, d, J = 5Hz), 9.04(4H, d, J = 5.6Hz). MALDI-TOF-MS *m/z:* calcd. for $C_{42}H_{26}Br_2N_6$ 774.51 obs. 774.53.

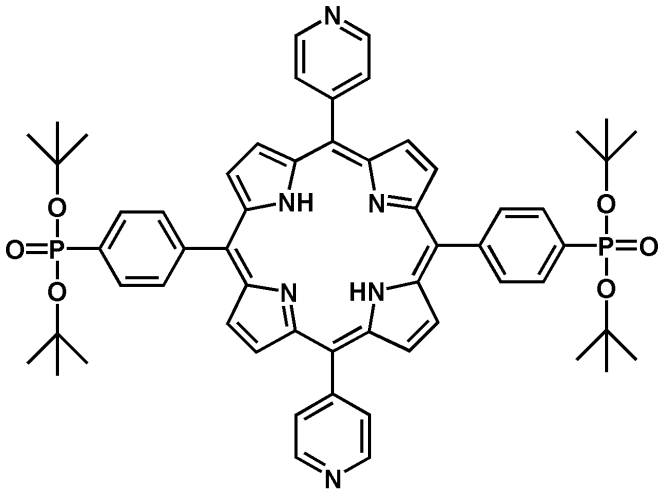

18

5,15-Bis(4-di-*tert*-butoxyphosphorylphenyl)-10,20-bis(4-pyridyl)porphyrin (18)

Porphyrin **17** (436 mg, 0.56 mmol) and di-*tert*-butylphosphite (2.17 gm, 11.25 mmol) were coupled using $Pd(PPh_3)_4$ (126 mg, 0.11 mmol) in toluene/triethylamine [16 mL, (1:1)] at 80°C under argon with the reaction lasting 20 h. The reaction mixture was concentrated and purified by column chromatography on silica gel using 5% methanol in dichloromethane as solvent. Yield 256 mg (45%). ^{1}H NMR: (400 MHz, $CDCl_3$, RT): δ –2.84 (s, 2H, NH), 1.68 (s, 36H, *t*-butyl), 8.17–8.30(m, 12H), 8.84–8.88(m, 8H), 9.05(4H, d, J = 6Hz). MALDI-TOF-MS *m/z:* calcd. for $C_{58}H_{62}N_6O_6P_2$ 1001.10 obs. 1001.15.

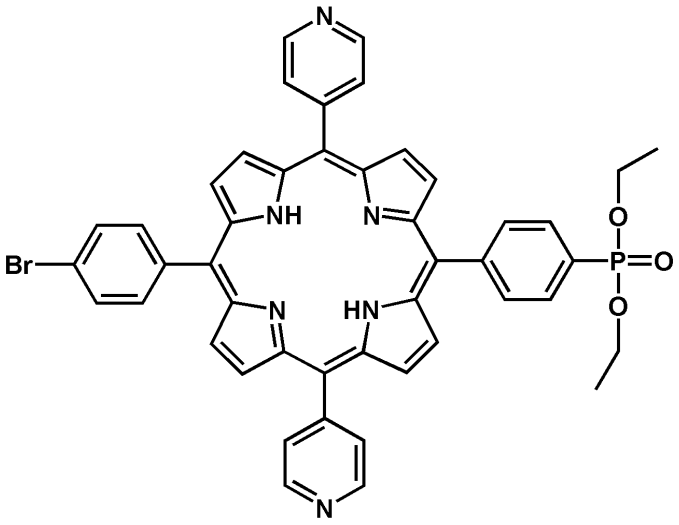

20

5-(4-Bromophenyl)-15-[4-(diethoxyphosphoryl)phenyl]-10,20-(4-pyridyl)porphyrin (20)

Compound **16** (100 mg, 0.448 mmol), 4-brombenzaldehyde (41 mg, 0.22 mmol), and 4-(di-ethyloxyphosphoryl)benzaldehyde (70.85 mg, 0.224 mmol) were refluxed in 10 mL of propionic acid for 1 h. The reaction mixture was cooled and the excess propionic acid was removed under vacuum. The residue was dissolved in 2% methanol in dichloromethane and filtered through silica to remove the tar. The filtrate was concentrated and purified by column chromatography using silica gel using 1-5% methanol in dichloromethane. The product obtained was crystallized using methanol/dichloromethane. Yield: 25 mg (9.5%). ^{1}H NMR: (400 MHz, $CDCl_3$, RT): δ –2.96 (s, 2H, NH), 1.46 (t, 6H, J = 7 Hz, ethyl-CH_3), 4.24–4.38 (m, 4H, CH_2), 7.86(d, 2H, J = 8.2 Hz), 8.0(d, 2H, J = 8.2 Hz), 8.12–8.18(6H, m), 8.25–8.29(2H, d), 8.66–8.99(12H, m). MALDI-TOF-MS *m/z:* calcd. for $C_{46}H_{36}BrN_6O_3P$ 831.70 obs. 831.74.

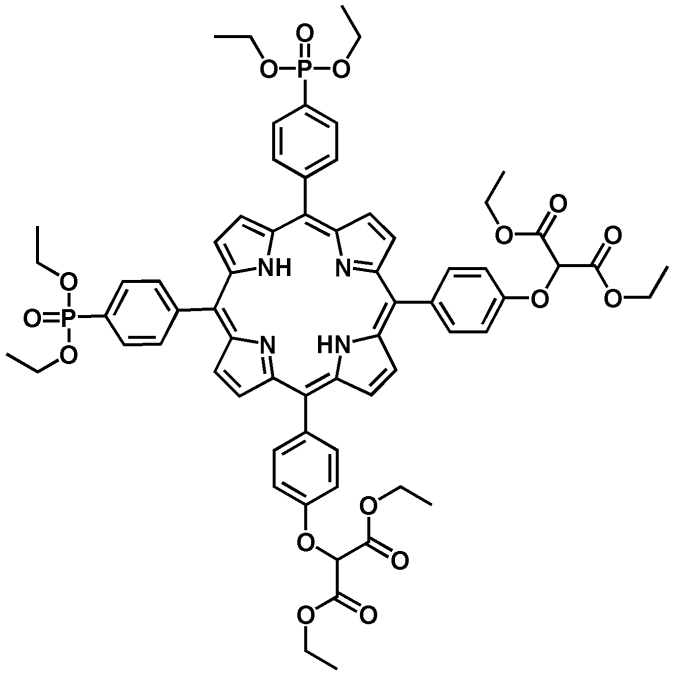

22

5,10-Bis(4-diethyl oxyphenylmalonate)-15,20-bis(4-diethoxyphosphorylphenyl]porphyrin (22)

To 1.5 L of dichloromethane were added 4.2 g (15 mmol) of diethyl 2-(4-formylphenoxy)malonate, 3.63 g (15 mmol) of 4-(di-*tert*-butyloxyphosphoryl)benzaldehyde dimethylacetal and 2.01 g (30 mmol, 2.17 mL) of freshly distilled pyrrole. The resulting solution was stirred for 15 min before 422 mg (3 mmol, 0.387 mL) of $BF_3.Et_2O$ were added and the solution was stirred at room temperature. After 75 min 4.8 g (30 mmol, 5.63 mL) of triethyl orthoacetate was added and stirred for 15 min. Then 0.387 mL of $BF_3.Et_2O$ were added once more and the reaction was stirred for 1 h. A portion of DDQ 5.4 g (23 mmol), was added and stirred for 20 hr at room temperature in the dark. The reaction mixture was concentrated and purified by column chromatography on

silica gel using 5–10% methanol in dichloromethane Yield: 356 mg (2%).[1]H NMR: (400 MHz, $CDCl_3$, RT): δ –2.84 (s, 2H, NH), 1.42 (t, 12H, *J* = 7 Hz, ethyl-CH_3), 1.51(t, 12H, *J* = 7.16 Hz, ethyl-CH_3), 4.3–4.5 (m, 8H, CH_2), 5.52(s, 2H, -CH), 4.23–4.34(m, 8H, 7.58, CH_2), 7.35(d, 4H, *J* = 8.6 Hz), 8.12(d, 4H, *J* = 8.6 Hz), 8.18–8.22(4H, m), 8.30–8.32(4H, m), 8.78(4H, d, *J*= 6Hz), 8.84(4H, d, *J*= 6Hz). MALDI-TOF-MS *m/z:* calcd. for $C_{66}H_{68}N_4O_{16}P_2$ 1235.21, obsd. 1235.17; UV-vis (dichloromethane): λ_{max} 419, 515, 551, 591, and 648 nm.

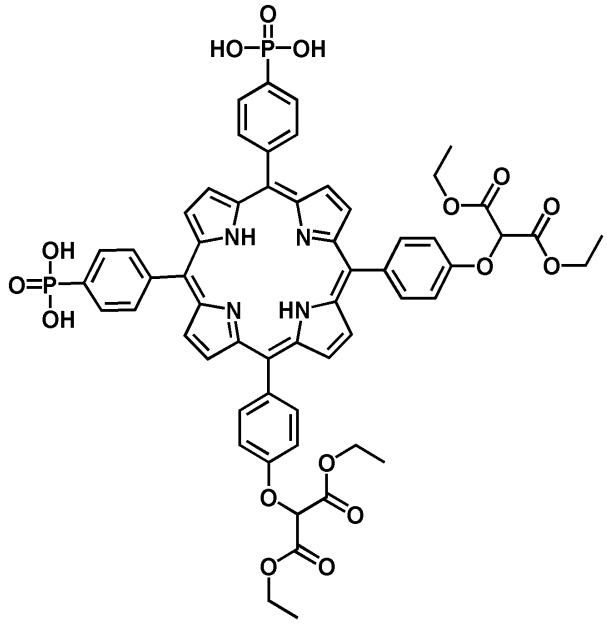

23

5,10-Bis(4-dihydroxyphosphorylphenyl)-15,20-bis(4-diethyl oxyphenylmalonate)porphyrin (23)

Chlorotrimethylsilane (10.5 mg, 0.10 mmol) was added to a mixture of porphyrin **22** (50 mg, 0.04 mmol) and sodium iodide (14.5 mg, 0.10 mmol) in 10 mL of acetonitrile. The mixture was stirred for 2 h. The reaction mixture was washed with water, followed by brine, and then dried over sodium sulfate and evaporated

under vacuum. Yield: 36 mg (79%) MALDI-TOF-MS m/z: calcd. for $C_{58}H_{52}N_4O_{16}P_2$ 1122.99 obs. 1124.92 (Compound +2H) and 1146.31 (Compound +Na).

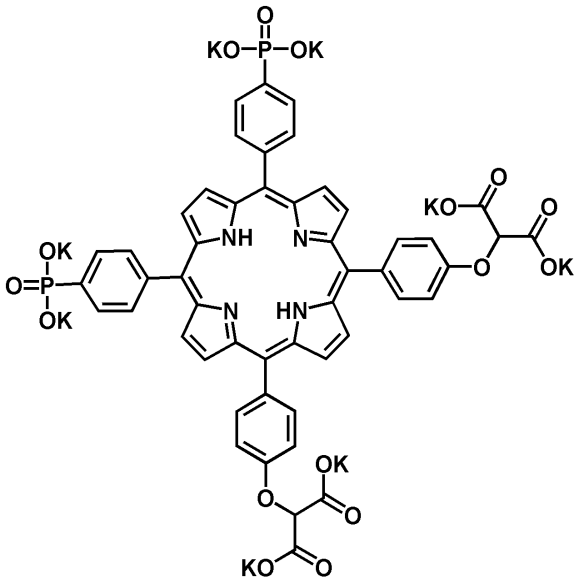

24

Octapotassium 5,10-bis(4-phenylphosphonate)-15,20-bis(4-oxyphenylmalonate)porphyrin (24)

Porphyrin **23** (30 mg, 0.03 mmol) was dissolved in 10 mL of dichloromethane. To this solution 20 mL of 20% KOH solution and 0.3 mL of water was added. The mixture was refluxed for 3 h and stirred for 12 h at room temperature. The compound was filtered and washed with ice-cold ethanol and dried in high vacuum. Yield: 28 mg (82%). ^{1}H NMR: (400 MHz, D_2O, RT): δ 5.09(s, 2H, -CH), 7.27(d, 4H, *J* = 8.1 Hz), 7.97–8.16(m, 12H), 8.73–9.18(8H, bs). MALDI-

TOF-MS *m/z:* calcd. for $C_{50}H_{36}N_4O_{16}P_2$ 1010.78, obsd. 1012.60 (compound +2H); UV-vis (water): λ_{max} 416, 519, 557, 582, and 640 nm.

VII. References

(1) Gust, D.; Moore, T. A.; Moore, A. L. *Accounts of Chemical Research* **1993**, *26*, 198.

(2) Gust, D.; Moore, T. A. *Science* **1989**, *244*, 35.

(3) Gust, D.; Moore, T. A.; Moore, A. L. *Accounts of Chemical Research* **2001**, *34*, 40.

(4) Lewis, N. S.; Nocera, D. G. *Proceedings of the National Academy of Sciences of the United States of America* **2007**, *104*, 20142.

(5) Youngblood, W. J.; Lee, S. H. A.; Maeda, K.; Mallouk, T. E. *Accounts of Chemical Research* **2009**, *42*, 1966.

(6) Kuwabara, T.; Tomita, E.; Sakita, S.; Hasegawa, D.; Sone, K.; Yagi, M. *Journal of Physical Chemistry C* **2008**, *112*, 3774.

(7) Gratzel, M. *Nature* **2001**, *414*, 338.

(8) Alstrum-Acevedo, J. H.; Brennaman, M. K.; Meyer, T. J. *Inorganic Chemistry* **2005**, *44*, 6802.

(9) Gust, D.; Moore, T. A.; Moore, A. L. *Accounts of Chemical Research* **2009**, *42*, 1890.

(10) Barber, J. *Chemical Society Reviews* **2009**, *38*, 185.

(11) McEvoy, J. P.; Brudvig, G. W. *Chemical Reviews* **2006**, *106*, 4455.

(12) Ni, M.; Leung, M. K. H.; Leung, D. Y. C.; Sumathy, K. *Renewable & Sustainable Energy Reviews* **2007**, *11*, 401.

(13) Concepcion, J. J.; Jurss, J. W.; Brennaman, M. K.; Hoertz, P. G.; Patrocinio, A. O. T.; Iha, N. Y. M.; Templeton, J. L.; Meyer, T. J. *Accounts of Chemical Research* **2009**, *42*, 1954.

(14) Kudo, A. *International Journal of Hydrogen Energy* **2007**, *32*, 2673.

(15) Fujishima, A.; Honda, K. *Nature* **1972**, *238*, 37.

(16) Oregan, B.; Gratzel, M. *Nature* **1991**, *353*, 737.

(17) Kudo, A.; Miseki, Y. *Chemical Society Reviews* **2009**, *38*, 253.

(18) Kiwi, J.; Gratzel, M. *Journal of the American Chemical Society* **1979**, *101*, 7214.

(19) Kanan, M. W.; Nocera, D. G. *Science* **2008**, *321*, 1072.

(20) Zong, R.; Thummel, R. P. *Journal of the American Chemical Society* **2005**, *127*, 12802.

(21) Concepcion, J. J.; Jurss, J. W.; Templeton, J. L.; Meyer, T. J. *Proceedings of the National Academy of Sciences of the United States of America* **2008**, *105*, 17632.

(22) Concepcion, J. J.; Jurss, J. W.; Templeton, J. L.; Meyer, T. J. *Journal of the American Chemical Society* **2008**, *130*, 16462.

(23) Harriman, A.; Pickering, I. J.; Thomas, J. M.; Christensen, P. A. *Journal of the Chemical Society-Faraday Transactions I* **1988**, *84*, 2795.

(24) Harriman, A.; Richoux, M. C.; Christensen, P. A.; Mosseri, S.; Neta, P. *Journal of the Chemical Society-Faraday Transactions I* **1987**, *83*, 3001.

(25) Harriman, A.; Thomas, J. M.; Millward, G. R. *New Journal of Chemistry* **1987**, *11*, 757.

(26) Hara, M.; Waraksa, C. C.; Lean, J. T.; Lewis, B. A.; Mallouk, T. E. *Journal of Physical Chemistry A* **2000**, *104*, 5275.

(27) Nahor, G. S.; Neta, P.; Hambright, P.; Thompson, A. N.; Harriman, A. *Journal of Physical Chemistry* **1989**, *93*, 6181.

(28) Campbell, W. M.; Jolley, K. W.; Wagner, P.; Wagner, K.; Walsh, P. J.; Gordon, K. C.; Schmidt-Mende, L.; Nazeeruddin, M. K.; Wang, Q.; Gratzel, M.; Officer, D. L. *Journal of Physical Chemistry C* **2007**, *111*, 11760.

(29) Wang, Q.; Carnpbell, W. M.; Bonfantani, E. E.; Jolley, K. W.; Officer, D. L.; Walsh, P. J.; Gordon, K.; Humphry-Baker, R.; Nazeeruddin, M. K.; Gratzel, M. *Journal of Physical Chemistry B* **2005**, *109*, 15397.

(30) Hara, M.; Mallouk, T. E. *Chemical Communications* **2000**, 1903.

(31) Hoertz, P. G.; Kim, Y. I.; Youngblood, W. J.; Mallouk, T. E. *Journal of Physical Chemistry B* **2007**, *111*, 6845.

(32) Younpblood, W. J.; Lee, S. H. A.; Kobayashi, Y.; Hernandez-Pagan, E. A.; Hoertz, P. G.; Moore, T. A.; Moore, A. L.; Gust, D.; Mallouk, T. E. *Journal of the American Chemical Society* **2009**, *131*, 926.

(33) Yagi, M.; Tomita, E.; Sakita, S.; Kuwabara, T.; Nagai, K. *Journal of Physical Chemistry B* **2005**, *109*, 21489.

(34) Nakagawa, T.; Beasley, C. A.; Murray, R. W. *Journal of Physical Chemistry C* **2009**, *113*, 12958.

(35) Nakagawa, T.; Bjorge, N. S.; Murray, R. W. *Journal of the American Chemical Society* **2009**, *131*, 15578.

(36) Sherman, B. D.; Pillai, S.; Kodis, G.; Bergkamp, J.; Mallouk, T. E.; Gust, D.; Moore, T. A.; Moore, A. L. *Canadian Journal of Chemistry-Revue Canadienne De Chimie* **2011**, *89*, 152.

(37) Garbayjaureguiberry, C.; McCorttranchepain, I.; Barbe, B.; Ficheux, D.; Roques, B. P. *Tetrahedron-Asymmetry* **1992**, *3*, 637.

(38) Yokomatsu, T.; Minowa, T.; Murano, T.; Shibuya, S. *Tetrahedron* **1998**, *54*, 9341.

(39) Muthukumaran, K.; Loewe, R. S.; Ambroise, A.; Tamaru, S. I.; Li, Q. L.; Mathur, G.; Bocian, D. F.; Misra, V.; Lindsey, J. S. *Journal of Organic Chemistry* **2004**, *69*, 1444.

(40) Oza, V. B.; Corcoran, R. C. *Journal of Organic Chemistry* **1995**, *60*, 3680.

(41) Guldi, D. M.; Zilbermann, I.; Anderson, G.; Li, A.; Balbinot, D.; Jux, N.; Hatzimarinaki, M.; Hirsch, A.; Prato, M. *Chemical Communications* **2004**, 726.

(42) Wen, L. Q.; Li, M.; Schlenoff, J. B. *Journal of the American Chemical Society* **1997**, *119*, 7726.

(43) Scalise, I.; Durantini, E. N. *Journal of Photochemistry and Photobiology a-Chemistry* **2004**, *162*, 105.

(44) Ruzie, C.; Michaudet, L.; Boitrel, B. *Tetrahedron Letters* **2002**, *43*, 7423.

(45) Lottner, C.; Bart, K. C.; Bernhardt, G.; Brunner, H. *Journal of Medicinal Chemistry* **2002**, *45*, 2079.

(46) Lindsey, J. S.; Schreiman, I. C.; Hsu, H. C.; Kearney, P. C.; Marguerettaz, A. M. *Journal of Organic Chemistry* **1987**, *52*, 827.

Chapter 3

ARTIFICIAL ANTENNA MODELS COMPOSED OF NANOPARTICLES AND PORPHYRINS LINKED BY DNA

I. Introduction

Absorption of light is the first step in the photosynthesis process and is performed by antenna systems that absorb the sun's energy and transfer this excitation energy to the reaction centers.[1] Photosynthetic organisms have evolved in ways that favor adaptation of their antenna systems to the environment in which they live.[2] Chlorophyll and carotenoid pigments are the most common chromophores found in antennas: collectively they absorb in the range of ~350 and 700 nm of the solar spectrum.[3] The challenge in building an efficient artificial light harvesting system relies on designing structures with high absorption cross sections that are able to absorb most of the incoming radiation from the sun.[4] Artificial antenna systems using various molecular assemblies have been reported, most of which include cyclic tetrapyrrole systems related to those found in nature.[3] Recent advances in nanotechnology and improvement in spectroscopic methods have allowed researchers to develop hybrid systems including nanomaterials, biomolecules and organic fluorophores.[5] Among different nanomaterials, noble metal nanoparticles (NP) have gained increasing attention in this field because of their characteristic bands at visible and infrared wavelengths.[6,7] These bands, because of their localized surface plasmons, make them viable candidates for artificial light harvesting systems. Efficient coupling between the fluorophore and the plasmons of nanoparticles can be observed and

characterized by plasmon resonance energy transfer (PRET) and metal enhanced fluorescence. It is reported in the literature that interaction between a nanoparticle and a fluorophore is distance-dependent and in relation to such distance there is either fluorescence enchantment or quenching of the fluorescence of the fluorophore.[7-9] We focused our attention on building an efficient antenna system using silver nanoparticles, and porphyrins as fluorophores. To study the distance-dependent interaction between the two components, various lengths of double stranded DNA were used to control the separation between the silver nanoparticle and the porphyrin. Double stranded DNA serves as an ideal linker due to its rigidity and its well-established chemistry for attaching it to the nanoparticles.

Nanoparticles (NPs)

"Nanoparticulate metal colloids are generally defined as isolable particles between 1 and 50 nm in size that are prevented from agglomerating by protective shells."[10] NPs have received much attention in the recent past because of their special electronic structure and their large surface area. In general there are five methods for transition metal NP synthesis: (1) transition metal salt reduction, (2) thermal decomposition and photochemical methods, (3) ligand reduction and displacement from organometallics, (4) metal vapor synthesis and (5) electrochemical synthesis. Once synthesized these NPs need to be stabilized to prevent agglomeration of these particles.[10] NPs are kinetically stable but they can aggregate into larger particles and form bulk material which are thermodynamically more stable.[11] Stabilization can be accomplished either by electrostatic stabilization, by steric hindrance stabilization or both (Figure 1). In

electrostatic stabilization there is columbic repulsion between the particles due to adsorption of ions (e.g., citrate ions) to an electrophilic metal surface causing an electrical double layer. Metal clusters can be surrounded by organic molecules, which are sterically bulky such as polymers, copolymers, surfactants or organometallics creating a steric barrier that prevents the close contact of the metal particles. Functionalization of NPs is necessary in order to preserve the plasmonic properties while making them stable and compatible with organic and biological materials. NPs can be functionalized either by using chemical functional group or biological molecules such as DNA.[12]

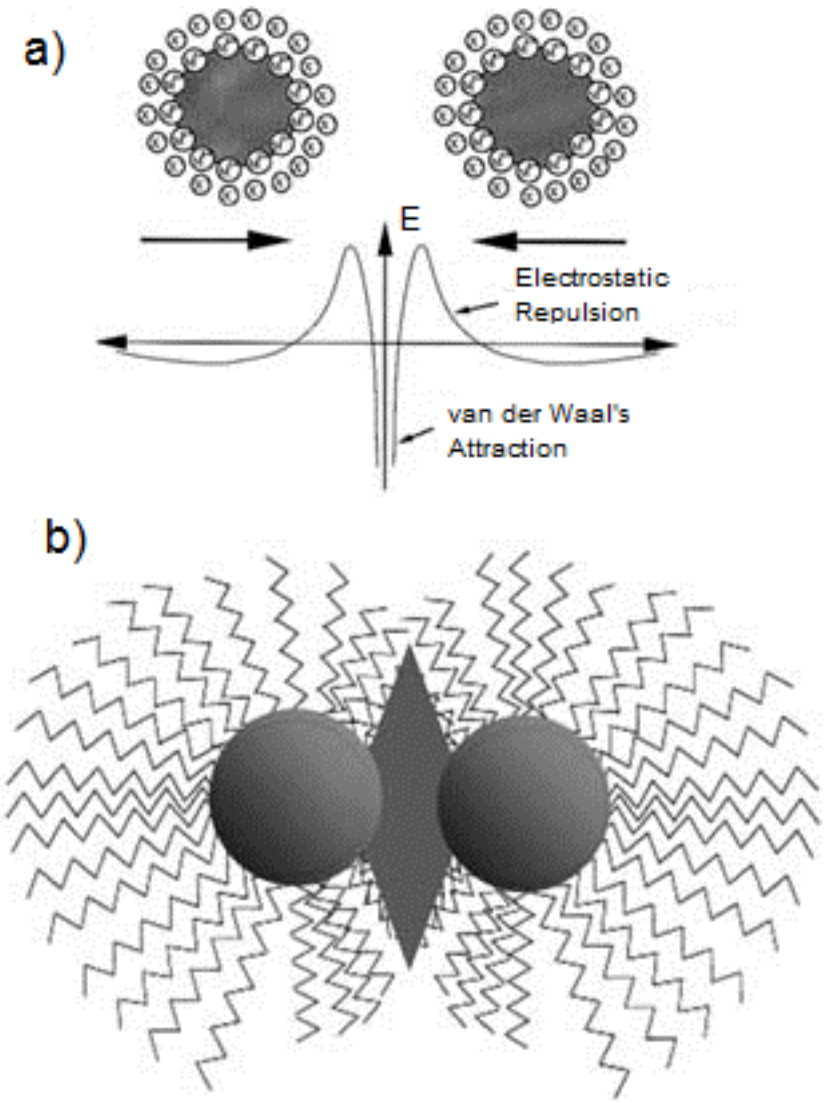

Figure 1: a) Electrostatic stabilization of nanoparticles, b) steric stabilization of nanoparticles.[10]

Nanoparticle functionalization

Nanoparticle functionalization can be achieved by chemical functional groups such as hydrocarbon chains functionalized with a thiol group on one end

and a carboxylic group at the other end. This method has been used extensively as these functional groups can stabilize the NPs in aqueous medium by electrostatic repulsion. Alternatively polyethylene glycol group (PEG) ligands can be used because NPs with PEG are kept separated from each other for steric reasons and can be further functionalized by ligand exchange. NPs fabricated with PEG are robust, water soluble and do not aggregate under extreme pH or in presence of proteins.[12]

Biological molecules such as proteins and oligonucleotides (DNA/RNA) have also been used to functionalize NPs. Thiolated biomolecules can directly be attached to NPs surface due to thiol-gold/silver affinity interactions. DNA mediated assembly of NPs provides an attractive way to organize both metallic and semiconducting NPs into periodic or discrete one-, two-, and three-dimensional architectures. Some of the factors that affect the stability of the NP are the length of the oligonucleotide, and the surface coverage of DNA. The enhanced stability of the NP-DNA is the highly charged and high molecular weight of DNA, which provides both surface charge and steric hindrance.[12]

Nanoparticle characterization

Common techniques used for NPs characterization are nuclear magnetic spectroscopy (NMR), infrared spectroscopy (IR), elemental analysis and energy dispersive spectroscopy (EDS). Transmission electron microscopy (TEM) is also often used for characterizing the size of the NPs. Techniques like UV-visible spectroscopy are used for NPs whose plasmon resonance lies in the visible region. As the particle size increases, the characteristic plasmon band shifts to a longer

wavelength. Therefore, by simple light absorption methods it is possible to determine the degree of aggregation of the NPs.[10]

Synthetic DNA and formation of nanoparticle DNA-conjugates

DNA synthesis was been developed several years ago and has now reached a stage where desired sequence can be obtained commercially. DNA can be synthesized by coupling a protected nucleotide to the growing end of the DNA chain followed by removal of the protecting group. This process is repeated to acquire the desired sequence. There are multiple ways of attaching DNA on the NPs surface, among these methods the direct adsorption of alkylthiol or disulfide terminated oligonucleotides functionalized at 3' or 5' is commonly used.[13]

In 1996, Mirkin and coworkers reported that by simply mixing gold (Au) particles with alkanethiol terminated oligonucleotides it is possible to generate a dense monolayer of DNA molecules on each particle.[14,15] The Watson-Crick base pairing of an oligonucleotide is thermally stable at room temperature when there are at least 12 bases that are approximately within an area of 4 nm; this is sufficient for the placement of NP in a desired assembly.[15] Discrete number of oligonucleotides on each particle can be achieved by using methods similar to those developed by Alivisatos and coworkers.[16] These conjugates are stable for years even when exposed to light, oxidants, and high temperatures. Dickson and coworkers successfully prepared fluorescent silver nanoparticles with good biocompatibility and water solubility by using DNA as a template.[17]

Effect of metal nanoparticles on fluorophores

The most widely studied interactions between metal NPs and fluorophores are those that result in the enhancement and/or quenching of the fluorescence of the fluorophore. Incident light induces an enhanced electric field around the metal NP that can interact with the spectral properties of the fluorophore. There are many factors, which govern the interaction between the fluorophore and the NP. Some of these are: a) the distance between the fluorophore and the NP, b) the geometry and orientation of the fluorophore with respect to the NP, c) size and shape of the NP, and d) the overlap of the molecule emission with the NP absorption spectrum.[10]

Gold (Au) nanoparticles have attracted great attention because of their strong absorption/scattering properties and very low toxicity.[18,19] Hayashi and coworkers used Rose Bengal as the fluorophore to study the fluorescence enchantment of the dye attached to Au NP, the size varying from 20 to 250 nm in diameter and observed maximum enhancement of the dye fluorescence with a 100 nm Au nanoparticle.[20] Dulkeith and coworkers observed a decrease in the radiative decay of a fluorophore (lissamine) placed near Au NP.[21] Schneider and coworkers showed that the degree of quenching of the fluorescence of a fluorophore as a function of the distance between a Au NP and the fluorophore.[22] Similar studies were performed on silver (Ag) NP by Lakowicz and coworkers using Cy5 as a fluorophore; the fluorophore was attached to NPs with diameter varying from 5 to 100 nm via a DNA double strand of 8 nm length. Fluorescence intensity of the dye attached to 50 nm Ag NP showed maximum enhancement of

the fluorescence.[23] Recently the same group reported the enhanced Förster resonance energy transfer (FRET) between a nearby donor and acceptor pair to Ag NP with a 20 nm diameter.[6,21]

For the development of protein-based solar cells, researchers are attempting to increase the absorption of major light harvesting proteins found in nature. Carmeli and coworkers developed a hybrid system in which the Au or Ag NPs were capped with PS1. They observed an increase in absorption over the entire absorption band of the protein rather than at the specific wavelengths of the NPs.[24] Imahori and coworkers reported porphyrin-modified metal alloy nanoclusters where they used silver, platinum, palladium, and Ag-Au alloy as the metal core. They observed that the interaction between a surface of mono-metal cluster and the porpyhrin excited singlet state is greater than their alloy (Ag/Au).[25]

In this chapter we report the distance-dependent fluorescence enhancement of porphyrin molecules by silver NPs using DNA as a spacer. We chose porphyrin as the fluorophore because of its strong Soret absorption band, which overlaps efficiently with Ag NP plasmonic band. Porphyrin also provides us with widely separated absorption and emission bands that allow us to separate absorption enhancement from emission enhancement phenomena. We intend to demonstrate the effect of the plasmon properties of Ag NP on the porphyrin photophysics by steady-state and transient spectroscopy.

II. Results and discussion

1. Synthesis and Purification

Synthesis of porphyrin **1** was achieved by reacting isonicotine aldehyde and methyl 4-formylbenzoate with pyrrole under Adler Longo conditions. The desired porphyrin was then obtained by basic hydrolysis of the ester.[26]

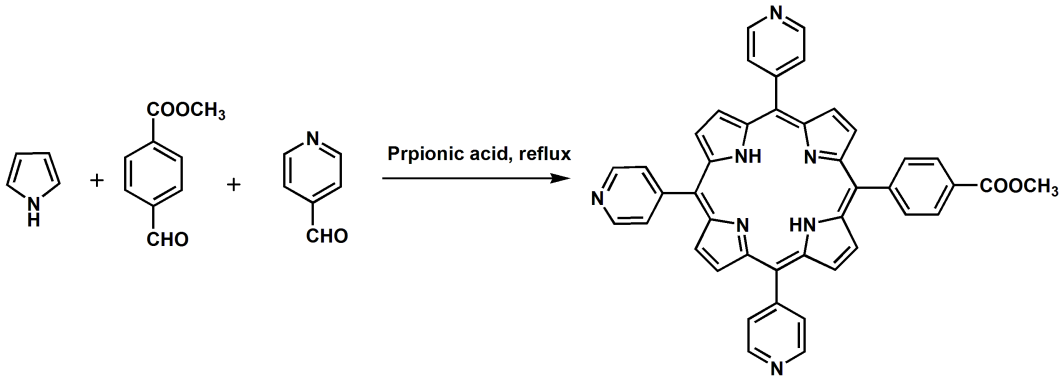

1

Scheme 1: Synthesis of porphyrin **1.**

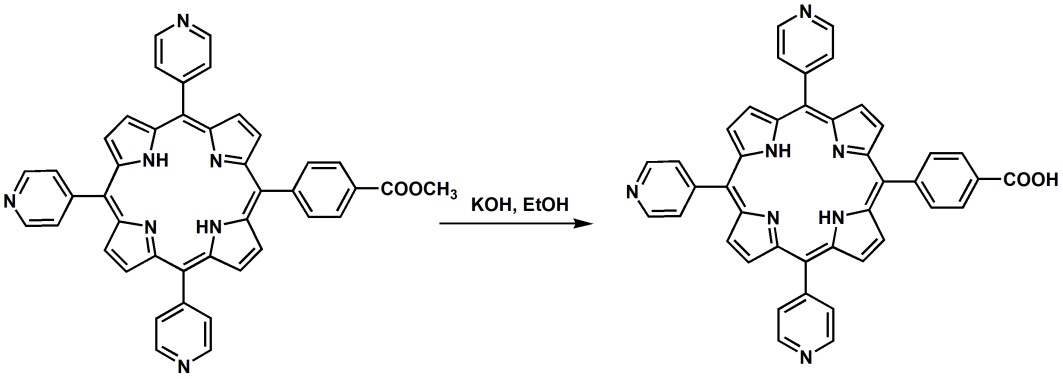

1 2

Scheme 2: Synthesis of porphyrin **2.**

The carboxylic acid group of porphyrin **2** was then further activated with N-hydroxysuccinimide in the presence of EDC and DMF as solvent to give porphyrin **3**.

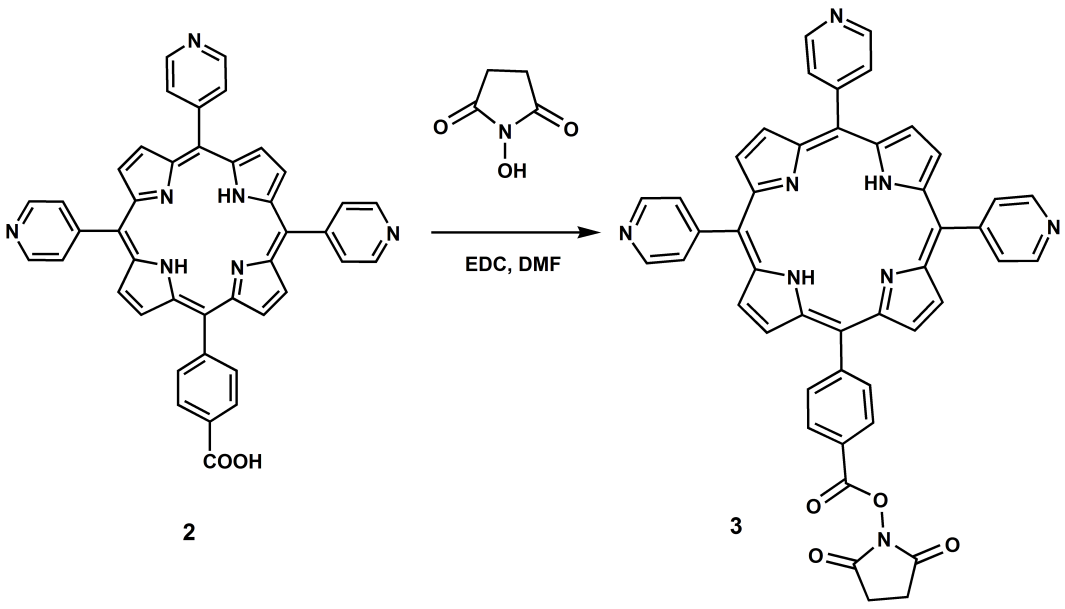

Scheme 3: Synthesis of porphyrin **3.**

Our intention was to attach the activated porphyrin **3** to the amino-modified DNA, via an amide linkage. The reaction conditions required aqueous medium and as the porphyrin had very little solubility in water this scheme was unsuccessful. Consequently, the reaction scheme was modified to make a water-soluble porphyrin which was achieved by methylating the pyridyl groups with methyl iodide.[26]

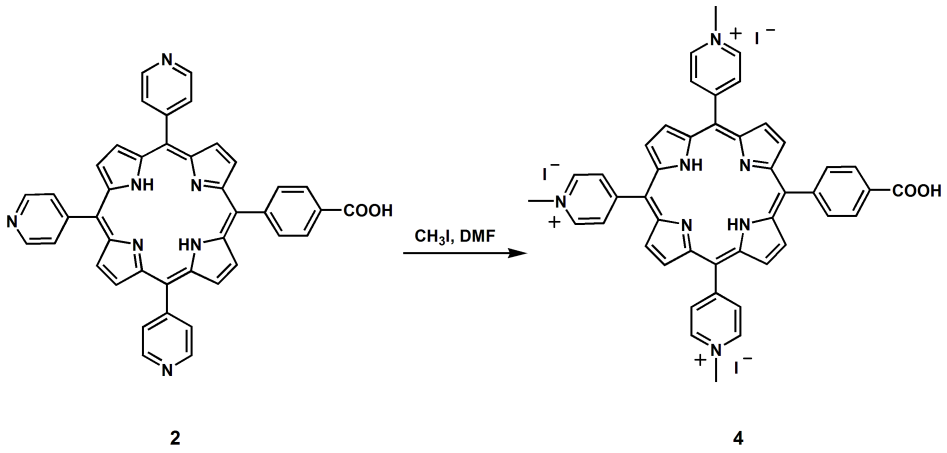

2 4

Scheme 4: Synthesis of porphyrin **4.**

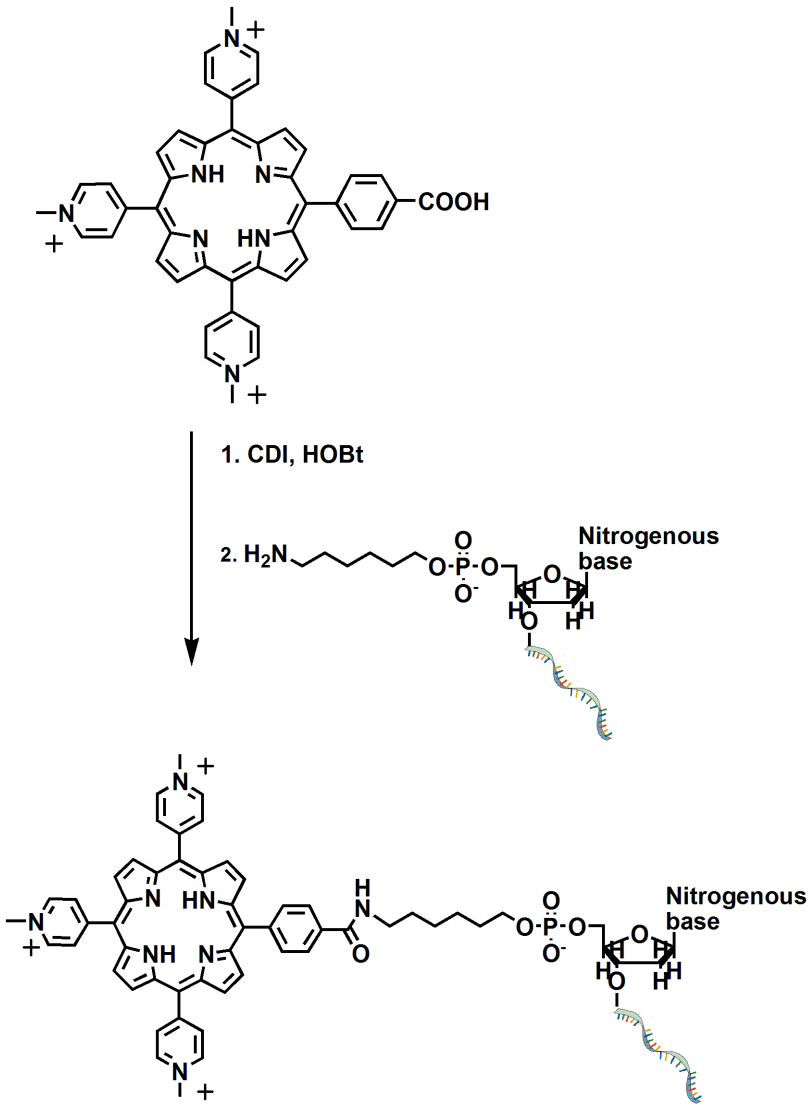

Scheme 5: General scheme for ligating DNA to porphyrin **4**.

Porphyrin **4** was completely water-soluble and was attached to the DNA via an amide linkage. The reaction was achieved by activating the porphyrin carboxylic acid by CDI and HOBt. The activated porphyrin was then treated with the respective single stranded DNA containing the amino group and incubated at 37ºC for 3 h.[27] All the DNA-porphyrin conjugates (10, 15, 20, 25, 30, 40, 50 base)

were then purified by reverse phase high performance liquid chromatography (HPLC) by gradient elution using 50 mM ammonium acetate (solvent A) and acetonitrile (solvent B) with a flow rate of 0.9 mL/min. The purified DNA-porphyrin conjugates were characterized by matrix-assisted laser desorption ionization (MALDI) mass spectrometry.

1. **10 base sequence**: Eluted at 18% B

5'-/5AmMC6/CGT GAC CGT C-3'

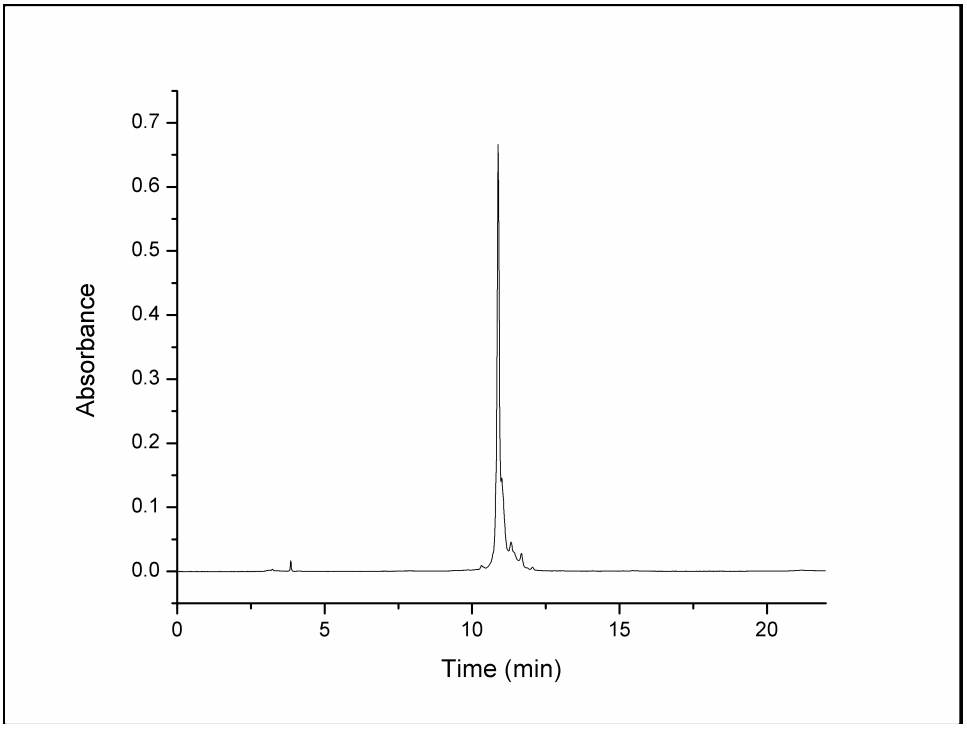

Figure 2: Chromatogram of **10-base DNA-porphrin** conjugate using a C4 analytical column with 50 mM ammonium acetate (solvent A) and 18% acetonitrile (solvent B) as eluent.

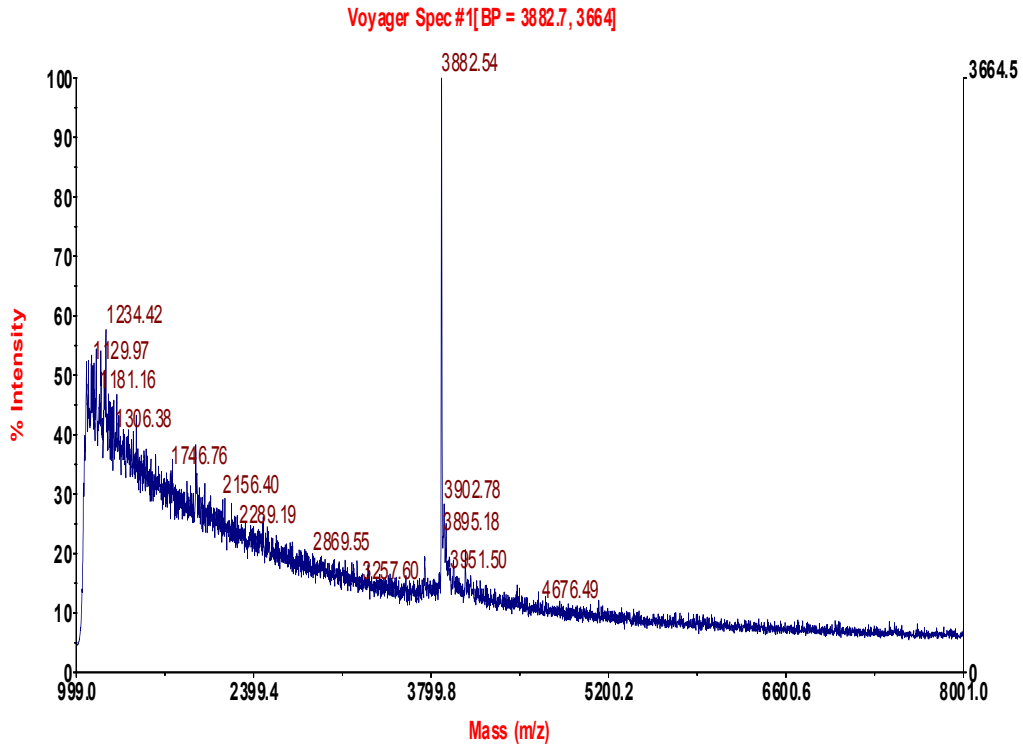

Figure 3: MALDI-TOF spectra of **10-base DNA-porphrin**, purified by HPLC, eluted at 18%B (see text) from a C4 analytical column. The major peak corresponds to the expected molecular weight of **10-base DNA-porphrin:** 3881.54.

2. **15 base sequence:** Eluted at 16% B

5'-/5AmMC6/TGA CTC GTG ACC GTC-3'

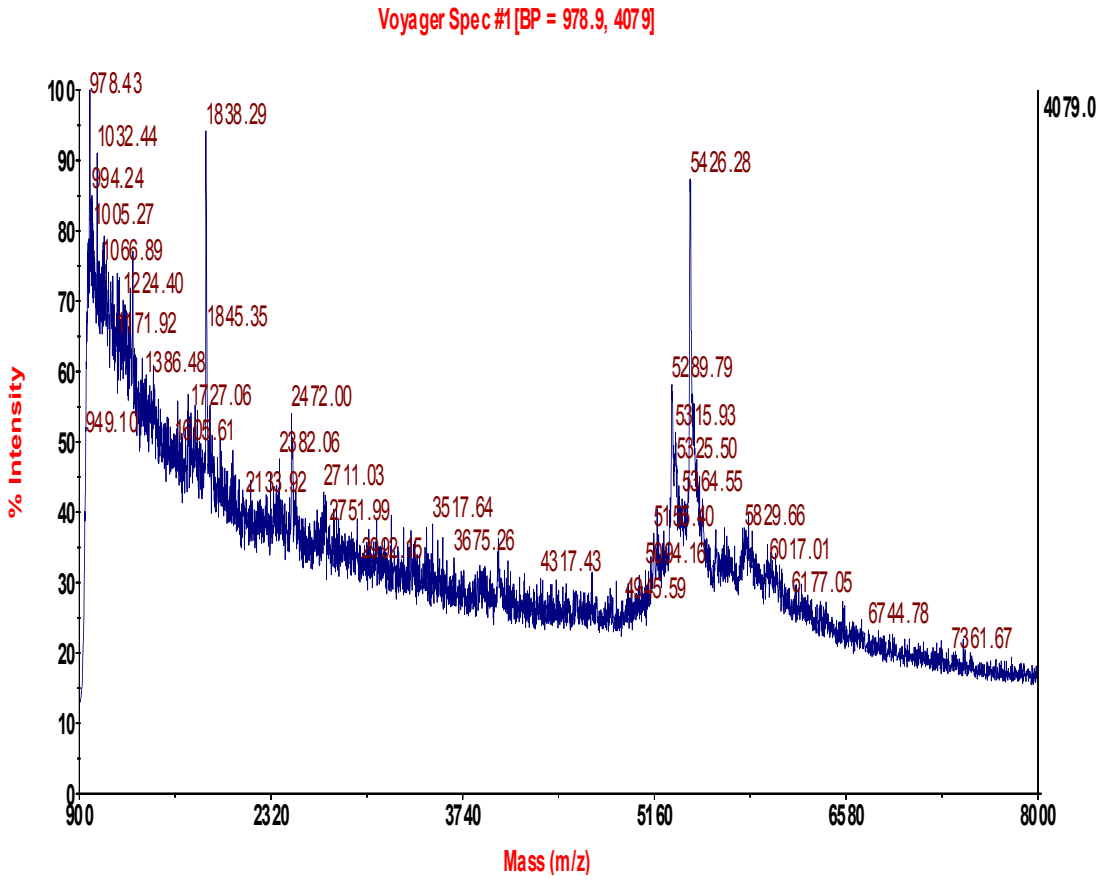

Figure 4: MALDI-TOF spectra of **15-base DNA-porphrin**, purified by HPLC, eluted with 16%B (see text) from C4 analytical column. The major peak corresponds to the expected molecular weight of **15-base DNA-porphrin:** 5423.37.

3. **20 base sequence:** Eluted at 15% B

5'-/5AmMC6/GGC TGT GAC TCG TGA CCG TC-3'

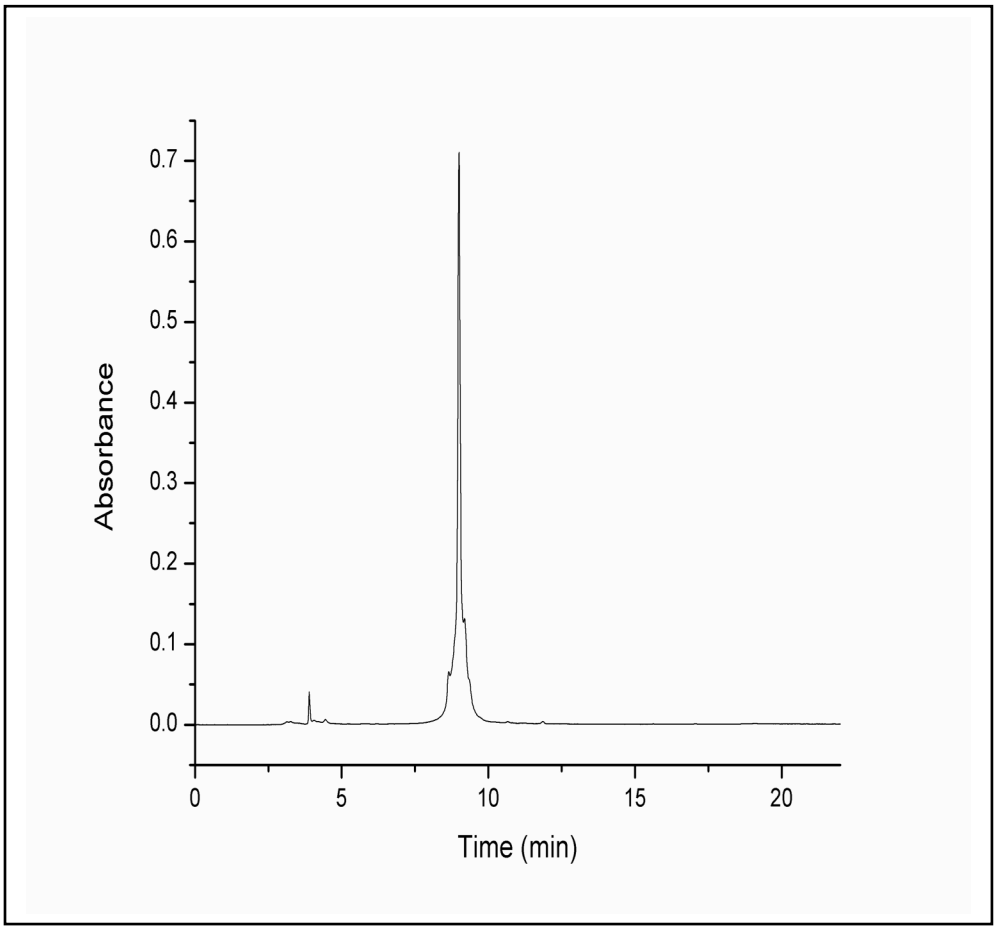

Figure 5: Chromatogram of **20-base DNA-porphrin** conjugate using a C4 analytical column with 50 mM ammonium acetate (solvent A) and 15% acetonitrile (solvent B) as eluent.

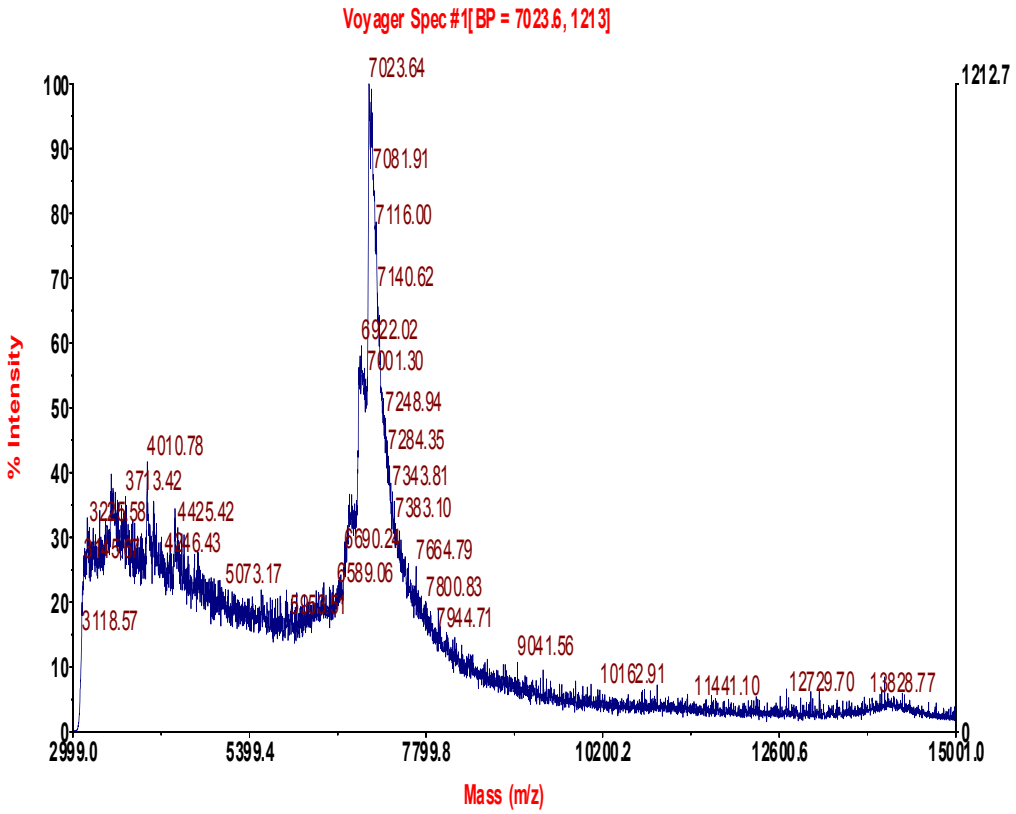

Figure 6: MALDI-TOF spectra of **20-base DNA-porphrin**, purified by HPLC, eluted at 15% B (see text) from a C4 analytical column. The major peak corresponds to the expected molecular weight + sodium ion of **20-base DNA-porphrin:** 7001.73.

4. **25 base sequence**: Eluted at 13.26% B

5'-/5AmMC6/GAC TCG GCT GTG ACT CGT GAC CGT C-3'

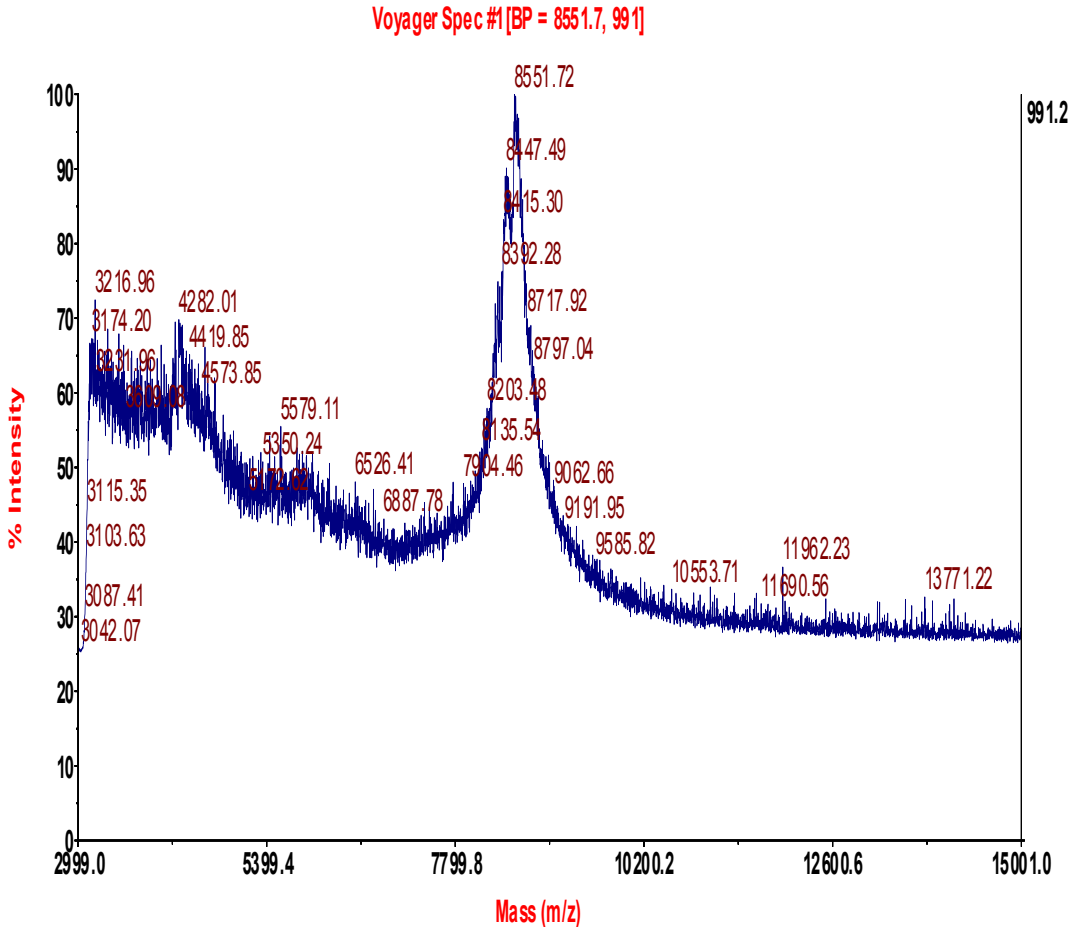

Figure 7: MALDI-TOF spectra of **25-base DNA-porphrin**, purified by HPLC, eluted with 13% B (see text) from a C4 analytical. The major peak corresponds to the expected molecular weight of **25-base DNA-porphrin:** 8547.23.

5. **30 base sequence**: Eluted at 12.93% B

5'-/5AmMC6/GTG CAG ACT CGG CTG TGA CTC GTG ACC GTC-3'

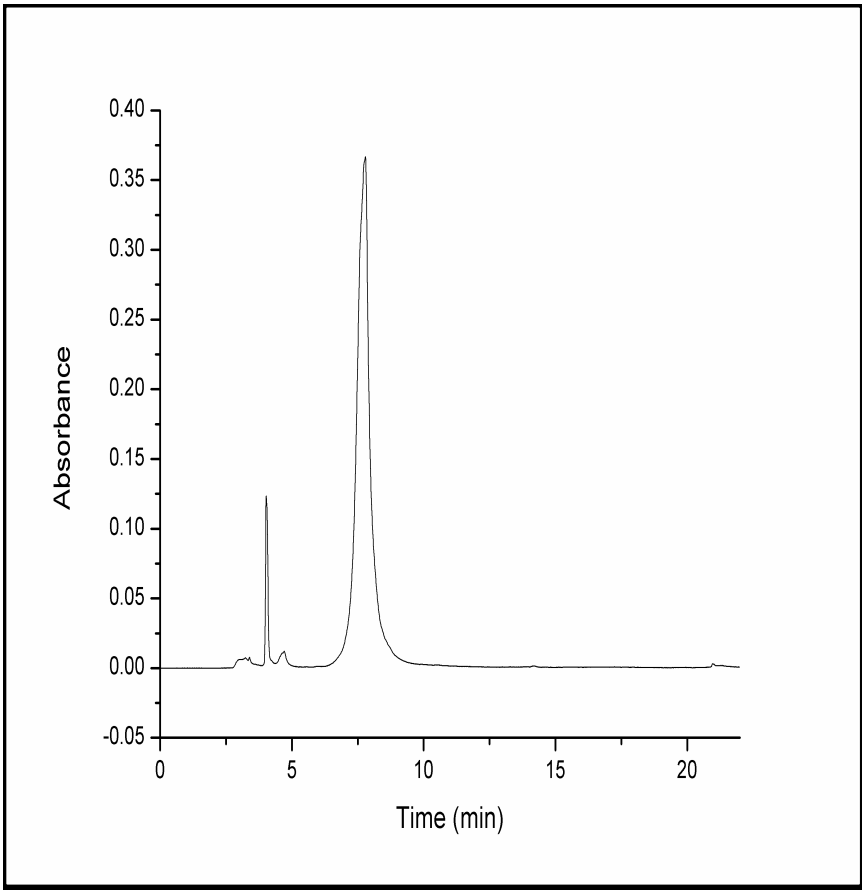

Figure 8: Chromatogram of **30-base DNA-porphrin** using on a C4 analytical column with 50 mM ammonium acetate (solvent A) and 13% acetonitrile (solvent B) as eluent.

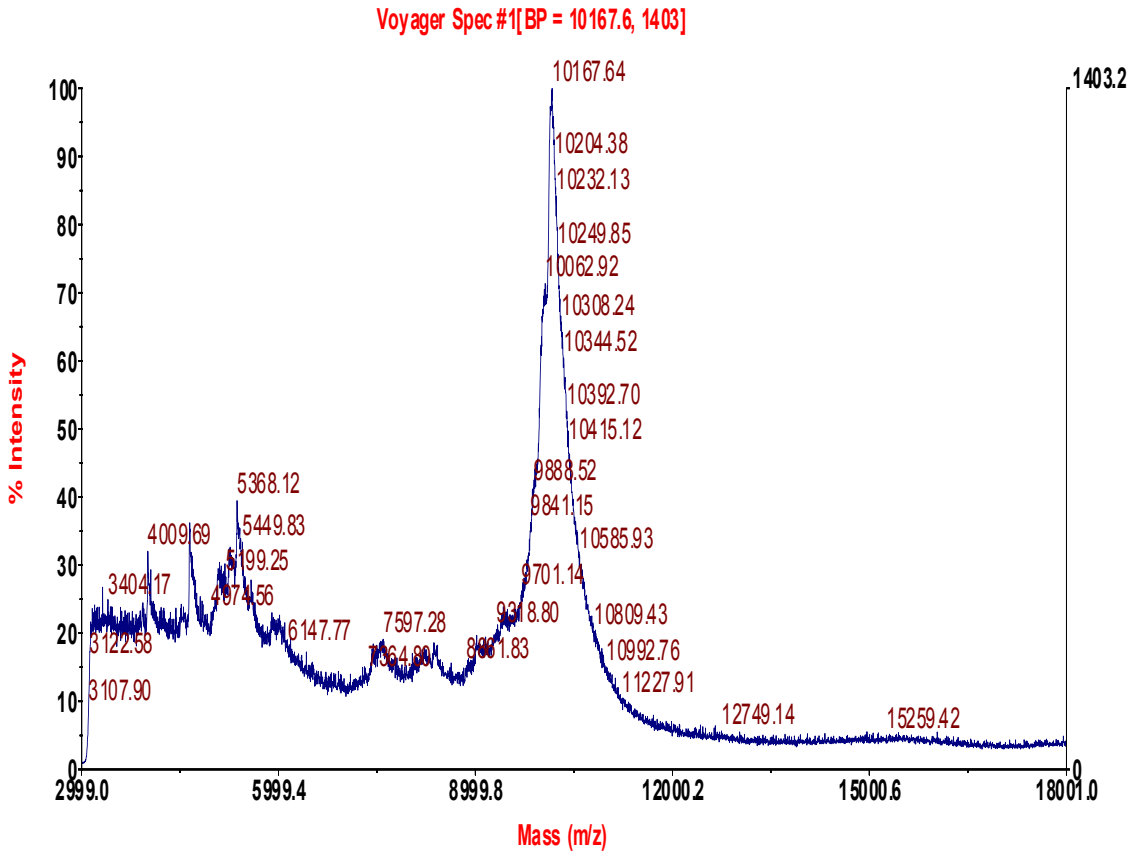

Figure 9: MALDI-TOF spectra of **30-base DNA-porphrin,** purified by HPLC, eluted at 13%B (see text) from a C4 analytical column. The major peak corresponds to the expected molecular weight of **30-base DNA-porphrin:** 10150.37.

6. **40 base sequence**: Eluted at 19.35% B

5'-/5AmMC6/TAC GGT GAT AGT GCA GAC TCG GCT GTG ACT CGT GAC CGT C-3'

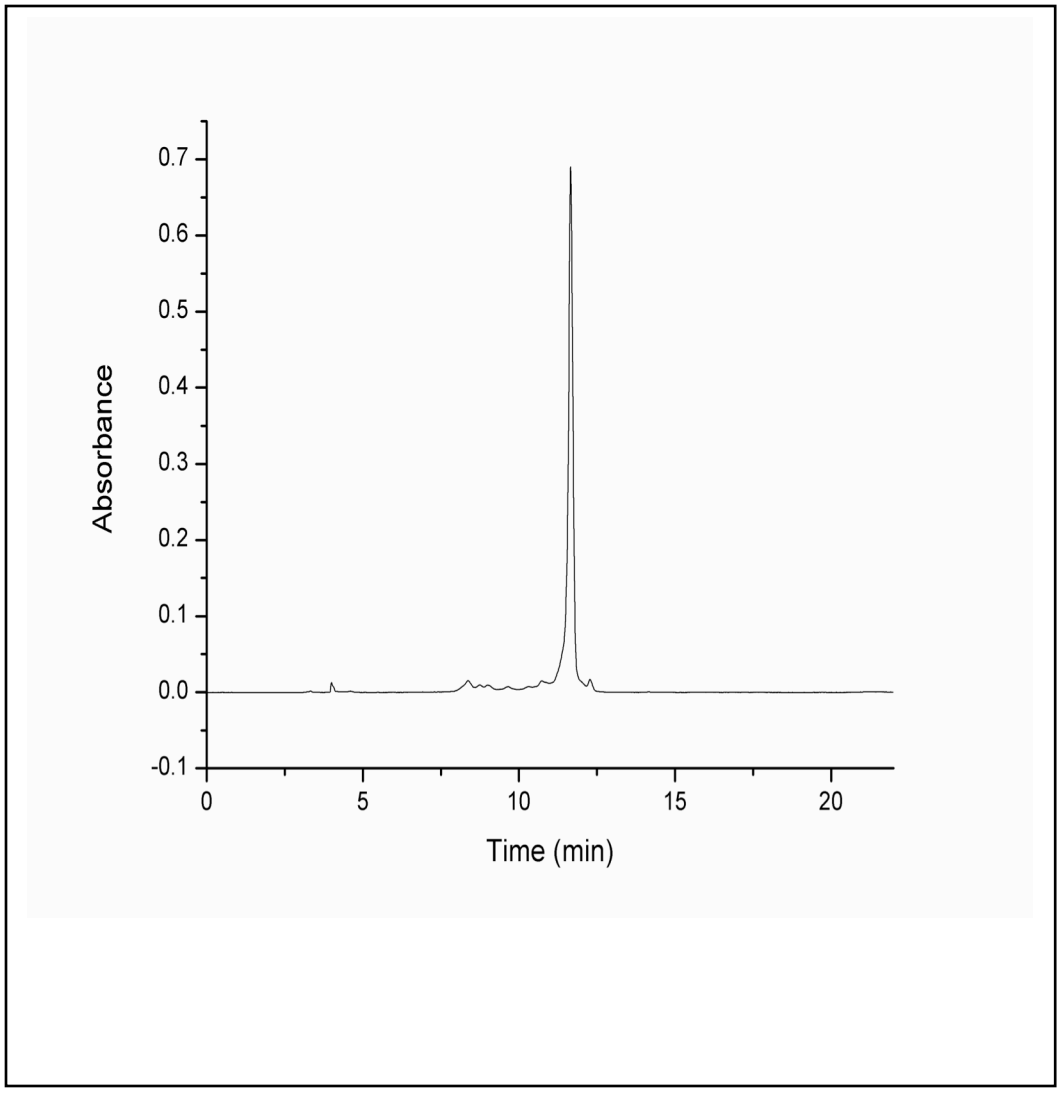

Figure 10: Chromatogram of **40-base DNA-porphrin** using a C4 analytical column with 50 mM ammonium acetate (solvent A) and 19.35% (solvent B) as eluent.

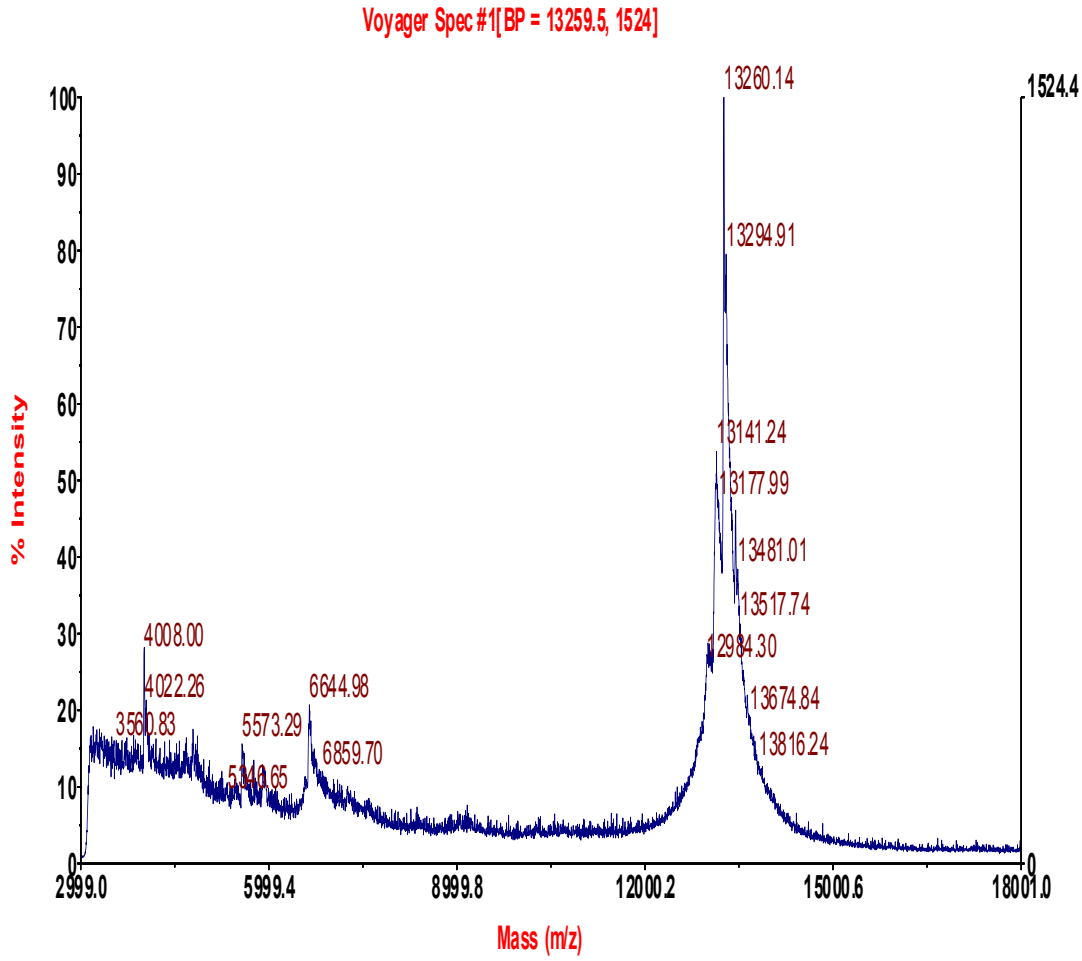

Figure 11: MALDI-TOF spectra of **40-base DNA-porphrin**, purified by HPLC, eluted with 19.35% B (see text) from a C4 analytical column. The major peak corresponds to the expected molecular weight of **40-base DNA-porphrin** 13265.63.

7. **50 base sequence:** Eluted at 14% B

5'-/5AmMC6/ACC TCC TGA GTA CGG TGA TAG TGC AGA CTC GGC TGT GAC TCG TGA CCG TC-3'

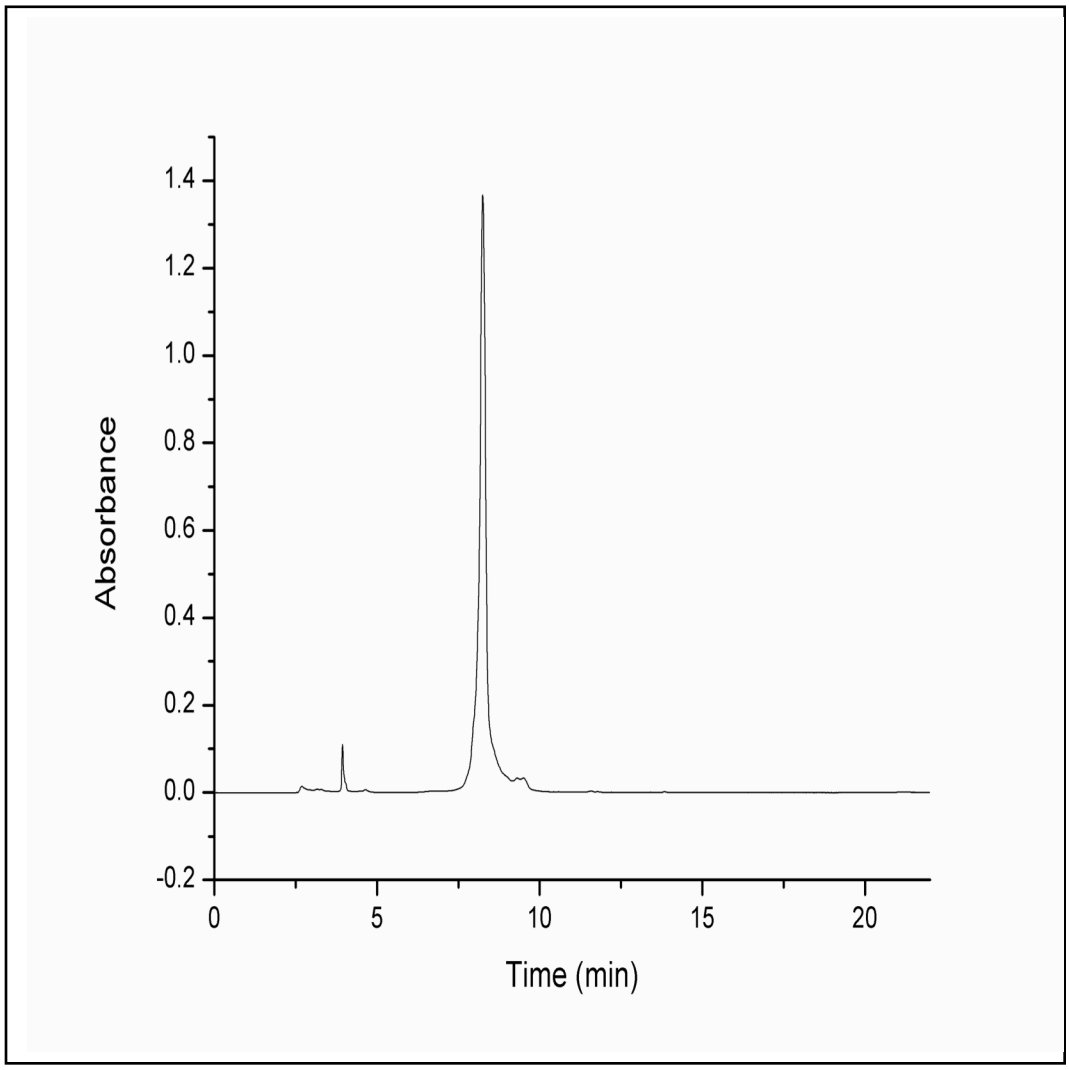

Figure 12: Chromatogram of **50-base DNA-porphrin** using on a C4 analytical column with 50 mM ammonium acetate (solvent A) and 14% acetonitrile (solvent B) as eluent.

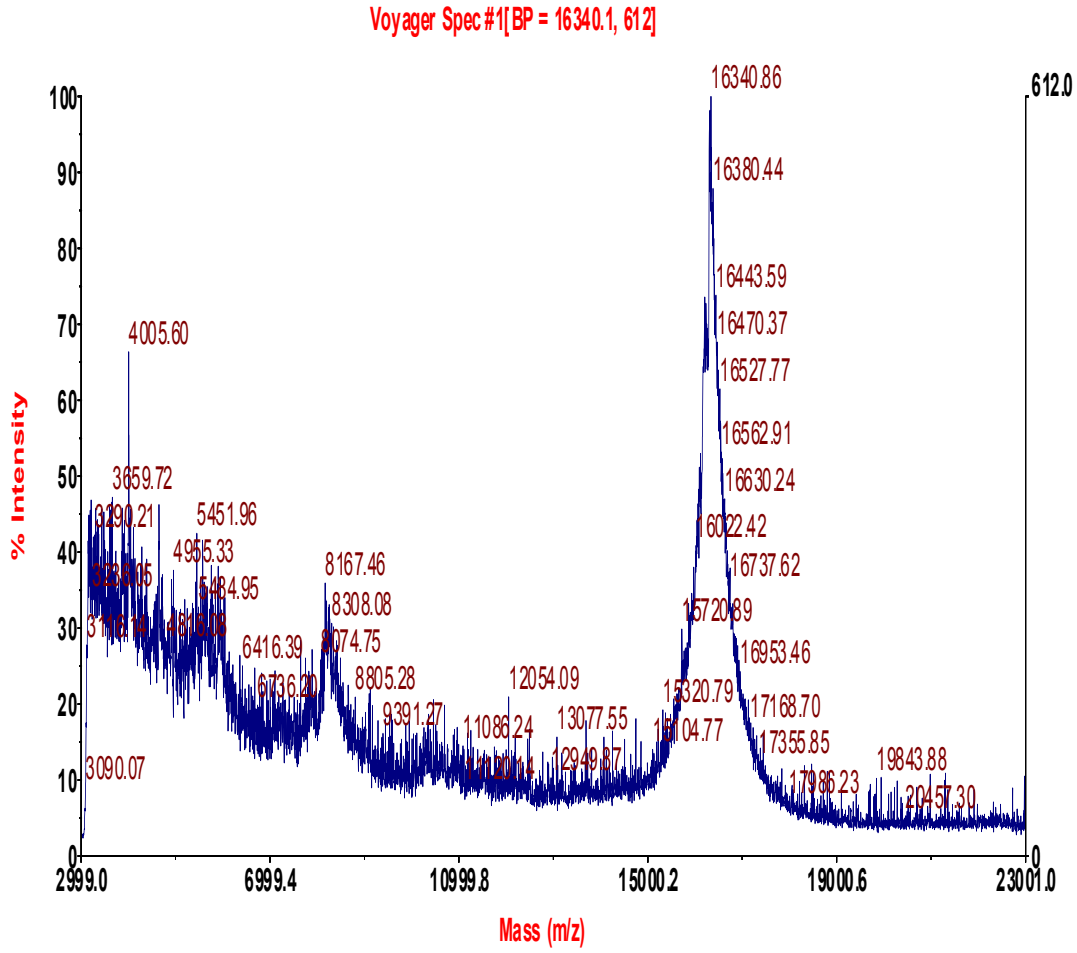

Figure 13: MALDI-TOF spectra of **50-base DNA-porphrin**, purified by HPLC, eluted at 14% B (see text) on C4 analytical column. The major peak corresponds to the expected molecular weight **of 50-base DNA-porphrin** 16337.97.

The concentrations of the oligonucleotides were determined by UV absorption measurements at 260 nm (see Figure 14) as the length of the DNA increases the extinction coefficient of DNA increases. The absorption spectra shows a Soret-band at 435 nm, Q_y bands are located at 520 and 550 nm, and Q_x bands are located at 590 and 653 nm.

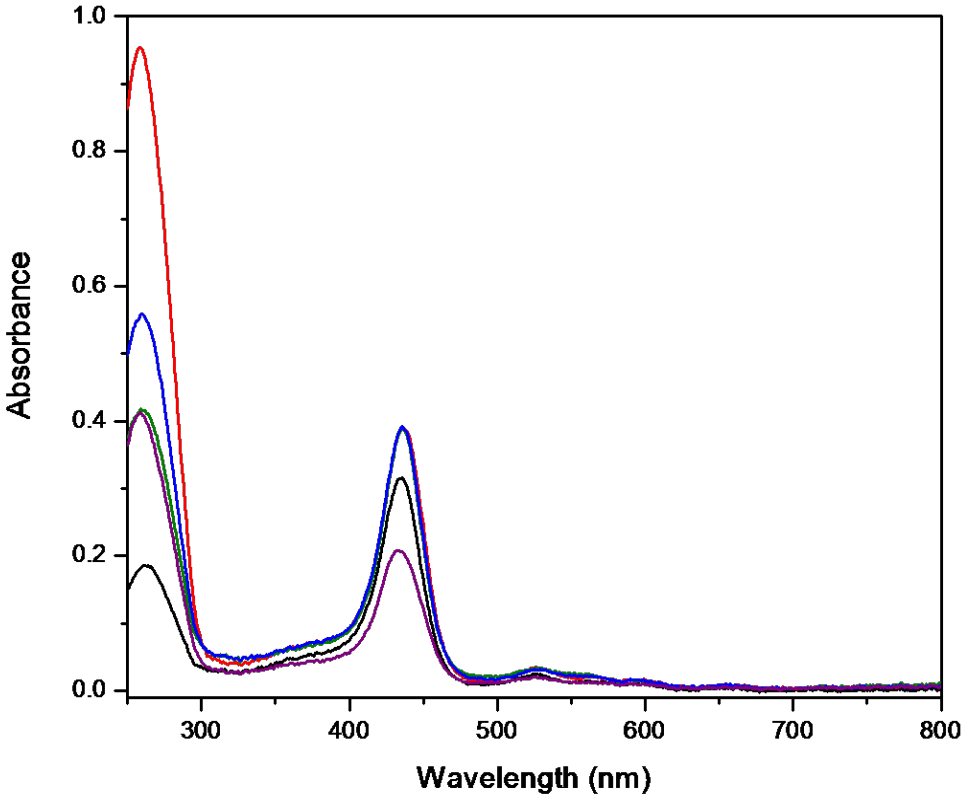

Figure 14: Absorption spectra of DNA-porphyrin conjugates: 10-base (black), 20-base (purple), 30-base (green), 40-base (blue), 50-base (red).

2. Preparation of porphyrin-nanoparticle conjugates. (In collaboration with Suchetan Pal from Hao Yan's Lab)

Silver nanoparticles were functionalized with oligonucleotides containing multiple phosphorothioate linkages in which a sulfur atom replaces non-bridging oxygen in the phosphate backbone of the oligonucleotide. The sulfur atom on DNA facilitates the attachment of the oligonucleotide on the nanoparticle.[28] The nanoparticles are surrounded with DNA and there are multiple interactions between the silver nanoparticles and sulfur; the addition of PEG stabilizes the nanoparticles from aggregation. One end of the DNA is attached to NP while the rest of the DNA sequence is free and presumably pointing away from the surface; it can be hybridized with its complimentary strand. Our collaborators at Hao Yan's lab at Arizona State University have developed such a method. The porphyrin was attached to the complimentary DNA strand via amide linkage, as described above. Using DNA as a spacer, the porphyrin molecules were attached to the nanoparticle with varying distances. The length of the double stranded DNA ranged from 3.4 to 17 nm, which corresponds to 10 to 50 base-pairs. The double stranded DNA that is fully conjugated is expected to behave as a rigid rod, with one helical turn of the duplex to be around 3.4 nm.[28] Even though the electrostatic repulsion between the double stranded DNA-porphyrin and the DNA monolayer on the surface of the NP should allow an upright configuration, the flexibility due to the alkyl chains connecting the porphyrin and DNA cannot be neglected therefore the values for the distance are approximate.

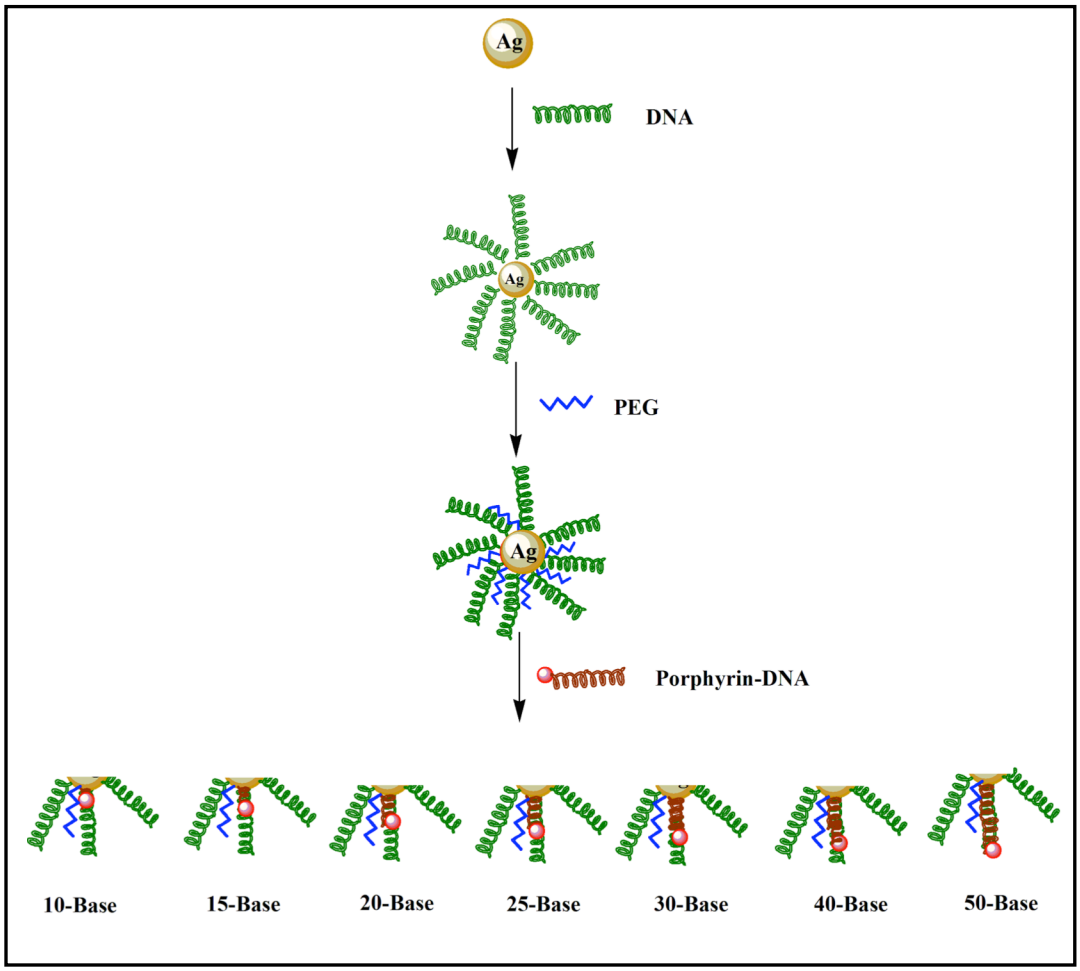

Scheme 5: General scheme for attaching porphyrin to Ag NP using various lengths of double stranded DNA.

Two sets of Ag NP solutions, named the sample and control were prepared named sample and control. The sample solution contained the Ag Np coated with 55 base phosphothiorated DNA complimentary to the DNA-porphyrin conjugates. The control solution contained the Ag NP coated with single stranded DNA non

complimentary to the DNA-porphyrin conjugates. Both these sets of Ag NP solution were additionally coated with thiolated PEG to prevent any coagulation of the nanoparticles. Concentration of these two sets of Ag NP solution was matched by checking their absorbance at 408 nm.

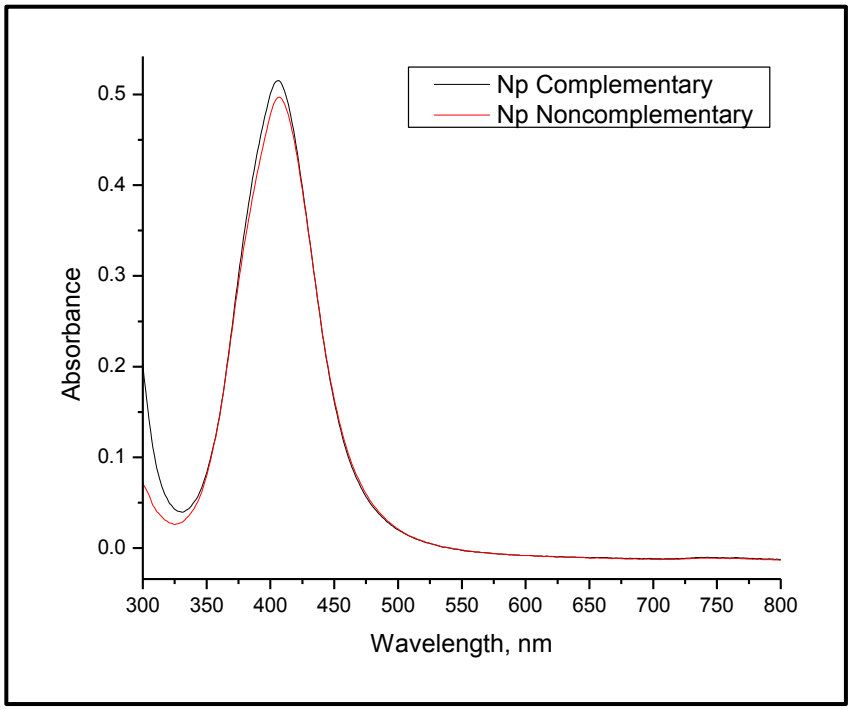

Figure 15: Absorption spectra of Ag NPs solutions coated with a monolayer of complementary stranded DNA to the DNA-porphyrin conjugates (black) and with a monolayer of non-complimentary stranded DNA to the DNA-porphyrin conjugates (red).

For each DNA-porphyrin conjugate, two solutions were made:

1. Sample: DNA-porphyrin conjugate and complementary DNA-nanoparticle solution.

2. Control: DNA-porphyrin conjugate and non–complementary DNA-nanoparticle solution.

After hybridization, the absorbance from the nanoparticle did not show significant change for either sample. Due to the much higher extinction coefficient of the AgNP, the absorbance from porphyrin (dye) could not be observed, however it could be monitored by means of a fluorescence excitation and emission. Figure 16-43 shows the steady state absorption, the steady-state emission spectra (at 408 nm excitation), the steady-state emission spectra (at 435 nm excitation), and the steady state emission spectra (at 660 nm excitation) for 10-, 15-, 20-, 30-, 40-, 50-base DNA porphyrins.

1. 10-base DNA-porphyrin (Figures 16–19)

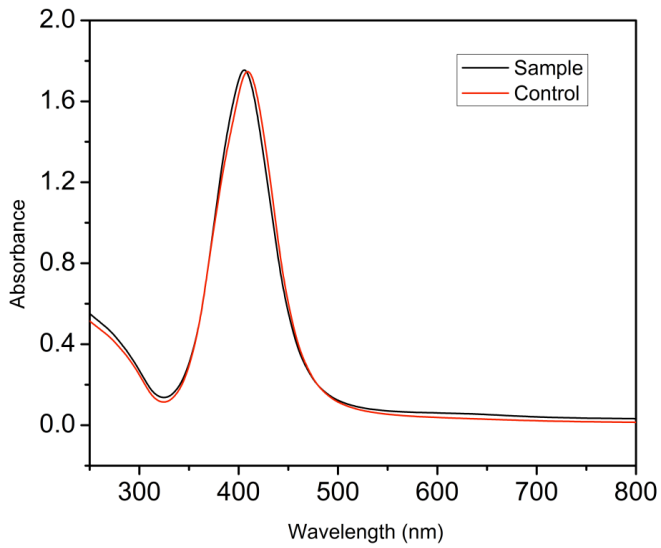

Figure 16: Steady state absorption: **10-base DNA-porphyrin** and complementary DNA-nanoparticle solution (black); mixture of **10-base DNA-porphyrin** and noncomplementary DNA-nanoparticle solution (red).

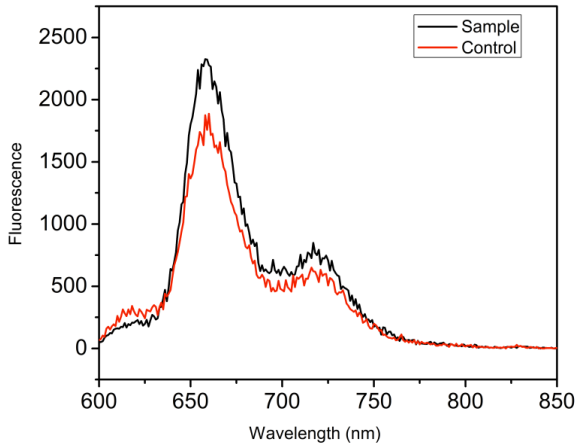

Figure 17: Steady state emission spectra (408 nm excitation): **10-base DNA-porphyrin** and complementary DNA-nanoparticle solution (black); **10-base DNA-porphyrin** and noncomplementary DNA-nanoparticle solution (red).

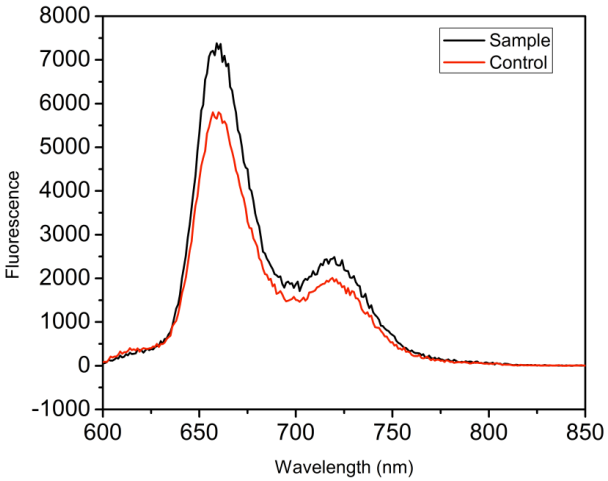

Figure 18: Steady state emission spectra (435 nm excitation): **10-base DNA-porphyrin** and complementary DNA-nanoparticle solution (black); **10-base DNA-porphyrin** and noncomplementary DNA-nanoparticle solution (red).

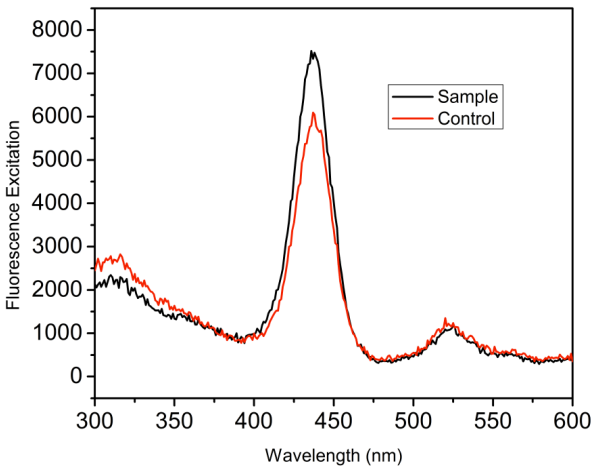

Figure 19: Steady state excitation spectra (660 nm emission): **10-base DNA-porphyrin** and complementary DNA-nanoparticle solution (black); **10-base DNA-porphyrin** and noncomplementary DNA-nanoparticle solution (red).

2. 15-base DNA-porphyrin (Figures 20–23)

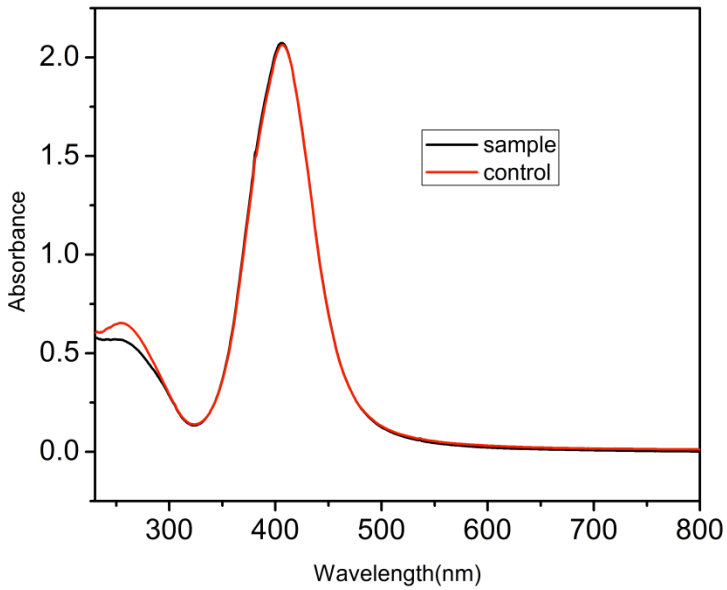

Figure 20: Steady state absorption: **15-base DNA-porphrin** and complementary DNA-nanoparticle solution (black); mixture of **15-base DNA-porphyrin** and noncomplementary DNA-nanoparticle solution (red).

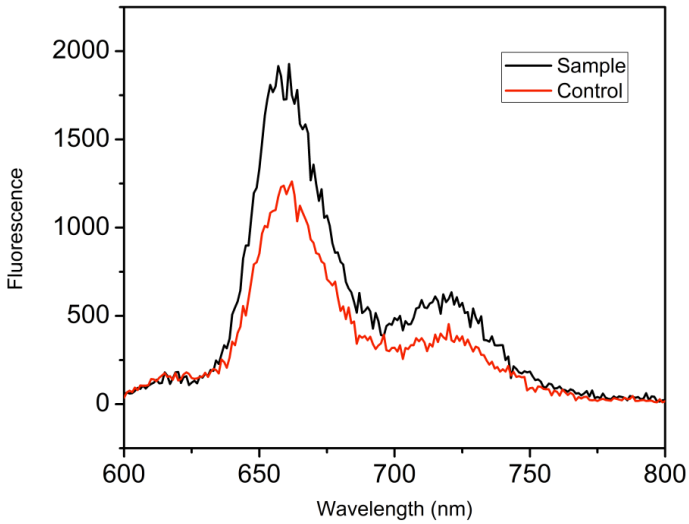

Figure 21: Steady state emission spectra (408 nm excitation): **15-base DNA-porphyrin** and complementary DNA-nanoparticle solution (black); mixture of **15-base DNA-porphyrin** and noncomplementary DNA-nanoparticle solution (red).

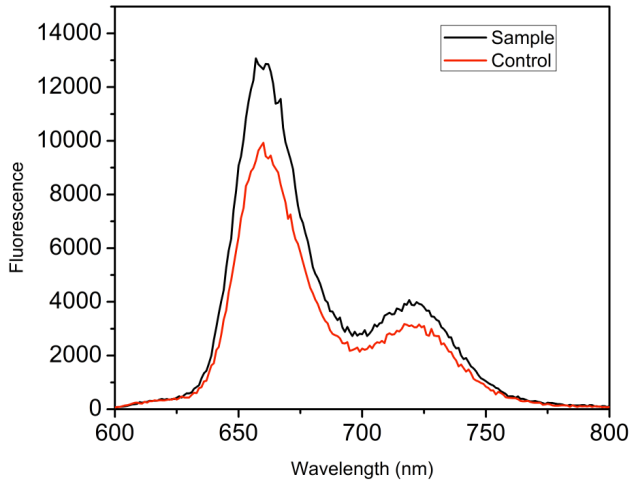

Figure 22: Steady state emission spectra (435 nm excitation): **15-base DNA-porphyrin** and complementary DNA-nanoparticle solution (black); mixture of **15-base DNA-porphyrin** and noncomplementary DNA-nanoparticle solution (red).

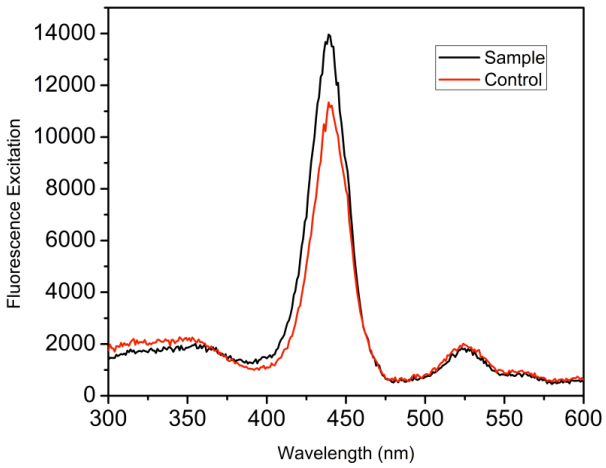

Figure 23: Steady state excitation spectra (660 nm emission): **15-base DNA-porphyrin** and complementary DNA-nanoparticle solution (black); mixture of **15-base DNA-porphyrin** and noncomplementary DNA-nanoparticle solution (red).

3. 20-base DNA-porphyrin (Figures 24–27)

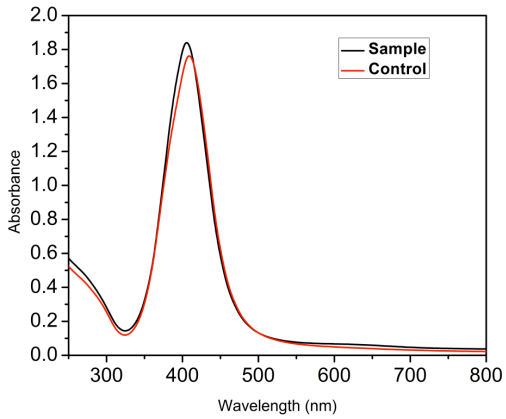

Figure 24: Steady state absorption: **20-base DNA-porphrin** and complementary DNA-nanoparticle solution (black); mixture of **20-base DNA-porphyrin** and noncomplementary DNA-nanoparticle solution (red).

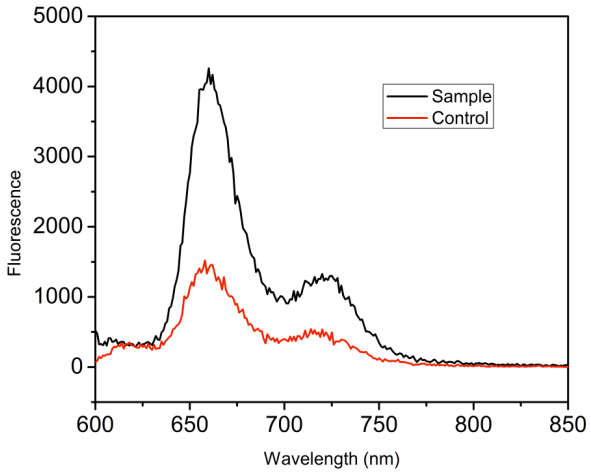

Figure 25: Steady state emission spectra (408 nm excitation): **20-base DNA-porphyrin** and complementary DNA-nanoparticle solution (black); mixture of **20-base DNA-porphyrin** and noncomplementary DNA-nanoparticle solution (red).

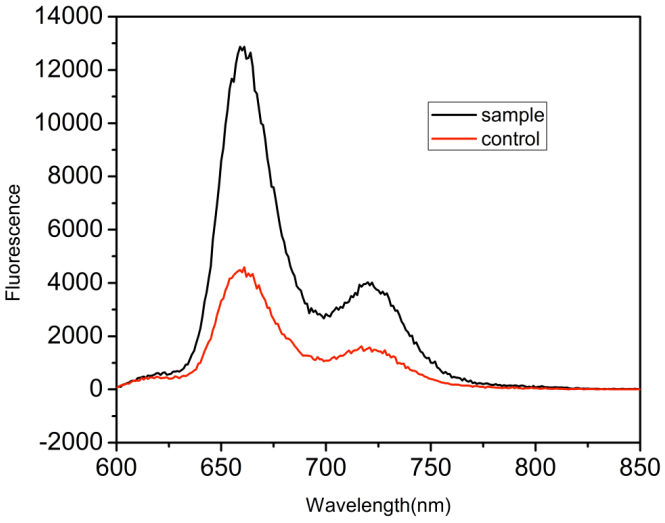

Figure 26: Steady state emission spectra (435 nm excitation): **20-base DNA-porphyrin** and complementary DNA-nanoparticle solution (black); mixture of **20-base DNA-porphyrin** and noncomplementary DNA-nanoparticle solution (red).

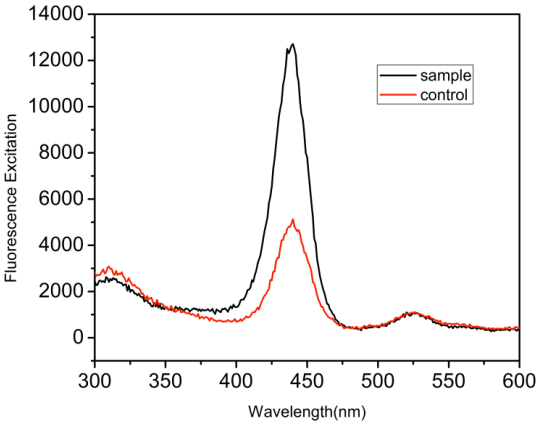

Figure 27: Steady state excitation spectra (660 nm excitation): **20-base DNA-porphyrin** and complementary DNA-nanoparticle solution (black); mixture of **20-base DNA-porphyrin** and noncomplementary DNA-nanoparticle solution (red).

4. 25-base DNA-porphyrin (Figures 28–31)

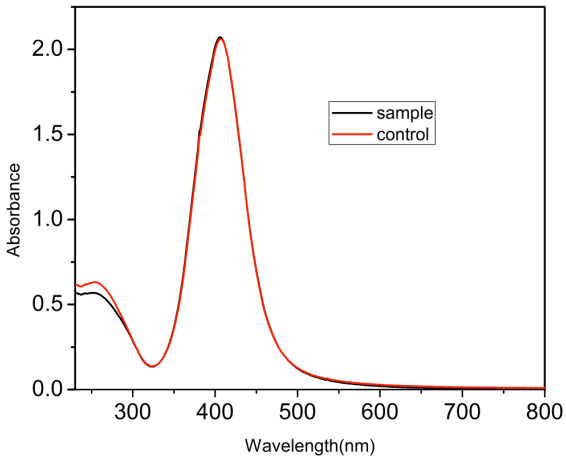

Figure 28: Steady state absorption: **25-base DNA-porphrin** and complementary DNA-nanoparticle solution (black); mixture of **25-base DNA-porphyrin** and noncomplementary DNA-nanoparticle solution (red).

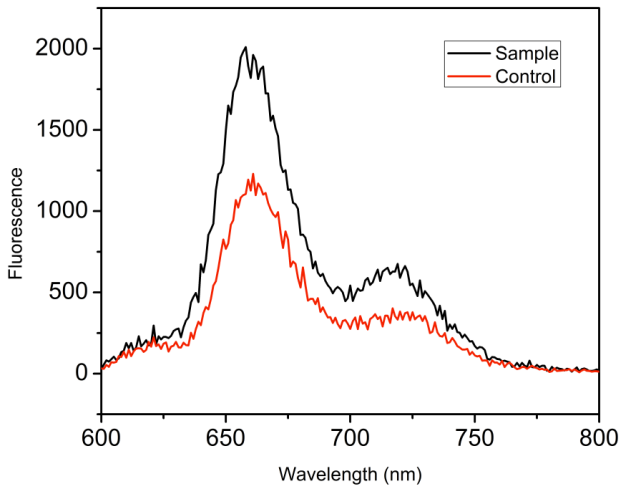

Figure 29: Steady state emission spectra (408 nm excitation): **25-base DNA-porphyrin** and complementary DNA-nanoparticle solution (black); mixture of **25-base DNA-porphyrin** and noncomplementary DNA-nanoparticle solution (red).

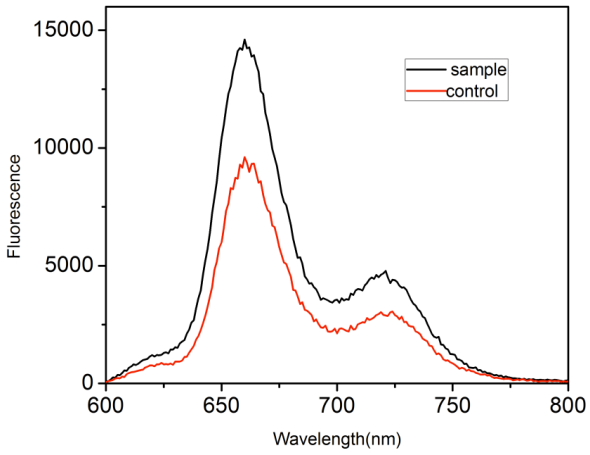

Figure 30: Steady state emission spectra (435 nm excitation): **25-base DNA-porphyrin** and complementary DNA-nanoparticle solution (black); mixture of **25-base DNA-porphyrin** and noncomplementary DNA-nanoparticle solution (red).

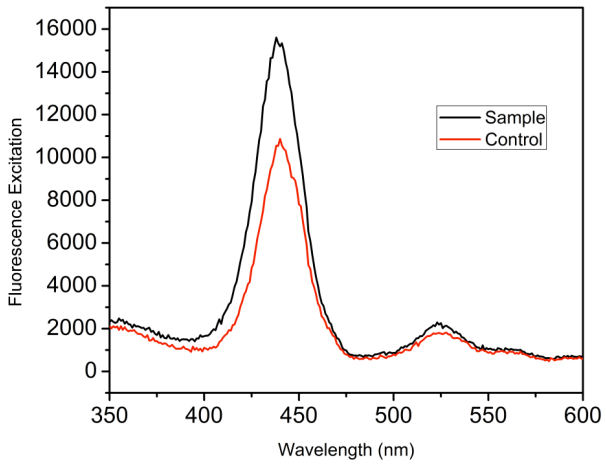

Figure 31: Steady state excitation spectra (660 nm emission): **25-base DNA-porphyrin** and complementary DNA-nanoparticle solution (black); mixture of **25-base DNA-porphyrin** and noncomplementary DNA-nanoparticle solution (red).

4. 30-base DNA-porphyrin (Figures 31–35)

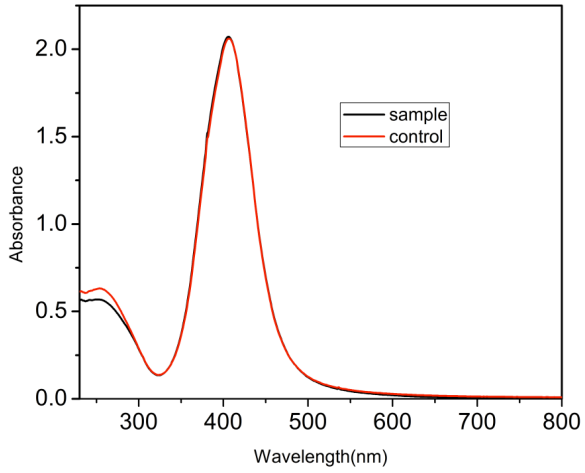

Figure 32: Steady state absorption: **30-base DNA-porpyhrin** and complementary DNA-nanoparticle solution (black); mixture of **30-base DNA-porphyrin** and noncomplementary DNA-nanoparticle solution (red).

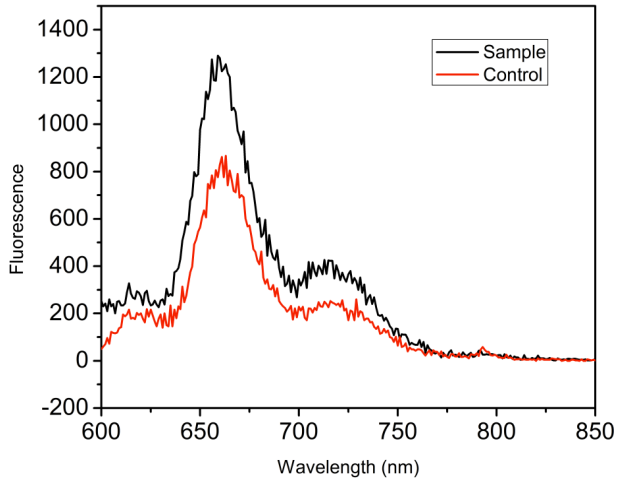

Figure 33: Steady state emission spectra (408 nm excitation): **30-base DNA-porphyrin** and complementary DNA-nanoparticle solution (black); mixture of **30-base DNA-porphyrin** and noncomplementary DNA-nanoparticle solution (red).

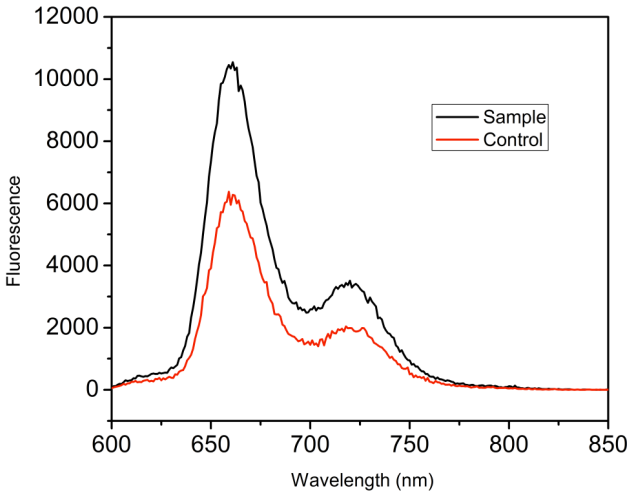

Figure 34: Steady state emission spectra (435 nm excitation): **30-base DNA-porphyrin** and complementary DNA-nanoparticle solution (black); mixture of **30-base DNA-porphyrin** and noncomplementary DNA-nanoparticle solution (red).

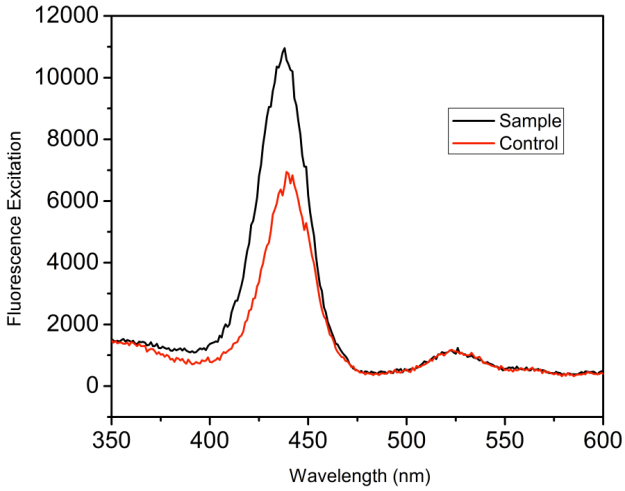

Figure 35: Steady state excitation spectra (660 nm emission): **30-base DNA-porphyrin** and complementary DNA-nanoparticle solution (black); mixture of **30-base DNA-porphyrin** and noncomplementary DNA-nanoparticle solution (red).

5. 40-base DNA-porphyrin (Figures 36–39)

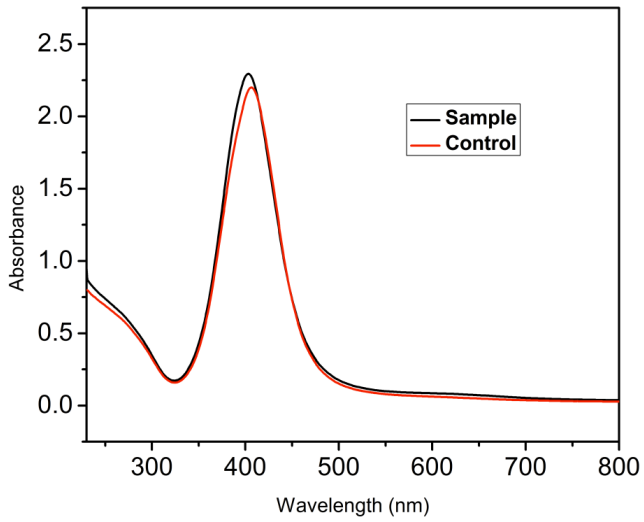

Figure 36: Steady state absorption: **40-base DNA-porphrin** and complementary DNA-nanoparticle solution (black); mixture of **40-base DNA-porphyrin** and noncomplementary DNA-nanoparticle solution (red).

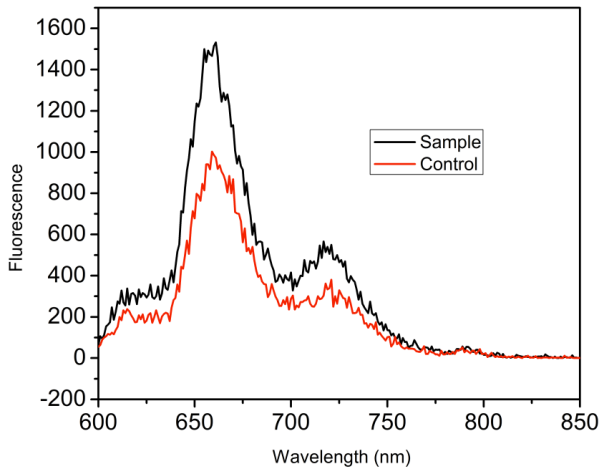

Figure 37: Steady state emission spectra (408 nm excitation): **40-base DNA-porphyrin** and complementary DNA-nanoparticle solution (black); mixture of **40-base DNA-porphyrin** and noncomplementary DNA-nanoparticle solution (red).

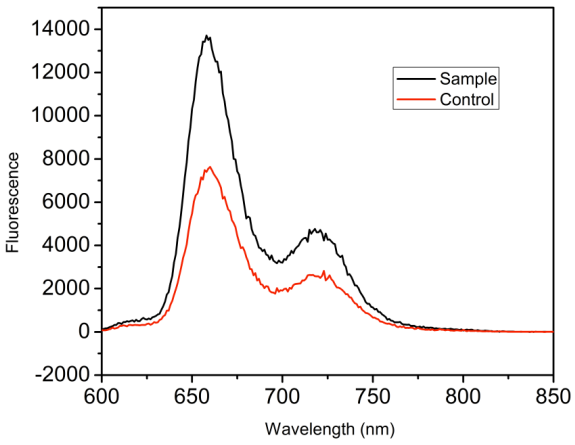

Figure 38: Steady state emission spectra (435 nm excitation): **40-base DNA-porphyrin** and complementary DNA-nanoparticle solution (black); mixture of **40-base DNA-porphyrin** and noncomplementary DNA-nanoparticle solution (red).

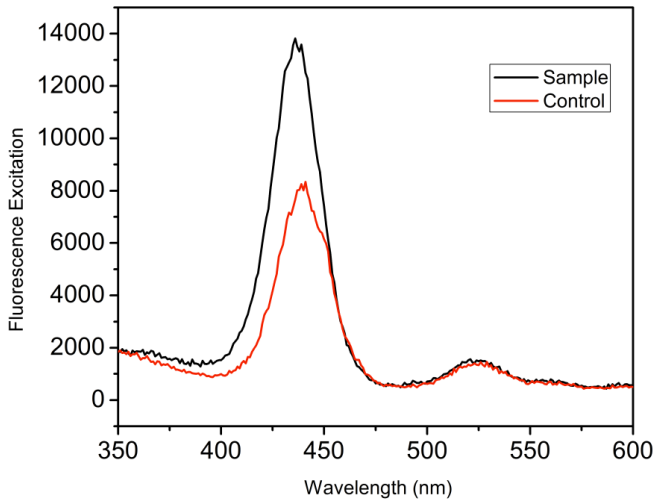

Figure 39: Steady state excitation spectra (660 nm emission): **40-base DNA-porphyrin** and complementary DNA-nanoparticle solution (black); mixture of **40-base DNA-porphyrin** and noncomplementary DNA-nanoparticle solution (red).

5. 50-base DNA-porphyrin (Figures 40–43)

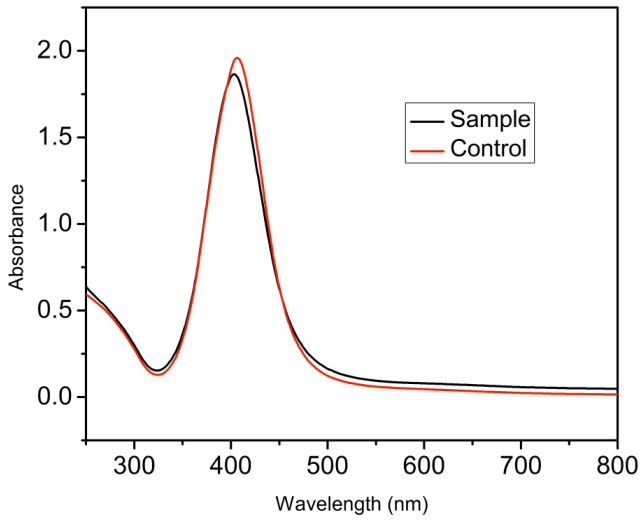

Figure 40: Steady state absorption: **50-base DNA-porphrin** and complementary DNA-nanoparticle solution (black); mixture of **50-base DNA-porphyrin** and noncomplementary DNA-nanoparticle solution (red).

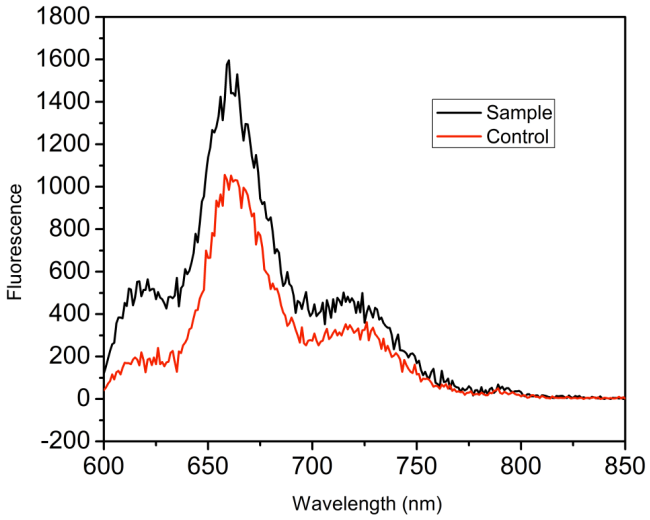

Figure 41: Steady state emission spectra (408 nm excitation): **50-base DNA-porphyrin** and complementary DNA-nanoparticle solution (black); mixture of **50-base DNA-porphyrin** and noncomplementary DNA-nanoparticle solution (red).

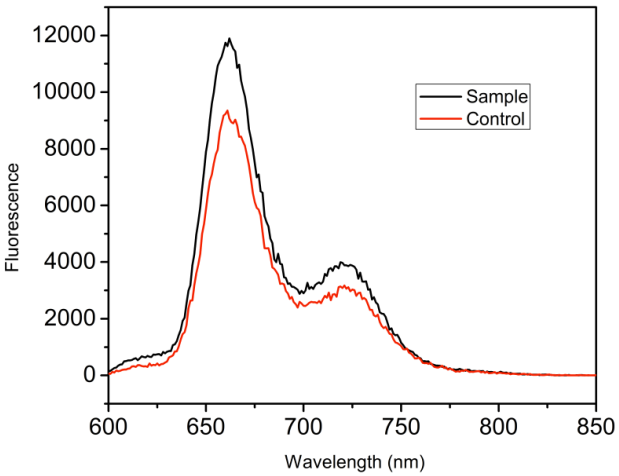

Figure 42: Steady state emission spectra (435 nm excitation): **50-base DNA-porphyrin** and complementary DNA-nanoparticle solution (black); mixture of **50-base DNA-porphyrin** and noncomplementary DNA-nanoparticle solution (red).

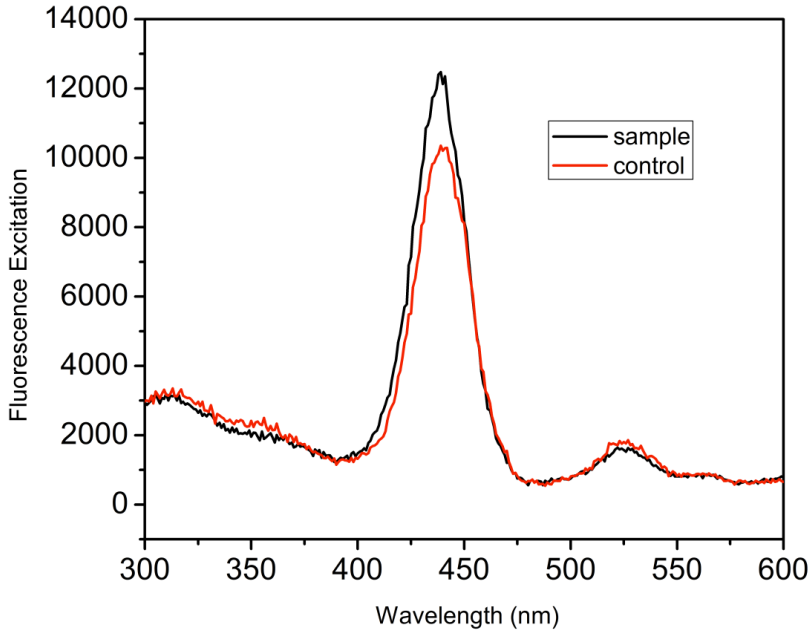

Figure 43: Steady state excitation spectra (660 nm emission): **50-base DNA-porphyrin** and complementary DNA-nanoparticle solution (black); mixture of **50-base DNA-porphyrin** and noncomplementary DNA-nanoparticle solution (red).

The absorption of light by the porphyrin responsible for its fluorescence at the various distances from the Ag NP was observed by measuring the excitation spectrum (by setting emission at 660 nm) and the fluorescence spectra was obtained by setting the excitation at 408 nm or at 435 nm and scanning the emission spectra. The typical free-base porphyrin fluorescence at 600–800 nm originates from the Q_x state. The fluorescence bands are located at ~675 and ~725 nm for 10–50 base DNA-porphyrin attached to Ag NP. The ratio of fluorescence intensity enhancement is defined as $F(Q/Q_0)$, where FQ and FQ_0 are the fluorescence intensities of sample and control respectively. The above figures

provide a clear evidence of fluorescence enhancement in the DNA-porphyrin Ag NP constructs. The preliminary results for fluorescence lifetime measurements of the DNA-porphyrin Ag NP constructs with excitation at 420 nm and emission at 660 nm are shown in Table 1 below for the sample, control and model (DNA-porphyrin double stranded without Ag NP).

Table 1: Fluorescence lifetimes: **10–50-base DNA-porphyrin** and complementary DNA-nanoparticle solution (sample); mixture of **10–50-base DNA-porphyrin** and noncomplementary DNA-nanoparticle solution (control), and **DNA-porphyrin double stranded** without nanoparticle (model).

	τ1 ns	A1 %	τ2 ns	A2 %	τ3 ns	A3 %	χ_{R^2}	<τ> (amp.ave)	<τ>
10-sample	0.13	12	2.10	21	9.78	67	0.94	7.01	4.00
10-control	0.16	12	2.19	14	10.14	74	0.96	7.83	4.16
10- model	0.25	9	2.87	10	10.41	81	0.94	8.74	4.51
15-sample	0.27	11	2.51	28	10.01	61	0.96	6.84	4.26
15-control	0.14	10	2.39	15	10.37	75	0.96	8.15	4.30
15- model	0.25	4	2.95	14	10.28	82	1.13	8.85	4.49
20-sample	0.39	13	2.70	25	9.76	62	0.95	6.78	4.28
20-control	0.33	13	2.65	20	10.25	67	1.00	7.44	4.41
20-model	0.36	10	2.55	21	10.67	69	0.97	7.93	4.53
25-sample	0.21	15	1.98	32	9.35	53	0.99	5.62	3.85
25-control	0.18	12	1.93	27	10.02	61	1.01	6.65	4.04
25-model	0.10	16	1.85	21	9.76	63	1.12	6.55	3.90
30-sample	0.20	17	2.15	28	9.31	55	0.95	5.76	3.87
30-control	0.16	18	2.26	19	10.06	63	0.93	6.80	4.16
30-model	0.20	11	2.63	19	10.52	70	0.94	7.89	4.45
40-sample	0.10	10	2.08	16	10.38	74	0.98	8.02	4.19
40-control	0.30	14	2.86	19	10.18	67	0.95	7.41	4.45
40-model	0.52	11	4.14	20	11.64	68	0.95	8.80	5.43
50-sample	0.15	16	2.32	21	9.96	63	0.94	6.79	4.14
50-control	0.34	11	2.88	21	10.47	68	0.95	7.76	4.56
50-model	0.41	10	3.97	19	11.29	71	0.97	8.81	5.22

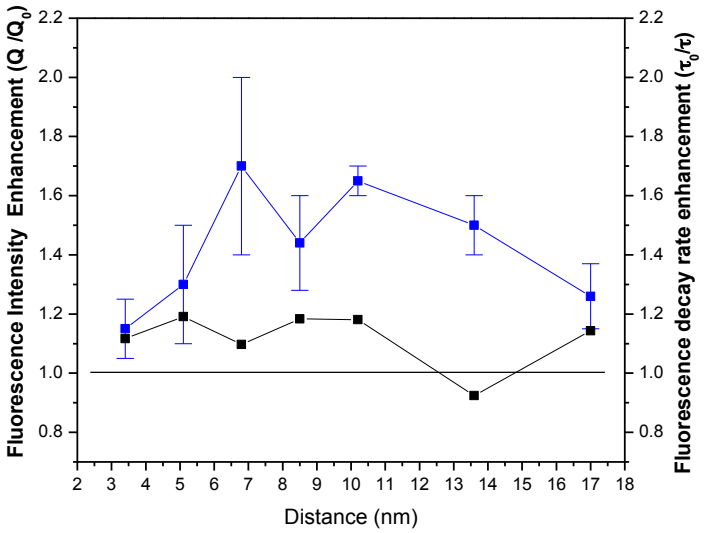

Figure 44: Fluorescence intensity enhancement (blue) and fluorescence decay rate enhancement (black) dependence on distance between porphyrin and Ag NP.

The results of the study of a set of seven DNA-porphyrin Ag NP constructs are summarized in Figure 44. From the steady state measurements optimal distance between the porphyrin and Ag NP to observed fluorescence intensity enhancement was found to be about 7–10 nm, but the enhancement appears to be no more than a factor of 1.5. The fluorescence lifetime data were fitted with three time constants in every case (Table 1) and a picture associated with distance dependence is not immediately evident. In addition, the interaction between the porphyrin and the DNA (see model data in Table 1) appears to play a more important role in the fluorescence lifetime than in the presence of the nanoparticle. The modest enhancement of fluorescence observed at shorter distances, in the steady state measurements, could be due to either enhanced absorption or changes in the radiative rate constant by the proximity of the

nanoparticle. Which one of these two factors explains the experimental observation cannot be specified at this time. Experiments will be repeated in the future using uncharged porphyrin such that the interaction between the DNA and porphyrin can be minimized.

III. Conclusion

In this chapter we have discussed the synthesis and spectral properties of a porphyrin attached to Ag NP surface via a DNA linker. Preliminary results shows that the porphyrin fluorescence is enhanced in the 20–base conjugate as compared to the 50–base conjugate, most likely due to closer proximity and therefore stronger interaction between the photons absorbed by the dye and the plasmons generated in the neighboring Ag nanoparticle. However, the effect is small and additional experiments need to be performed to evaluate the exact causes for the observed enhancement of the fluorescence. If the effect could be further enhanced, it would open the opportunity to use these hybrid plasmonic nanostructures as efficient artificial light harvesting systems.

IV. Experimental

General methods

The NMR spectra were recorded on Varian spectrometers at 400 MHz. Mass spectra were obtained with matrix-assisted laser desorption/ionization time-of-flight spectrometer (MALDI-TOF) in positive mode. Terthiophene matrix was used for the all porphyrins. 3-hydroxy picolinic acid was used as matrix for porphyrin-DNA conjugates.

Steady state fluorescence spectra were obtained with NanoLog spectrometer manufactured by HORIBA Jobin Yvon equipped with a thermoelectrically cooled PMT (R928 in the range 200 to 850 nm) and CW 450W Xenon lamp.

Fluorescence decay measurements were performed by the time-correlated single-photon-counting method. The excitation source for the system was a mode-locked Ti:Sapphire laser (Spectra Physics, Millennia-pumped Tsunami) with a 130 fs pulse duration operating at 80 MHz. The laser output was sent through a frequency doubler and pulse selector (Spectra Physics Model 3980) to obtain 370–450 nm pulses at 4 MHz. Fluorescence emission was detected at the magic angle using a double grating monochromator (Jobin Yvon Gemini-180) and a microchannel plate photomultiplier tube (Hamamatsu R3809U-50). The instrument response function was 35–55 ps. The spectrometer was controlled by software based on the LabView programming language and data acquisition was done using a single photon counting card (Becker-Hickl, SPC-830). Data analysis was carried out using locally written software (ASUFIT) developed in a

MATLAB environment (Mathworks Inc.). Random errors associated with the reported lifetimes obtained from fluorescence were typically ≤ 5%.

Solvents and reagents

The chemicals used were purchased from Aldrich, or Alfa Aesar and solvents were bought from EM Science. Dichloromethane used was distilled from calcium hydride. Dimethylformamide was dried over activated 4Å molecular sieves. Thin layer chromatography was done using silica coated glass plates from Analtech. Column chromatography was carried out using Silicycle silica gel 60 with 230–400 mesh. Unless otherwise specified all reactions were carried out under a nitrogen atmosphere.

The DNA-porphyrin conjugates were purified using reverse phase high performance liquid chromatography (HPLC) on a Beckman system. The column used for the analytical separation was an AappTec N42608 C4 reversed phase TR-AA010087 (5μm 25×0.46). Silver nanoparticles (diameter 20 ± 5 nm reported by the manufacturer) were purchased from Ted Pella Inc. (catalog number 15705-5sc). The size and distribution were analyzed by TEM imaging and was found to be 32 ± 5 nm. All oligonucleotides used for the experiments were obtained from Integrated DNA Technologies.

Synthesis

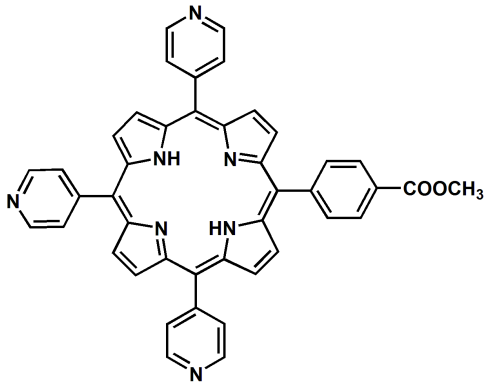

1

Porphyrin (1)

4-Pyridinecarboxaldehyde (2.32 g, 22 mmol) and methyl4-formylbenzoate (1.19 g, 7.3 mmol) were added to propionic acid (100 mL). The reaction mixture was refluxed under nitrogen atmosphere. Pyrrole (2 mL) was added to the refluxing mixture within 15 min. The reaction mixture was heated under reflux for 1.5 h and then it was allowed to cool to room temperature. Propionic acid was removed under vacuum, and the crude product was purified by silica gel column chromatography using 1-4% methanol in dicloromethane as eluent. Yield: 206 mg (4.2%). ^{1}H NMR: (400 MHz, $CDCl_3$, RT): δ –2.9 (2H, s, NH), 4.1 (3H, s), 8.14(6H, d, J = 8Hz), 8.28(2H, d, J = 7.8Hz), 8.45(2H, d, J = 8Hz), 8.8–8.86(8H, m), 9.02-9.06(6H, m). MALDI-TOF-MS *m/z:* calcd for $C_{43}H_{29}N_7O_2$ 675.74 obs 675.71.

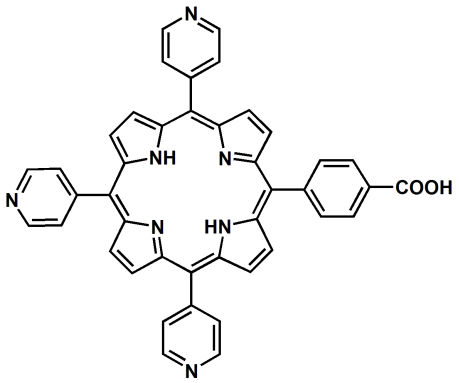

2

Porphyrin (2)

Porphyrin **1** (113 mg, 0.167 mmol) was dissolved in 10 mL of 2M KOH in 80% ethanol and was stirred at room temperature for 2 days. The product was extracted by $CHCl_3$ and dried over anhydrous sodium sulphate. The solvent was removed under reduced pressure and the product was dried under vacuum. Yield: 86 mg (78%). ^{1}H NMR: (400 MHz, $CDCl_3$, RT): δ –3.03 (2H, s, -NH), 8.09(6H, d, J = 4.64Hz), 8.17(2H, d, J = 8.16Hz), 8.36(2H, d, J = 8.16Hz), 8.58–8.89(14H, m). MALDI-TOF-MS *m/z:* calcd for $C_{42}H_{27}N_7O_2$ 661.71 obs 661.73.

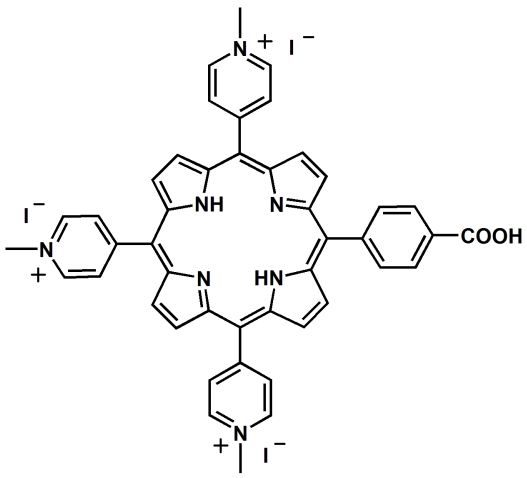

4

Porphyrin (4)

Porphyrin **2** (19.5 mg, 29.4 mmol) was dissolved in DMF (3 mL), CH_3I (3 mL, 48 mmol) was then added to the solution and the mixture was heated under reflux for 2 h. The solution was poured into acetone (50 mL) and the resulting precipitate was then washed with $CHCl_3$ and dried under vacuum. Yield: 27 mg (84%). ^1H NMR: (400 MHz, DMSO, RT): δ –3.07 (2H, s, -NH), 4.68 (9H, s), 8.32(2H, d, J = 8Hz), 8.4(2H, d, J = 8Hz), 8.92-9.17(14H, m), 9.44(6H, d, J = 6.56Hz). MALDI-TOF-MS *m/z:* calcd for $C_{45}H_{36}N_7O_2$ 706.81 obs 706.78.

General Procedure for the synthesis of DNA-porphyrin conjugates

To 42 μL of 476 μM solution of porphyrin **4** in DMF, 1,1'-carbonyldiimidazole 77.16 μL of 5.71 mM in dry DMF was added. The reaction mixture was stirred at room temperature for 90 min. Then 64 μL of 5.71 mM hydroxybenzotriazole in dry DMF was added. After 1 h, 240 μL of 20 mM MOPS buffer (pH 7.5) was added to hydrolyze the excess reagent. After 15 min this solution of the activated ester was added to 100 μL of 476 μM solution of 5'-amino modified C6 oligonucleotide in 200μL of 20 mM MOPS buffer. The solution was incubated at 37ºC for 3 h. Ice-cold isopropanol, 1 mL was added and the mixture was centrifuged. After removal of the supernatant the residue was washed with methanol (3× 500 μL).

DNA-porphyrin conjugates were purified using reverse phase high performance liquid chromatography (HPLC) on a Beckman system. The crude product (1mg/ml) was dissolved in Millipore water. The column used for analytical separation of this DNA was an AappTec N42608 C4 reversed phase TR-AA010087 (5μm 25× 0.46).

The purification was achieved by gradient elution using 50 mM ammonium acetate (Solvent A) and acetonitrile (Solvent B) with a flow rate of 0.9 mL/min. During sample injection, more hydrophilic solvent compostion (95% A + 5%B) was used which was changed gradually to 1.67 % B /min till more hydrophobic solvent composition (70% A + 30% B). These column elutions were monitored by waters 2487 Dual λ Detector at 254 nm. The peaks collected were frozen and lyophilized to give purified DNA-porphyrin conjugates.

DNA-porphyrin conjugates

1. 10-base sequence

5'-/5AmMC6/CGT GAC CGT C-3' with extinction coefficient: 90,100 L/ (mole.cm) was eluted with 18% B.

2. 15-base sequence

5'-/5AmMC6/TGA CTC GTG ACC GTC-3' with extinction coefficient: 136,500 L/ (mole.cm) was eluted with 16% B.

3. 20-base sequence

5'-/5AmMC6/GGC TGT GAC TCG TGA CCG TC-3' with extinction coefficient: 182,100 L/ (mole.cm) was eluted with 14.95% B.

4. 25-base sequence:

5'-/5AmMC6/GAC TCG GCT GTG ACT CGT GAC CGT C-3' with extinction coefficient: 227,500 L/ (mole.cm) was eluted with 13.26%B.

5. 30-base sequence:

5'-/5AmMC6/GTG CAG ACT CGG CTG TGA CTC GTG ACC GTC-3' with extinction coefficient: 275,800 L/ (mole.cm) was eluted with 12.93% B.

6. 40-base sequence:

5'-/5AmMC6/TAC GGT GAT AGT GCA GAC TCG GCT GTG ACT CGT GAC CGT C-3' with extinction coefficient: 378,400 L/ (mole.cm) was eluted with 19.35% B.

7. 50-base sequence: Eluted at 13.71% B.

5'-/5AmMC6/ACC TCC TGA GTA CGG TGA TAG TGC AGA CTC GGC TGT GAC TCG TGA CCG TC-3' with extinction coefficient: 470,500 L/ (mole.cm) was eluted with13.71% B.

General procedure for the preparation of silver nanoparticle solution

The silver colloid (1 mL) was concentrated 10 times by centrifugation (8,000 rpm, 40 min) and re-dispersed in 1×TBE buffer. To the 100 μL of silver nanoparticle solution, phosphorothioated DNA was added so that the final concentration of DNA becomes 8 μM. The nanoparticle solution was kept on a shaker with gentle shaking overnight. Then 5 M NaCl was added by small aliquots over 48 h to raise the final NaCl concentration to 350 mM. Then 5 μL of 1 mM thiolated PEG-500 solution was added and the solution was incubated overnight. The excess of oligonucleotides and PEG (polyethylene glycol) was removed by centrifugation (8,000 rpm, 40 min) and re-dispersed into a buffer solution that contains 1× TBE, with 350 mM NaCl. This centrifugation and re-dispersion procedure was repeated three times to get rid of the excess of unattached DNA. The concentration of Ag NPs was determined by measuring the absorbance at 400 nm using the extinction coefficient provided by the manufacturer (7.1×10^8).

IV. References

(1) Gust, D.; Moore, T. A. *Science* **1989**, *244*, 35.

(2) Barber, J. *Chemical Society Reviews* **2009**, *38*, 185.

(3) Gust, D.; Moore, T. A.; Moore, A. L. *Accounts of Chemical Research* **2009**, *42*, 1890.

(4) Mihailescu, G.; Olenic, L.; Garabagiu, S.; Blanita, G.; Cosma, E. F.; Biris, A. S. *Journal of Nanoscience and Nanotechnology* **2010**, *10*, 2527.

(5) Ray, P. C.; Darbha, G. K.; Ray, A.; Walker, J.; Hardy, W. *Plasmonics* **2007**, *2*, 173.

(6) Zhang, J.; Fu, Y.; Chowdhury, M. H.; Lakowicz, J. R. *Journal of Physical Chemistry C* **2007**, *111*, 11784.

(7) Nerambourg, N.; Werts, M. H. V.; Charlot, M.; Blanchard-Desce, M. *Langmuir* **2007**, *23*, 5563.

(8) Lakowicz, J. R. *Analytical Biochemistry* **2001**, *298*, 1.

(9) Andrew, P.; Barnes, W. L. *Science* **2004**, *306*, 1002.

(10) Bonnemann, H.; Richards, R. M. *European Journal of Inorganic Chemistry* **2001**, 2455.

(11) Aiken, J. D.; Finke, R. G. *Journal of Molecular Catalysis a-Chemical* **1999**, *145*, 1.

(12) DeLong, R.; Reynolds, C.; Malcolm, Y.; Schaeffer, A.; Severs, T.; Wanekaya, A. *Nanotechnology, Science and Applications* **2010**, *3*, 53.

(13) Li, Z.; Jin, R. C.; Mirkin, C. A.; Letsinger, R. L. *Nucleic Acids Research* **2002**, *30*, 1558.

(14) Fischler, M.; Simon, U. *Journal of Materials Chemistry* **2009**, *19*, 1518.

(15) Mirkin, C. A.; Letsinger, R. L.; Mucic, R. C.; Storhoff, J. J. *Nature* **1996**, *382*, 607.

(16) Zanchet, D.; Micheel, C. M.; Parak, W. J.; Gerion, D.; Alivisatos, A. P. *Nano Letters* **2001**, *1*, 32.

(17) Petty, J. T.; Zheng, J.; Hud, N. V.; Dickson, R. M. *Journal of the American Chemical Society* **2004**, *126*, 5207.

(18) Panyala, N. R.; Pena-Mendez, E. M.; Havel, J. *Journal of Applied Biomedicine* **2009**, *7*, 75.

(19) Bhattacharya, R.; Mukherjee, P. *Advanced Drug Delivery Reviews* **2008**, *60*, 1289.

(20) Nakamura, T.; Hayashi, S. *Japanese Journal of Applied Physics Part 1-Regular Papers Brief Communications & Review Papers* **2005**, *44*, 6833.

(21) Dulkeith, E.; Morteani, A. C.; Niedereichholz, T.; Klar, T. A.; Feldmann, J.; Levi, S. A.; van Veggel, F.; Reinhoudt, D. N.; Moller, M.; Gittins, D. I. *Physical Review Letters* **2002**, *89*.

(22) Schneider, G.; Decher, G.; Nerambourg, N.; Praho, R.; Werts, M. H. V.; Blanchard-Desce, M. *Nano Letters* **2006**, *6*, 530.

(23) Zhang, J.; Fu, Y.; Chowdhury, M. H.; Lakowicz, J. R. *Journal of Physical Chemistry C* **2008**, *112*, 18.
(24) Carmeli, I.; Lieberman, I.; Kraversky, L.; Fan, Z. Y.; Govorov, A. O.; Markovich, G.; Richter, S. *Nano Letters* **2010**, *10*, 2069.
(25) Imahori, H.; Kashiwagi, Y.; Hanada, T.; Endo, Y.; Nishimura, Y.; Yamazaki, I.; Fukuzumi, S. *Journal of Materials Chemistry* **2003**, *13*, 2890.
(26) Yamaguchi, H.; Tsubouchi, K.; Kawaguchi, K.; Horita, E.; Harada, A. *Chemistry-a European Journal* **2004**, *10*, 6179.
(27) Mestre, B.; Pratviel, G.; Meunier, B. *Bioconjugate Chemistry* **1995**, *6*, 466.
(28) Pal, S.; Deng, Z. T.; Ding, B. Q.; Yan, H.; Liu, Y. *Angewandte Chemie-International Edition* **2010**, *49*, 2700.

REFERENCES

Chapter 1

(1) Gust, D.; Moore, T. A. *Science* **1989**, *244*, 35.

(2) Gust, D.; Moore, T. A.; Moore, A. L. *Accounts of Chemical Research* **1993**, *26*, 198.

(3) Muller, P.; Li, X. P.; Niyogi, K. K. *Plant Physiology* **2001**, *125*, 1558.

(4) Polivka, T.; Sundstrom, V. *Chemical Reviews* **2004**, *104*, 2021.

(5) Vaswani, H. M.; Holt, N. E.; Fleming, G. R. *Pure and Applied Chemistry* **2005**, *77*, 925.

(6) Ahn, T. K.; Avenson, T. J.; Ballottari, M.; Cheng, Y. C.; Niyogi, K. K.; Bassi, R.; Fleming, G. R. *Science* **2008**, *320*, 794.

(7) Ruban, A. V.; Berera, R.; Ilioaia, C.; van Stokkum, I. H. M.; Kennis, J. T. M.; Pascal, A. A.; van Amerongen, H.; Robert, B.; Horton, P.; van Grondelle, R. *Nature* **2007**, *450*, 575.

(8) Standfuss, R.; van Scheltinga, A. C. T.; Lamborghini, M.; Kuhlbrandt, W. *Embo Journal* **2005**, *24*, 919.

(9) Ishizaki, A.; Calhoun, T. R.; Schlau-Cohen, G. S.; Fleming, G. R. *Physical Chemistry Chemical Physics* **2010**, *12*, 7319.

(10) Papagiannakis, E.; Larsen, D. S.; van Stokkum, I. H. M.; Vengris, M.; Hiller, R. G.; van Grondelle, R. *Biochemistry* **2004**, *43*, 15303.

(11) Dreuw, A.; Fleming, G. R.; Head-Gordon, M. *Physical Chemistry Chemical Physics* **2003**, *5*, 3247.

(12) Fungo, F.; Otero, L.; Durantini, E.; Thompson, W. J.; Silber, J. J.; Moore, T. A.; Moore, A. L.; Gust, D.; Sereno, L. *Physical Chemistry Chemical Physics* **2003**, *5*, 469.

(13) Frank, H. A.; Cogdell, R. J. *Photochemistry and Photobiology* **1996**, *63*, 257.

(14) Polivka, T.; Kaligotla, S.; Chabera, P.; Frank, H. A. *Physical Chemistry Chemical Physics* **2011**, *13*, 10787.

(15) Wehling, A.; Walla, P. J. *Journal of Physical Chemistry B* **2005**, *109*, 24510.

(16) Polivka, T.; Sundstrom, V. *Chemical Physics Letters* **2009**, *477*, 1.

(17) Polivka, T.; Frank, H. A. *Accounts of Chemical Research* **2010**, *43*, 1125.

(18) Liao, P. N.; Bode, S.; Wilk, L.; Hafi, N.; Walla, P. J. *Chemical Physics* **2010**, *373*, 50.

(19) Frank, H. A.; Farhoosh, R.; Gebhard, R.; Lugtenburg, J.; Gosztola, D.; Wasielewski, M. R. *Chemical Physics Letters* **1993**, *207*, 88.

(20) Wehling, A.; Walla, P. J. *Photosynthesis Research* **2006**, *90*, 101.

(21) Bode, S.; Quentmeier, C. C.; Liao, P. N.; Hafi, N.; Barros, T.; Wilk, L.; Bittner, F.; Walla, P. J. *Proceedings of the National Academy of Sciences of the United States of America* **2009**, *106*, 12311.

(22) Liao, P. N.; Holleboom, C. P.; Wilk, L.; Kuhlbrandt, W.; Walla, P. J. *Journal of Physical Chemistry B* **2010**, *114*, 15650.

(23) Walla, P. J.; Yom, J.; Krueger, B. P.; Fleming, G. R. *Journal of Physical Chemistry B* **2000**, *104*, 4799.

(24) Schulten, K.; Ohmine, I.; Karplus, M. *Journal of Chemical Physics* **1976**, *64*, 4422.

(25) Tavan, P.; Schulten, K. *Journal of Chemical Physics* **1979**, *70*, 5407.

(26) Tavan, P.; Schulten, K. *Physical Review B* **1987**, *36*, 4337.

(27) Zigmantas, D.; Hiller, R. G.; Sharples, F. P.; Frank, H. A.; Sundstrom, V.; Polivka, T. *Physical Chemistry Chemical Physics* **2004**, *6*, 3009.

(28) Frank, H. A.; Bautista, J. A.; Josue, J.; Pendon, Z.; Hiller, R. G.; Sharples, F. P.; Gosztola, D.; Wasielewski, M. R. *Journal of Physical Chemistry B* **2000**, *104*, 4569.

(29) Polivka, T.; Pellnor, M.; Melo, E.; Pascher, T.; Sundstrom, V.; Osuka, A.; Naqvi, K. R. *Journal of Physical Chemistry C* **2007**, *111*, 467.

(30) Enriquez, M. M.; Fuciman, M.; LaFountain, A. M.; Wagner, N. L.; Birge, R. R.; Frank, H. A. *Journal of Physical Chemistry B* **2010**, *114*, 12416.

(31) Kosumi, D.; Kusumoto, T.; Fujii, R.; Sugisaki, M.; Iinuma, Y.; Oka, N.; Takaesu, Y.; Taira, T.; Iha, M.; Frank, H. A.; Hashimoto, H. *Physical Chemistry Chemical Physics* **2011**, *13*, 10762.

(32) Pascal, A. A.; Liu, Z. F.; Broess, K.; van Oort, B.; van Amerongen, H.; Wang, C.; Horton, P.; Robert, B.; Chang, W. R.; Ruban, A. *Nature* **2005**, *436*, 134.

(33) Young, A. J.; Phillip, D.; Ruban, A. V.; Horton, P.; Frank, H. A. *Pure and Applied Chemistry* **1997**, *69*, 2125.

(34) Liao, P. N.; Pillai, S.; Gust, D.; Moore, T. A.; Moore, A. L.; Walla, P. J. *Journal of Physical Chemistry A* **2011**, *115*, 4082.

(35) Kloz, M.; Pillai, S.; Kodis, G.; Gust, D.; Moore, T. A.; Moore, A. L.; van Grondelle, R.; Kennis, J. T. M. *Journal of the American Chemical Society* **2011**, *133*, 7007.

(36) van Amerongen, H.; van Grondelle, R. *Journal of Physical Chemistry B* **2001**, *105*, 604.

(37) Delasrivas, J.; Telfer, A.; Barber, J. *Biochimica Et Biophysica Acta* **1993**, *1142*, 155.

(38) Berera, R.; van Stokkum, I. H. M.; Kodis, G.; Keirstead, A. E.; Pillai, S.; Herrero, C.; Palacios, R. E.; Vengris, M.; van Grondelle, R.; Gust, D.; Moore, T. A.; Moore, A. L.; Kennis, J. T. M. *Journal of Physical Chemistry B* **2007**, *111*, 6868.

(39) Berera, R.; Herrero, C.; van Stokkum, I. H. M.; Vengris, M.; Kodis, G.; Palacios, R. E.; van Amerongen, H.; van Grondelle, R.; Gust, D.; Moore, T. A.; Moore, A. L.; Kennis, J. T. M. *Proceedings of the National Academy of Sciences of the United States of America* **2006**, *103*, 5343.

(40) Fungo, F.; Otero, L.; Durantini, E. N.; Silber, J. J.; Sereno, L.; Marino-Ochoa, E.; Moore, T. A.; Moore, A. L.; Gust, D. *Journal of Physical Chemistry B* **2001**, *105*, 4783.

(41) Pillai, S. T.; Berera, R.; Kennis, J.; Gust, D.; Moore, T. A.; Moore, A. L. *Abstracts of Papers of the American Chemical Society* **2009**, *238*, 507.

(42) S.M, M.; Telegina, N. I.

(43) Reddy, P. V.; Rabago-Smith, M.; Borhan, B. *Journal of Labelled Compounds & Radiopharmaceuticals* **2002**, *45*, 79.

(44) Cardoso, S. L.; Nicodem, D. E.; Moore, T. A.; Moore, A. L.; Gust, D. *Journal of the Brazilian Chemical Society* **1996**, *7*, 19.

(45) Wolfe, J. P.; Buchwald, S. L. *Journal of Organic Chemistry* **2000**, *65*, 1144.

(46) Sadighi, J. P.; Singer, R. A.; Buchwald, S. L. *Journal of the American Chemical Society* **1998**, *120*, 4960.

(47) Wolfe, J. P.; Wagaw, S.; Marcoux, J. F.; Buchwald, S. L. *Accounts of Chemical Research* **1998**, *31*, 805.

(48) Byramova, N. E.; Mochalova, L. V.; Belyanchikov, I. M.; Matrosovich, M. N.; Bovin, N. V. *Journal of Carbohydrate Chemistry* **1991**, *10*, 691.

(49) Gust, D.; Moore, T. A.; Moore, A. L.; Devadoss, C.; Liddell, P. A.; Hermant, R.; Nieman, R. A.; Demanche, L. J.; Degraziano, J. M.; Gouni, I. *Journal of the American Chemical Society* **1992**, *114*, 3590.

(50) Maya, E. M.; Vazquez, P.; Torres, T. *Chemistry-a European Journal* **1999**, *5*, 2004.

(51) Avenson, T. J.; Ahn, T. K.; Niyogi, K. K.; Ballottari, M.; Bassi, R.; Fleming, G. R. *Journal of Biological Chemistry* **2009**, *284*, 2830.

(52) Bassi, R.; Avenson, T.; Ahn, T. K.; Zigmantas, D.; Zirong, L.; Matteo, B.; Li, Z.; Fleming, G. *Photosynthesis Research* **2007**, *91*, PS362.

(53) Holt, N. E.; Zigmantas, D.; Valkunas, L.; Li, X. P.; Niyogi, K. K.; Fleming, G. R. *Science* **2005**, *307*, 433.

(54) Berera, R.; van Stokkum, I. H. M.; d'Haene, S.; Kennis, J. T. M.; van Grondelle, R.; Dekker, J. P. *Biophysical Journal* **2009**, *96*, 2261.

(55) Li, Z. R.; Ahn, T. K.; Avenson, T. J.; Ballottari, M.; Cruz, J. A.; Kramer, D. M.; Bassi, R.; Fleming, G. R.; Keasling, J. D.; Niyogi, K. K. *Plant Cell* **2009**, *21*, 1798.

(1) Gust, D.; Moore, T. A.; Moore, A. L. *Accounts of Chemical Research* **1993**, *26*, 198.

(2) Gust, D.; Moore, T. A. *Science* **1989**, *244*, 35.

(3) Gust, D.; Moore, T. A.; Moore, A. L. *Accounts of Chemical Research* **2001**, *34*, 40.

(4) Lewis, N. S.; Nocera, D. G. *Proceedings of the National Academy of Sciences of the United States of America* **2007**, *104*, 20142.

(5) Youngblood, W. J.; Lee, S. H. A.; Maeda, K.; Mallouk, T. E. *Accounts of Chemical Research* **2009**, *42*, 1966.

(6) Kuwabara, T.; Tomita, E.; Sakita, S.; Hasegawa, D.; Sone, K.; Yagi, M. *Journal of Physical Chemistry C* **2008**, *112*, 3774.

(7) Gratzel, M. *Nature* **2001**, *414*, 338.

(8) Alstrum-Acevedo, J. H.; Brennaman, M. K.; Meyer, T. J. *Inorganic Chemistry* **2005**, *44*, 6802.

(9) Gust, D.; Moore, T. A.; Moore, A. L. *Accounts of Chemical Research* **2009**, *42*, 1890.

(10) Barber, J. *Chemical Society Reviews* **2009**, *38*, 185.

(11) McEvoy, J. P.; Brudvig, G. W. *Chemical Reviews* **2006**, *106*, 4455.

(12) Ni, M.; Leung, M. K. H.; Leung, D. Y. C.; Sumathy, K. *Renewable & Sustainable Energy Reviews* **2007**, *11*, 401.

(13) Concepcion, J. J.; Jurss, J. W.; Brennaman, M. K.; Hoertz, P. G.; Patrocinio, A. O. T.; Iha, N. Y. M.; Templeton, J. L.; Meyer, T. J. *Accounts of Chemical Research* **2009**, *42*, 1954.

(14) Kudo, A. *International Journal of Hydrogen Energy* **2007**, *32*, 2673.

(15) Fujishima, A.; Honda, K. *Nature* **1972**, *238*, 37.

(16) Oregan, B.; Gratzel, M. *Nature* **1991**, *353*, 737.

(17) Kudo, A.; Miseki, Y. *Chemical Society Reviews* **2009**, *38*, 253.

(18) Kiwi, J.; Gratzel, M. *Journal of the American Chemical Society* **1979**, *101*, 7214.

(19) Kanan, M. W.; Nocera, D. G. *Science* **2008**, *321*, 1072.

(20) Zong, R.; Thummel, R. P. *Journal of the American Chemical Society* **2005**, *127*, 12802.

(21) Concepcion, J. J.; Jurss, J. W.; Templeton, J. L.; Meyer, T. J. *Proceedings of the National Academy of Sciences of the United States of America* **2008**, *105*, 17632.

(22) Concepcion, J. J.; Jurss, J. W.; Templeton, J. L.; Meyer, T. J. *Journal of the American Chemical Society* **2008**, *130*, 16462.

(23) Harriman, A.; Pickering, I. J.; Thomas, J. M.; Christensen, P. A. *Journal of the Chemical Society-Faraday Transactions I* **1988**, *84*, 2795.

(24) Harriman, A.; Richoux, M. C.; Christensen, P. A.; Mosseri, S.; Neta, P. *Journal of the Chemical Society-Faraday Transactions I* **1987**, *83*, 3001.

(25) Harriman, A.; Thomas, J. M.; Millward, G. R. *New Journal of Chemistry* **1987**, *11*, 757.

(26) Hara, M.; Waraksa, C. C.; Lean, J. T.; Lewis, B. A.; Mallouk, T. E. *Journal of Physical Chemistry A* **2000**, *104*, 5275.

(27) Nahor, G. S.; Neta, P.; Hambright, P.; Thompson, A. N.; Harriman, A. *Journal of Physical Chemistry* **1989**, *93*, 6181.

(28) Campbell, W. M.; Jolley, K. W.; Wagner, P.; Wagner, K.; Walsh, P. J.; Gordon, K. C.; Schmidt-Mende, L.; Nazeeruddin, M. K.; Wang, Q.; Gratzel, M.; Officer, D. L. *Journal of Physical Chemistry C* **2007**, *111*, 11760.

(29) Wang, Q.; Carnpbell, W. M.; Bonfantani, E. E.; Jolley, K. W.; Officer, D. L.; Walsh, P. J.; Gordon, K.; Humphry-Baker, R.; Nazeeruddin, M. K.; Gratzel, M. *Journal of Physical Chemistry B* **2005**, *109*, 15397.

(30) Hara, M.; Mallouk, T. E. *Chemical Communications* **2000**, 1903.

(31) Hoertz, P. G.; Kim, Y. I.; Youngblood, W. J.; Mallouk, T. E. *Journal of Physical Chemistry B* **2007**, *111*, 6845.

(32) Younpblood, W. J.; Lee, S. H. A.; Kobayashi, Y.; Hernandez-Pagan, E. A.; Hoertz, P. G.; Moore, T. A.; Moore, A. L.; Gust, D.; Mallouk, T. E. *Journal of the American Chemical Society* **2009**, *131*, 926.

(33) Yagi, M.; Tomita, E.; Sakita, S.; Kuwabara, T.; Nagai, K. *Journal of Physical Chemistry B* **2005**, *109*, 21489.

(34) Nakagawa, T.; Beasley, C. A.; Murray, R. W. *Journal of Physical Chemistry C* **2009**, *113*, 12958.

(35) Nakagawa, T.; Bjorge, N. S.; Murray, R. W. *Journal of the American Chemical Society* **2009**, *131*, 15578.

(36) Sherman, B. D.; Pillai, S.; Kodis, G.; Bergkamp, J.; Mallouk, T. E.; Gust, D.; Moore, T. A.; Moore, A. L. *Canadian Journal of Chemistry-Revue Canadienne De Chimie* **2011**, *89*, 152.

(37) Garbayjaureguiberry, C.; McCorttranchepain, I.; Barbe, B.; Ficheux, D.; Roques, B. P. *Tetrahedron-Asymmetry* **1992**, *3*, 637.

(38) Yokomatsu, T.; Minowa, T.; Murano, T.; Shibuya, S. *Tetrahedron* **1998**, *54*, 9341.

(39) Muthukumaran, K.; Loewe, R. S.; Ambroise, A.; Tamaru, S. I.; Li, Q. L.; Mathur, G.; Bocian, D. F.; Misra, V.; Lindsey, J. S. *Journal of Organic Chemistry* **2004**, *69*, 1444.

(40) Oza, V. B.; Corcoran, R. C. *Journal of Organic Chemistry* **1995**, *60*, 3680.

(41) Guldi, D. M.; Zilbermann, I.; Anderson, G.; Li, A.; Balbinot, D.; Jux, N.; Hatzimarinaki, M.; Hirsch, A.; Prato, M. *Chemical Communications* **2004**, 726.

(42) Wen, L. Q.; Li, M.; Schlenoff, J. B. *Journal of the American Chemical Society* **1997**, *119*, 7726.

(43) Scalise, I.; Durantini, E. N. *Journal of Photochemistry and Photobiology a-Chemistry* **2004**, *162*, 105.

(44) Ruzie, C.; Michaudet, L.; Boitrel, B. *Tetrahedron Letters* **2002**, *43*, 7423.

(45) Lottner, C.; Bart, K. C.; Bernhardt, G.; Brunner, H. *Journal of Medicinal Chemistry* **2002**, *45*, 2079.
(46) Lindsey, J. S.; Schreiman, I. C.; Hsu, H. C.; Kearney, P. C.; Marguerettaz, A. M. *Journal of Organic Chemistry* **1987**, *52*, 827.

(1) Gust, D.; Moore, T. A. *Science* **1989**, *244*, 35.
(2) Barber, J. *Chemical Society Reviews* **2009**, *38*, 185.
(3) Gust, D.; Moore, T. A.; Moore, A. L. *Accounts of Chemical Research* **2009**, *42*, 1890.
(4) Mihailescu, G.; Olenic, L.; Garabagiu, S.; Blanita, G.; Cosma, E. F.; Biris, A. S. *Journal of Nanoscience and Nanotechnology* **2010**, *10*, 2527.
(5) Ray, P. C.; Darbha, G. K.; Ray, A.; Walker, J.; Hardy, W. *Plasmonics* **2007**, *2*, 173.
(6) Zhang, J.; Fu, Y.; Chowdhury, M. H.; Lakowicz, J. R. *Journal of Physical Chemistry C* **2007**, *111*, 11784.
(7) Nerambourg, N.; Werts, M. H. V.; Charlot, M.; Blanchard-Desce, M. *Langmuir* **2007**, *23*, 5563.
(8) Lakowicz, J. R. *Analytical Biochemistry* **2001**, *298*, 1.
(9) Andrew, P.; Barnes, W. L. *Science* **2004**, *306*, 1002.
(10) Bonnemann, H.; Richards, R. M. *European Journal of Inorganic Chemistry* **2001**, 2455.
(11) Aiken, J. D.; Finke, R. G. *Journal of Molecular Catalysis a-Chemical* **1999**, *145*, 1.
(12) DeLong, R.; Reynolds, C.; Malcolm, Y.; Schaeffer, A.; Severs, T.; Wanekaya, A. *Nanotechnology, Science and Applications* **2010**, *3*, 53.
(13) Li, Z.; Jin, R. C.; Mirkin, C. A.; Letsinger, R. L. *Nucleic Acids Research* **2002**, *30*, 1558.
(14) Fischler, M.; Simon, U. *Journal of Materials Chemistry* **2009**, *19*, 1518.
(15) Mirkin, C. A.; Letsinger, R. L.; Mucic, R. C.; Storhoff, J. J. *Nature* **1996**, *382*, 607.
(16) Zanchet, D.; Micheel, C. M.; Parak, W. J.; Gerion, D.; Alivisatos, A. P. *Nano Letters* **2001**, *1*, 32.
(17) Petty, J. T.; Zheng, J.; Hud, N. V.; Dickson, R. M. *Journal of the American Chemical Society* **2004**, *126*, 5207.
(18) Panyala, N. R.; Pena-Mendez, E. M.; Havel, J. *Journal of Applied Biomedicine* **2009**, *7*, 75.
(19) Bhattacharya, R.; Mukherjee, P. *Advanced Drug Delivery Reviews* **2008**, *60*, 1289.
(20) Nakamura, T.; Hayashi, S. *Japanese Journal of Applied Physics Part 1-Regular Papers Brief Communications & Review Papers* **2005**, *44*, 6833.
(21) Dulkeith, E.; Morteani, A. C.; Niedereichholz, T.; Klar, T. A.; Feldmann, J.; Levi, S. A.; van Veggel, F.; Reinhoudt, D. N.; Moller, M.; Gittins, D. I. *Physical Review Letters* **2002**, *89*.
(22) Schneider, G.; Decher, G.; Nerambourg, N.; Praho, R.; Werts, M. H. V.; Blanchard-Desce, M. *Nano Letters* **2006**, *6*, 530.
(23) Zhang, J.; Fu, Y.; Chowdhury, M. H.; Lakowicz, J. R. *Journal of Physical Chemistry C* **2008**, *112*, 18.

(24) Carmeli, I.; Lieberman, I.; Kraversky, L.; Fan, Z. Y.; Govorov, A. O.; Markovich, G.; Richter, S. *Nano Letters* **2010**, *10*, 2069.

(25) Imahori, H.; Kashiwagi, Y.; Hanada, T.; Endo, Y.; Nishimura, Y.; Yamazaki, I.; Fukuzumi, S. *Journal of Materials Chemistry* **2003**, *13*, 2890.

(26) Yamaguchi, H.; Tsubouchi, K.; Kawaguchi, K.; Horita, E.; Harada, A. *Chemistry-a European Journal* **2004**, *10*, 6179.

(27) Mestre, B.; Pratviel, G.; Meunier, B. *Bioconjugate Chemistry* **1995**, *6*, 466.

(28) Pal, S.; Deng, Z. T.; Ding, B. Q.; Yan, H.; Liu, Y. *Angewandte Chemie-International Edition* **2010**, *49*, 2700.

APPENDIX A

Additional Molecules

I. Porphyrin was obtained from Antaeres Antoniuk-pablant from our group.

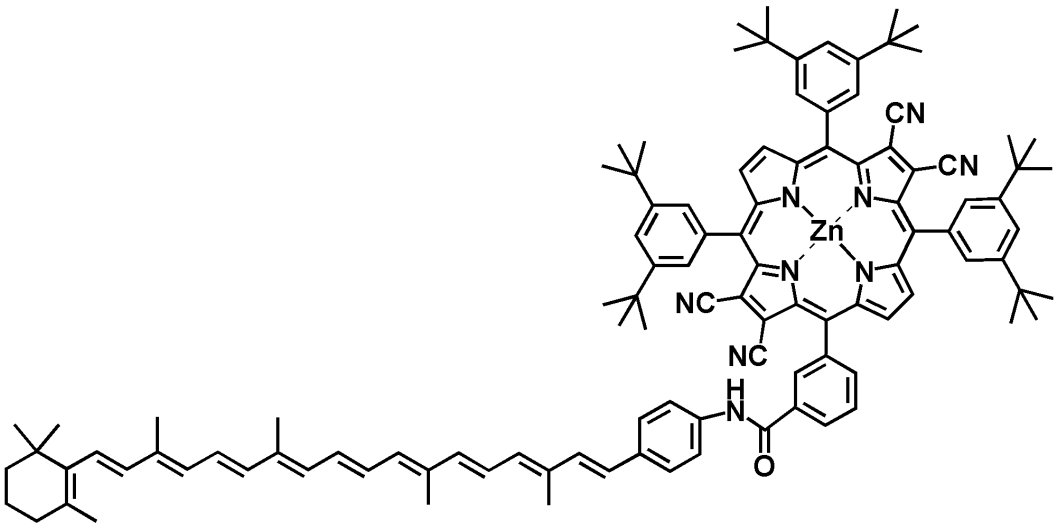

44

Compound 44: Porphyrin (14 mg, 0.01 mmol) and 7'-apo-7'-(4-aminophenyl)-β-carotene (6.72 mg, 0.01 mmol) were dissolved in 10 mL DCM. EDCI (3.47 mg, 0.018 mmol) and DMAP (2.95 mg, 0.03 mmol) were added and the reaction mixture was stirred for 5.5 h at room temperature. The reaction mixture was then washed with water and brine. The organic layer was then dried over sodium sulfate and evaporated. The crude product was then purified by column chromatography on silica gel using 20% ethyl acetate and hexane. Yield: 8.5 mg (43%). ^{1}HNMR (400MHz, $CDCl_3$): δ 1.02 (6H, s, CH_3-16C and CH_3-17C), 1.41 (11H, bs), 1.46 (12H, bs), 1.5 (14H, bs), 1.58(12H, bs), 1.7 (12H, bs), 1.93-2.02(14H, m), 6.1-6.84 (14H, m), 6.96(1H, bs), 7.09 (1H, bs), 7.29(1H, s), 7.33(1H, bs), 7.63(1H, s),7.72-8.09(11H, m), 8.16(1H, s), 8.82-9(4H, m).

MALDI-TOF-MS *m/z:* calcd. for $C_{110}H_{117}N_9OZn$ 1646.55, obsd. 1646.57; UV-vis (CH_2Cl_2): 353, 373, 445, 454, 506, 597, and 649 nm.

II.

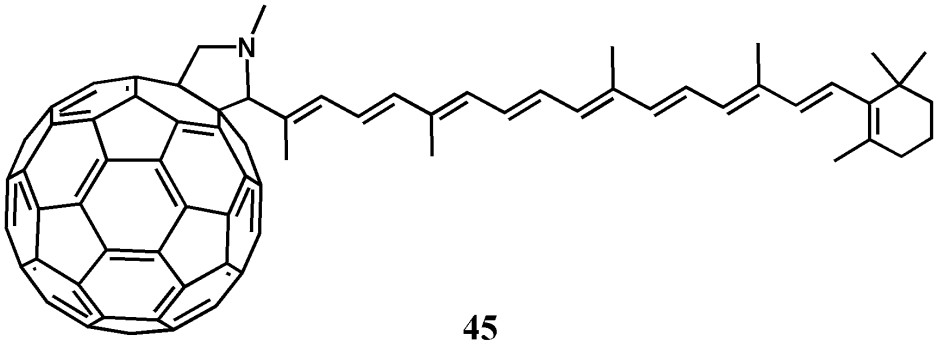

45

Compound 45: 8-'Apo-*β*-caroten-8'-al (50 mg, 0.12 mmol), C_{60} (179 mg, 0.25 mmol), sarcosine (108.2 mg, 1.2 mmol) was refluxed in 50 mL chlorobenzene for 24 h. The reaction mixture was cooled and the solvent was removed under vacuum. The crude reaction mixture was purified by column chromatography on silica gel using 5% CS_2, 5% ethyl acetate with 90% hexanes. Yield: 105 mg (75%). ^{1}HNMR (400MHz, $CDCl_3/CS_2$): δ 1.02 (6H, s, CH_3-16C and CH_3-17C), 1.43-1.5 (2H, m, CH_2-2C), 1.57-1.64 (2H, m, CH_2-3C), 1.7(3H, s, CH_3-19C), 1.91-2 (11H, m, CH_3-18C, CH_3-20C, CH_3-20'C, CH_2-4C), 2.26(3H, s, CH_3-19'C), 2.82(3H, s, CH_3), 4.16(1H, d, *J*=12Hz), 4.48(1H, bs), 4.93(1H, bs), 5.98-6.84 (12H, m vinyl H). MALDI-TOF-MS *m/z*: calcd. for $C_{92}H_{45}N$ 1163.35, obsd. 1163.39; UV-vis (CH_2Cl_2) 328, 417, 439, 466, and 698 nm.

III.

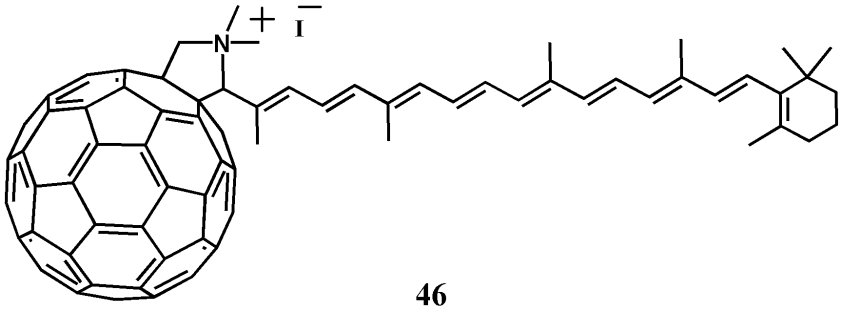

46

Compound 46: Compound **45** (25 mg, 0.02 mmol) was suspended in a mixture of 1 mL DMSO and 3 mL iodomethane in a screw cap vial. The reaction mixture was stirred at room temperature for 36 h. Most of the iodomethane was removed under a nitrogen stream to give a wet brown colored compound. The compound was then dissolved in 10mL of CH_2Cl_2 and filtered, the filtrate was then washed with water and then the organic solvent was concentrated under reduced pressure. The crude product was purified by column chromatography on silica gel using 5% MeOH 15% CS_2 in DCM. Yield: 17 mg (60%). ^{1}HNMR [(400MHz, $CDCl_3/CS_2$(1:1)]: δ 0.01 (6H, s, CH_3-16C and CH_3-17C), 1.42-1.48 (2H, m, CH_2-2C), 1.58-1.64 (2H, m, CH_2-3C), 1.69(3H, s, CH_3-19C), 1.91-2.04(11H, m, CH_3-18C, CH_3-20C, CH_3-20'C, CH_2-4C), 2.43(3H, s, CH_3-19'C), 4.32(6H, s, -CH_3), 5.9(1H, d, *J*=12Hz), 6.02-6.83(12H, m vinyl H), 7.21(1H, s), 7.34(1H, bs). ^{1}HNMR [(400MHz, $CDCl_3/CS_2$/MeOD(1:1:0.2)]: δ 0.95 (6H, s, CH_3-16C and

CH_3-17C), 1.37-1.42 (2H, m, CH_2-2C), 1.5-1.58 (2H, m, CH_2-3C), 1.63(3H, s, CH_3-19C), 1.85-1.97 (11H, m, CH_3-18C, CH_3-20C, CH_3-20'C, CH_2-4C), 2.37(3H, s, CH_3-19'C), 4.01(3H, s, -CH_3), 4.21(3H, s, -CH_3), 5.75(1H, d, *J* =13Hz), 5.98-6.66 (12H, m vinyl H), 6.78(1H, s), 7.15(1H, s). MALDI-TOF-MS *m/z*: calcd. for $C_{93}H_{48}N$ 1178.58, obsd. 1178.62; UV-vis (CH_2Cl_2) 325, 423, 445, 465, and 690 nm.

IV.

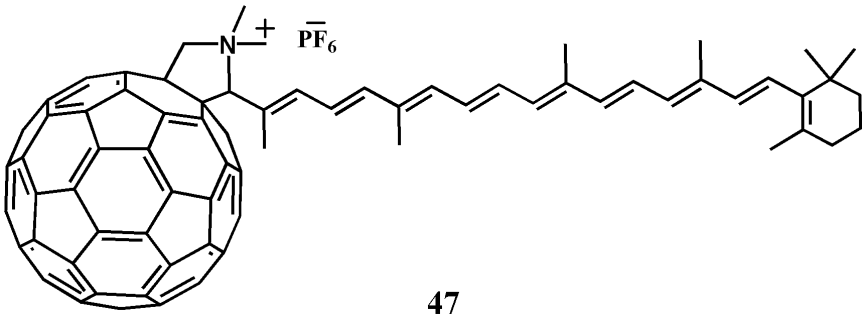

47

Compound 47: Compound **46** (10 mg, 0.009 mmol) was dissolved in 5 mL THF, KPF_6 (6.24 mg, 0.034 mmol) was added in 2mL water and the reaction mixture was stirred at room temperature for 3 h. The product was then extracted in CH_2Cl_2 and washed with water several times. The solvent was evaporated under reduced pressure. Yield: 8.6 mg (80%). ^{19}FNMR [(400MHz, $CDCl_3/CS_2$ (1:1)]: δ -67.67(d, 6F).

APPENDIX B

UV SPECTRAS

Chapter 1

Absorption spectra 11'-apo-11'-(4-amino-N-[4-methlphenylphenyl)-*β*-carotene in dichloromethane.

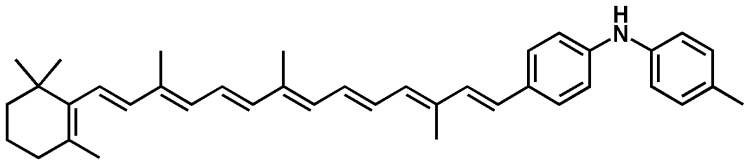

36

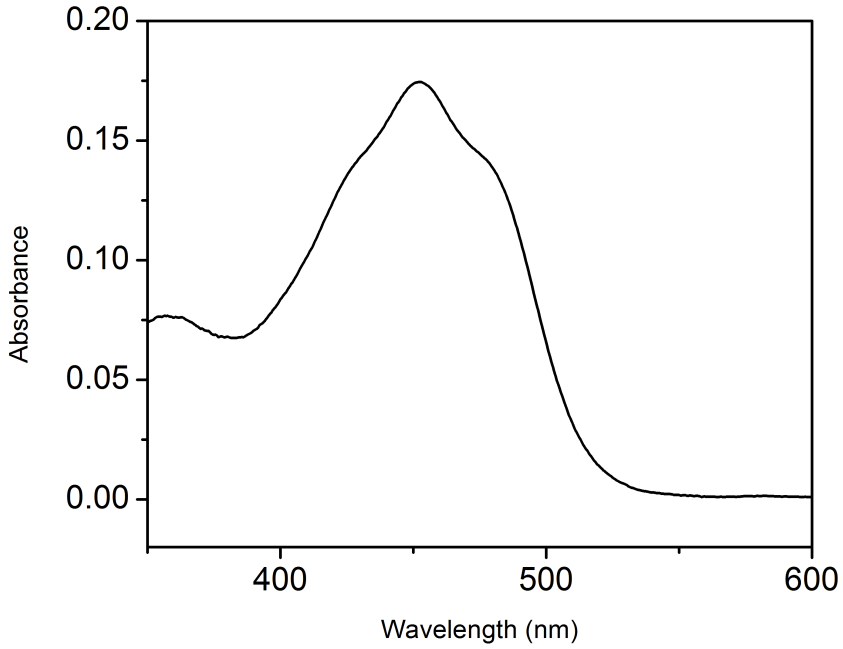

Absorption spectra 9'-apo-9'-(4-amino-N-[4-methlphenylphenyl)-*β*-carotene in dichloromethane.

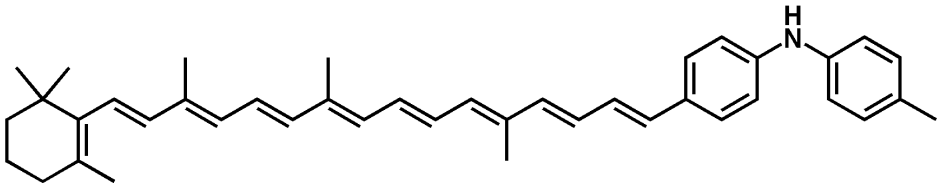

41

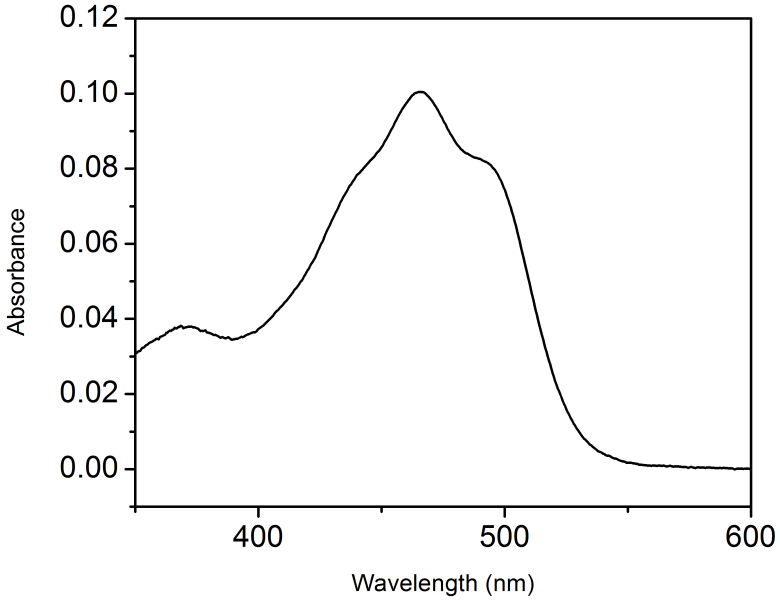

Absorption spectra 7'-apo-7'-(4-amino-N-[4-methlphenylphenyl)-β-carotene in dichloromethane.

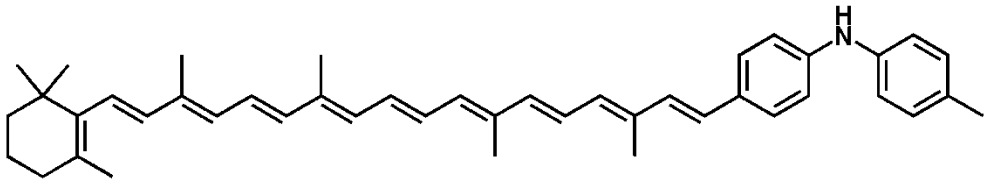

42

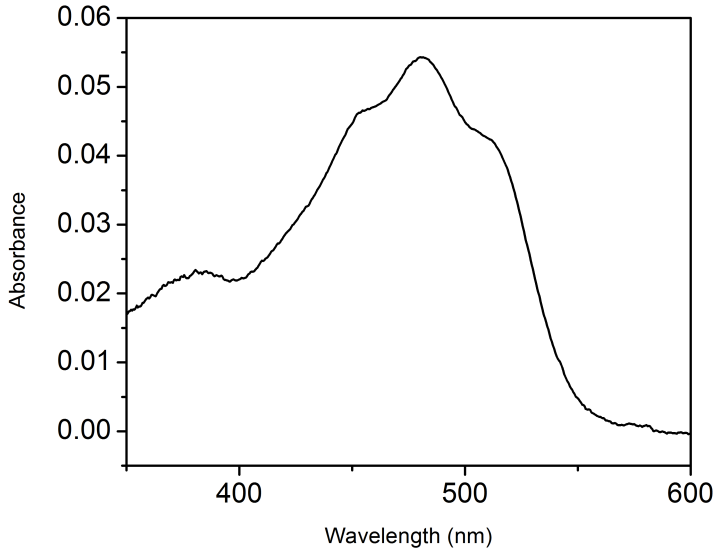

Absorption spectra 5'-apo-5'-(4-amino-N-[4-methlphenylphenyl)-*β*-carotene in dichloromethane.

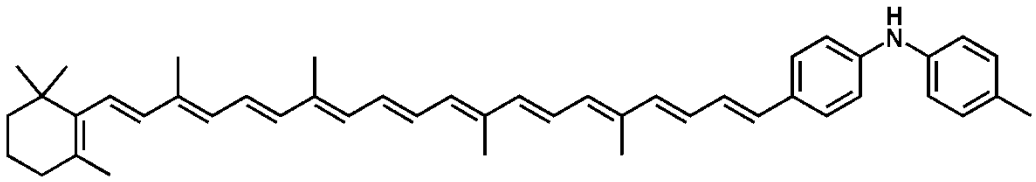

43

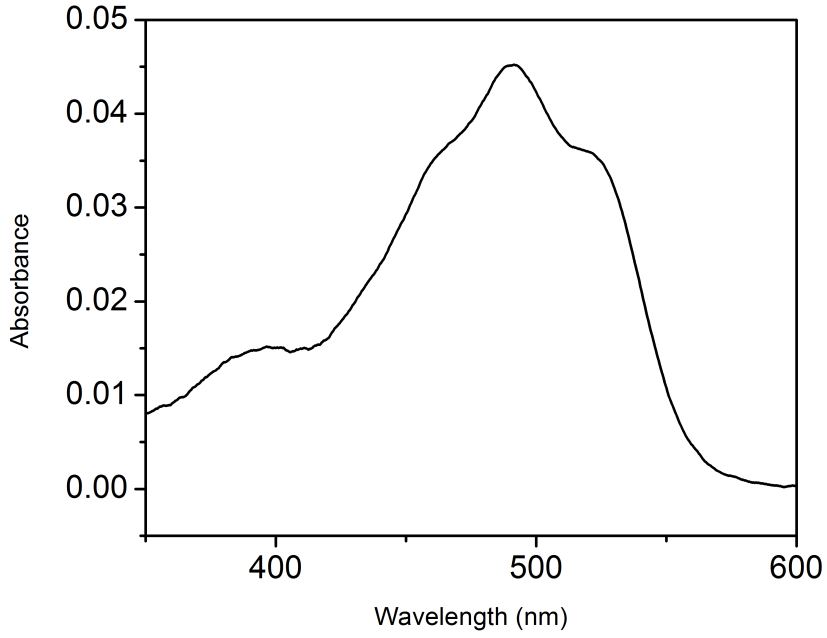

Absorption spectra of compound 45 (black) and 47 (red) in toluene.

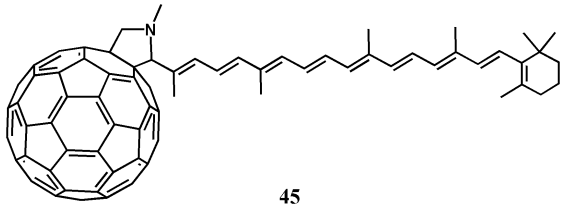

45

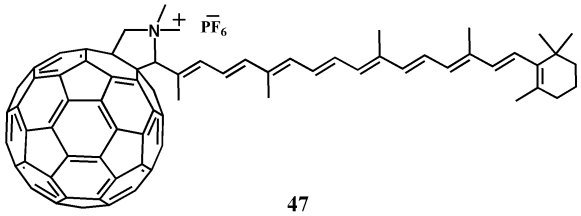

47

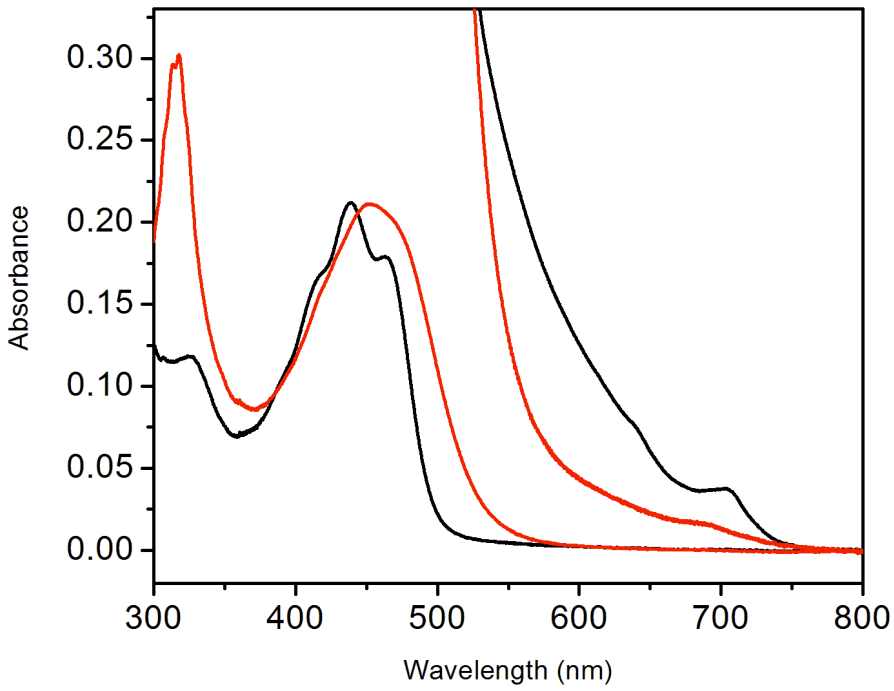

Absorption spectra of compound 44 in toluene.

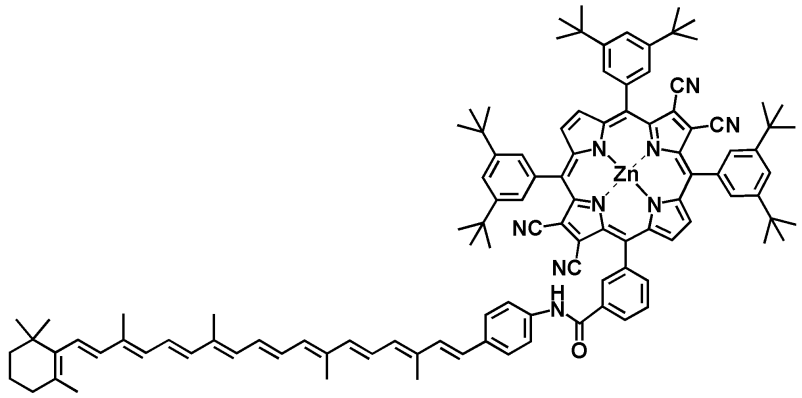

44

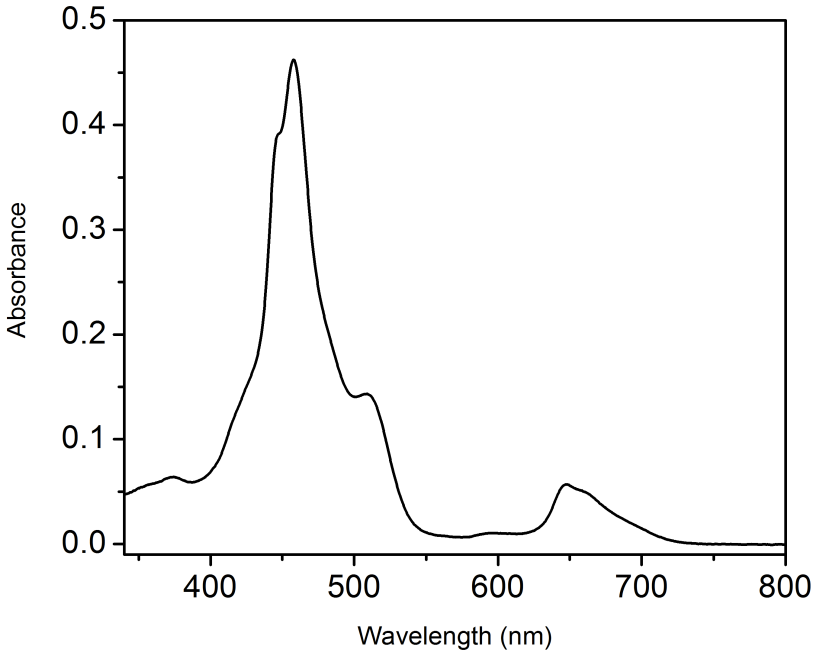

Chapter 2

Absorption spectra porphyrin 7 in dichloromethane.

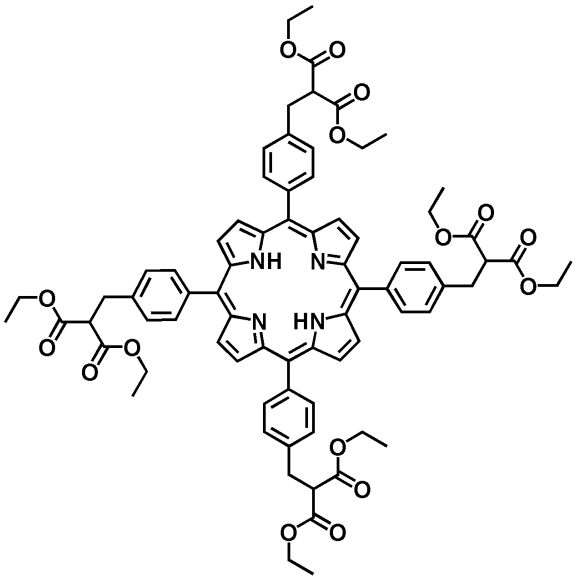

7

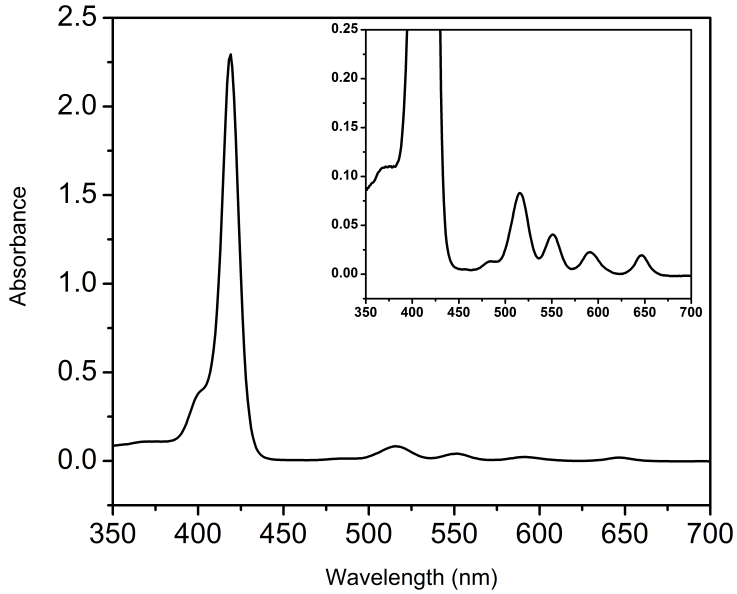

Absorption spectra porphyrin 8 in dichloromethane.

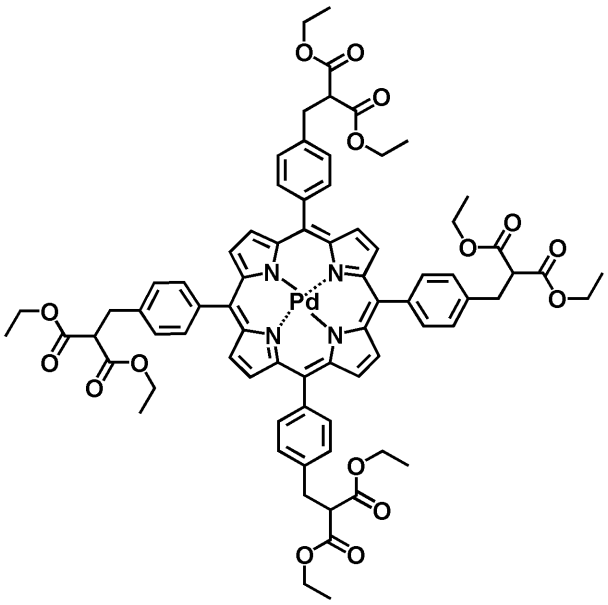

8

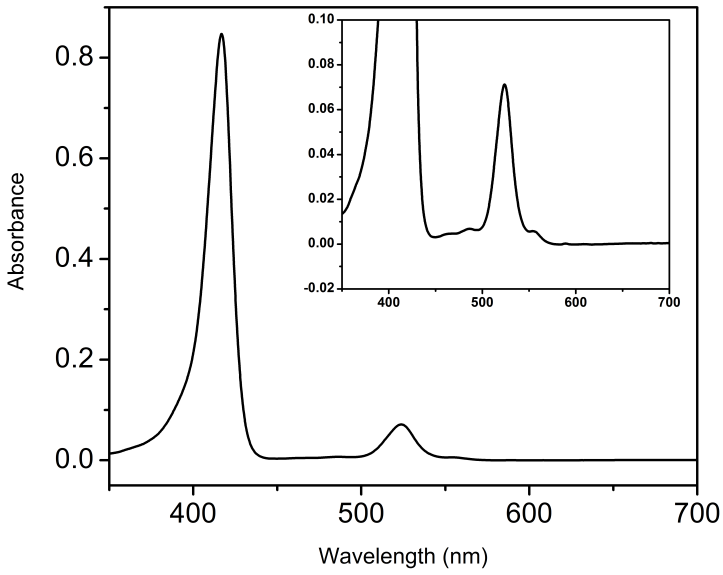

Absorption spectra porphyrin 9 in water.

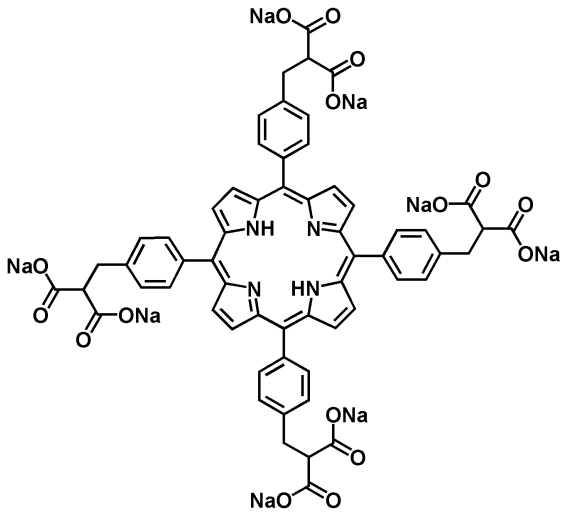

9

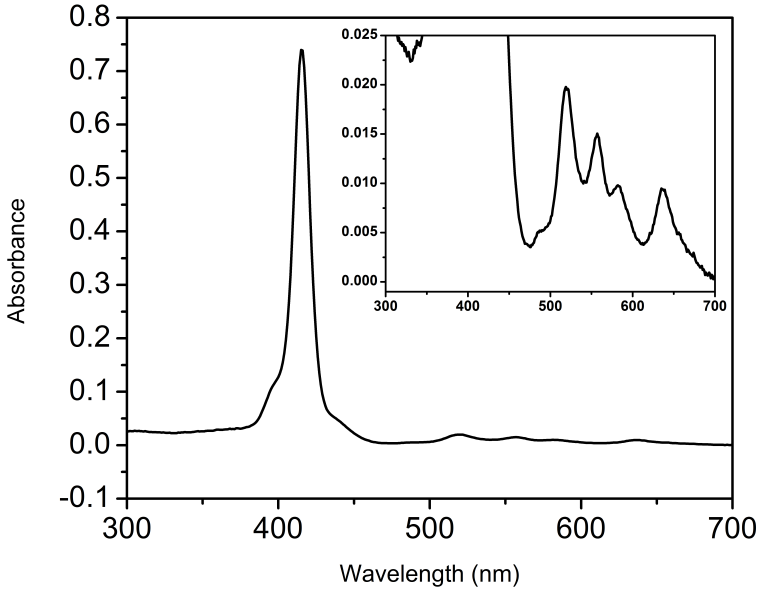

Absorption spectra porphyrin 10 in water.

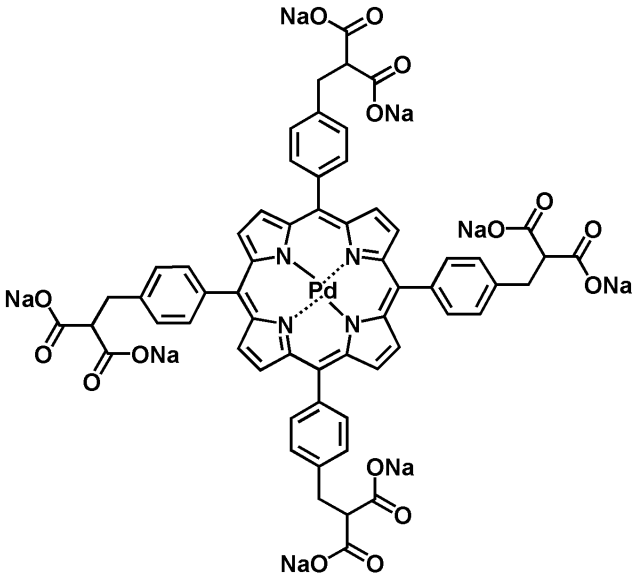

10

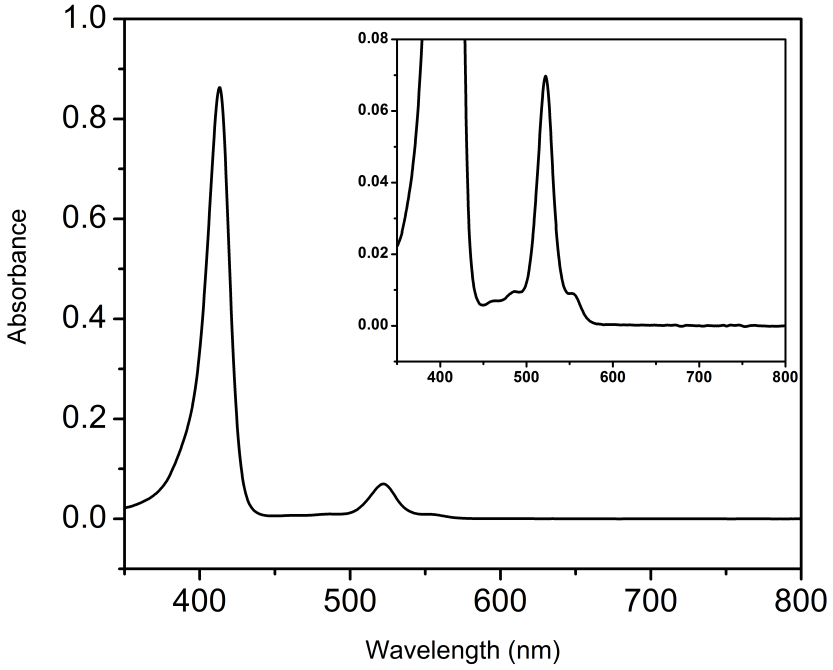

Absorption spectra porphyrin 12 in dichloromethane.

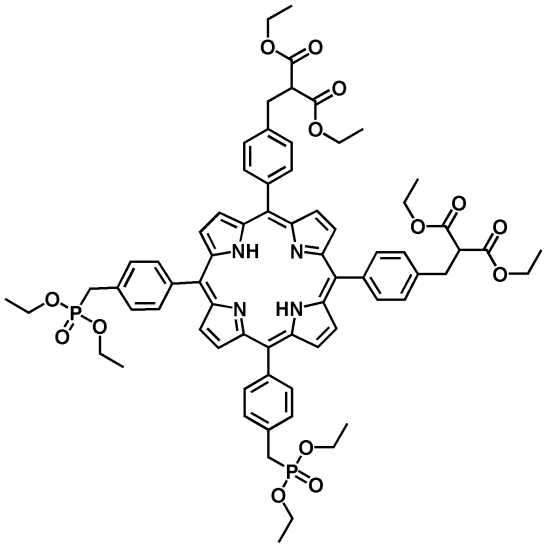

12

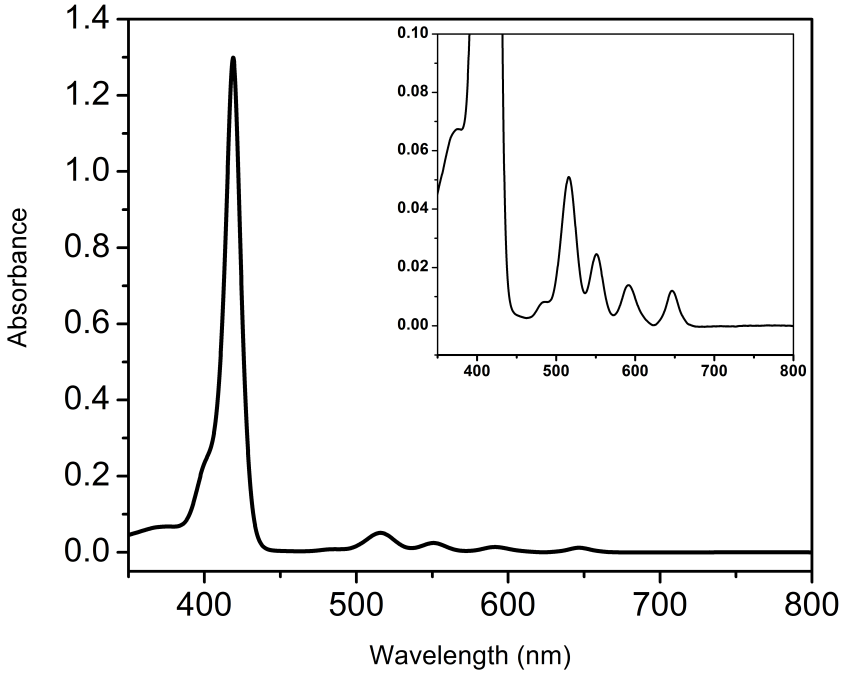

Absorption spectra porphyrin 13 in dichloromethane.

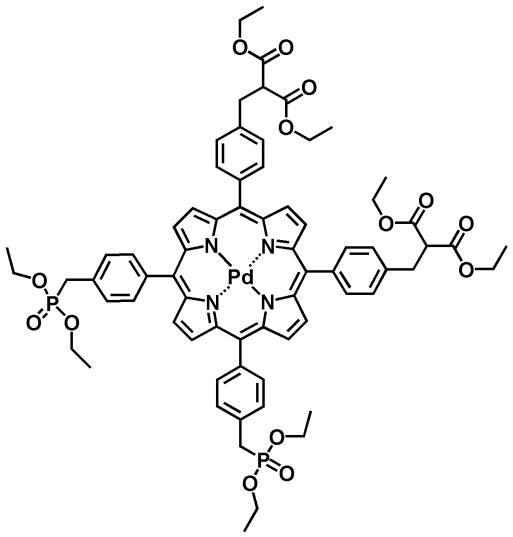

13

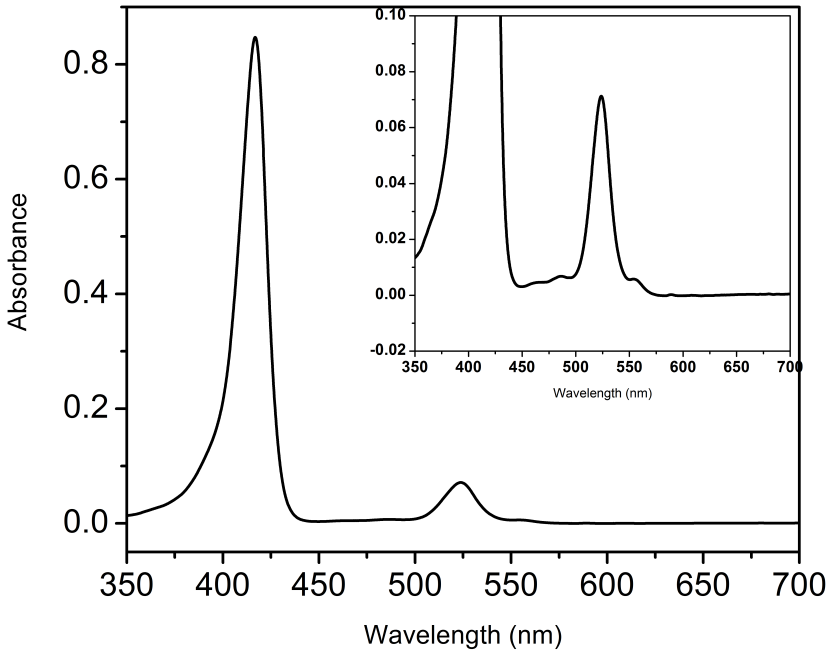

Absorption spectra porphyrin 15 in water.

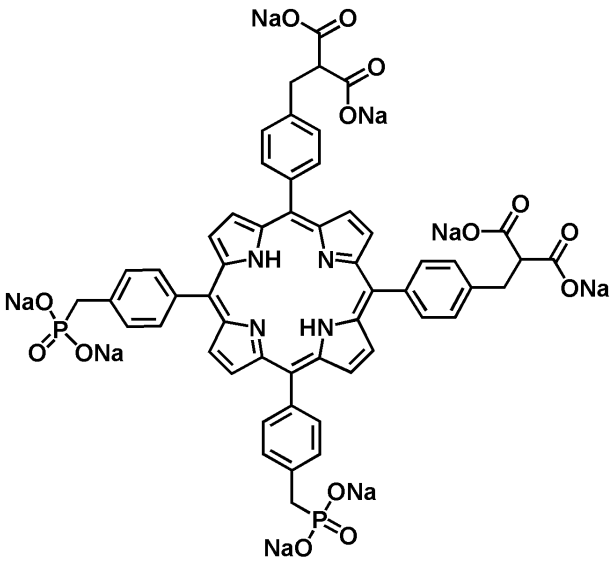

15

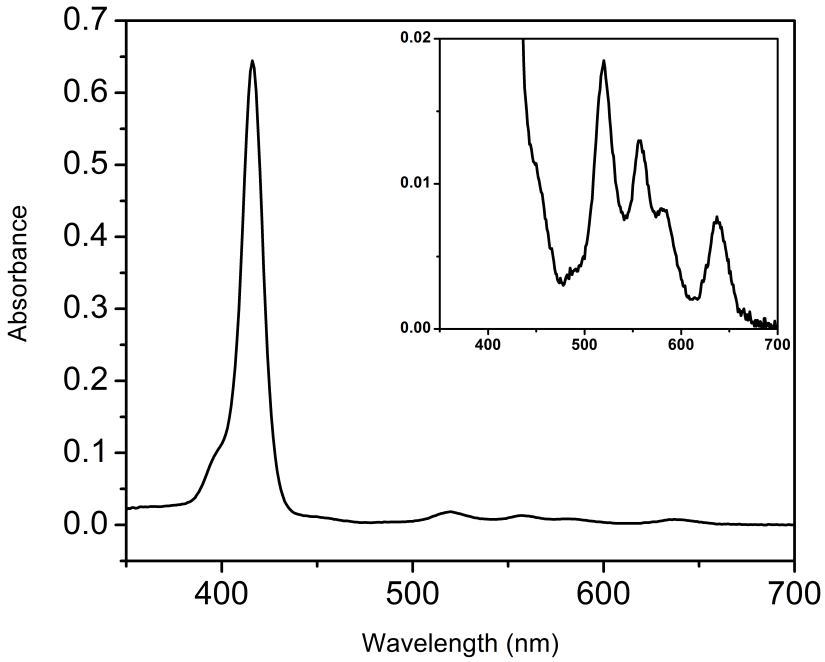

APPENDIX C

NMR SPECTRAS

Chapter 1

400MHz ^{1}H NMR spectrum 12'-apo-*β*-caroten-12'-al recorded in chloroform –*d.*

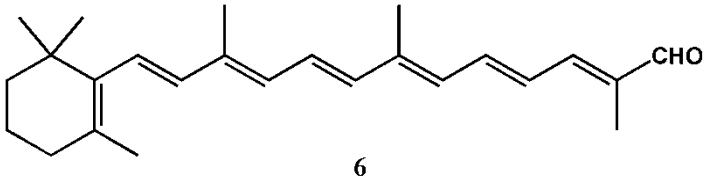

6

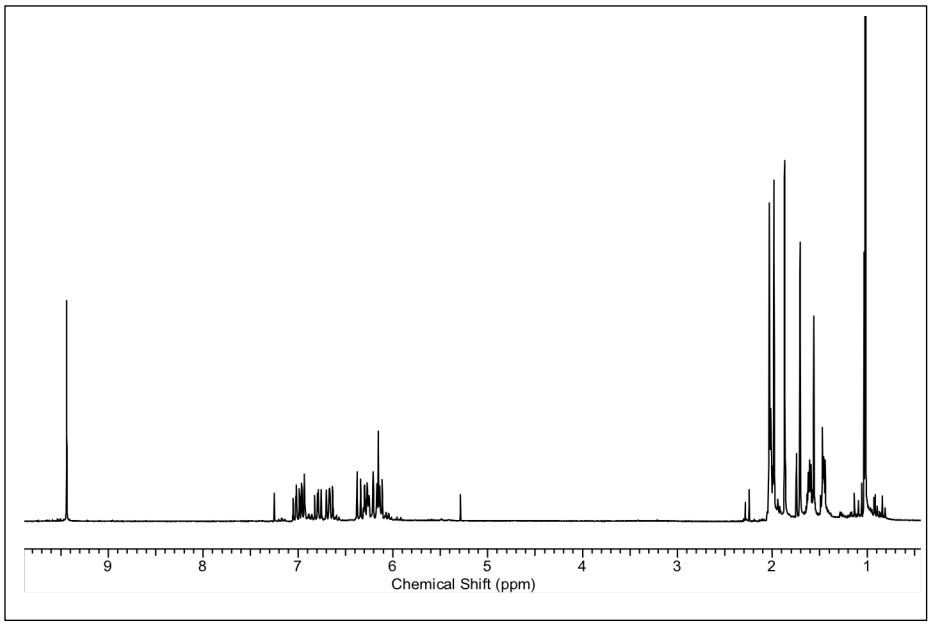

400MHz ^{1}H NMR spectrum 12'-apo-*β*-caroten-12'-al recorded in chloroform –*d.*

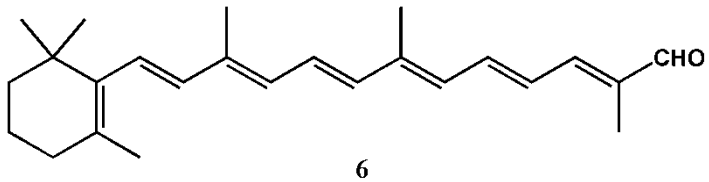

6

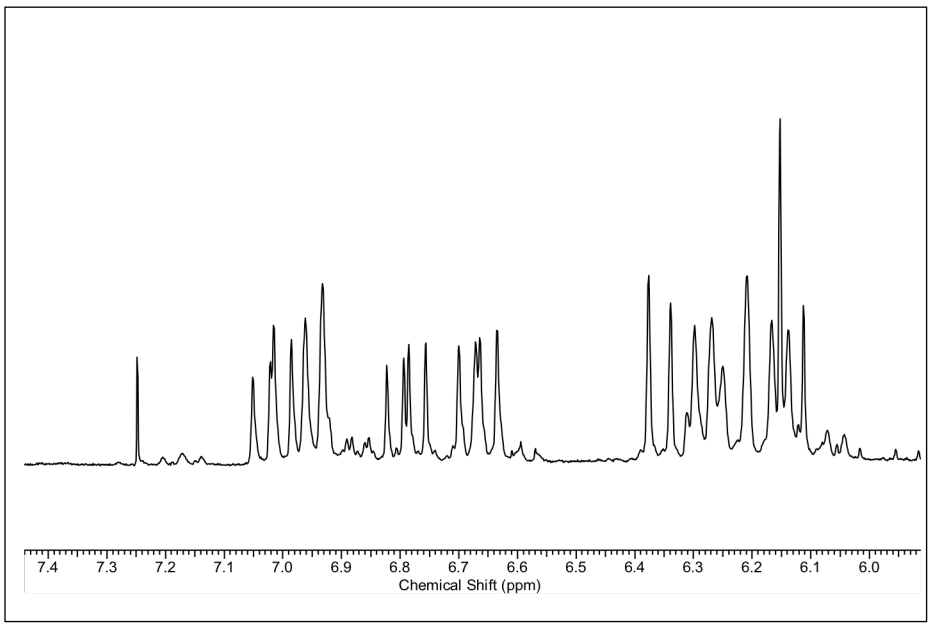

400MHz ^{1}H NMR spectrum 10'-apo-*β*-caroten-10'-al recorded in chloroform –*d.*

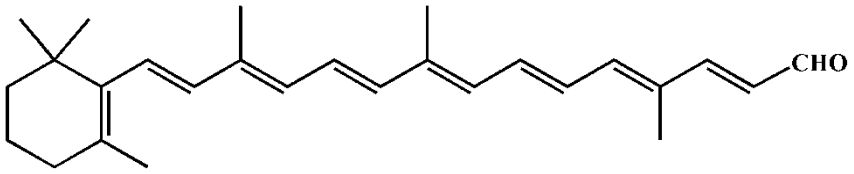

9

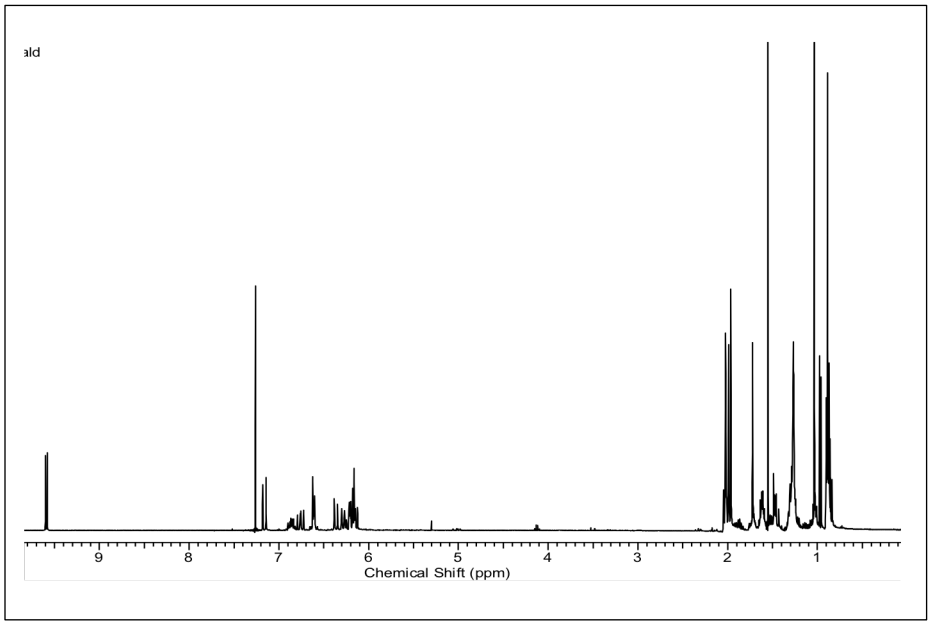

400MHz ^{1}H NMR spectrum 10'-apo-*β*-caroten-10'-al recorded in chloroform –*d.*

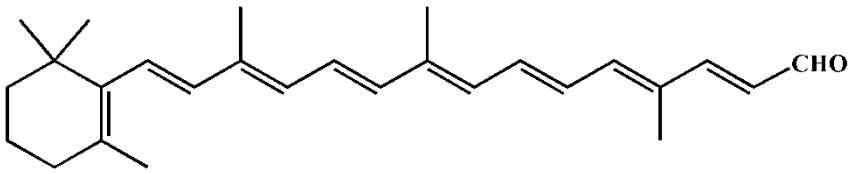

9

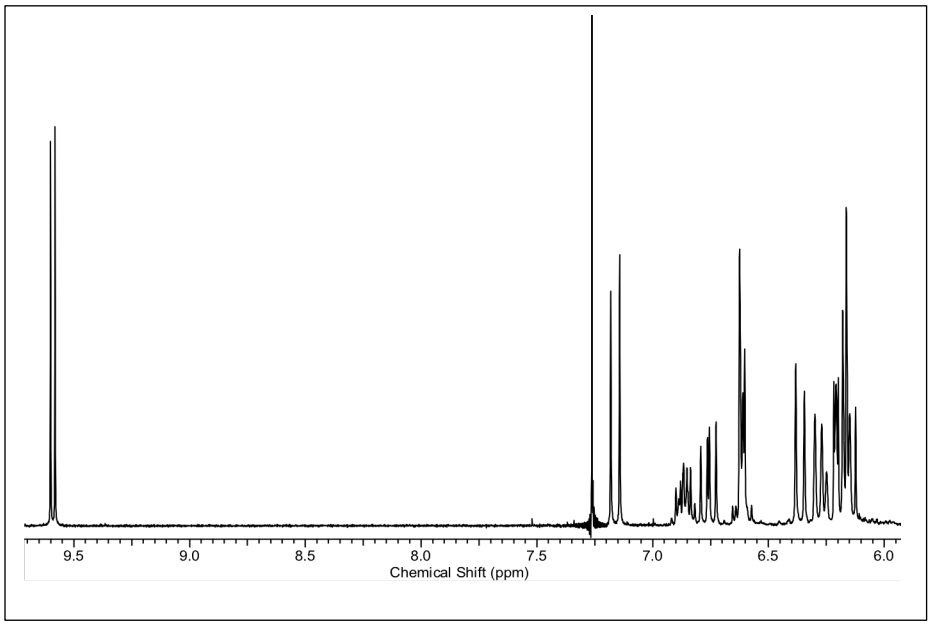

400MHz ^{1}H NMR spectrum 6'-apo-*β*-caroten-6'-al recorded in chloroform –*d.*

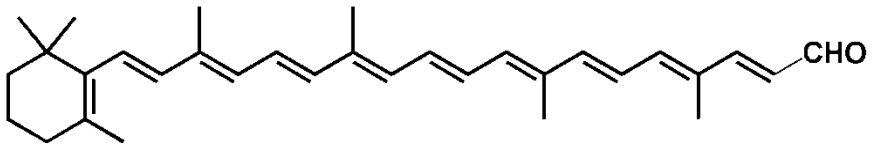

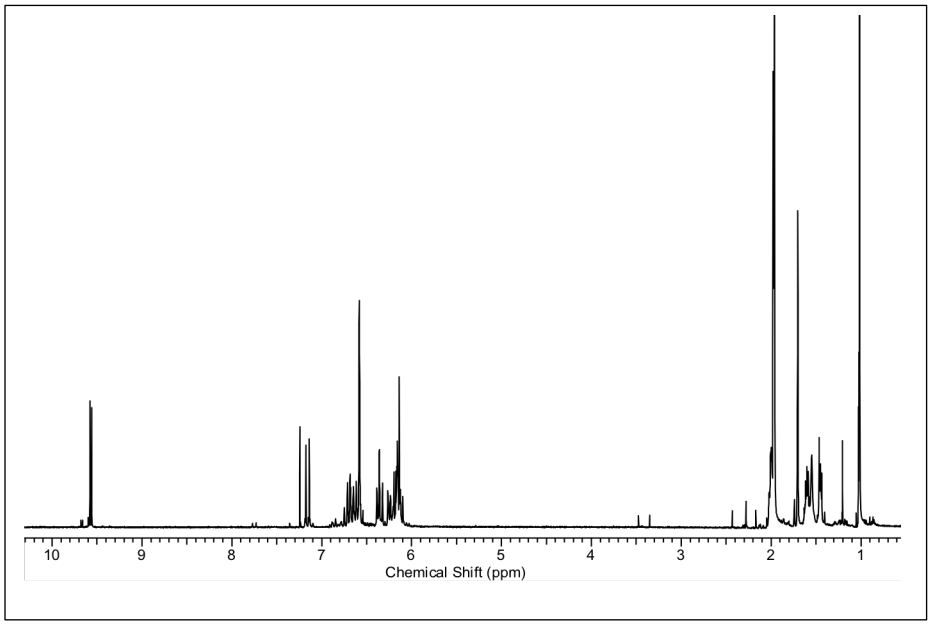

400MHz ^{1}H NMR spectrum 6'-apo-*β*-caroten-6'-al recorded in chloroform –*d.*

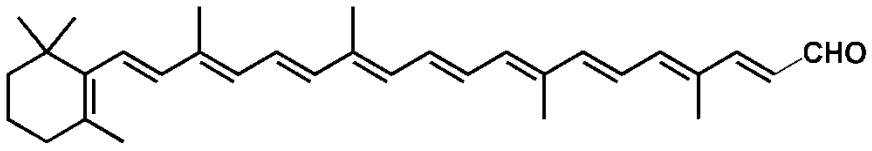

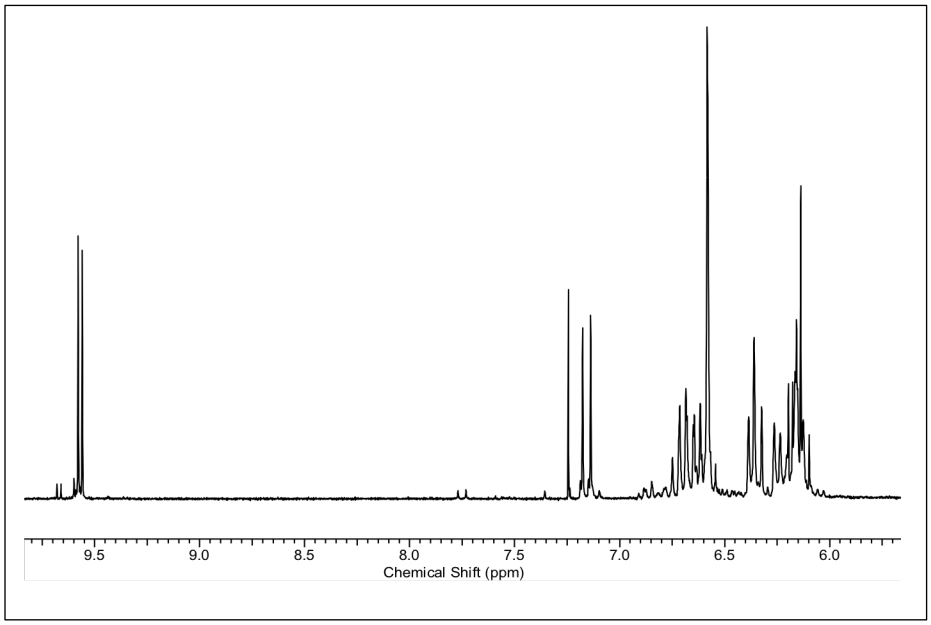

400MHz ^{1}H NMR spectrum compound (28A) recorded in chloroform –*d*.

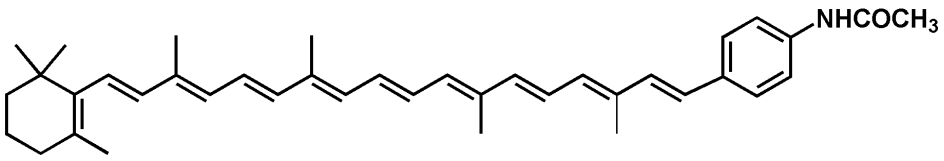

28A

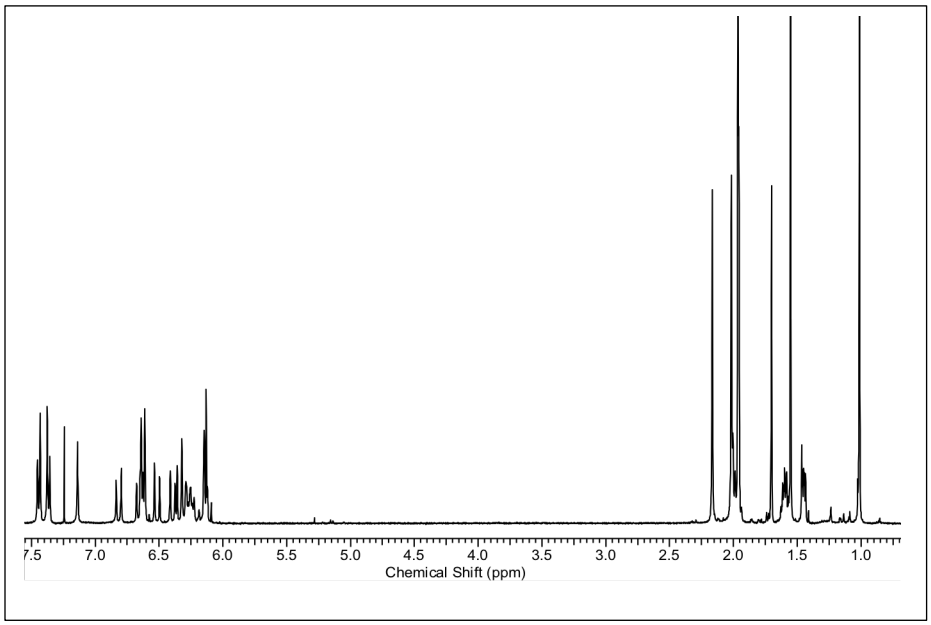

400MHz ^{1}H NMR spectrum compound (28A) recorded in chloroform –*d*.

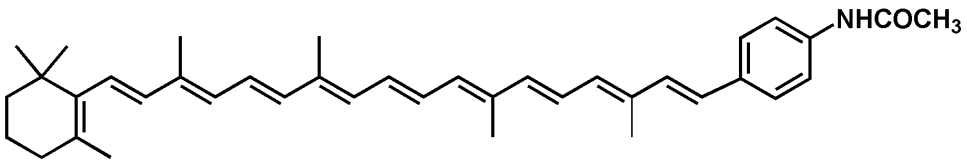

28A

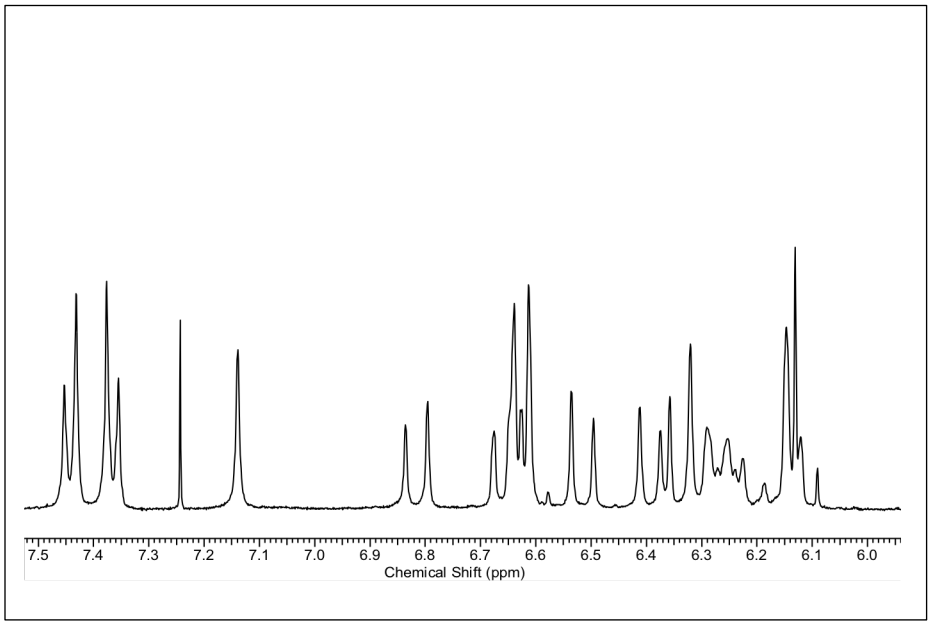

400MHz ^{1}H NMR spectrum (29A) recorded in chloroform –*d.*

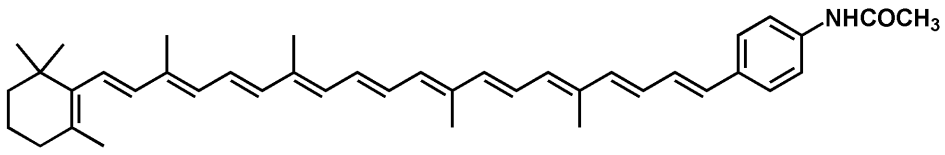

29A

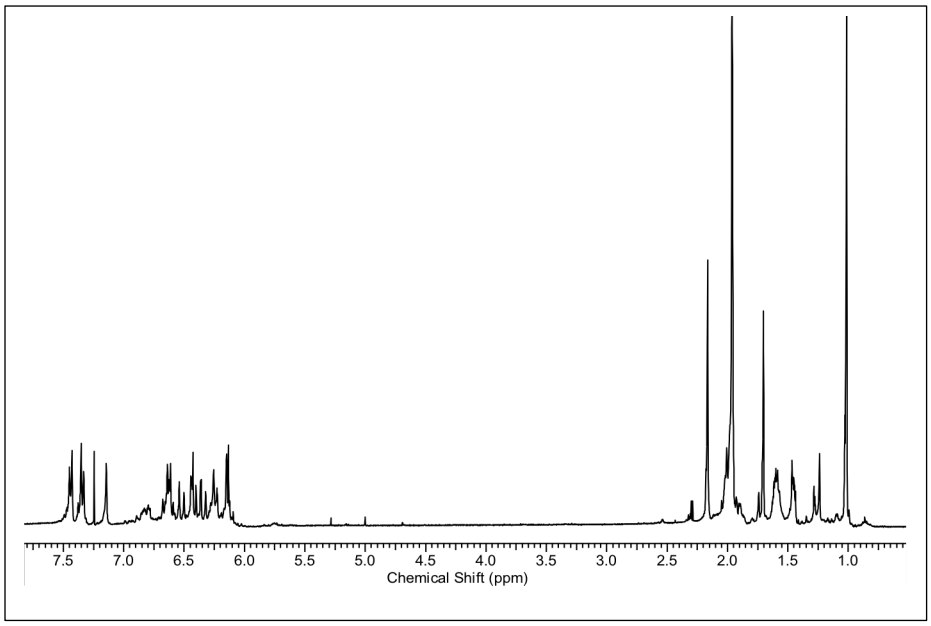

400MHz ^{1}H NMR spectrum (29A) recorded in chloroform –*d.*

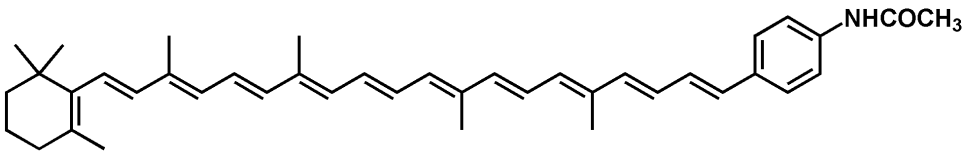

29A

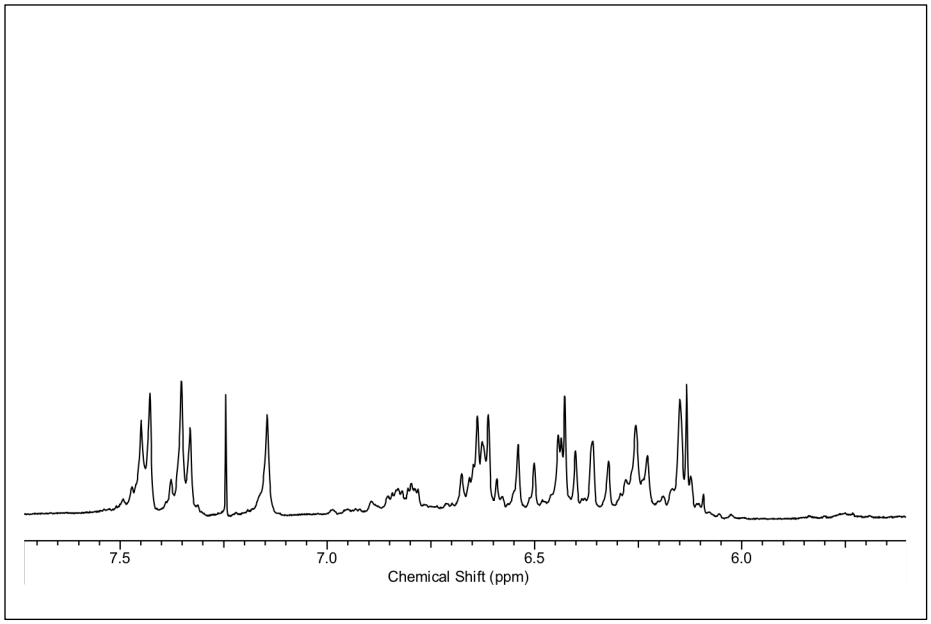

400MHz ^{1}H NMR spectrum 7'-apo-7'-(4-aminophenyl)-β-carotene recorded in chloroform –*d*.

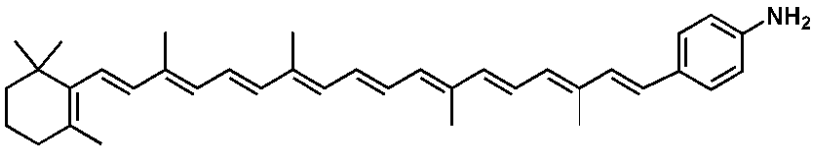

27

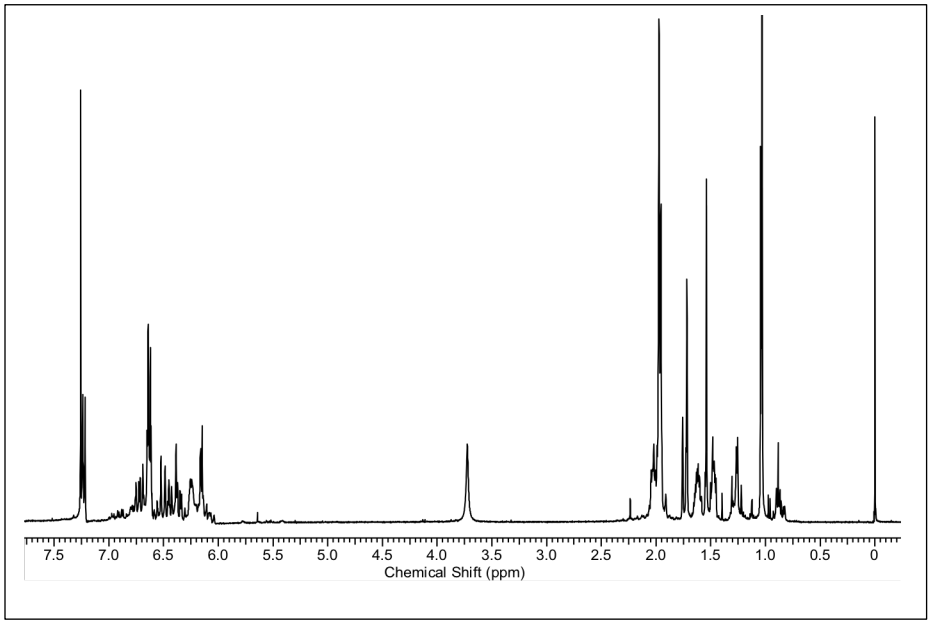

400MHz ^{1}H NMR spectrum 7'-apo-7'-(4-aminophenyl)-β-carotene recorded in chloroform –*d.*

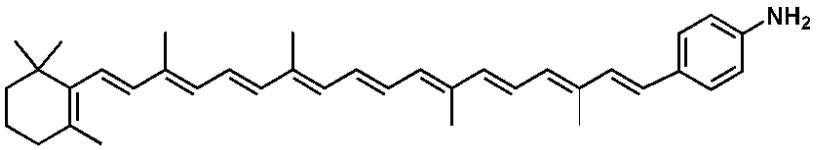

27

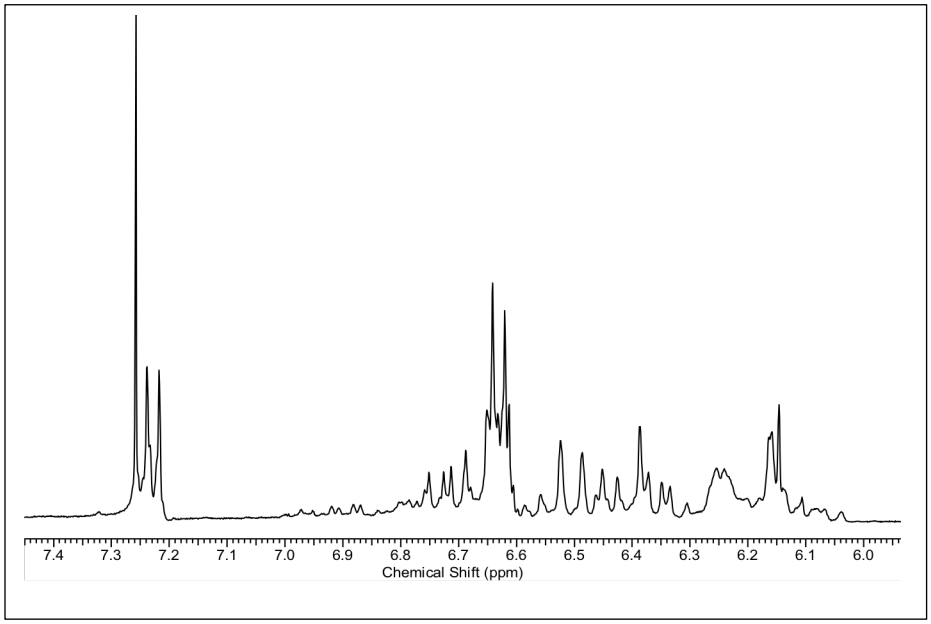

400MHz ^{1}H NMR spectrum 5'-apo-'5-(4-aminophenyl)-*β*-carotene recorded in chloroform –*d*.

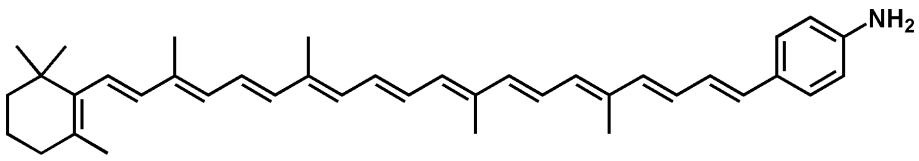

29

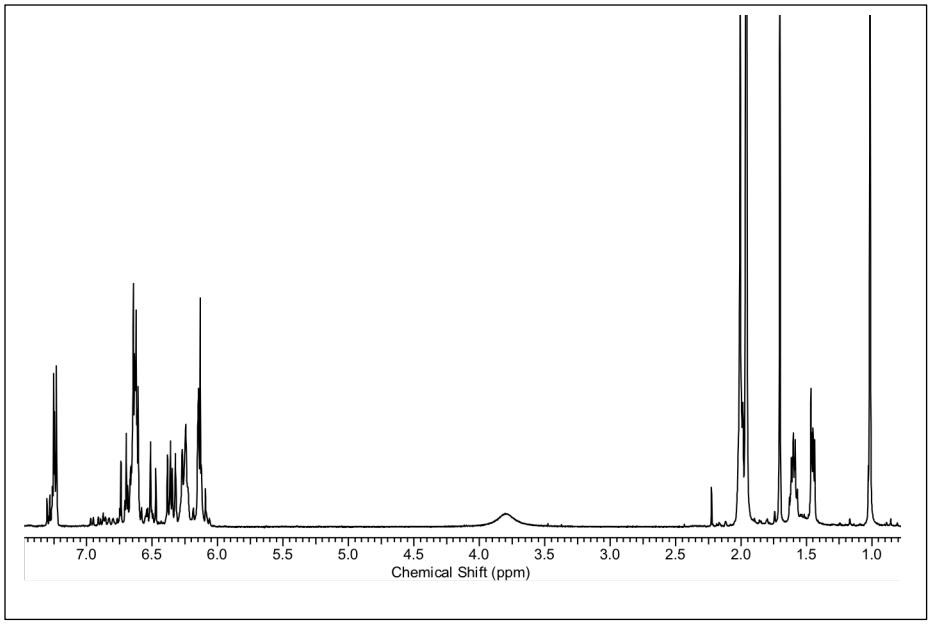

400MHz ^{1}H NMR spectrum 5'-apo-5'-(4-aminophenyl)-β-carotene recorded in chloroform –*d*.

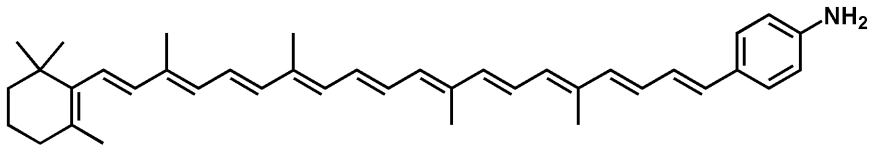

29

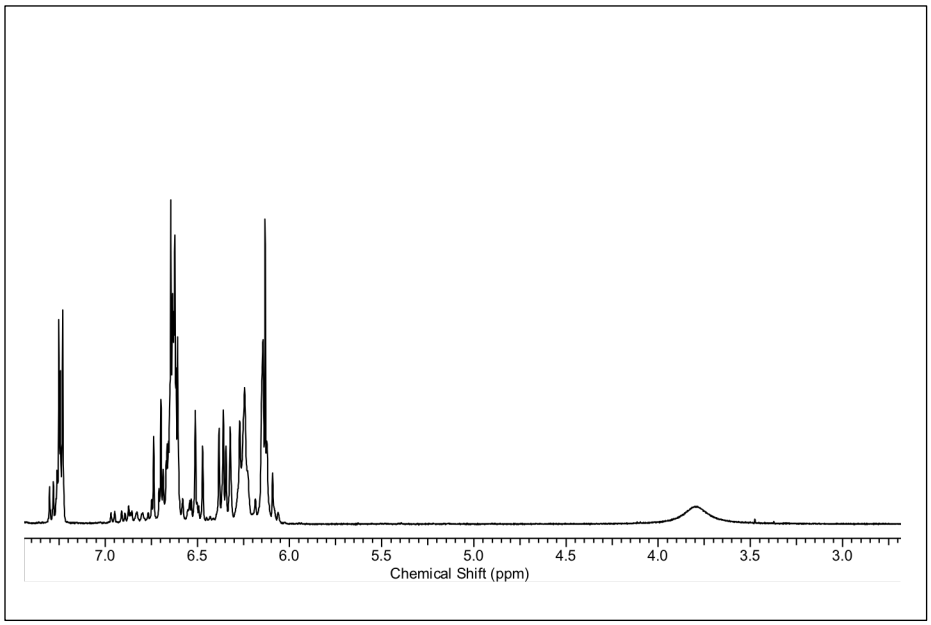

400MHz ^{1}H NMR spectrum compound (35) recorded in chloroform –*d*.

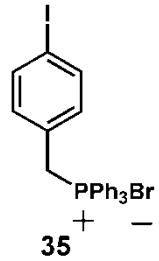

35

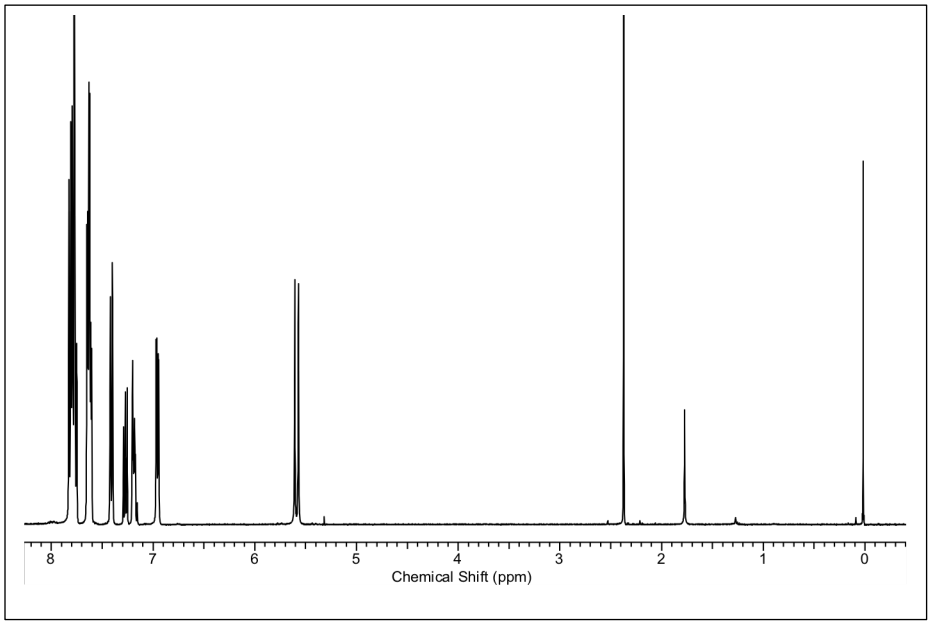

400MHz ^{1}H NMR spectrum 11'-Apo-11'-(4-iodophenyl)-*β*-carotene recorded in chloroform –*d.*

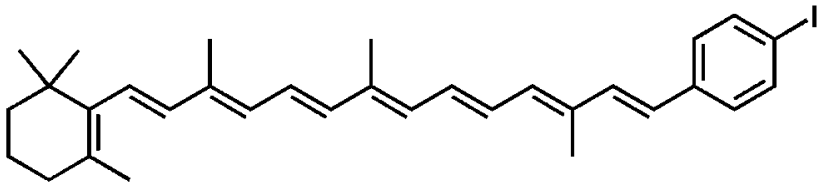

36

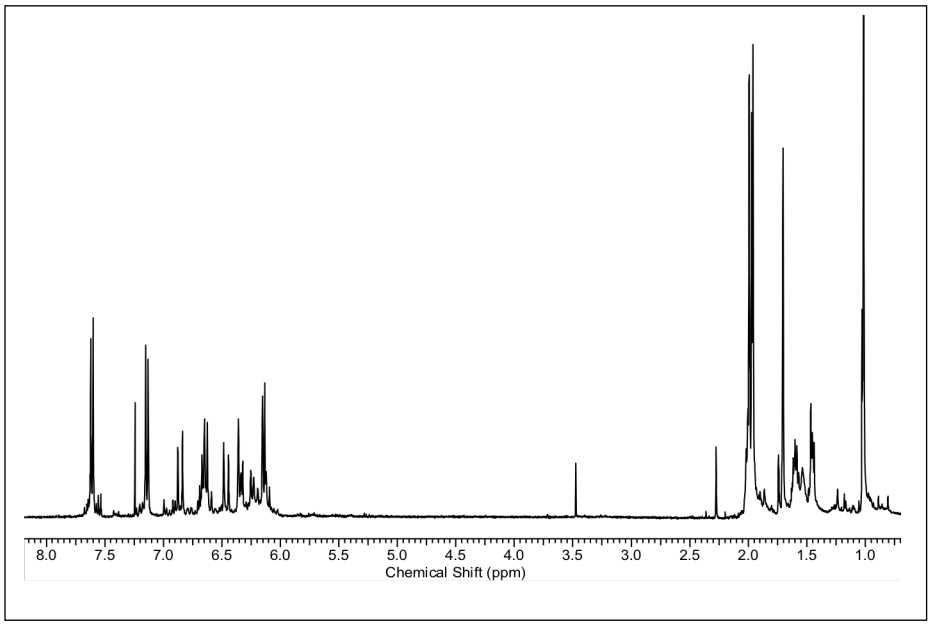

400MHz ^{1}H NMR spectrum 11'-Apo-11'-(4-iodophenyl)-*β*-carotene recorded in chloroform –*d*.

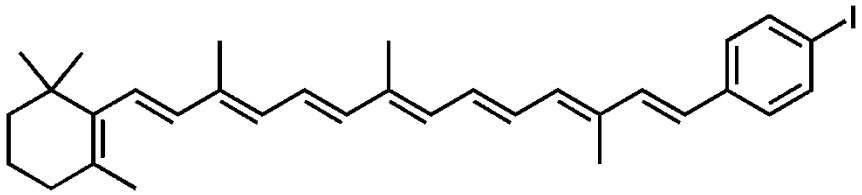

36

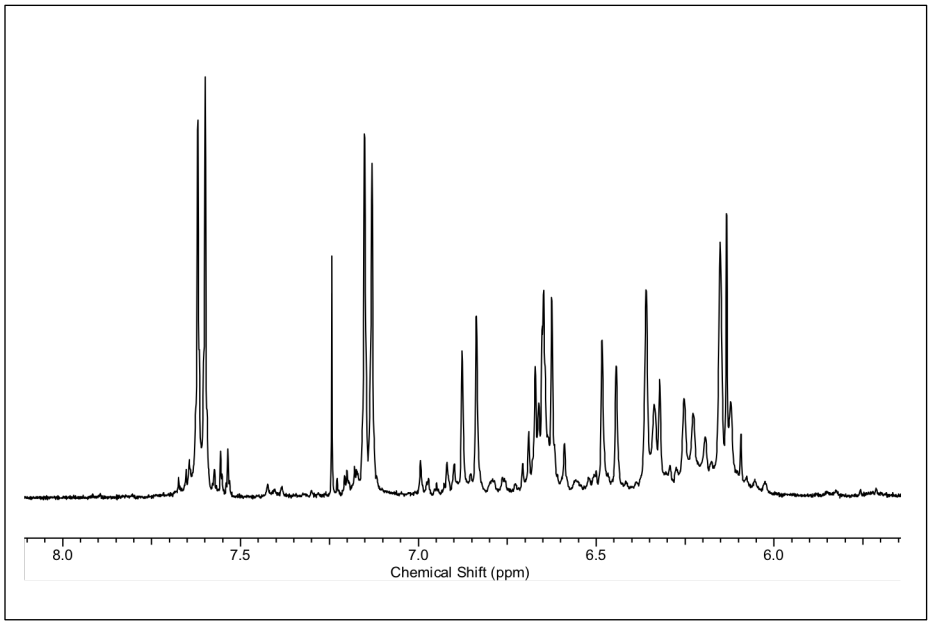

400MHz ^{1}H NMR spectrum 7'-Apo-7'-(4-iodophenyl)-β-carotene recorded in chloroform –*d*.

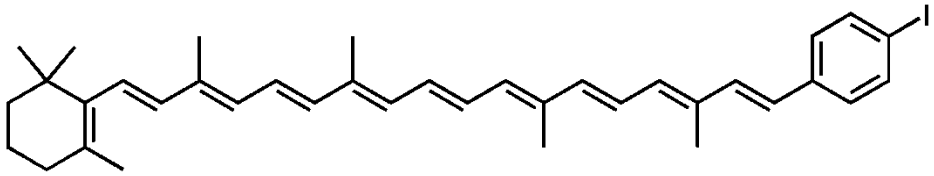

38

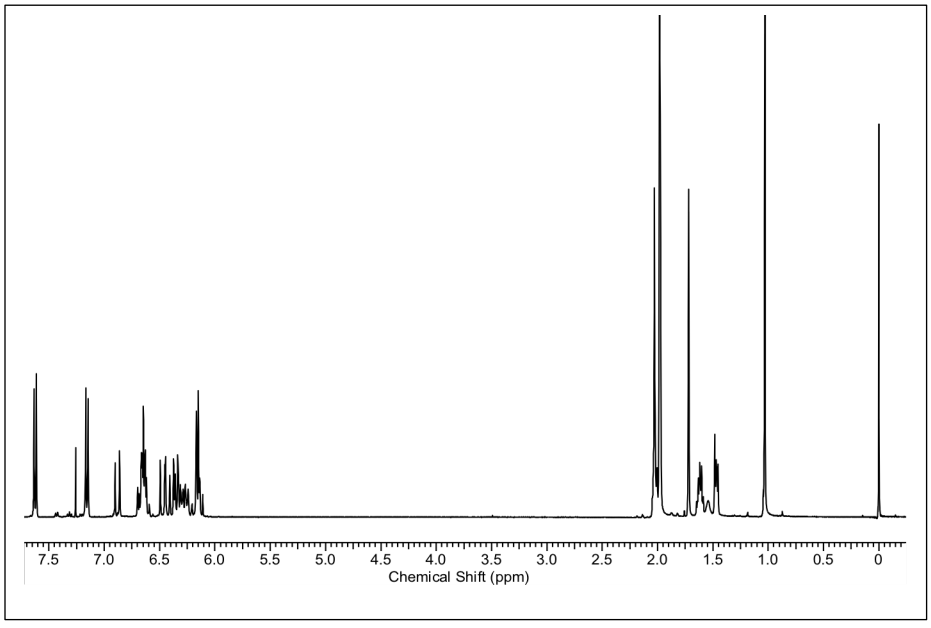

400MHz ^{1}H NMR spectrum 7'-Apo-7'-(4-iodophenyl)-*β*-carotene recorded in chloroform –*d*.

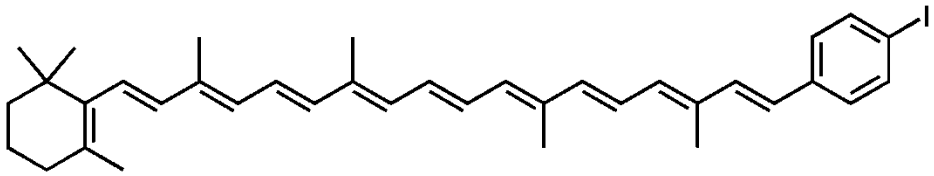

38

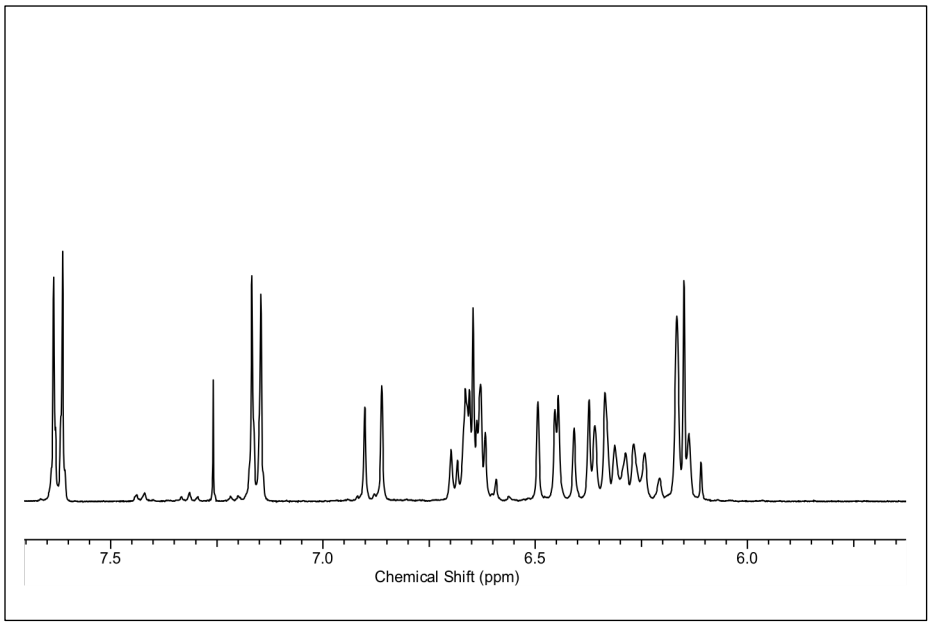

400MHz ^{1}H NMR spectrum 11'-apo-11'-(4-amino-N-[4-methylphenyl]phenyl)-*β*-carotene recorded in chloroform –*d*.

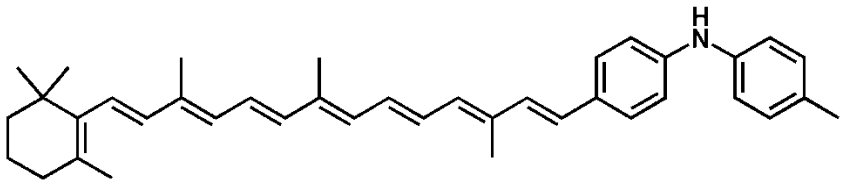

40

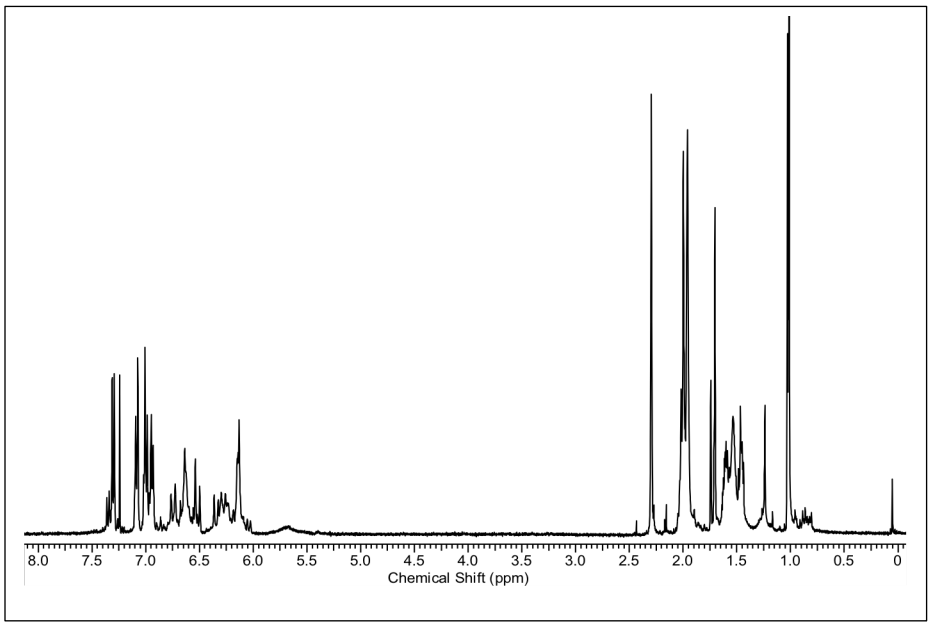

400MHz ^{1}H NMR spectrum 11'-apo-11'-(4-amino-N-[4-methylphenyl]phenyl)-*β*-carotene recorded in chloroform –*d*.

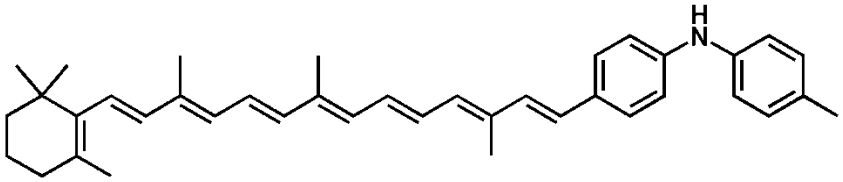

40

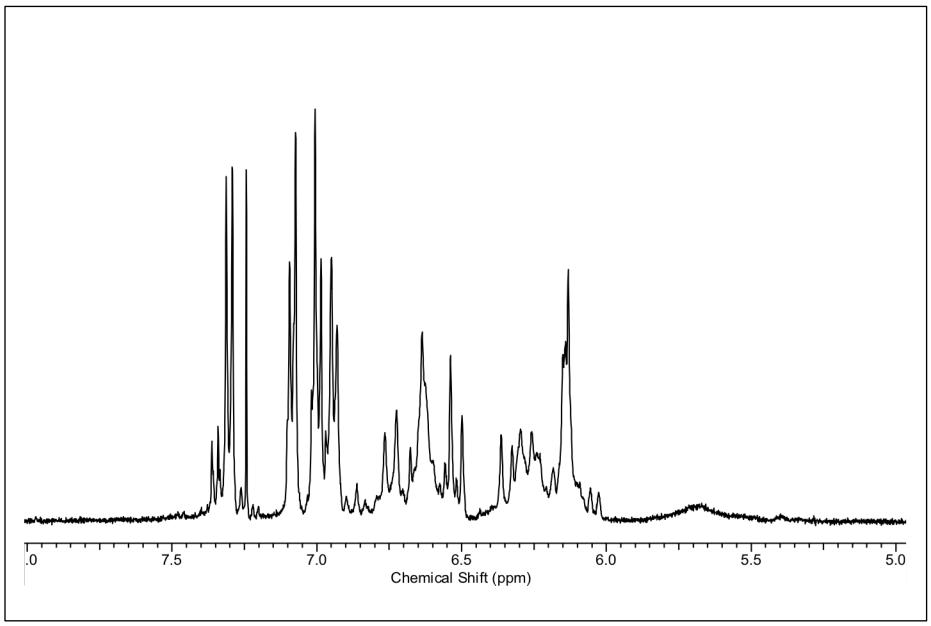

400MHz ^{1}H NMR spectrum 7'-apo-7'-(4-amino-N-[4-methylphenyl]phenyl)-*β*-carotene recorded in chloroform –*d*.

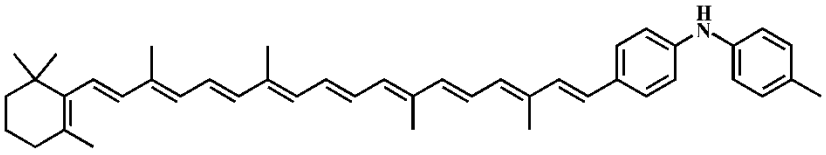

42

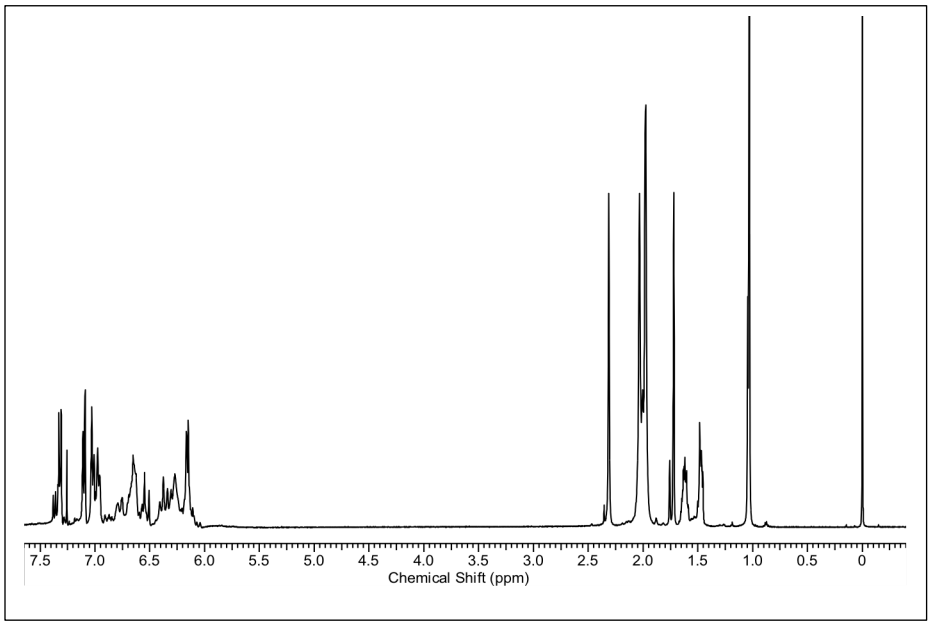

400MHz ^{1}H NMR spectrum 7'-apo-7'-(4-amino-N-[4-methylphenyl]phenyl)-*β*-carotene recorded in chloroform –*d*.

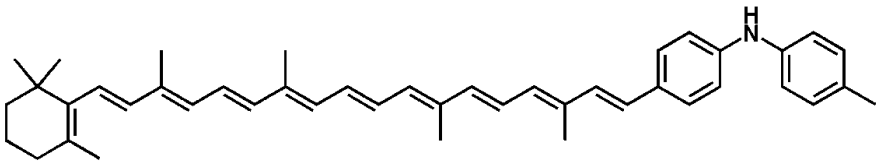

42

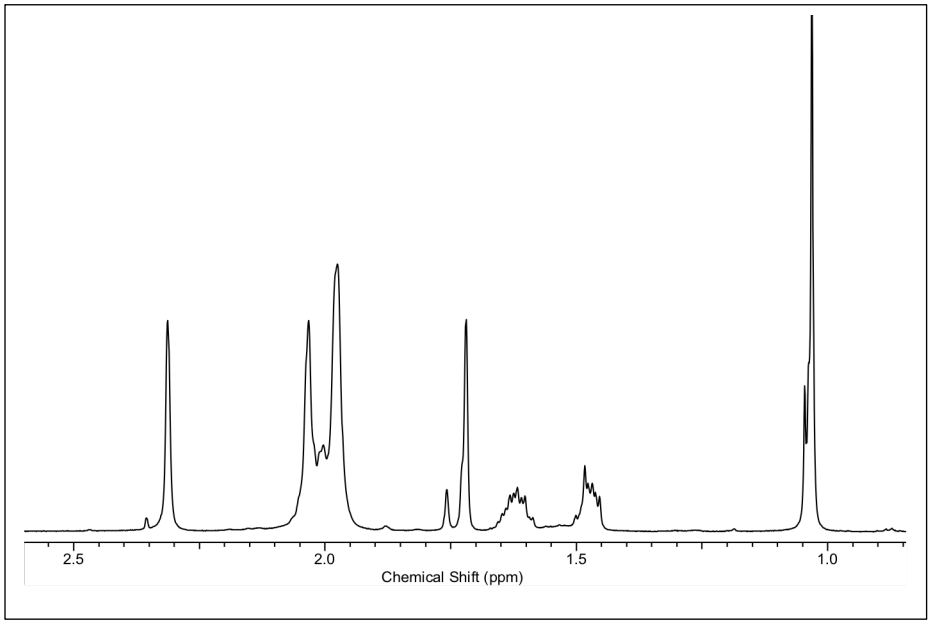

400MHz ^{1}H NMR spectrum 5'-apo-5'-(4-amino-N-[4-methylphenyl]phenyl)-*β*-carotene recorded in chloroform –*d*.

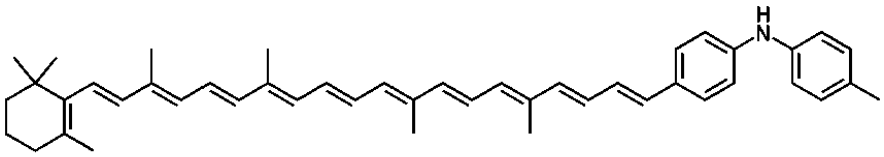

43

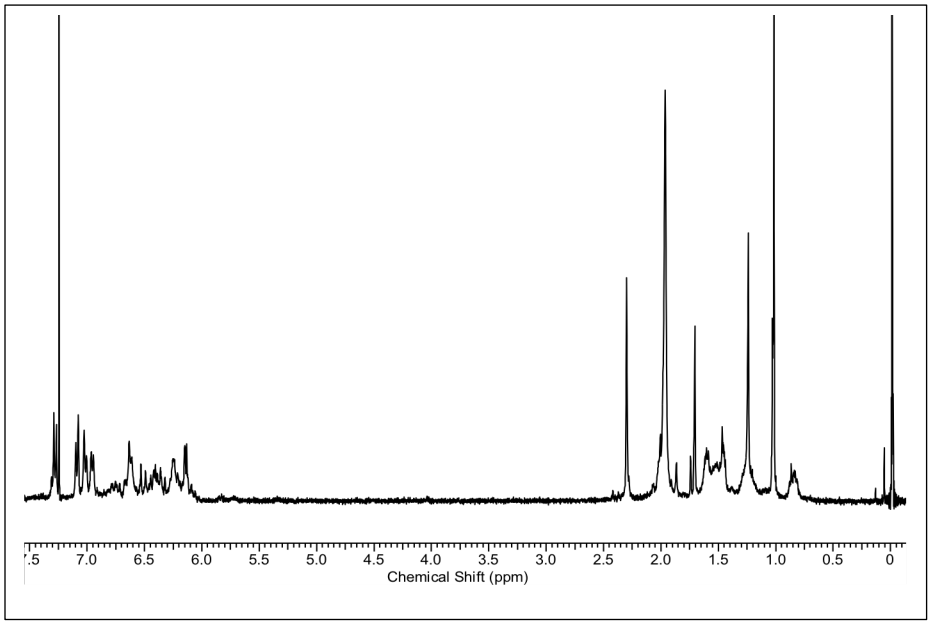

400MHz ^{1}H NMR spectrum 5'-apo-5'-(4-amino-N-[4-methylphenyl]phenyl)-*β*-carotene recorded in chloroform –*d*.

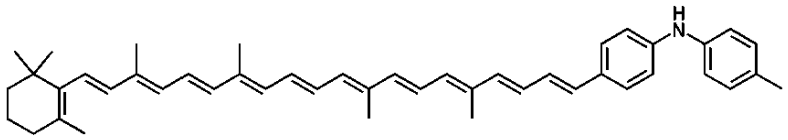

43

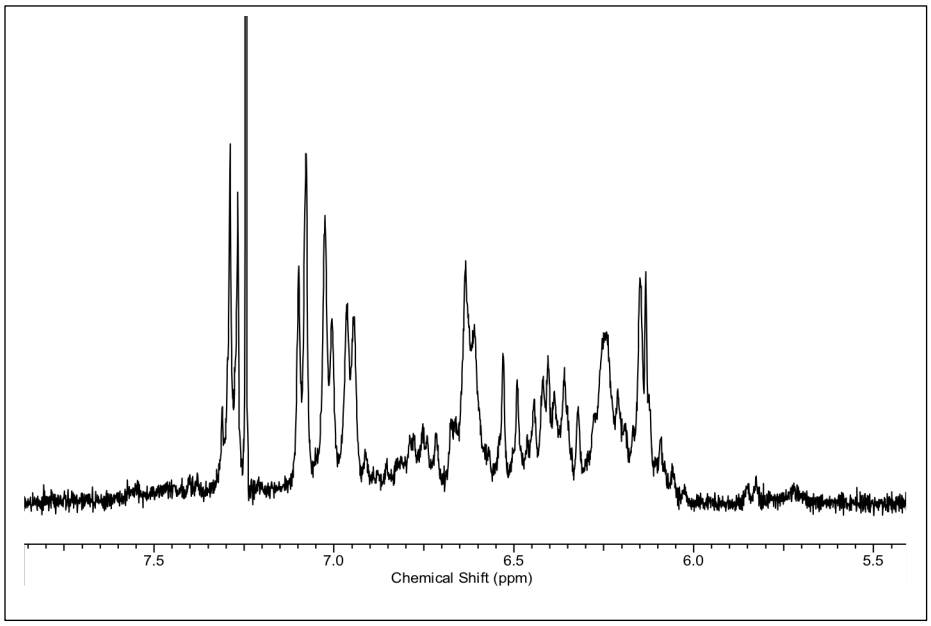

500MHz ^{1}H NMR spectrum amine-dyad-8-db recorded in THF-d_8.

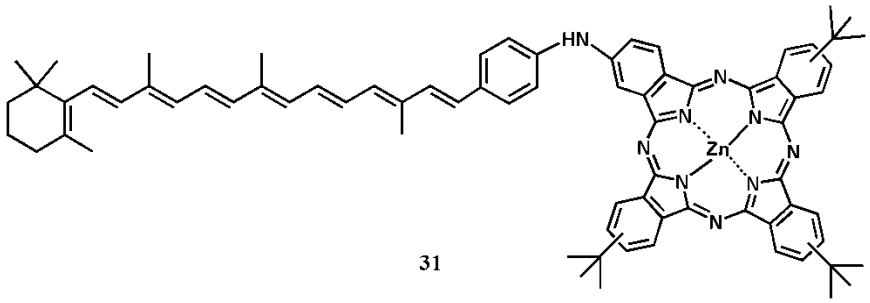

31

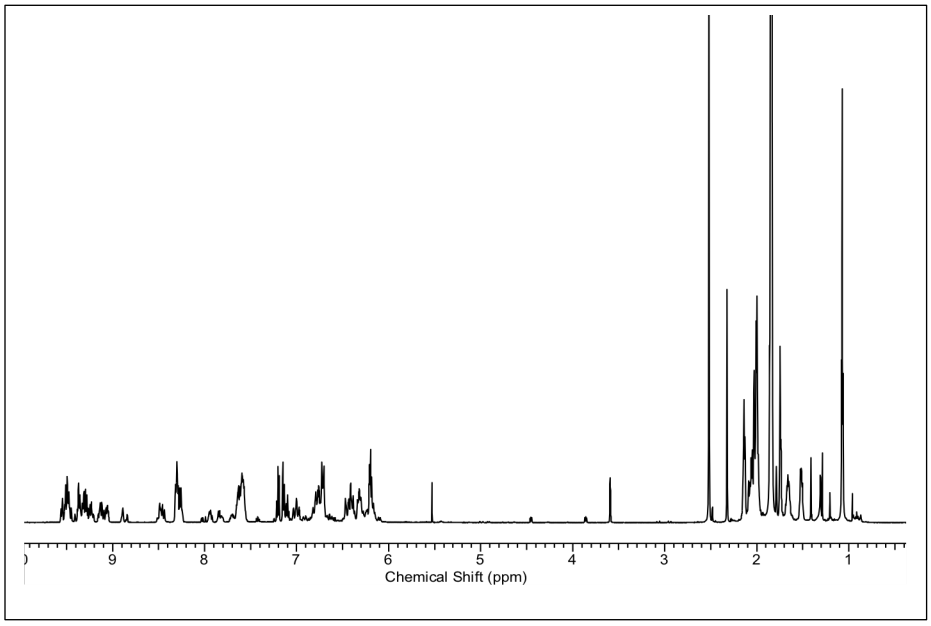

500MHz ^{1}H NMR spectrum amine-dyad-8-db recorded in THF-d_8.

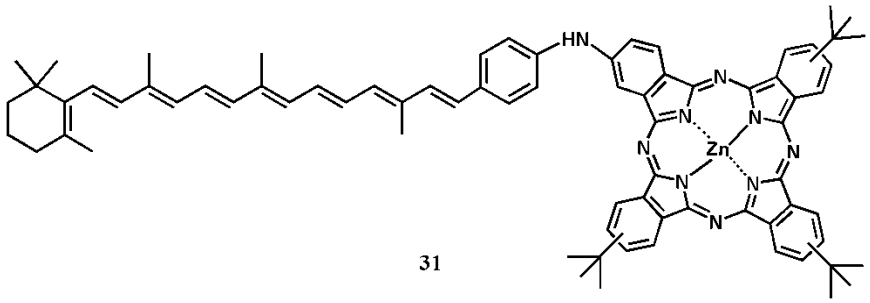

31

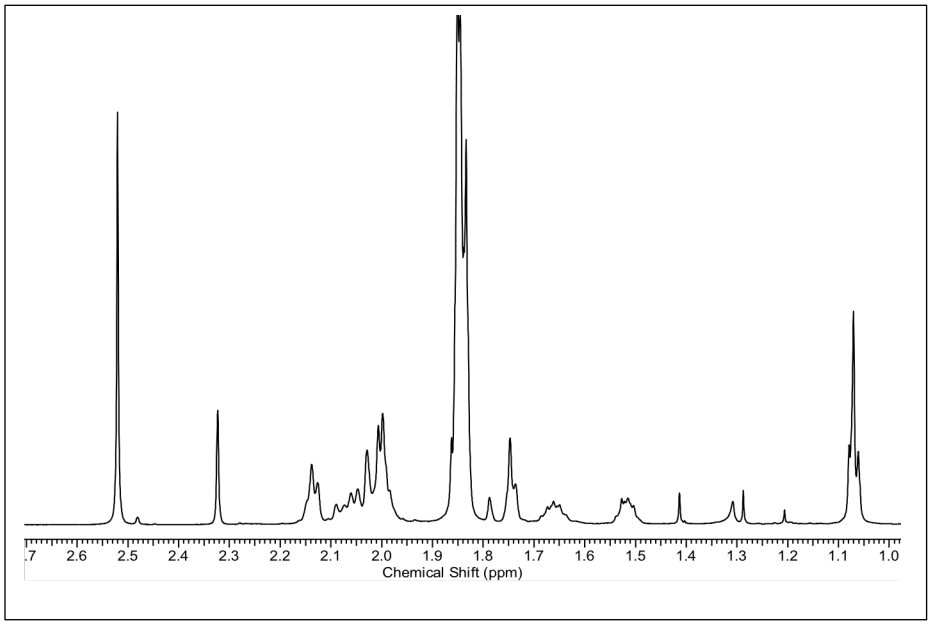

500MHz ^{1}H NMR spectrum amine-dyad-8-db recorded in THF-d_8.

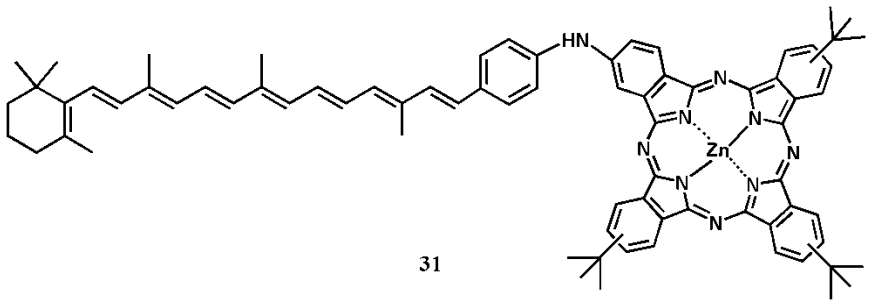

31

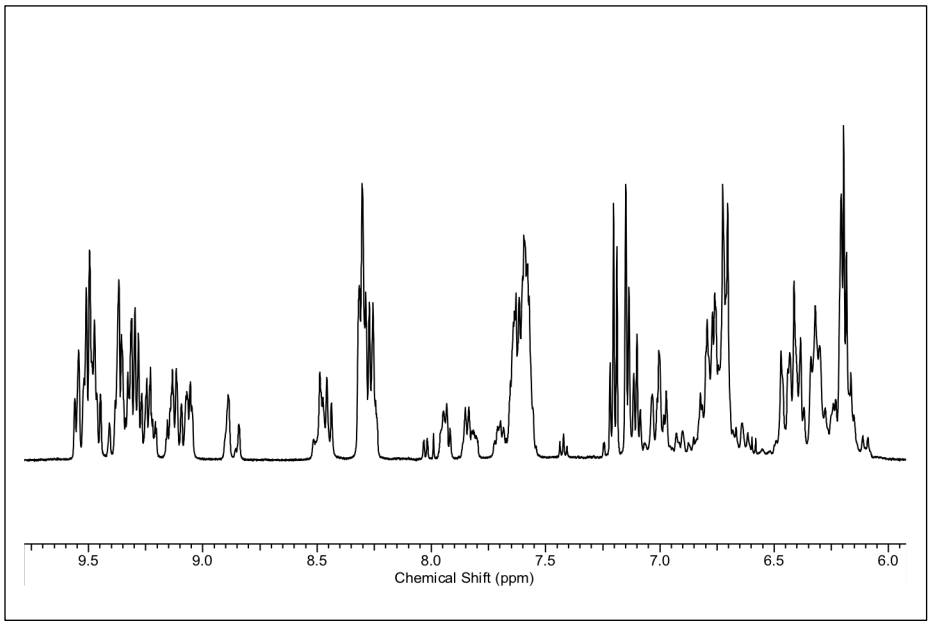

500MHz ^{1}H NMR spectrum amine-dyad-9-db recorded in THF-d_8.

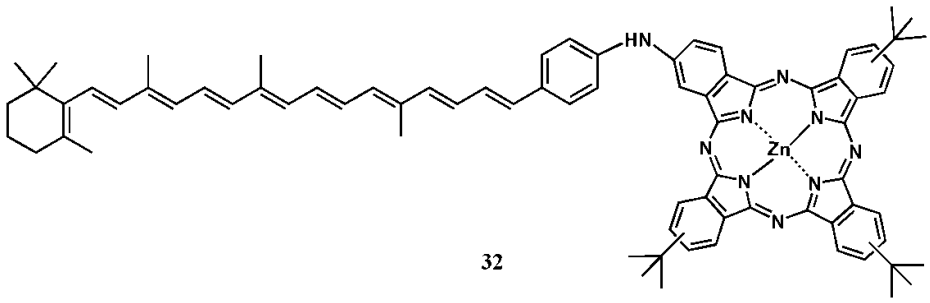

32

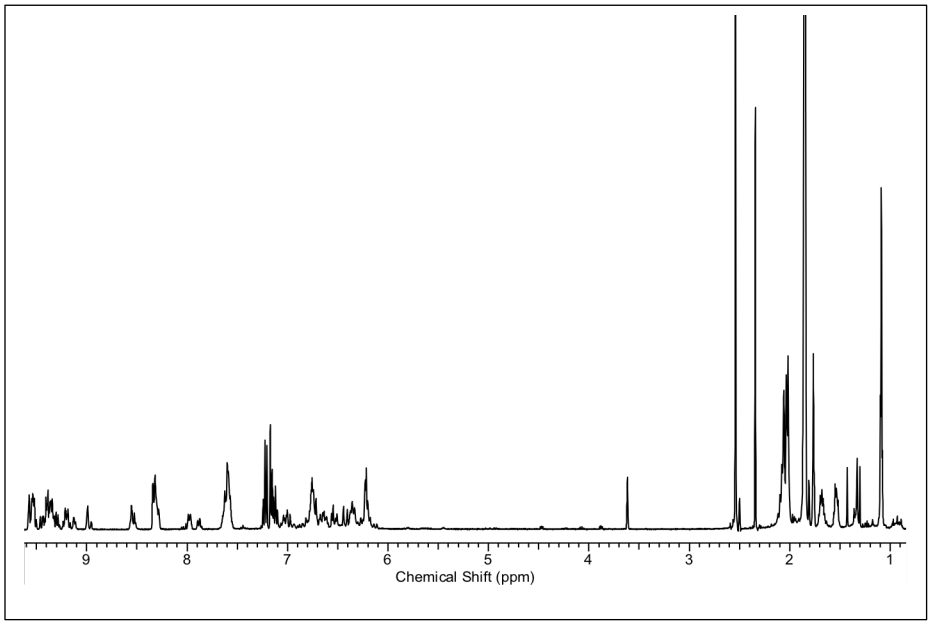

500MHz ^{1}H NMR spectrum amine-dyad-9-db recorded in THF-d_8.

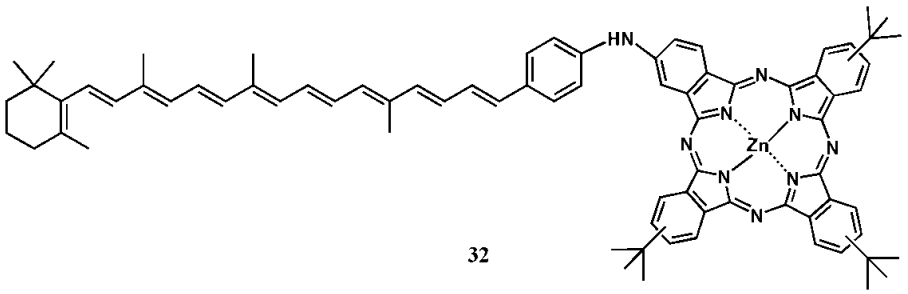

32

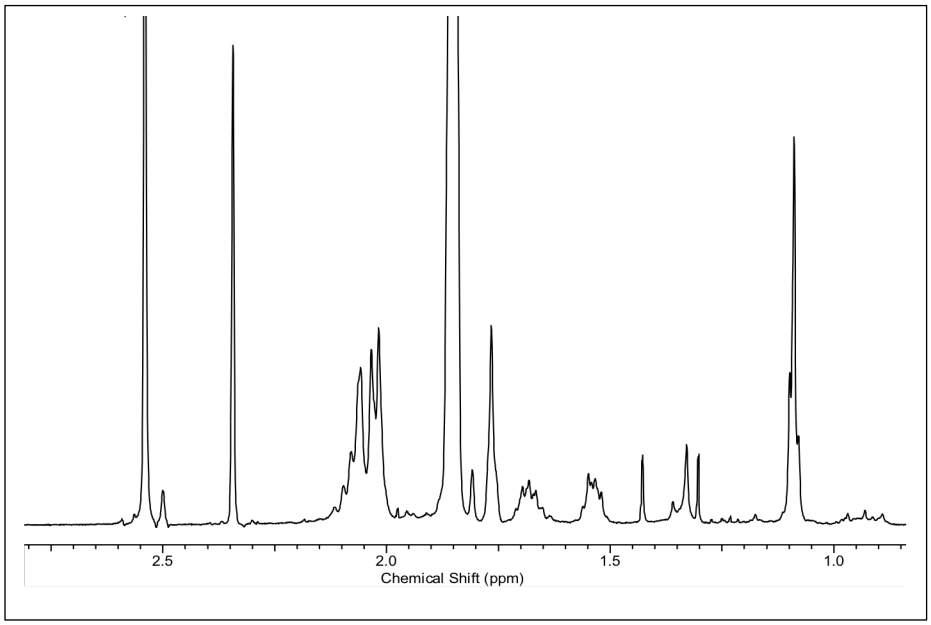

500MHz ^{1}H NMR spectrum amine-dyad-9-db recorded in THF-d_8.

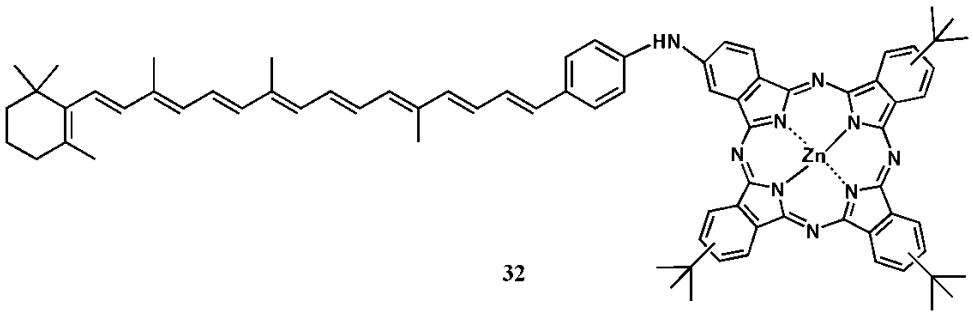

32

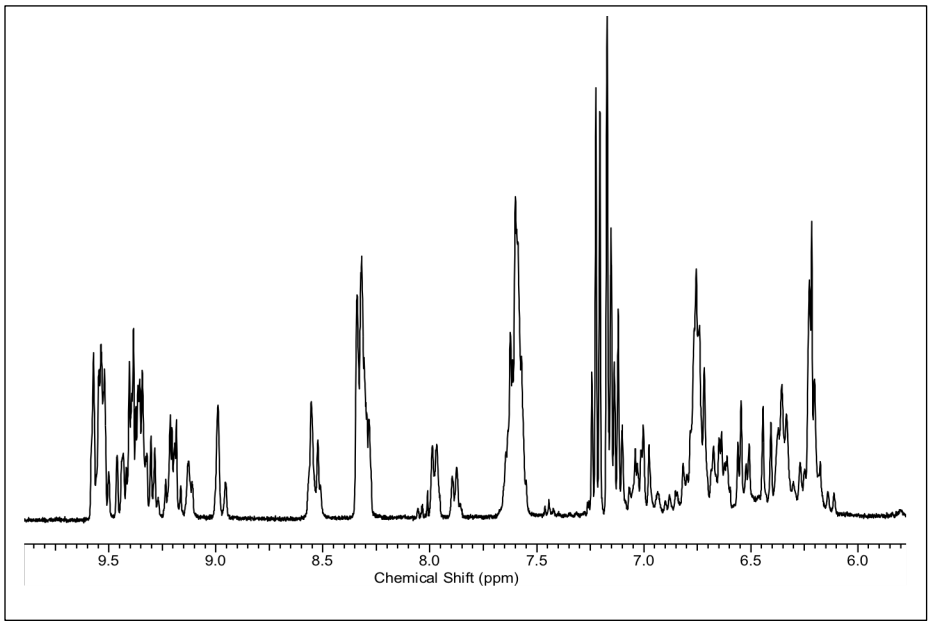

500MHz HMBC spectrum amine-dyad-9-db recorded in THF-d_8.

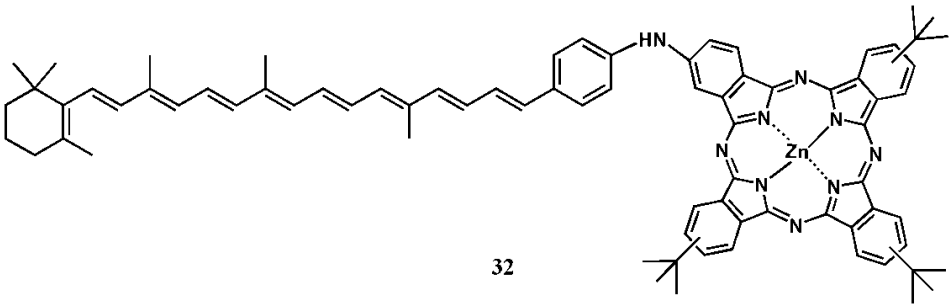

32

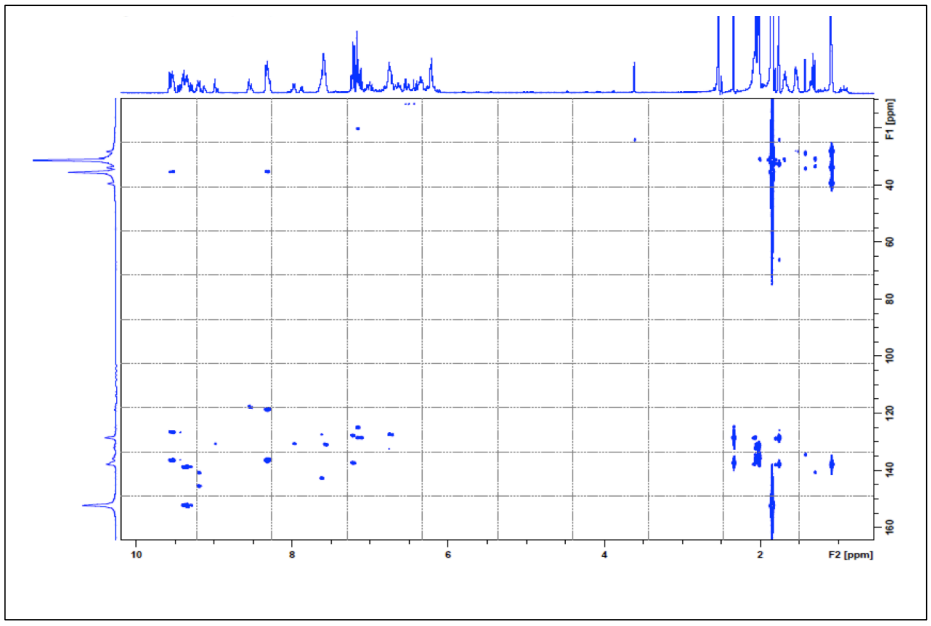

500MHz HMBC spectrum amine-dyad-9-db recorded in THF-d_8.

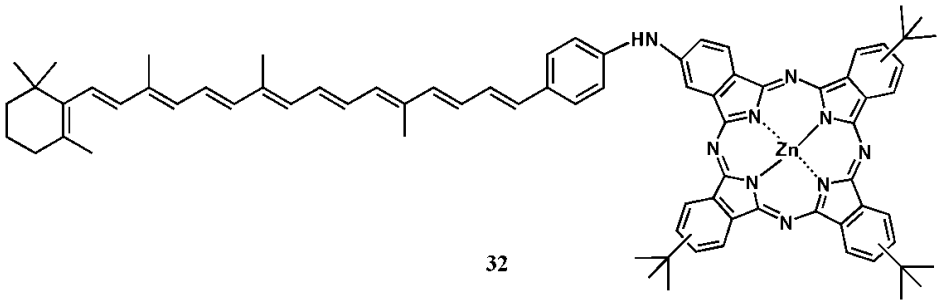

32

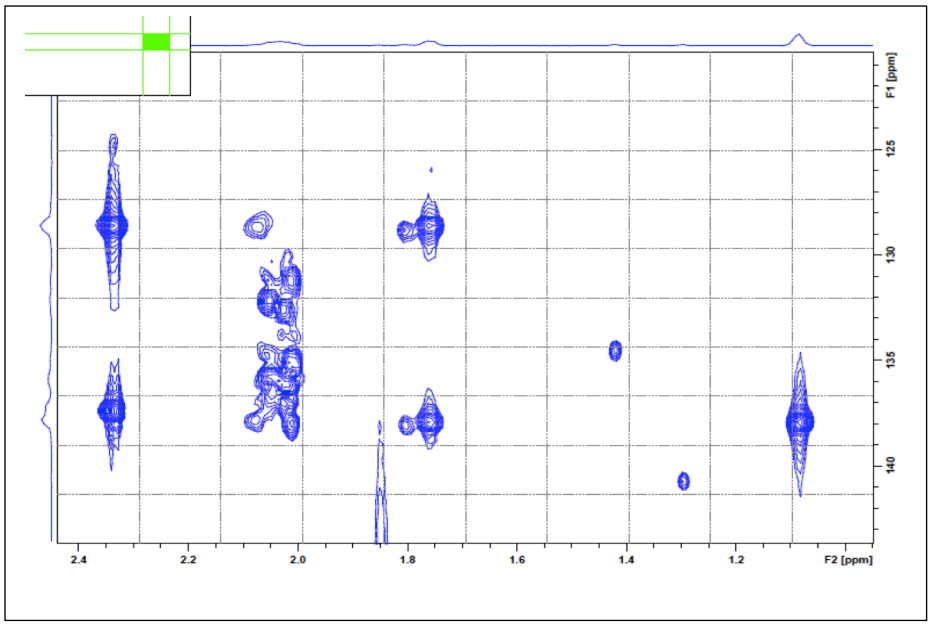

500MHz HMBC spectrum amine-dyad-9-db recorded in THF-d_8.

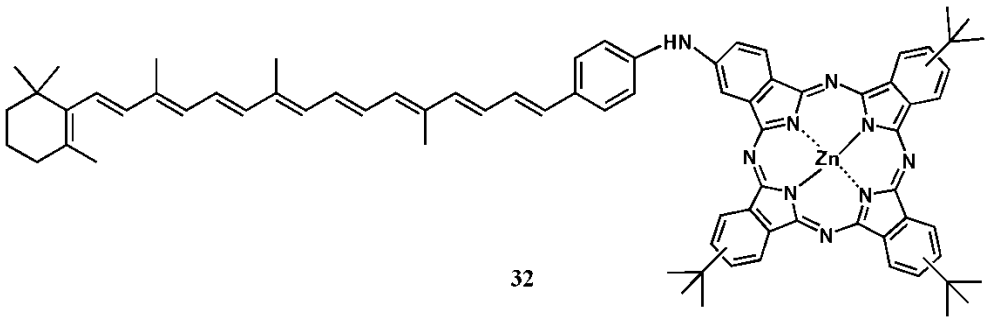

32

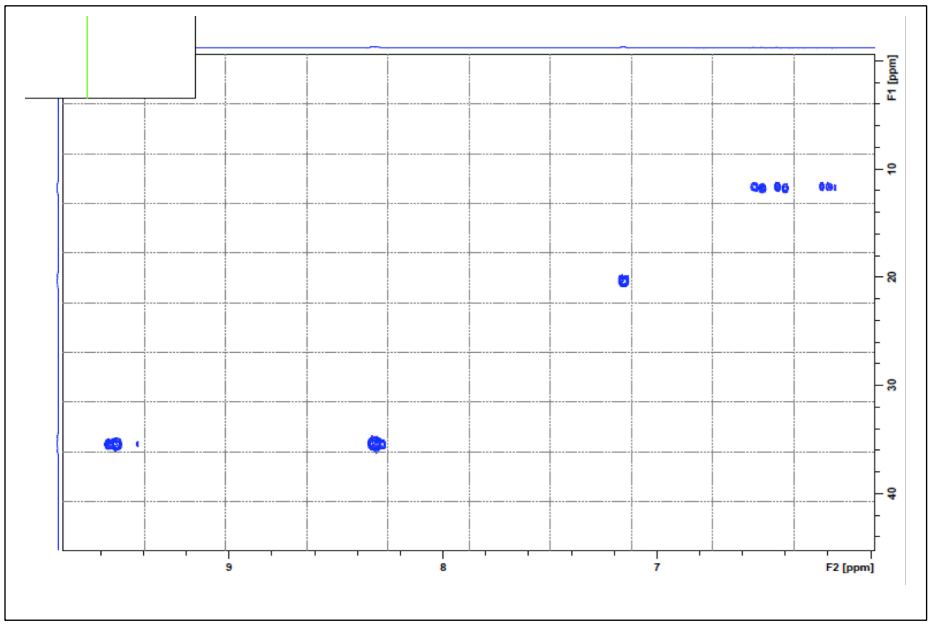

500MHz HSQC spectrum amine-dyad-9-db recorded in THF-d_8.

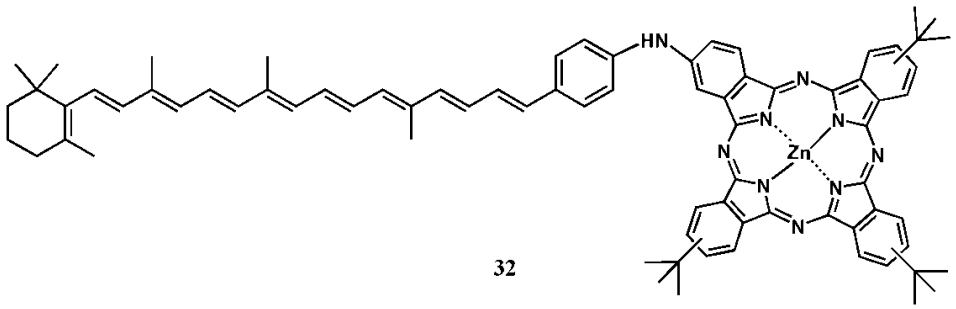

32

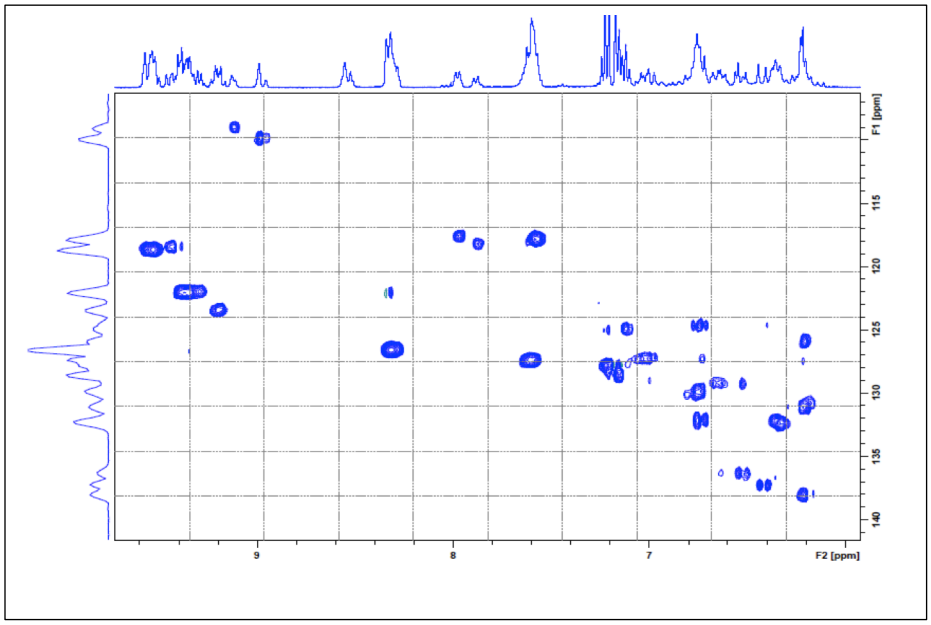

500MHz HMBC overlaid HSQC spectrum amine-dyad-9-db recorded in THF-d_8.

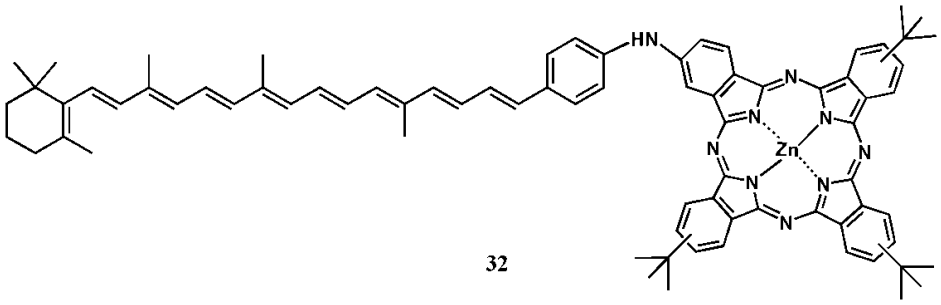

32

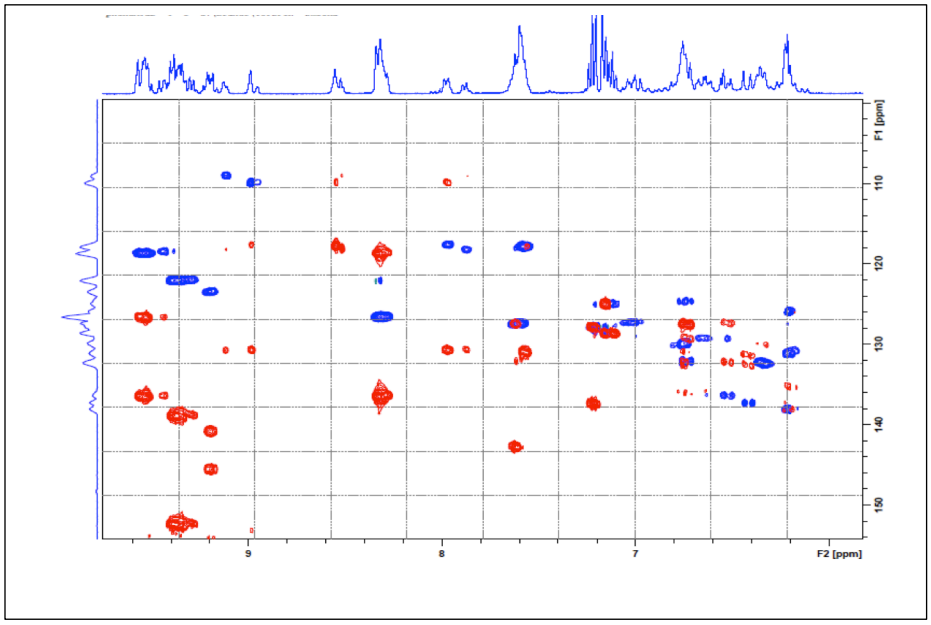

400MHz ^{1}H NMR spectrum compound (45) recorded in chloroform –*d.*

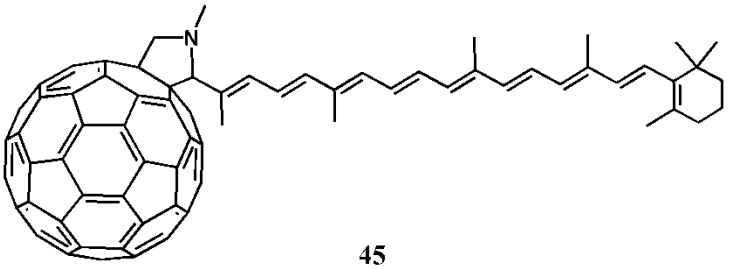

45

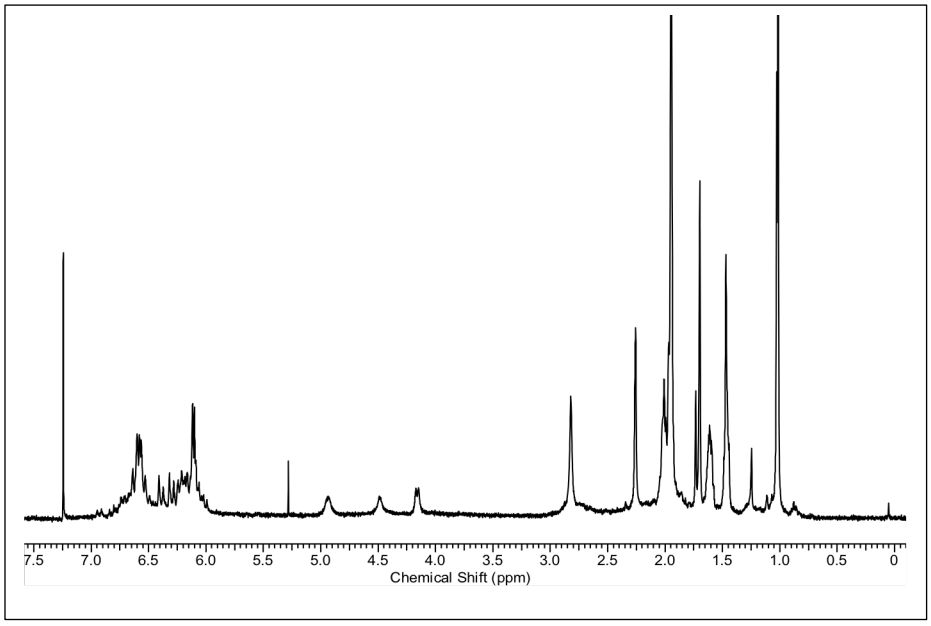

400MHz ^{1}H NMR spectrum compound (45) recorded in chloroform –*d*.

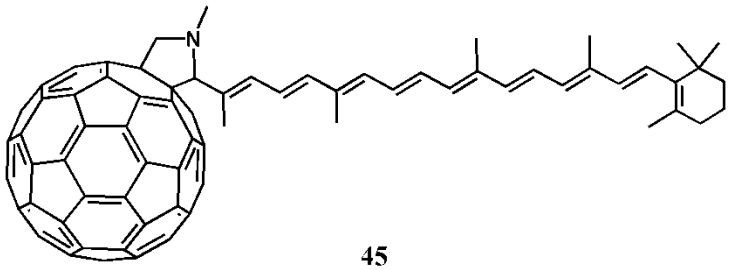

45

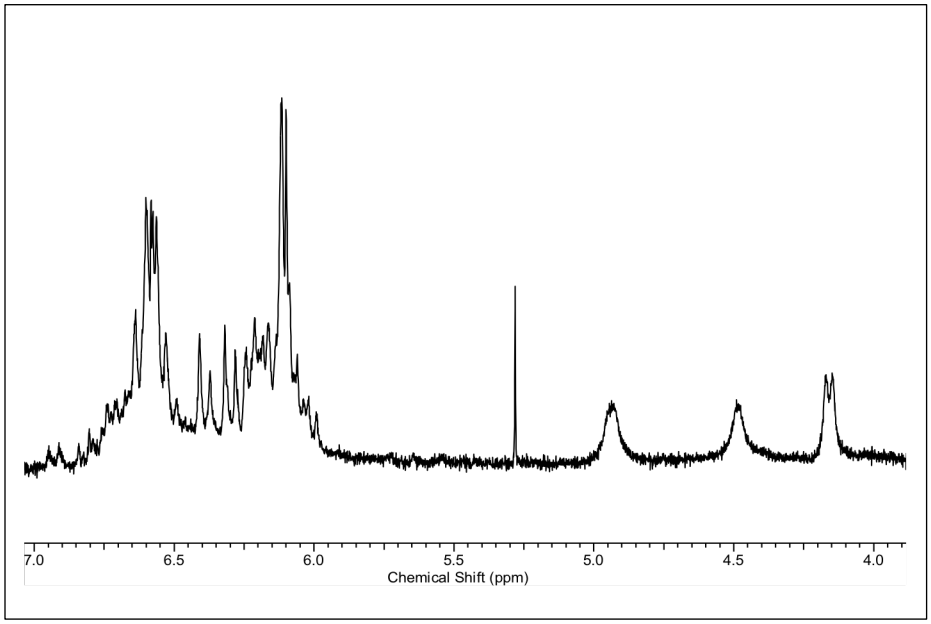

400MHz ^{1}H NMR spectrum compound (46) recorded in chloroform –*d.*

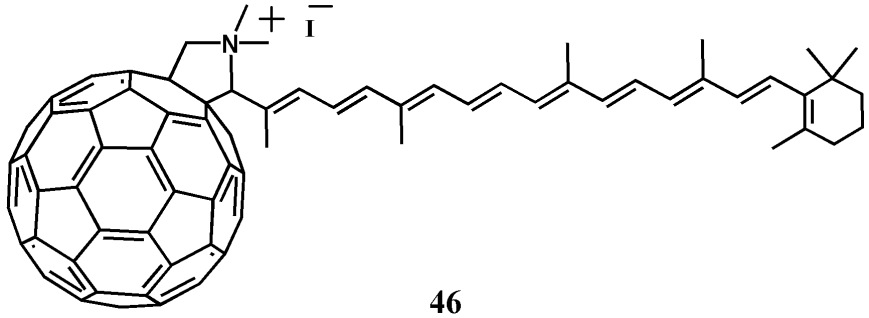

46

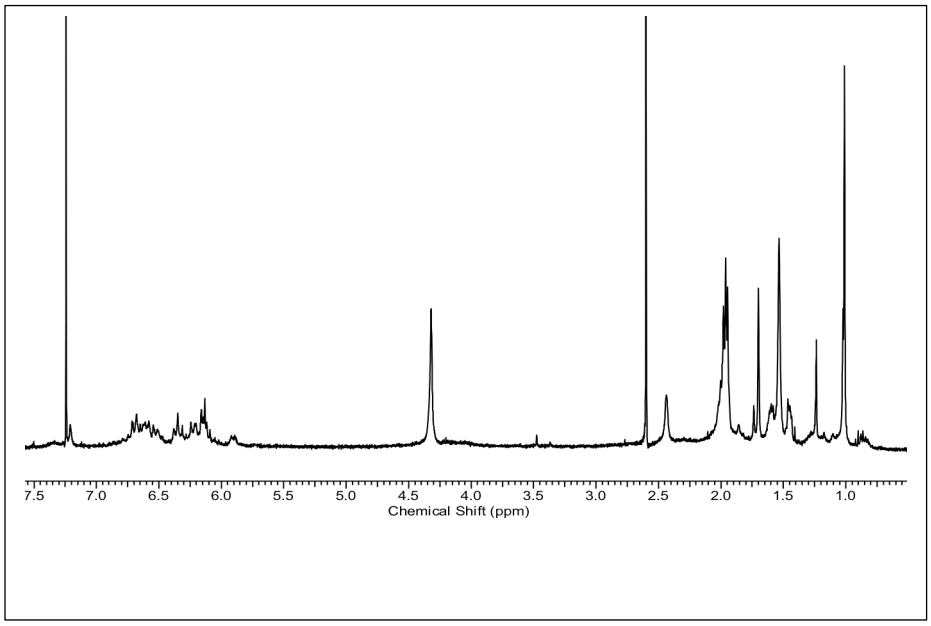

400MHz ^{1}H NMR spectrum compound (46) recorded in chloroform –*d*.

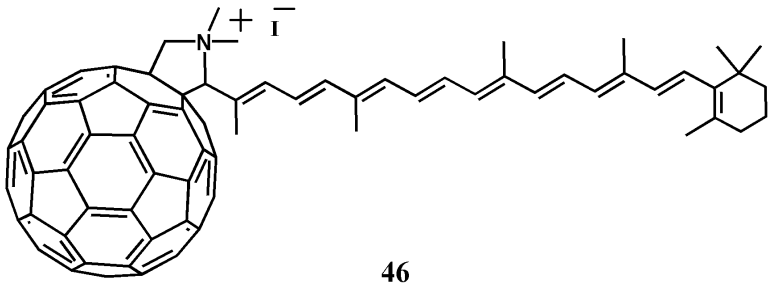

46

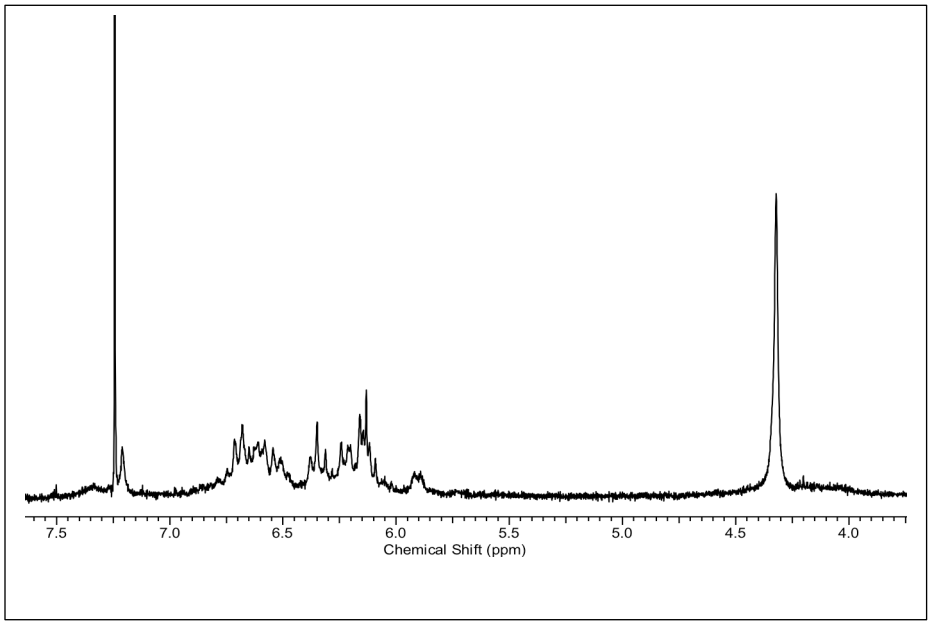

400MHz ^{1}H NMR spectrum compound (2) recorded in chloroform –*d*.

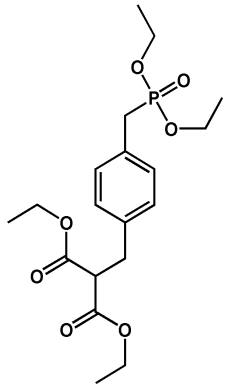

2

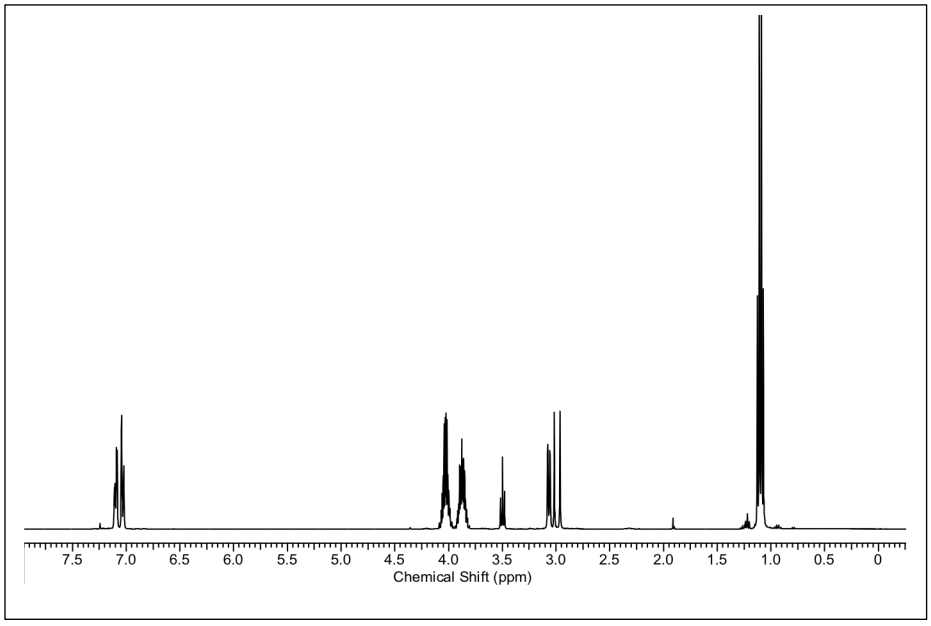

400MHz ^{1}H NMR spectrum compound (2) recorded in chloroform –*d*.

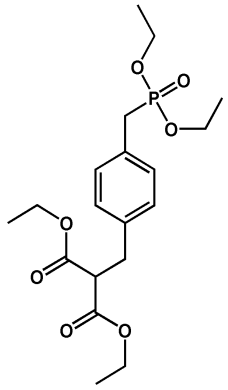

2

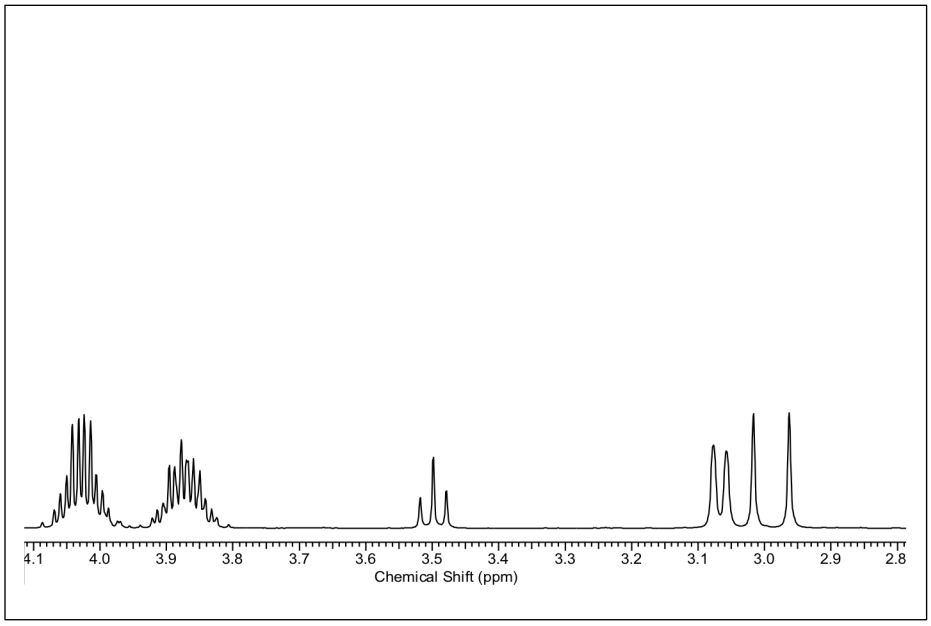

400MHz ^{1}H NMR spectrum compound (4) recorded in deuterium oxide.

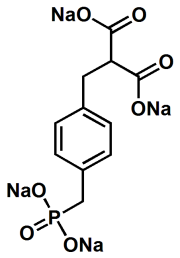

4

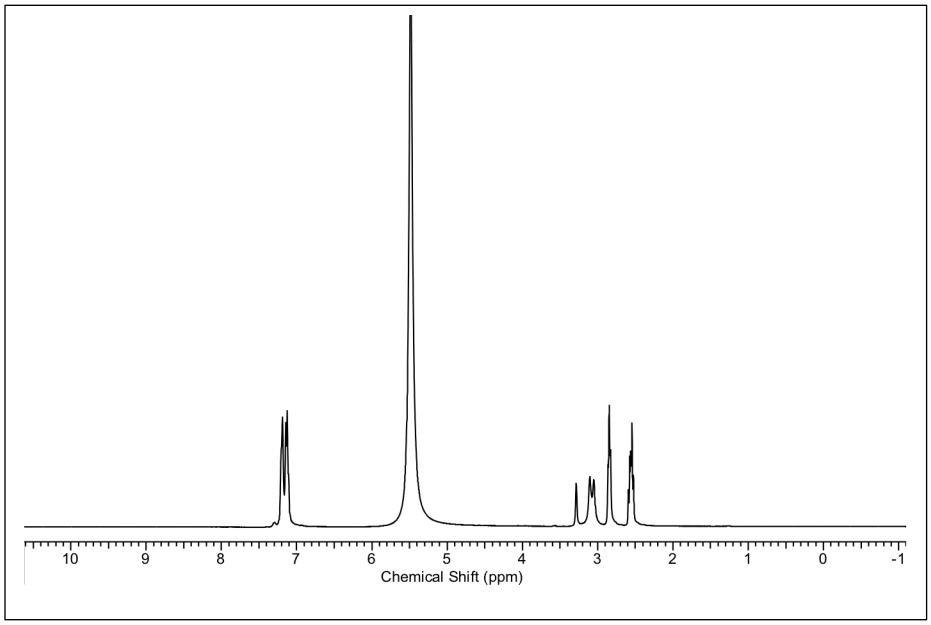

400MHz ^{1}H NMR spectrum porphyrin (7) recorded in chloroform –*d.*

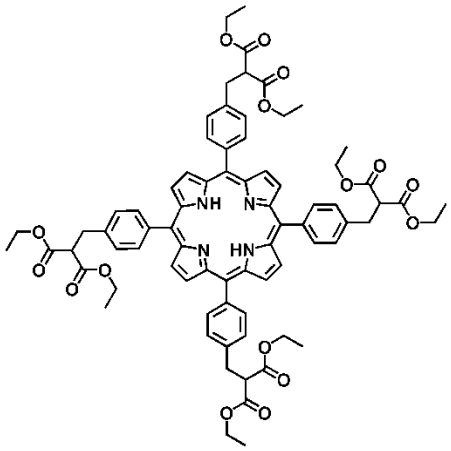

7

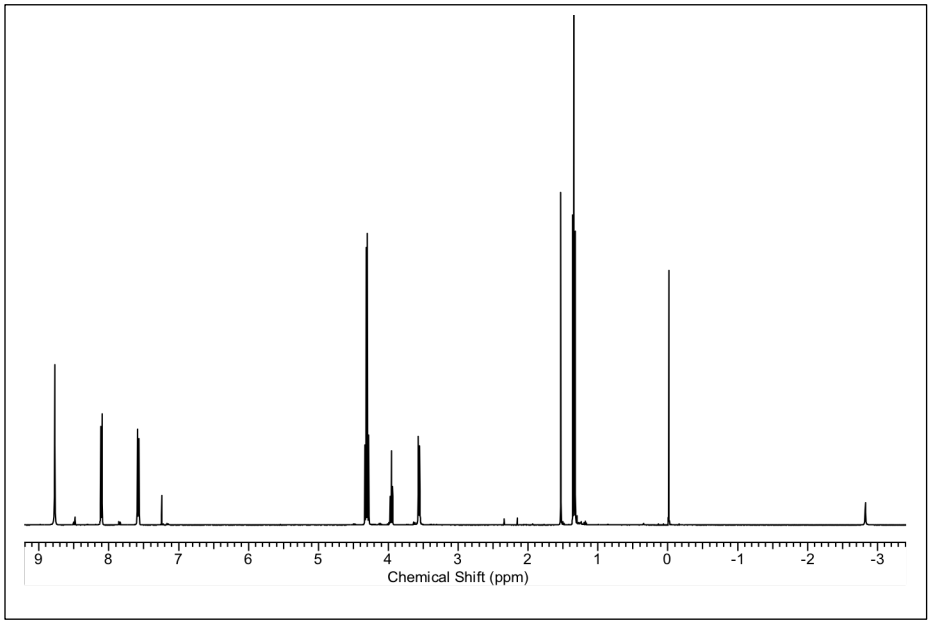

400MHz ^{1}H NMR spectrum porphyrin (7) recorded in chloroform –*d.*

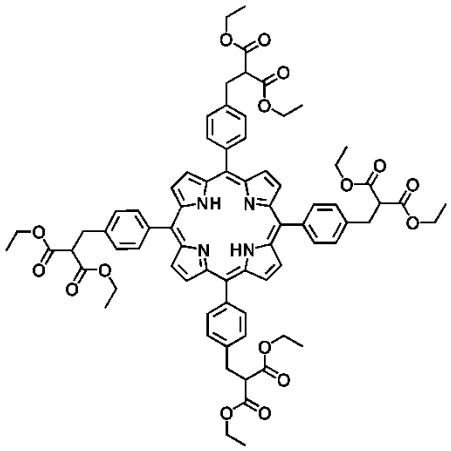

7

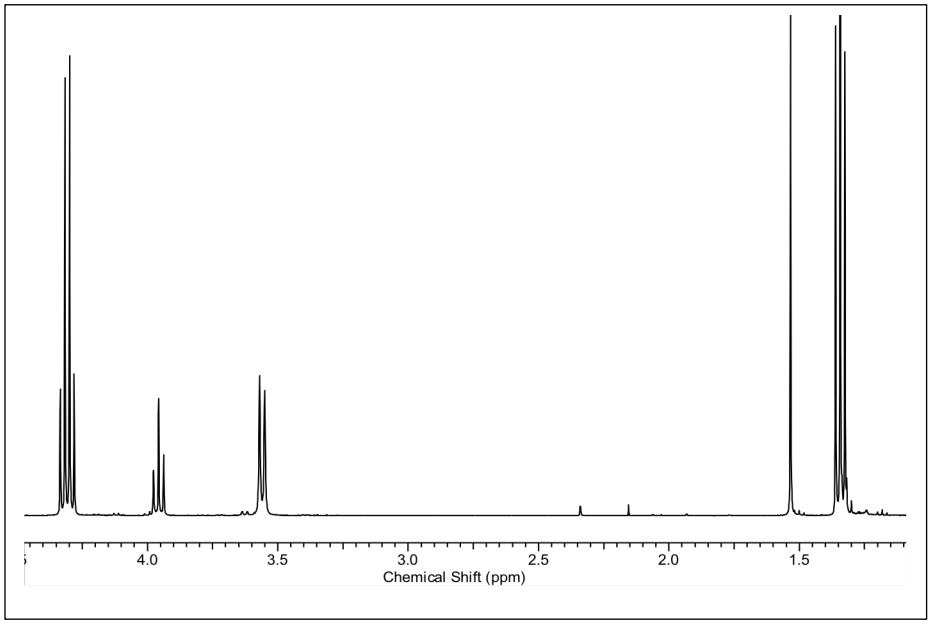

400MHz ^{1}H NMR spectrum porphyrin (11) recorded in chloroform –*d*.

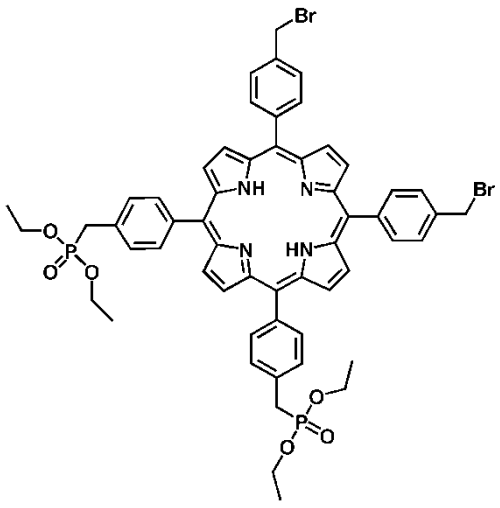

11

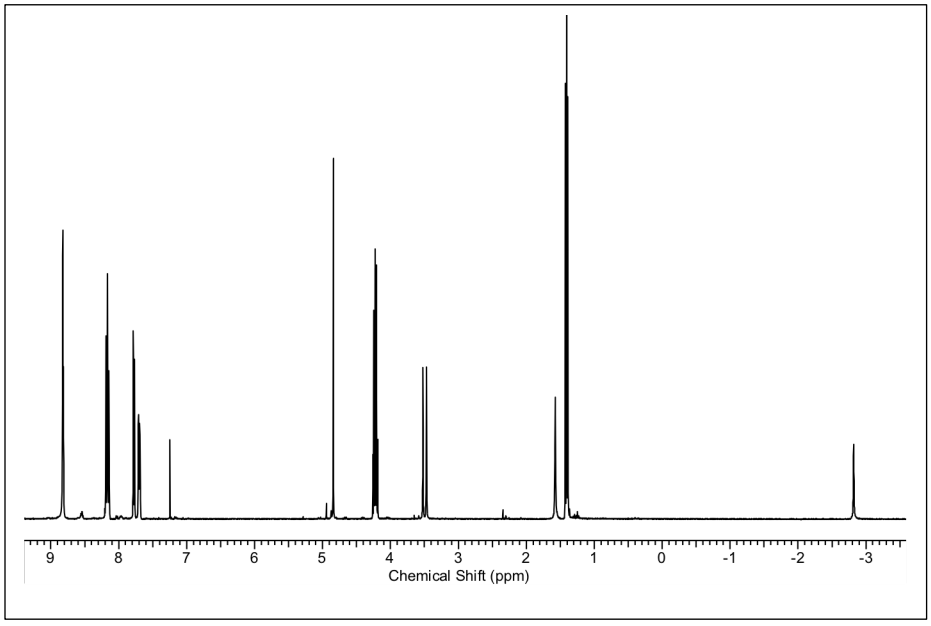

400MHz ^{1}H NMR spectrum porphyrin (11) recorded in chloroform –*d.*

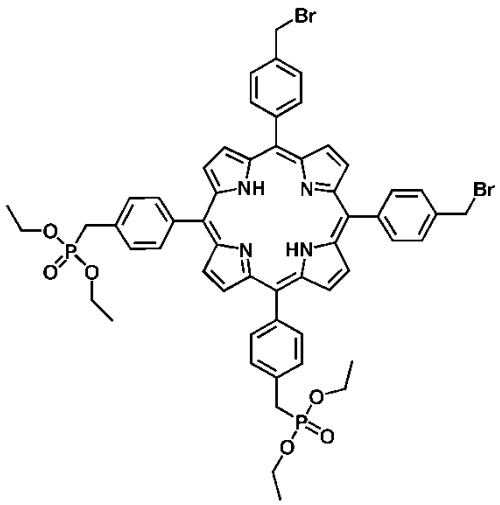

11

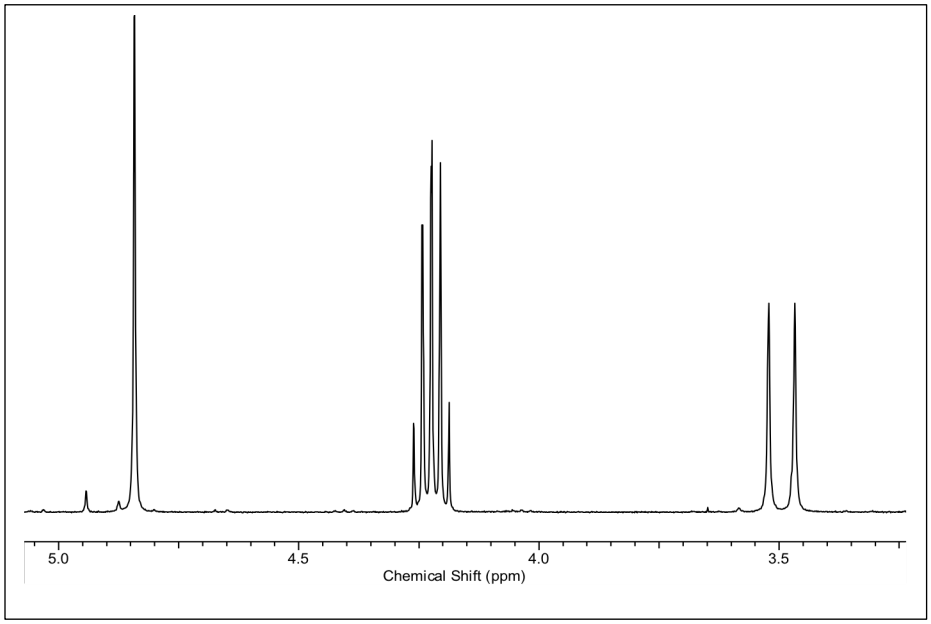

400MHz ^{1}H NMR spectrum porphyrin (12) recorded in chloroform –*d.*

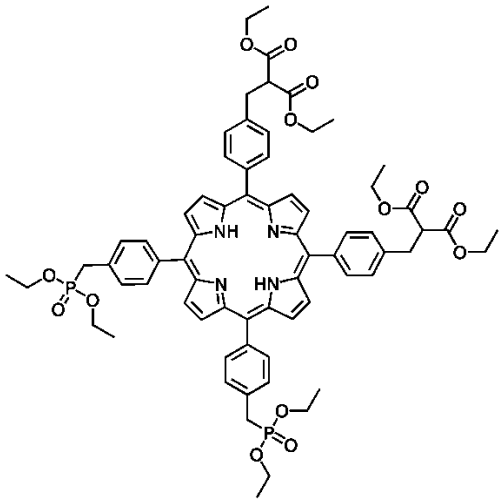

12

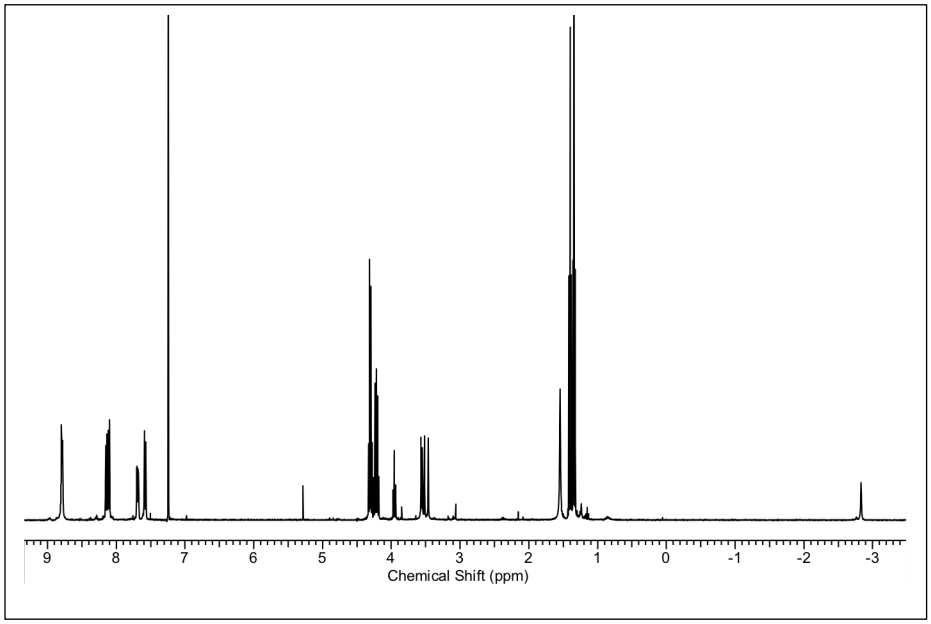

400MHz ^{1}H NMR spectrum porphyrin (12) recorded in chloroform –*d.*

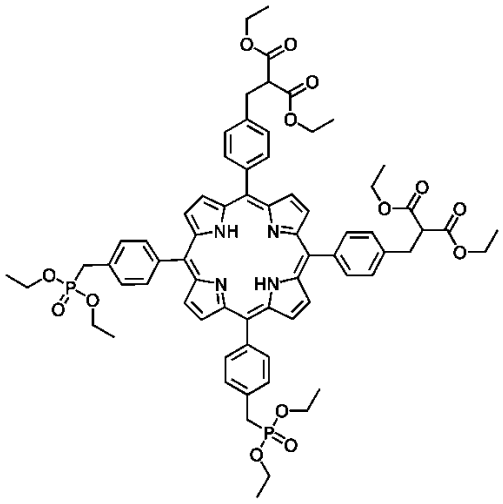

12

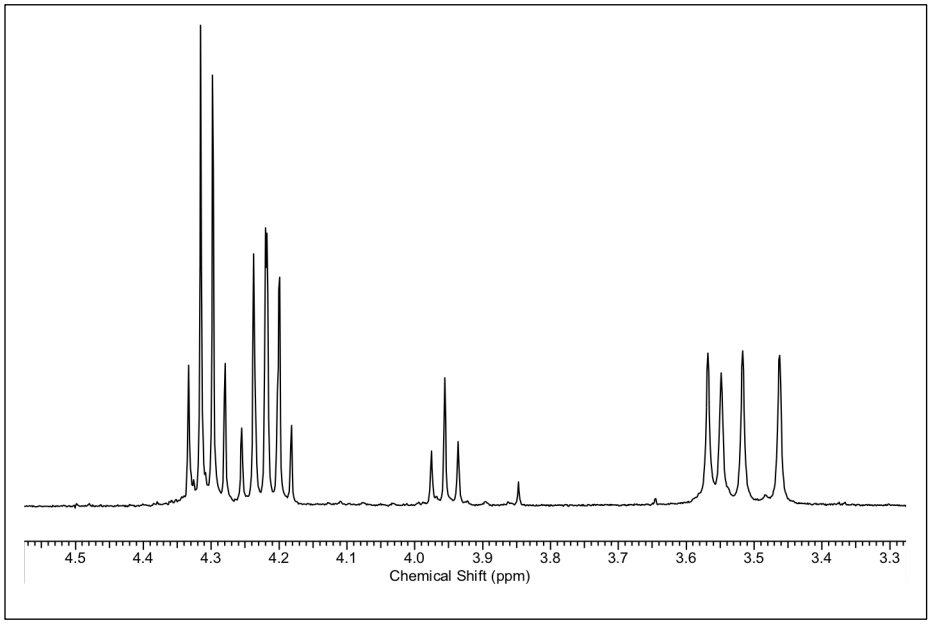

400MHz ^{1}H NMR spectrum porphyrin (22) recorded in chloroform –*d.*

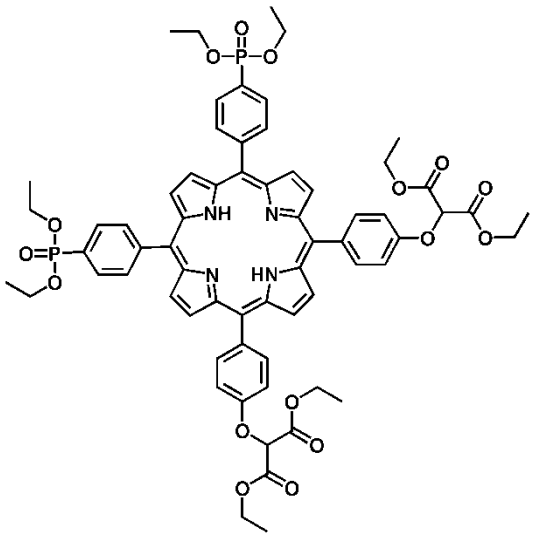

22

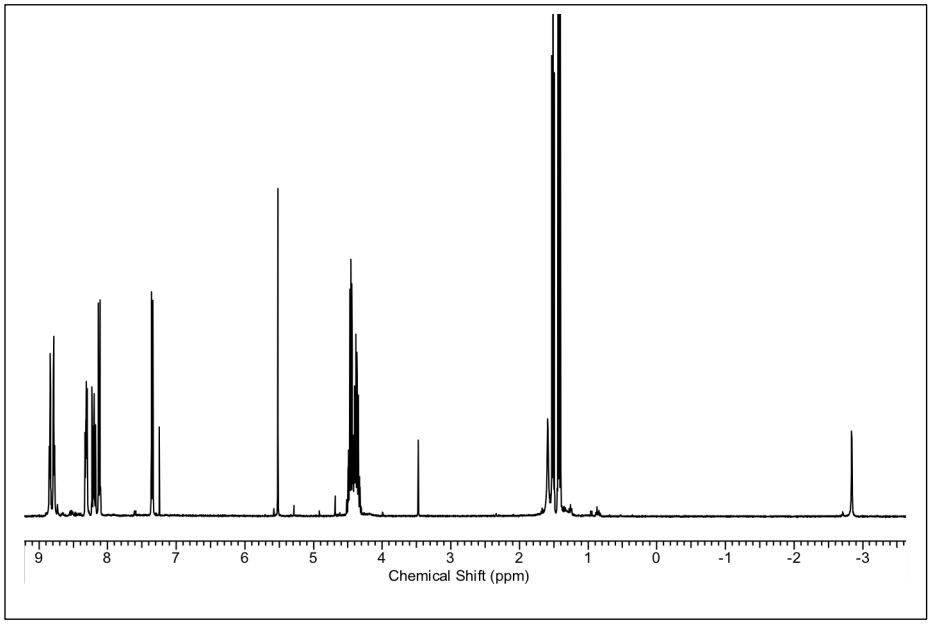

400MHz ^{1}H NMR spectrum porphyrin (22) recorded in chloroform –*d.*

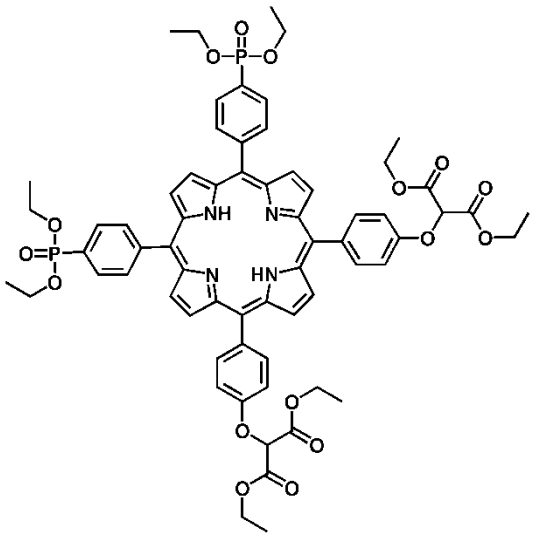

22